PARTIAL MELTING EXPERIMENTS ON CHONDRITIC PRECURSORS:

A POSSIBLE ORIGIN FOR EUCRITES

AND THE BASALTIC ACHONDRITE PLANETOID

BY JOSEPH S. BOESENBERG

A thesis submitted to the

Graduate School - New Brunswick

Rutgers, The State University of New Jersey

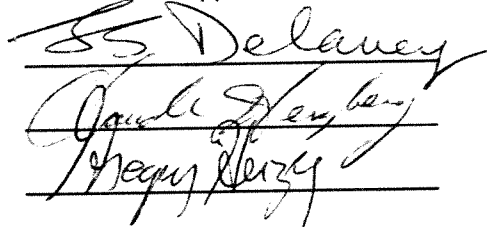in partial fulfillment of the requirements

for the degree of

Master of Science

Graduate Program in the Geological Sciences

Written under the direction of

Dr. Jeremy S. Delaney

and approved by

New Brunswick, New Jersey

May, 1995

ABSTRACT OF THE THESIS

Partial Melting Experiments on Chondritic Precursors:

A Possible Origin for Eucrites and the Basaltic Achondrite Planetoid

by JOSEPH S. BOESENBERG

Thesis Director

Dr. Jeremy S. Delaney

Partial melting experiments on synthetic analogues and natural samples of Murchison and a mixture of 70% H-chondrite - 30% CM-chondrite were conducted to investigate the origins of eucrites and the basaltic achondrite planetoid (BAP). The experiments show that if eucrites were produced by partial equilibrium melting of a chondritic precursor, fractionation of Fe metal and olivine is required on BAP to produce appropriate Fe-Mn-Mg systematics. The eucrites can also be produced by equilibrium crystallization, as well as by fractional melting of the modified H-CM precursor. A comparison between the experiments indicates that the H-CM composition not only matches the oxygen isotope constraint, but is a more appropriate precursor than Murchison since less extensive fractionation is required to produce eucritic melts. The only problem with H-CM composition is a massive overabundance of alkali elements. Production of an H-CM precursor is possible through the collision of two asteroids, and the subsequent melting of that newly formed parent planetoid.

Acknowledgments

TABLE OF CONTENTS

LIST OF TABLES

LIST OF FIGURES

APPENDICES

Introduction

Meteorites can be classified into three major families: the iron meteorites, the stony meteorites, and the stony-iron meteorites (GLASS, 1982). The iron meteorites consist almost exclusively of iron and nickel metal, while the stony meteorites consist of mainly silicate material, and the stony-irons consist of both silicate and metal. Of these three groups, the stony meteorites are by far the most abundant and can be further subdivided into two groups: the chondrites or those meteorites which contain small silicate spheres called chondrules, and the achondrites, those meteorites which do not have chondrules (GLASS, 1982). Eucrites, which are the meteorites of interest in this study, belong to a subgroup of the achondritic meteorites known as the basaltic achondrites. The basaltic achondrites constitute the largest group of achondritic meteorites (JUREWICZ et al., 1993; MASON et al. 1979), with the eucrites being their most numerous member.

The mineralogy of eucrites consists predominantly of pigeonite, plagioclase, the silica polymorphs of tridymite and quartz, with small additions of accessory phases such as augite, ilmenite, chromite, phosphates, troilite, and metal.

Texturally, most eucrites are breccias, containing lithic clasts with basaltic textures. However, some eucrites are interpreted to have cumulate textures (CONSOLMAGNO and DRAKE, 1977).

The two other members of the basaltic achondrites, that are often associated with the eucrites, are the diogenites and the howardites. The diogenites consist almost entirely of orthopyroxene with minor amounts of the accessory phases of augite, pigeonite, plagioclase, olivine, chromite, troilite, tridymite, quartz, and metal, while the howardites are breccias that have a mineralogy similar, but not identical, to a combination of diogenites and eucrites (McCARTHY et al, 1973; MASON et al, 1979). Based on overlapping oxygen isotope signatures, the eucrites, diogenites and howardites appear to originate from the same parent body (CLAYTON, 1993). Since the eucrites and diogenites both appear to have crystallized in relatively low pressure environments, probably at or near the surface, they may represent

different lithologic provinces of the same parent body that are dominated by different rock types or they may be two different lithologies in a layered crust on the parent body (TAKEDA, 1979; DELANEY 1986b, 1986c). The howardites, in either case, probably resulted from impact events that mixed and further processed pre-existing eucrite and diogenite lithologies (WARREN, 1985).

At present, the best candidate for the parent body of the eucrites, as well as the diogenites and howardites, is the asteroid 4 Vesta. Vesta has an optical reflectance spectral pattern that is similar to the spectral data obtained from actual samples, such as the eucrites Nuevo Laredo (McCORD et al., 1970), Nobleborough (FEIERBERG and DRAKE, 1980), Béréba, and Pasamonte (BINZEL and XU, 1993); the diogenite, Johnstown (BINZEL and XU, 1993), and the howardite, Kapoeta (CHAPMAN and SALISBURY, 1973). The samples that match Vesta best are the eucrite, Béréba, and the howardite, Kapoeta. A recent discovery by BINZEL and XU (1993) shows that 20 main belt asteroids (less than 10km diameter) that are in orbits associated with Vesta all have spectral patterns that are consistent with the basaltic achondrites. The asteroidal spectra vary from asteroid to asteroid, with some being nearly identical to Vesta, while others match spectra taken from diogenites, like Johnstown (BINZEL and XU, 1993). Therefore, sufficient variability appears to exist to indicate that the eucrites, diogenites, and howardites (HED) were all derived from the same parent body.

The probability that Vesta is a source of the basaltic achondrites is further strengthened by the BINZEL and XU (1993) investigation of the orbits of their 20 newly discovered asteroids. Twelve asteroids were found to have orbits similar to that of Vesta, while the remaining eight were found to have orbits between Vesta and the Jovian 3:1 orbital resonance. Assuming that Vesta was the parent body of these smaller asteroids, the ejection velocities necessary to place the asteroids into their present orbits was determined. According to BINZEL and XU (1993), the positions of the asteroids span the distance between Vesta and the 3:1 resonance and suggest that other asteroids may have entered the resonance. Since the sizes of ejected fragments from an impact are inversely proportional to their ejection

velocities (BINZEL and XU, 1993), the ejection velocities of small (0.1 to 1.0 km) fragments should be sufficient to reach the resonance, and thereby allow fragments of eucrite, diogenite, and howardite lithologies from these asteroids to be delivered into Earth-crossing orbits. A study by FARINELLA et al (1993) argues that fragments from asteroids like Vesta, can be injected into the resonance in approximately 10^6 years. Subsequent ejection of the fragments from the resonance into an Earth-crossing orbit, based on numerical calculations of fictitious bodies near 2.4 AU (Vesta's location) by FARINELLA et al (1992), indicate that the fragments could reach Earth in an additional 10^6 years. Considering the cosmic-ray exposure ages of eucrites, diogenites, and howardites vary between 5-40 x 10^6 years (HERZOG and CRESSY, 1977; SCHULTZ, 1987), there appears to be agreement between the existing data and the model, facilitating the possibility that Vesta is the parent asteroid to the HED meteorites. Associating Vesta and its related asteroids with the basaltic achondrites, however, does not explain how the parent body or the eucrites, diogenites, and howardites formed.

There are two general types of models that try to explain the formation of the eucrites. The first model, a fractional crystallization model (MASON, 1962; McCARTHY et al., 1973), suggests that eucrites crystallized from a residual liquid. This residual liquid resulted when a presumably chondritic precursor (olivine-rich) melt experienced olivine fractionation at depth inside its parent body. Fractionated olivine was left behind to form the mantle, while the melt continued to rise towards the surface. Subsequent fractionation of mafic mineral cumulates, near the surface, produced cumulate orthopyroxenites, which are represented by the diogenites, leaving a residual liquid behind to crystallize into the eucrites. A mass balance constraint by WARREN (1985) on the howardites supports this model, arguing that if the eucrites are identical to the basaltic component and the diogenites are identical to the pyroxenite component in the howardites, then more than half of the eucrites probably formed as residual liquids of melts that had previously fractionated from diogenites. The second type of model (STOLPER 1975, 1977; HEWINS and NEWSOM, 1988) suggests that the noncumulate eucrites formed as partial melts of an olivine rich source region and

experienced little or no fractional crystallization during their formation, while the diogenites formed from separate melts.

However, since the achondrite models are attempting to describe the petrogenetic history of a planetoid, it strains credibility to assume that a single style of magmatism was responsible for all of the lithologies sampled by the basaltic achondrites. (The older terminology of planetoid is used here instead of parent body or asteroid to avoid any preconceived ideas about such bodies. Planetoid simply implies a relatively small planetary body which experienced geological processes that are usually associated with planets, such as magmatism or impacts.) More likely, both partial melting and fractional crystallization mechanisms acted to varying extents in different geographical areas of the source planetoid (DELANEY, 1986a, b, c; DELANEY et al., 1981). The distribution of the igneous lithologies on the Earth and Moon are quite variable in composition and regionally are dominated by different lithologies that formed under different stratigraphic, lateral, or temporal conditions on the planetary body. The Earth and Moon therefore provide precedents for the basaltic achondrite planetoid (BAP) having a provincial distribution of igneous lithologies, with some areas of crust being dominated by eucrites, while others contain more abundant diogenite or ultramafic lithologies. The cosmic ray exposure ages for basaltic achondrites (AYLMER et al., 1986; HERZOG and CRESSY, 1977; HERZOG et al., 1978; SCHULTZ, 1987) indicate that approximately three to seven cratering events (depending on the interpretation of the data) within the last 40 million years were responsible for the ejection of samples from their parent body. A single igneous province on BAP, therefore, is unlikely to have been sampled.

STOLPER (1977) demonstrated that partial melting experiments on eucrites at low temperatures (1160 to 1180°C) and at oxygen fugacity conditions of one log unit below the iron-wüstite or Fe-FeO buffer yielded a glass composition that was multiply-saturated with olivine, pigeonite, plagioclase, spinel, and metal. The multiple saturation indicates that the melt probably formed at or near an invariant point and is likely to be a significant source of magmas of constant composition. Since this mineralogy is compatible with the partial melting

of a chondritic meteorite, an implication of STOLPER'S results is that eucrites might be formed by the fairly simple process of partial melting of a chondritic precursor.

Since STOLPER'S (1977) study, there have been several studies concerning the melting of chondritic meteorites. Some experiments, such as those done by TAKAHASHI (1983) and WALKER and AGEE (1988) concentrated on aspects of melting that are not directly applicable to the eucrite problem, such as very high pressure 30 kilobars (TAKAHASHI, 1983) or thermal gradients (WALKER and AGEE, 1988). However, others did partial melting experiments that are very relevant to achondrite genesis. KUSHIRO and MYSEN (1979) did partial melting experiments on the L6 chondrite, Y74354, and showed that their 1200°C glasses were within the compositional range of the eucrites and howardites and therefore suggested chondrites may have a genetic relationship with the basaltic achondrites. BARTELS and GROVE (1991) experimented with partially melting magnesian eucrite clasts from howardites, at one atmosphere and one kilobar pressure, to determine constraints on the composition of eucritic precursor material, as well as, the melting and crystallization processes on the parent body of the eucrites. JUREWICZ *et al* (1991, 1993) did partial melting experiments on Allende (CV3) and Murchison (CM2) and produced melts that are remarkably similar to the true eucrites and to eucritic melts produced by STOLPER (1977). However, they noted that the MnO content of their resulting glasses was systematically lower than in natural eucrites.

These melting experiments provide evidence that partial melting of a chondritic precursor produces melts that resemble the major and minor element chemistry of the eucrites and therefore suggest the possibility that a chondritic precursor to the basaltic achondrites may have existed. However, two major problems become apparent if any single chondritic class of meteorite is the eucrite precursor. The first problem is that the oxygen isotopic signature of the eucrites does not match any known class of chondritic meteorite. The second problem, as highlighted by JUREWICZ *et al.* (1993) and recognizable in the experiments of KUSHIRO

and MYSEN (1979), is that melting experiments on typical chondrites produce melts with unrealistically high molar Fe/Mn ratios.

In an attempt to reconcile these problems, DELANEY (1993) calculated a eucritic precursor composition constrained by the oxygen isotopic ratios of basaltic achondrite samples. The model (Table 1 and Figure 1) involves mixing material from two different types of chondrite meteorite in proportions that give the oxygen isotopic signature of the eucrites in the mixture. As both mixing components are chondritic, the major element chemistry of the mixture remains chondritic. The only mixing constraint on the model (in a two component mixture) is that the two components must be on opposite sides of the BAP oxygen mass fractionation line, so that the resulting mixture has the isotopic signature of the eucrites. The two major types of meteorites that were involved in the mixing models were carbonaceous chondrites and ordinary chondrites. They were used because the closest chondritic meteorites to the BAP fractionation line are the H chondrites (a type of ordinary chondrite) on the $\delta^{17}O$ enriched side and the CM or CV chondrites (two types of carbonaceous chondrites) on the $\delta^{17}O$ depleted side. However, other members of the two types of meteorites were also explored as possible mixing members. The model subsequently uses some of the carbon present within the precursor to reduce sufficient iron metal from the silicate FeO component so that appropriate silicate molar Fe/Mn ratios for the eucritic precursor are reproduced. The results of DELANEY'S calculations yielded several chondritic mixtures [nicknamed "cocktails"] (shown in Table 1) that might be used as a eucritic precursor. One cocktail, produced by mixing 70% H chondrite with 30% CM chondrite, has a remarkable compositional similarity to the 'eucritic parent body' [precursor] calculated by DREIBUS and WÄNKE (1980) and appears to be promising as a model precursor.

This study reports on three series of experiments that used both synthetic and natural starting compositions of the chondritic cocktail (70% H - 30% CM) described above and the CM chondritic meteorite, Murchison. The experiments were designed to: 1) investigate the Fe-Mn-Mg systematics resulting from the removal of iron from a partially melted chondritic

precursor of the eucrites; 2) determine and compare the phase relationships resulting from the partial melting of different chondritic starting compositions; 3) test the DELANEY (1993) model to determine whether an appropriate precursor to the eucrites could be derived from the cocktail (70% H - 30% CM); and 4) allow direct reproduction and confirmation of the experiments done by JUREWICZ et al. (1993).

Experimental and Analytical Techniques

Before any experiments could be run, strict procedures had to be developed so that the experiments were tightly constrained compositionally and to ensure precise and reproducible run temperatures and oxygen fugacities. Without precisely defined constraints a comparison between these experiments and the experiments of other researchers would be impossible. The procedures involved 1) the preparation of the synthetic and natural starting compositions, 2) the calibration of the temperature and oxygen fugacity, or the activity of oxygen present, within the furnace, and 3) the calibration of the electron microprobe analyses, the means by which the experiments were characterized.

Sample Preparation

Three series of experiments were run for this research. The first series of experiments were essentially the test experiments. They were designed to explore whether synthetic compositions were a feasible alternative to using natural materials and to understand the effects of Fe loss on the Fe-Mn-Mg systematics. The understanding of the Fe loss in the experiments is critical, since it can occur due to several factors, both wanted and unwanted. The oxygen fugacity, which controls the amount of iron being reduced and removed from the silicates in the experiment, is the major "wanted" factor since it can be calibrated precisely. A second factor, which can at least be accounted for, is the amount of carbon present within the sample. Carbon reacts with FeO to produce Fe-metal and carbon dioxide. The amount of Fe-metal produced by this reaction can be calculated and subtracted out of the total amount of

metal produced during the experiment to determine the effect of altering the oxygen fugacity settings. The third major factor, which is the most difficult to account for, is the amount of iron lost to the platinum wire that holds the experiment inside the furnace. Since iron readily diffuses into platinum, either the iron that diffuses into the platinum wire from the experiment must be accounted for, or an equilibrium must be attained between the experimental charge and the platinum wire, allowing the experiment to neither gain nor lose iron to the wire. This equilibrium is accomplished by pre-saturating the platinum wire with iron and will be discussed in greater detail later.

The Series I experiments were simplified synthetic equivalents of the CM chondritic meteorite, Murchison (Table 2A) (based on the analysis of JAROSEWICH, 1990). Four analogue compositions (Table 2B) were made and contained seven oxides: SiO_2, Al_2O_3, Cr_2O_3, FeO, MnO, MgO, CaO. The oxides of SiO_2, Al_2O_3, Cr_2O_3, MnO, and MgO were added as pure oxide powders, the "FeO" was from Fe_2O_3 powder, and the "CaO" was taken from $CaCO_3$ powder (Table 3). The compositions were prepared by heating up the individual oxides and carbonates to 250°C to drive off any adsorbed water that was present. The oxide powders were then weighed and assumed to be anhydrous. The compositions were finally assembled and ground into a fine powder (to about 75 microns) using a SPEX grinder. The four analogue compositions had four different bulk molar Fe/Mn ratios. Despite the attempt to remove the adsorbed water from the compositions, the effects of the added water in the oxides resulted in the incorrect Fe/Mn ratios in the four analogue compositions. Although the nominal Murchison Fe/Mn ratio of 140 was initially intended to be used (along with Fe/Mn ratios of 100, 60 and 20), microprobe analyses of glasses made from the four compositions showed that the errors resulted in the highest bulk Fe/Mn ratio being 85. The three other compositional ratios turned out to be 65, 45, and 20. Although the ratios were not those planned, the analogues were used anyway and served their planned purposes. Table 2B shows the nominal Murchison composition (Fe/Mn 140) and the averaged microprobe analyses of the four analogue compositions used.

The Series II experiments were used to investigate eucritic origins. These experiments were run with two compositions that were prepared from _synthetic_ materials (Table 2A and 2C). The compositions consisted of a Murchison analogue and a modified version of the 70% H chondrite - 30% CM chondrite mixture proposed by DELANEY (1993). This series of compositions consisted of the same oxides as in the first series, but also included the oxides TiO_2, Na_2O, and NiO (for the Murchison composition only). The TiO_2 and NiO were pure oxides, but the Na_2O was taken from $NaHCO_3$ (Table 3). These compositions were heated, weighed, assembled, and ground during their preparation in the same manner as the compositions of the first series. Table 2C shows that the Series II synthetic compositions also did not yield the desired abundances of the oxides. The experimental compositions (especially the H-CM analogue) for these experiments however actually proved quite useful and will be discussed later.

The Series III experiments were run using _natural_ samples of Murchison and a mixture of 70% of the H chondrite, Allegan, and 30% Murchison (Table 2A). Allegan and Murchison were initially received as chips and were ground into fine powders (to about 75 microns) before they were used. The powders were then individually baked at 400°C for two hours, and then weighed out. For the (70%) Allegan - (30%) Murchison mixture, the samples were then ground a second time.

To insure that starting compositions for the synthetic (Series I and II) experiments were homogeneous, high temperature glasses were made from each of the starting compositions. For the Series I compositions, two glasses were made for each of the four starting compositions, while three glasses were made for each of the two Series II starting compositions. After making the glasses, the glasses were analyzed by electron microprobe for the oxide abundances contained within them. The two (Series I) or three (Series II) glass compositions for each starting composition were than averaged and the deviation of each glass composition from the average was determined. Since only two or three glasses were made for each starting composition, the standard deviations were very large, being either

50% (2 glasses) or 33% (3 glasses). The tests, therefore, only prove that there were no large scale heterogeneities present, not that the compositions were homogeneous. Ultimately, to insure homogeneity, a greater number of sample glasses should have been taken. Fortunately, the differences between the glasses for each starting composition were extremely small (less than 2% from the average glass composition for the major elements, and less than 5% from the average for the minor elements for all of the compositions) and the absence of large-scale heterogeneity could be assured.

Since there was limited amount of actual meteoritic material available for the Series III experiments, high temperature glasses were not made to test for homogeneity. Instead, modal analysis was used in conjunction with the compositions of the silicate phases within each experiment to calculate the starting bulk composition. The calculated bulk composition in each experiment was then compared to the nominal bulk composition of either natural Murchison or natural Allegan-Murchison. In general, there was excellent agreement between the calculated and nominal bulk compositions, with only one experiment not yielding good results (Natural Murchison, 1180°C, IW-0.5). This experiment experienced olivine fractionation during quenching, which made the calculation extremely difficult.

Furnace Temperature Calibration

Furnace Description

The furnace that was used for the experiments was a Deltech 31 VTOS/C vertical muffle tube gas mixing furnace (Figure 2). The furnace design was fairly simple, containing a 4 centimeter diameter, 60 centimeter long, alumina tube (called the muffle tube), surrounded by six equally spaced U-shaped Kanthall molybdenum disilicide heating elements, which are capable of sustained operation in air at temperatures up to 1800°C. Encompassing the heating elements and muffle tube, is a steel box which contains 12 cm of insulation. Brass cooling heads attach to and seal against both ends of the muffle tube causing an isolated chamber to be made. The internal atmosphere of the muffle tube can subsequently be

monitored and regulated for the ambient oxygen (or other gas) fugacity. An access port within each cooling head allows the regulated gases to pass through the muffle tube. For the Deltech furnace used, the gases entered at the upper cooling head and exited at the lower cooling head, however, the reverse setup could have just as easily been used. As long as the position of the oxygen fugacity calibration, temperature calibration, and experimental charges are in the same spot, there is no advantage to the direction of the flow of the gases. The brass cooling heads' primary purpose, in addition to providing an isolated chamber, is to water cool the ends of the muffle tube, allowing a stable thermal gradient to exist inside the furnace. This stable gradient prevents erratic temperature fluctuations caused by air drafts. The cooling heads also prevent the instrumentation ports and the access ports from becoming dangerously hot (TURRIN, 1984).

The furnace temperature was regulated by a Eurotherm 211 programmable temperature control unit that is connected to an internal, type B 94% platinum - 6% rhodium versus 70% platinum - 30% rhodium wire thermocouple (KINZIE, 1973; POWELL, 1972). The thermocouple is situated next to the heating elements and enters through an access port in the back wall of the furnace (TURRIN, 1984). This programmable temperature control unit allows the user to implement programmed heating and cooling paths.

Sample Rod and Thermocouple Assembly

To measure the temperature within the furnace, a thermocouple was needed that could function over the temperature range of the experiments (1100°C to 1600°). After looking at the various types of thermocouples, a type S thermocouple (KINZIE, 1973; POWELL, 1972) was decided upon. The thermocouple consists of two wires, one pure platinum wire and one 90% platinum-10% rhodium wire and is included within the sample rod assembly. To make the thermocouple (and sample rod), a 40 cm long, four bore hole alumina rod is attached to a brass cap (Figure 2). The Pt and Pt-Rh wires are each inserted into one of the holes in the alumina rod. The ends of the wires are then butt welded together at one end (the end that is

inserted into the furnace), using an oxygen-acetylene torch, to form a small uniformly melted sphere. When the welded end of the wires is at a different temperature than the unwelded ends, a thermoelectric current is produced. Since the wires are made of different materials, the resistance of each wire is different and a potential is created between them. When a potentiometer is attached to the unwelded ends, the potential can be measured between the two wires. The output voltage can than be monitored and calibrated to give the temperature at the welded end.

Two pieces of platinum wire are then inserted into the remaining two holes in the alumina rod and allow the experimental charges to be suspended slightly below the thermocouple (Figure 3).

Hotspot Location

Calibration of the furnace began by first determining where the hottest point in the furnace was. This point was found by carefully sliding the sample rod up and down within the muffle tube of the furnace, until the maximum possible temperature was read by the thermocouple. The hotspot was located 33 cm from the base of the brass head on the sample rod and remained fixed throughout the experiments. The size of the hotspot was found to be about three cm high and the temperature variation within the hotspot was 1-2°C.

Calibration of the Furnace and Sample Rod Thermocouples

In order to calibrate temperature correctly, the nominal temperature at which some process or event occurs must be known. One of the simplest and most precise methods for calibrating is to compare the measured and nominal melting point of an element or compound. Since the experiments were to be run over a temperature range of 1100°C to 1600°C and calibration temperatures comparable to the experimental range would be preferred, the melting points of gold (1064°C) and palladium (1554°C) were chosen to calibrate against.

The procedure for calibrating takes advantage of the fact that both gold and palladium are excellent conductors, by creating a circuit within the furnace and waiting for the circuit to break when the melting point of Au (or Pd) is reached. To set up the circuit, a piece of thin Pt wire is attached to each of the sample support wires. The thin Pt wires are attached to a piece of Au or Pd wire, by making tiny loops in the thin Pt wires and slipping the Au (or Pd) wire through each loop (Figure 4). The tips of the Au (or Pd) wire are then slightly bent so it does not slide off from the thin Pt wires. Next, a voltmeter is attached to the support wires at the top of the sample rod. If everything is set correctly, when the sample rod is placed in the furnace, there should be little or no resistance [in ohms (Ω)] through the Au (or Pd) and Pt wire circuit just made. The next step is to bring the furnace temperature, if possible, to within 20°C of the Au (or Pd) melting point and allow the furnace to equilibrate. Depending on the difference between the initial and final temperatures, the furnace may take up to 45 minutes to thermally equilibrate, however it is extremely important that the furnace be at thermal equilibrium. After the temperature appears to be stable (at equilibrium), the sample rod is carefully inserted into the furnace, while monitoring the voltmeter and insuring the circuit remains intact. The temperature is increased very slowly (1-2°C every 5-10 minutes) towards the melting point of Au (or Pd), while monitoring the thermocouple until the Au (or Pd) wire melts, breaks the circuit, and makes the voltmeter register infinite resistance. It is important to wait at least 5-10 minutes between each increase in temperature to allow the furnace to equilibrate. After the circuit is broken, the sample rod and furnace display temperatures are then noted for the calibration. If the difference between the sample rod thermocouple calibration temperature and the melting point is more than 3-5°C, a new thermocouple welding should be made to insure that corrosion or recrystallization of the wires does not further hamper the ability to measure the temperature precisely. [It is important for the reader to realize that the displayed furnace readings are not true temperatures, although the values would tend to imply this. In fact, the displayed furnace readings only estimate the desired temperature, but are actually used to control the amount of electrical current being supplied to

the heating elements. Since conductivity increases with decreasing temperature, more heat per ampere is produced at lower temperatures than at higher temperatures. The calibrated temperature path shown in Figure 5 demonstrates this effect by NOT being parallel to the nominal one to one line. At low temperatures, it is skewed to the right of the nominal line (current is more efficiently transformed into heat), but passes over to the left of the nominal line at high temperature (current is less efficiently transformed into heat. Table 4 lists the furnace display readings (Dfurn) and the corresponding nominal temperatures taken with sample rod (Tsr) thermocouple in ten degree increments shown in Figure 5.)]

To make a new welding, the lower 3-5 centimeters from both the Pt and Pt-Rh wires should be removed. The two cut ends then are butt welded into a small uniformly melted sphere at the base of the thermocouple. If the subsequent calibration is still off, replacement of the thermocouple wires is probably necessary. A good calibration should give consistent and extremely small temperature differences (1-2°C) for both the Au and Pd calibrations.

Table 5 shows the results of the thermocouple calibration experiments using the furnace display readings and sample rod thermocouple. The first calibration yielded consistent results for both Pd and Au, but needed a 20°C correction. The lower portion of the wire had undergone extensive recrystallization from its previous use, so a new welding was made. Calibration #2 gave inconsistent results, suggesting a completely new thermocouple was needed. Calibration #3 was run with the new thermocouple. The correction factor for the sample rod thermocouple is 0°C, since the thermocouple readings match the melting points. This thermocouple calibration procedure was carried out approximately every 100-200 hours of experimental time, depending on the running temperatures of the experiments.

Furnace Oxygen Fugacity Calibration

Fugacity is a thermodynamic function that is equivalent to activity in non-ideal gases, but can be used in place of partial pressure in reactions that involve real gases and mixtures. At low pressures (~1 atmosphere), such as those experienced within the furnace (TURRIN,

1984), fugacity is essentially equivalent to partial pressure. Inside the muffle tube of the furnace, carbon monoxide and carbon dioxide are used to control the reaction: $2CO_2 \rightarrow 2CO + O_2$. Thus, the oxygen fugacity is proportional to the fugacity of CO and inversely proportional to the fugacity of CO_2, assuming the temperature remains constant, since the sum of the partial pressures of the three gas species must equal one atmosphere (assuming ideal conditions). The oxygen fugacity is also controlled as a function of temperature, assuming the ratio of $CO:CO_2$ remains constant. An increase in temperature will result in a larger proportion of CO_2 dissociating and causing a proportional increase in the oxygen fugacity. A consequence of this reaction is that the $CO-CO_2$ system is buffered with respect to oxygen, and will dissociate readily to maintain the total pressure should oxygen be removed from the system. Maintaining a continuous replenishment of gas so that neither gas is ever completely consumed or dissociated allows control of the buffering process and the oxygen fugacity (TURRIN, 1984). Since gas flow rates are proportional to the partial pressure of a gas species, oxygen fugacity control can be attained by regulating the gas flow rates, which was accomplished for these experiments, using precision flowmeters.

The amount of each gas used to control the oxygen fugacity varied depending on the run temperature of the experiment and the specific desired oxygen fugacity value. Since one of the aims of the experiments was to study the effects of iron loss on the silicate portions of the chondritic compositions, all of the experiments were run below the iron-wüstite (Fe-FeO) buffer, where FeO dissociates to form iron metal. The ratio of the volumes of $CO:CO_2$ ranged generally between 8:1 and 50:1 for temperatures between 1180°C and 1400°C and oxygen fugacities of -0.5 to -1.5 log units below the iron-wüstite buffer.

The calibration of the oxygen fugacity was achieved by two different methods to insure its reliability and accuracy, and will be discussed in detail below. The first method involved the calculation of the electromotive force of a fugacity cell at the IW buffer and subsequently determining the flowmeter settings, by trial and error, that would result in that electromotive force. The second method involved using the flowmeters to determine the IW buffer. This

method took advantage of the reduction-oxidation reactions of iron at this buffer, by using iron foil as an indicator of the position of the buffer. Assuming both the first and second methods were correctly done, the flowmeter settings from each method should match.

Method I: Calculation and Measurement of the Fe-FeO Buffer

The first method used for determining the iron-wüstite (IW) buffer was to first calculate the electromotive force (e.m.f.) at the IW buffer using the equations from JUREWICZ (1986) and CHOU (1987):

General equation: 1) $e.m.f. = (-\Delta V/2.303 R) \times T \times \log (fO_2)$

IW buffer equation 2) $e.m.f. = (0.0496) \times T \times \log (fO_2)$

where the e.m.f is measured in volts, $(-\Delta V/2.303 R)$ is the molar volume and R is the gas constant that has a value of 8.314 J/K mol, T is the temperature in Kelvin, and (fO_2) is the oxygen fugacity in atmospheres. Next, the correct settings for the flowmeters were found, using an oxygen fugacity sensor and an electrometer, so that the calculated e.m.f. of the IW buffer appeared on the readout display of the electrometer.

NOTE: If the log (fO_2) was needed the more familiar equations:

General equation: 3) $\log (fO_2)P,T = A/T + B + C(P-1)/T$

IW buffer equation: 4) $\log (fO_2) = (-27215 / (273.15 + T)) + 6.57$

from CHOU (1987) could be used, where A, B, and C are constants relating to the specific buffer, in this case the IW buffer, where T is temperature measured in degrees Kelvin, (fO_2) is oxygen fugacity measured in atmospheres, and P is pressure measured in bars.

Oxygen Fugacity Sensor

The oxygen fugacity sensor used (KINZIE, 1973; SATO, 1971; HUEBNER, 1987; NAFZIGER *et al*, 1971) was a yttrium-zirconia cell that contains an internal four bore alumina tube. The alumina tube accommodates a Pt and 90%Pt-10%Rh thermocouple identical to the thermocouple on the sample rod. On the inside and outside of the closed end of the yttrium-zirconia cell is a piece of tightly attached Pt foil. Two pieces of platinum wire are attached to the Pt foil, one wire for the exterior, one for the interior (Figure 6).

The oxygen fugacity sensor works by having molecular oxygen, which is delivered to the interior of the sensor through one of the bore holes in the alumina tube, ionized inside the sensor. The oxygen becomes ionized when electrons are made available to the oxygen by the platinum electrode, which is in contact with the yttrium-zirconia cell wall. The oxygen ions then pass through the cell wall using the available vacancies in the crystalline structure of the wall. Once the ionized oxygen exits the cell wall, its electrons are stripped from it by the outer platinum electrode, which transports the electrons to the electrometer, which registers them as a current or e.m.f. Meanwhile, the de-ionized oxygen reacts with carbon monoxide to form carbon dioxide. This tendency for oxygen to travel out the cell wall will continue as long as there is a greater oxygen fugacity on the interior of the cell than on the exterior.

Results of Method I

The initial attempts to acquire flowmeter readings, based on the calculated e.m.f. values proved inconsistent, since the furnace did not equilibrate over a reasonable amount of time (1-2 hours). The e.m.f. readings varied widely with the same flowmeter settings and the flowmeter settings did not agree (even closely) with the values sent by the manufacturer. Also, the flowmeters measuring the CO and the exhaust gas output were erratic and did not work properly because the flowmeter floats had a tendency to stick. Since the furnace was previously being run with a mixture of hydrogen and carbon monoxide, the sticking was

probably due to water buildup inside the flowmeters as well as the fact that the flowmeters were not standing vertically, but were inclined.

Under normal conditions the flowmeters should have a high degree of precision. They should allow consistent oxygen fugacity results to within ± 0.05 log units or ± 5 millivolts on the e.m.f. electrometer. The accuracy of the flowmeters should also have been quite good. Estimates of the accuracy up to that point however were about 60% different from the specifications sent with the flowmeters.

To correct the problems with the exhaust flowmeter, it was simply bypassed. Due to its removal, there was no regulation of the exhaust gases. Its removal resulted in the $CO_2/(CO+CO_2)$ ratio coming to within 5-15% of the calculated values for the e.m.f. of the IW buffer. The e.m.f. readings also stabilized. The CO flowmeter was placed under vacuum in an attempt to rid it of H_2O and stop the float from sticking. Both the CO and CO_2 flowmeters were squared and leveled. To further correct the problems, the gas mixing connections, which were suspected of causing back pressure on the outlet side of the flowmeters, due to an inadequate initial setup, were redesigned and rebuilt to insure that pressure from the high volume gas (CO) line would not hinder the flow of the low volume (CO_2) gas line (Figure 7A). The restructured gas mixer is shown in Figure 7B.

After rebuilding the gas equipment, another problem was soon discovered. The available oxygen fugacity sensor was nine centimeters too short to reach the hotspot in the furnace by inserting it through the upper cooling head (the same way the sample rod is inserted). Unfortunately, it also could not be inserted through the basal cooling head due to its design. To further complicate the calibration procedure, the supplies were not available to make a new sensor at the time. Therefore, the initial calibration in Table 6 was taken by inserting the sensor through the upper cooling head, nine centimeters from the hotspot and in a temperature gradient.

Table 6 shows the flowmeter settings that are needed to acquire the e.m.f. values that were calculated using equations 2 and 4 discussed above in the beginning of this section. The

reader should note that there is a temperature difference between Table 6 and Table 4. This difference results because of the use of the thermocouple inside the oxygen fugacity sensor, instead of the sample rod thermocouple. Since the sensor is nine centimeters shorter than the sample rod, the temperature could not be taken in the hotspot. Also, as a result of the oxygen fugacity cell thermocouple being inside the oxygen fugacity sensor, it is surrounded and thermally shielded by the yttrium-zirconia walls and platinum foil.

Comparisons between calculated plots and observed plots of the $f(O_2)$ versus $CO_2/(CO+CO_2)$ and temperature versus $CO_2/(CO+CO_2)$, shown in Figures 8A, 8B, 9A and 9B, indicated that the atmosphere within the furnace was about 0.4 - 0.6 log units more oxidized than it should have been at the given $CO_2/(CO+CO_2)$ ratios (the positions of the observed fugacities are shifted to lower $CO_2/(CO+CO_2)$ ratios than calculated). Since there was a fairly consistent shift of $CO_2/(CO+CO_2)$ across the entire range of $f(O_2)$ and temperature, the shift suggested that a leak existed within the furnace. A test was therefore performed to determine if this was true.

The ratio of $CO_2/(CO+CO_2)$ and the temperature were held constant, while the total pressure (flow rates) of the gases was varied. If there was a leak, the e.m.f. would become more reduced (lower values) with increasing pressure, while the lower pressures would be more oxidized. If there was not a leak, there should be no change in the e.m.f. since the ratio and hence the partial pressure of each gas would remain constant and only the total pressure would change. The two tests that were run and are shown in Table 7, indicated that a leak did exist.

Shortly after determining the leak, it was discovered that the existing oxygen fugacity sensor could be altered and reassembled to allow it to fit into the basal cooling head and reach the hotspot. Due to this fortunate occurrence, it was possible to calibrate the leak. As long as the sensor could calibrate in the hotspot, the leak would be accounted for by the sensor. The decision was made to seal the leak only if the problems persisted, which they did not.

The new oxygen fugacity sensor was inserted into the bottom of the furnace, while the sample rod was also inserted from the top. This allowed a temperature reading from both thermocouples. The oxygen fugacity sensor thermocouple was found to read consistently 6°C lower than the sample rod thermocouple. This difference was caused by the shielding from the yttrium-zirconia cell and platinum foil which surrounds the thermocouple inside the oxygen fugacity sensor. The oxygen fugacity sensor thermocouple was not directly used for temperature calibration purposes, but was used to compare to the sample rod thermocouple readings when needed. Table 8 shows the results of the final oxygen fugacity calibration. Please note that the calculated e.m.f. readings in Table 8 need to have a fudge factor added to them after the iron foil calibration is run, to correct for the difference between the calculated e.m.f. values listed in Table 8 and the observed e.m.f. values determined by Method II with the iron foil.

Method II: Testing for the Iron-Wüstite Buffer Using Iron Foil

The second method for calibrating the oxygen fugacity was to determine the flowmeter settings where Fe^0 foil is first oxidized ($2Fe^0 + O_2 \rightarrow 2FeO$) at a given temperature (i.e. find the IW buffer). The procedure was to first set the temperature to the required value and set the flowmeters to an obvious reducing atmosphere within the furnace (high CO, low CO_2) and allow the furnace to equilibrate (about 15-20 minutes). Next, a piece of iron foil was placed onto the sample rod; a note of the CO_2 setting was made; the CO_2 flowmeter was turned down to limit the amount of oxygen mixing with the furnace atmosphere when opening the top of the muffle tube; and the sample rod was placed into the furnace. The CO_2 flowmeter was then reset to its original value. After 15 minutes, the sample rod was removed from the furnace and the iron foil was water quenched. If the foil was oxidized the entire surface of the foil would be cracked and brittle, while if it was still reduced, the surface would remain smooth and glossy. If the foil was still reduced, resetting the flowmeters for more oxidizing conditions and repeating the procedure would be necessary. If it was oxidized, a new piece of foil would

be needed and the flowmeters would need to be set to more extreme values than the initial ones.

The most efficient way to find the buffer, assuming the experimenter is not sure what the flowmeters should approximately read, is to use a binary search procedure. This is accomplished by taking one known oxidizing and one known reducing condition, and subsequently taking a measurement halfway between these two measurements, noting the result after each test. By using this procedure, the range needed to be covered can be quickly constricted, until the experimenter can determine the settings for the buffer. If, however, the flowmeters settings for the buffer are generally known, another method is to creep up on the buffer from the reducing side, and thereby not utilize as much iron foil. Table 9 shows the results of the calibration. These observed e.m.f. readings are the three values determined using the iron foil test. The observed e.m.f. readings differ by 4 millivolts from the calculated e.m.f. values listed in Table 8. Therefore, the list of calculated e.m.f. values shown in Table 8 need to have 4 millivolts added to their values in order to be consistent with this calibration (one millivolt is approximately equal to a change in $f(O_2)$ of 0.01 log units).

The final $CO_2/(CO+CO_2)$ ratios were 3-5% off from the calculated values, substantially better than 60% off when the calibration began. Figure 10 shows a graph derived from Tables 8 and 9 that indicates what $CO_2/(CO+CO_2)$ gas ratio is required at a given temperature to achieve the correct fugacity. The gas ratios on the graph are based on the flowmeter (ml/min) readings, not the arbitrary scale readings also printed on the flowmeters.

Experimental Methodology

The oxygen fugacity and sample rod thermocouple calibrations were performed regularly in between experimental runs to insure that the oxygen fugacity and temperature of the furnace did not deviate with time. The oxygen fugacities, which will be quoted in log units relative to the iron-wüstite buffer reaction, have a confidence interval within ± 0.1 log units for each experimental run. Most of the experiments were conducted at IW -0.5 log units or IW -

1.5 log units, in order to bracket the work of JUREWICZ *et al.* (1993), and to assess the influence of different imposed oxygen fugacities on the starting compositions. A few experiments were run at IW-1.0 so that our results could be correlated with those of JUREWICZ *et al* (1993).

Most of the experiments were run in pairs, however, a few of the Series I experiments were run with up to four charges simultaneously in the furnace, while a few of the Series II experiments were run individually. In each of the Series II and III experiments, the synthetic and natural mixtures respectively, the Murchison and cocktail mixture were run simultaneously so that the charges would be assured of experiencing identical experimental conditions, and permit one-on-one comparisons of the run products for each composition. The charges were either both synthetic compositions or both natural compositions when they were run together. Synthetic and natural compositions were not run simultaneously as these were believed to be sufficiently different that a simple comparison would not be easily made.

Aliquots of approximately 100 mg of powder were pressed into 6mm x 4mm pellets in all of the experiments. For the Series I experiments pure Pt wire was used to hold the experimental charges. Since the effect of Fe loss was to be studied, no attempt was made to impregnate the Pt wire with Fe to minimize Fe loss. The Pt wire was used as a proxy for a reducing atmosphere.

For the Series II experiments, Fe loss was minimized by use of pure Fe wire to hold the charges. However, for experiments above 1200°C, the Fe wire became too weak to support the charges for the duration of the run. The solution which was also employed for all of the experiments in the last series, was to impregnate Pt wire with Fe prior to its use with the experimental charges. Charges of powdered magnetite (100 mg) were heated on the Pt wire loops in the furnace at reducing conditions (1400°C and fO_2 at IW-1.5) for periods of about 48 hours. This resulted in diffusion of iron into the Pt wire. The Fe impregnated Pt wire was then etched in hydrochloric acid to remove the excess iron oxide from the surface. Pellets of the relevant experimental charges were then placed on these Pt-Fe wire loops and placed in

the furnace. The Pt-Fe wire loops were reused as often as possible and were placed in hydrofluoric acid after each run to remove any excess silicate material. Typically, the wire loops lasted for three to five experiments before they became so brittle that they disintegrated.

Microprobe analysis of the iron impregnated platinum wire showed that a decreasing gradient of iron existed through the cross section of wire. The edge of the wire that was in direct contact with the iron pellet contained approximately 40 wt% iron, while on the opposite side of the same piece of wire there was approximately 15 wt% iron. Since it was not practical to analyze each impregnated wire, there was always cause for skepticism during the experiments concerning whether the experimental charge was in equilibrium with the iron inside the wire. To identify the effects of either the loss or gain of iron between the experimental charge and the Pt-Fe wire, two methods were employed. For the synthetic experiments, reversal runs [Cooling/crystallization experiments instead of heating/melting experiments] were used. As long as both experiments yielded nearly the same results, there was a fair degree of confidence that little or no loss or gain of iron to the experiment occurred. For the natural experiments, however, reversal runs were not employed due to the limited amount of natural materials available. To insure these experiments remained in equilibrium with the iron impregnated wire, modal recombination of the bulk composition, using the abundances and microprobe analyses of the phases present within the experiment, was employed. Although a few experiments resulted in iron loss, as will be pointed out later, in general, the results of the experiments were extremely good.

Although platinum was used as the support wire for the charges, several other metals could have been used, with molybdenum being the most likely candidate. The reason platinum was chosen in favor of the others is mainly because 1) platinum does not oxidize and enter the silicate compositions at the range of conditions the experiments were being conducted at; 2) it is very malleable and therefore can be bent to properly support the charges; and 3) it has an extremely high melting point, an absolute necessity to support the

charge at higher temperatures. Molybdenum has certain advantages over platinum because it has a much lower affinity for iron and has an even higher melting point. Unfortunately, molybdenum oxidizes at high temperature, (even in iron reducing atmospheres) where it tends to start entering the structure of some minerals. As an example, STOLPER (1977) used open molybdenum foil capsules to support many of his experimental charges and noted that molybdenum was found to be present as a minor element in many of his experimental glasses, while it was present as a major element in his experimentally produced spinels. Since molybdenum was not part of his starting composition, its presence tends to further complicate any interpretation concerning the phase relationships. It was this last consideration that made platinum the prime choice for the support wire.

Once the charges were placed on the wire loops, they were inserted into the furnace for a period of time thought to be sufficient to allow equilibration for those running conditions. When this time period was up, the charges were quenched. The time necessary to reach equilibrium was initially estimated by looking at the work of other experimenters, such as JUREWICZ *et al* (1993) and STOLPER (1977). The duration for the experiments was then modified depending on the planned running conditions. If running conditions were either at a lower temperature or lower oxygen fugacity than previously published experiments, the duration was lengthened. The duration was lengthened because both lower $f(O_2)$ and lower temperature result in smaller amounts of melt being produced within the experimental system, and the amount of melt generally controls the time to equilibrate. The duration was shortened if higher $f(O_2)$ or a higher temperature were run. Since reversal experiments were run for about the same duration as the original, the experiments could be evaluated to determine if sufficient time was allowed for equilibration.

Because of mechanical limitations on the furnace used, the experimental charges had to be quenched by removing the sample rod from the furnace and placing the charges quickly into water, with the entire quench process taking three to five seconds. Drop quenching through the bottom of the furnace was not possible for these experiments. However, the

results suggest that problems associated with quenching were minor and do not influence the results significantly.

Analysis Procedure

<u>Preparation of Experimental Charges for Analysis</u>

Before the experimental charges from the furnace could be analyzed, they needed to be prepared. First, the charges were removed from the support Fe or Pt-Fe wire by either simply picking them up with clean tweezers or by breaking them off using a pair of pliers. The samples were then placed into short quarter-inch diameter brass tubes and impregnated with epoxy. Once the epoxy hardened, the samples were cut in half and were polished using ten micron, six micron, and one micron diamond laps on polishing wheels. Both halves of each sample were often polished to allow a greater analysis area.

After polishing the samples, they were coated with a layer of carbon, approximately 20 nanometers thick, using a high vacuum thermal evaporation unit. The carbon layer is placed over the sample to avoid an electrostatic build-up on the sample when the electron beam of the microprobe strikes the sample. The electrostatic build-up acts like an umbrella over the sample and deflects the electrons away from the sample, causing analytical errors. Since the carbon layer conducts, it causes any electrostatic charge to dissipate and be grounded. An estimate of the carbon layer thickness is made by inserting a piece of polished brass in with the samples. As the carbon is deposited onto the surface of the brass, the surface changes color. Small amounts of carbon produce a dull orange interference color, however a carbon layer about 20 nanometers thick on brass gives a brilliant purple interference color, which is easily recognizable and reproducible.

<u>Electron Microprobe Analysis</u>

The experimental charges were analyzed on the JEOL JXA-8600 Superprobe in the Department of Geological Sciences at Rutgers University. The charges were characterized

first using backscattered electron imaging and energy dispersive spectrometer (EDS) analysis. The EDS and backscattered imaging provided extremely fast, semi-quantitative and qualitative information concerning the chemistry, texture, mineralogy, and surface features of the experimental charges. However, the analyses were fully quantified for their chemical composition using wavelength dispersive spectrometer (WDS) analysis. An accelerating voltage of 15 keV and a beam current of 10nA, measured in a Faraday cup, were used to allow areas within the charges approximately one to two microns in diameter to be analyzed for their major (5 wt% or greater) and minor (0.1 to 5 wt%) element chemistry. High degrees of accuracy and precision were desired from the microprobe analyses. To ensure high accuracy, previously well-characterized, homogenous, natural and synthetic mineral standards were used (Table 10 and 11 and Appendix I) (JAROSEWICH et al, 1980; TAKEI, 1976, 1978; TAKEI and KOBAYASHI, 1974). Since the silicate phases within the experimental charges were the primary concern of the research, the selection of the standards was controlled by their mineral composition, while the metal and spinel phases, although of interest during the research, were of secondary concerns. Standards with similar elemental abundances and mineral characteristics as the phases within the experimental charges were chosen for the 10 elements contained within the starting compositions (Table 2). Thus, the standards used were olivines, pyroxenes, or feldspars, with chromite being the only non-silicate. To ensure reproducibility, a suite of additional standards were routinely analyzed to test the microprobe calibration. Only after the analyses of all standards were checked against their nominal compositions, and any consistent errors corrected, were any samples analyzed.

Because of the constraints of being able to analyze small volumes and still achieve high precision, the time taken for each analysis needed to be fairly long. The long analysis time needed derives from the fact that the detection limit of the microprobe varies inversely with the square root of time. Thus, for elements that are present within a given phase at trace levels (0.1 wt% or less), the time required to analyze them increases quadratically as the

detection limit is lowered. (e.g. increasing the analyzing time by a factor of 10, improves the precision by only about 3x). For the major elements, analyzing times were set for 40 seconds (of detector live time, which is slightly longer than real time), while the minor elements were analyzed for 100 seconds (GOLDSTEIN *et al*, 1992). In general, these analysis times resulted in a standard deviation of 3-7% for the minor elements, while the major elements had a standard deviation of 1%.

The compositions for all of the analyses were corrected using the ZAF model, which is a generalized procedure for transforming the measured x-ray intensities into estimates of the mass fraction (e.g. weight percent) of the elements present. The ZAF procedure assumes that there is a linear relationship between the observed intensity of the x-rays and the concentration of the element present. However, the effects of atomic number (Z), absorption (A), and fluorescence (F) cause the data to deviate from this linear relationship, so multiplication factors are used to correct the data, before the final mass fraction of each element present is calculated (HEINRICH, 1991). The problem with calculating the final mass fraction of each element however, is that Z, A, and F are all functions of the composition of the unknown. Since they are related by the equation: $k = C_n(ZAF)$, where $k = I/I_0$ is the intensity ratio for the unknown and standard, and C_n is the composition of the unknown, the equation cannot be solved analytically. An iterative procedure is used instead. In order to solve the equation, an estimate of the unknown composition must be made. Based on this estimated composition, the ZAF factors can be calculated. Once calculated, the ZAF factors are substituted into the above equation and the equation is solved for the composition, C_{n+1}. This new composition, C_{n+1}, is then compared to the original, C_n. If $C_{n+1} - C_n$ is less than some predetermined value [usually less than 0.00001, when C is expressed as a mass fraction (0.01%)], the composition is considered to have converged on the true composition. If the difference is greater than the predetermined value, than the new composition's ZAF factors are substituted into the equation above and another composition is calculated. This

process of iterating is continued until the difference between two consecutively calculated compositions is within the predetermined value limit.

Table 10 lists the analysis details used in calibrating the microprobe. The first column lists the elements that were analyzed, while second column shows the spectrometer diffraction crystal used for each element. Different crystals can be used for many elements depending on which x-ray line is being measured. In the third and fourth columns of Table 10, the background positions are given. These are positions on either side of a given x-ray peak, where x-rays are detected and used to calculate the background intensity. The relationship between the spectrometer position (measured in mm) and x-ray wavelength (measured in nm) is:

$$L = 2R\lambda\ /\ 2d$$

where: L = spectrometer position (measured in millimeters)

2d = d - spacing of the diffracting crystal (measured in nanometers)

R = radius of the spectrometer Rowland circle (measured in millimeters)

The wavelengths can subsequently be converted into x-ray energies (measured in eV) by use of the equation: $E = hc\ /\ \lambda$

where: E = energy of the x-ray

h = Planck's constant (= 4.1357×10^{-15} eV sec)

c = velocity of light in a vacuum (= 3×10^{8} m/sec)

The background intensity is then compared to the peak intensity to calculate the abundance of the element. The fifth column is the ZAF correction factor used in calculating the mass fraction of the element present. A correction factor must be calculated for each element in the standard that is used in the calibration (e.g. Si and Na both use Plagioclase from Lake County, and have different correction factors). The correction factor is calculated on the basis the bulk composition of the standard. The sixth, seventh, and eighth columns show the

baseline, window, and bias, which are three factors that deal with the detector electronics within the microprobe. The detector electronics, which in this case was a pulse height analyzer (PHA), integrates the total charge produced by an x-ray photon and converts the charge into a single voltage pulse that can be further processed for counting or display purposes. Since the PHA can only select and transmit pulses in a predetermined voltage range, a bias voltage is needed to adjust the incoming charge so the PHA can process it. The bias voltage required to adjust the incoming charge is inversely related to the atomic number of the element producing the photons. The baseline and window control the position and the range over which the pulse height intensity can be read (measured in volts) (GOLDSTEIN *et al*, 1992). Finally, the last column lists the description of the standard used.

Appendix II contains the list of analyses from all three series of experiments. The appendix lists all of the analyses in oxide weight percent and shows the same data converted into mineral formulas.

Approach to Equilibrium

Confidence that the charges were at, or close to, equilibrium was achieved in three ways. First, microprobe analysis allowed the author to insure that all of the minerals and glasses present within each charge were homogeneous. The second test was made by calculating partition coefficients for Fe, Mg, and Mn in the coexisting olivines and glasses, and comparing them to published results (JONES, 1984; TAKAHASHI, 1978; LONGHI *et al*, 1975*)*. These two tests, while not providing absolute evidence that equilibrium was approached, allowed disequilibria data to be rejected. The final and most reliable method to test for experimental equilibrium was to bracket the equilibrium conditions by running reversal experiments when possible. The normal experimental routine involved placing the charge(s) in the furnace at the target experimental temperature and at the target $f(O_2)$ after allowing the temperature and gas mixture to stabilize. The experiment was then continued for a duration deemed appropriate for the attainment of equilibrium. These experiments could be

considered to be heating experiments. Reversal experiments were performed in three steps. First, the charge(s) was placed in the furnace for two hours at a higher temperature (about 200°C higher) than the target temperature and in oxidizing conditions. After the two hours, the temperature of the furnace was reduced to the target temperature. Once the target temperature was achieved, the oxidizing gas mixture was adjusted to the required (reducing) oxygen fugacity and the charge was allowed to reequilibrate for a duration equal to the normal routine experiment. Thus the reversals were cooling experiments rather than heating experiments. The early stages of the reversals were performed in oxidizing conditions, instead of reducing ones, to minimize the amount iron metal that was lost to the platinum wire while at the higher temperature.

Although complete reversals (both fugacity and temperature) would have been preferred to only temperature reversals, there was no reliable means of assuring limited or no Fe loss to the Pt-Fe support wires. A complete reversal would involve going from high temperature, low $f(O_2)$, to the normal experimental conditions at a lower temperature, higher $f(O_2)$. This reversal will nearly always suffer from Fe loss, because a much greater proportion of Fe diffuses into Pt at higher temperatures and/or lower oxygen fugacities than Fe and FeO diffusing out of the Pt into the charge at a lower temperature and/or higher oxygen fugacities. Although ideally there should be an equilibrium eventually established with no net Fe loss to the charge, in practice some of the Fe will permanently be lost to the Pt during the higher temperature, lower oxygen fugacity portion of the reversal.

Results of Experiments

Series I Experiments

The first series of experiments used four analogues of Murchison, which were supposed to differ only, by their starting bulk molar Fe/Mn ratios (85, 65, 45, and 20). However, the starting compositions seen in Table 2B, show that relative to nominal Murchison, the compositions are MgO depleted. The MgO depletion results from adsorbed water in the MgO

powder. Even though the powder was dried at 250°C for two hours, as mentioned earlier, the attempt was obviously ineffective. The Fe/Mn ratios (140, 100, 60, 20) originally wanted were also not achieved and appear to result from either varied abundances of adsorbed water in the MnO and Fe_2O_3 oxide powders, or perhaps the incorrect weighing of the oxide powders. Although these four compositions bear little resemblance to nominal Murchison, they served their intended purposes.

A list of the experimental parameters and resulting phase compositions is shown in Table 12A, while Appendix IIA contains the microprobe analyses of all the Series I experiments.

This series of experiments, as mentioned earlier, were designed to explore the effects of iron loss on the Fe-Mn-Mg systematics of a partially melted chondritic meteorite, and to determine if synthetic compositions was a feasible alternative to using natural compositions. Since each of the experiments were analyzed by microprobe and the experimental conditions they were run at recorded, the experiments could be used to test whether any consistent problems existed with either the temperature or oxygen fugacity calibration.

The experiments were run at a number of temperatures, but oxygen fugacity was not tightly controlled. Instead, the oxygen fugacity was set for IW-0.5 at 1600°C and left untouched (constant $CO_2/CO+CO_2$ ratio). The effect on the experiments is that as temperature decreases, the oxygen fugacity decreases, and increases the amount of Fe-metal produced in the charge. However, since platinum was used to support the experiments and it is a siderophile element, bulk iron loss will occur in the charge, as some portion of the Fe-metal in the charge diffuses into the Pt wire, thus becoming fractionated and isolated from the charge. Essentially, two reactions are trying to reach an equilibrium state simultaneously. First, the Fe in the charge is trying to reach equilibrium with the Fe-metal in the Pt wire. This Fe-metal becomes fractionated from the charge. Secondly, the FeO in the charge is trying to reach equilibrium with the Fe-metal in the charge. This second equilibrium is caused by the presence of a reducing atmosphere (e.g. IW-0.5 or lower). This Fe-metal should ideally remain within the reacting system of the charge. If an inert support wire were used, the Fe-

metal should not diffuse into the support wire. As a result of these two reactions, a greater total amount of FeO is converted to Fe-metal, than normally would be converted. An additional result of these reactions is the silicates of the charge contain less FeO than would normally be expected given the same oxygen fugacity and supported by an inert wire. This diffusion effect simulates the production and fractionation of Fe-metal into the core during the formation of a planetoid.

An important point concerning the first series of experiments is that many of the charges did not reach equilibrium as planned. Many of the experimental glasses show a fairly wide range of compositions, while the coexisting olivines and pyroxenes show more uniform compositions (Appendix IIA). Many of the lower temperature experiments also contained many relic silica grains, causing certain areas of the charges to contain silica enriched or silica depleted glass pockets. The disequilibrium between the silica enriched or depleted pockets of glass and the remaining charge was caused by insufficient grinding of the starting materials (but mainly the silica), and insufficient time in allowing the charges to equilibrate in the furnace. The disequilibrium condition was recognized when investigating these charges, so the starting materials were more finely ground and the times were substantially extended (nearly four times longer in some cases) for the subsequent Series II and III experiments.

These experiments demonstrated that the bulk Fe/Mn ratio of a CM chondritic composition can be altered (DELANEY and BOESENBERG, 1993) to varying degrees, while leaving the remaining elements in the composition largely unaffected (Appendix IIA). Figure 11 demonstrates that the bulk Fe/Mn ratios from the Murchison Fe/Mn 85 analogues could produce compositions that contained Fe/Mn ratios of 5 to 50 in the glasses, depending on the conditions set. High temperature (1580°C) experiments (Exp. M19), where 90% of the iron in the charge diffused into the Pt wire, could produce similar compositions to very low oxygen fugacity conditions. At lower temperature (1250-1300°C) experiments (Exp. M3 and M4), oxygen fugacities are simulated closer to the range of conditions in which eucrites appear to crystallize.

Along with the reduction of the Fe/Mn ratio, an increase in the normative pyroxene content of the bulk chondritic composition occurs. This is important because eucrites lie essentially on the peritectic point in the olivine-plagioclase-silica pseudoternary (LONGHI and PAN, 1988a, b). A bulk CM chondritic composition, like Murchison, is initially too Fe-rich and olivine normative to produce a glass by partial melting that resembles a eucritic composition. However, with removal of Fe, the bulk CM composition moves directly towards the silica component of the pseudoternary, and towards the pyroxene field (Figure 12). As a result, the bulk composition moves into a position on the phase diagram that produces eucritic glasses when partially melted. The part of the phase diagram, where the most favorable eucritic precursor compositions, such as DREIBUS and WÄNKE (1980) and DELANEY (1993), is the area between where bulk Murchison and the "Fe-free" Murchison compositions plot.

The experiments also showed that a synthetic composition could be used as proxy to a natural composition, but extremely careful procedures must be followed if the starting composition is made from oxide powders. The experiments further indicated that the temperature calibration appeared to be correct, since the petrology of the resulting phases of each experiment was consistent with the settings for the temperature and the amount of Fe loss to the Pt wire.

Series II Experiments: Synthetic Compositions

The synthetic compositions of the Series II experiments did not duplicate the bulk compositions of the chondritic starting materials as planned either (Table 2C). The synthetic Murchison composition was calculated on the basis of the bulk meteorite and assumed *all* of the iron present within Murchison (FeO + Fe-metal + FeS) was present as FeO. The synthetic H-CM mixture was based on only the silicate portion of the precursor, thus the Fe-metal, FeS, and Ni-metal contents are not included in the composition. However, a problem was discovered with both synthetic compositions. Microprobe measurements of glasses quenched from high temperature revealed that the actual compositions of the synthetic compositions

deviated from those calculated. As with the previous series, the oxide powders retained an abundant amount of adsorbed water, despite the attempts to dehydrate them. The modification is minor for the synthetic Murchison, however the synthetic H-CM composition was affected much more extensively and turned out to be substantially depleted in MgO. However, both compositions were used. Both, the planned nominal compositions and the actual experimental compositions used are shown in Table 2C. Table 13 summarizes the Series II experimental results by showing the average experimental silicate compositions. The complete microprobe analyses of all the Series II experiments are shown in Appendix IIB.

Murchison Analogue Results

Fe-Mn-Mg Systematics of the Synthetic Murchison Analogue

Figure 13A demonstrates the effect of Fe removal during the experiments on the starting synthetic Murchison composition. Plotted in the diagram is the bulk starting composition, the coexisting glasses, and the coexisting olivines after reaction at a variety of temperatures and oxygen fugacities. The curved dashed line, going from the starting composition to the origin, is the path the bulk composition would take as iron is removed, while the curved dashed line passing through the glasses is a representative path for the calculated equilibrium glasses produced in the experiments as iron is removed from the bulk composition. The experiments show the influence on a fairly high Fe/Mn ratio in the starting composition. To reach typical eucritic levels for Fe/Mn within these glasses, approximately 50% iron fractionation is required at an oxygen fugacity between IW-0.5 and IW-1.0. It should be noted that the Fe loss path for the glasses does not pass through the eucrite compositional area on the diagram. In order for a glass to be produced with eucritic ratios for both Fe/Mn and Fe/(Fe+Mg), a starting composition with an initially higher Fe/(Fe+Mg) ratio is required. One way of increasing the Fe/(Fe+Mg) ratio, while maintaining the other elemental ratios within the glasses, is to fractionate out olivine. This is possible because many elements, such as Ti,

Al, Ca, and Na are incompatible to the olivine crystal structure, so their elemental abundances remain undisturbed in the coexisting phases.

Phase Equilibria of the Synthetic Murchison Analogue

Figure 14 shows a close-up portion of the olivine-plagioclase-silica pseudoternary calculated from the work of LONGHI and PAN (1988b) and projected from wollastonite. In the figure, bulk eucrites can be seen clustering near the peritectic point. This point is where the first melt will be produced from those bulk compositions projected into the Opx-Ol-Plag pseudoternary (the minimum melting point within the Opx-Ol-Plag pseudoternary), which includes all of the synthetic and natural compositions used during this research. The phase boundaries (shown as bands) are plotted to match the Fe/(Fe+Mg)x100 ratio of the glasses, which is about 60. Two of the more "eucritic" synthetic Murchison glasses are shown along the olivine-pyroxene peritectic and demonstrate that there is an increase in temperature away from the peritectic point along the olivine-pyroxene boundary. Because temperature effects the formation at which a given phase can crystallize, with decreased temperature, the synthetic Murchison composition (and other compositions similar to Murchison), causes a more pyroxene and plagioclase normative (more eucritic), and less olivine glass to form (Table 14).

Many of the data points shown in Figure 14 are shifted away from the peritectic point and plot inside the pyroxene field. This shift is caused by varying abundances of sodium within each experiment, because the phase boundaries shift as a function of the Na/(Na+Ca) ratio within the glass. The shift is similar to that caused by varying the Fe/(Fe+Mg) ratio. The phase boundaries shown [and based on the work of LONGHI AND PAN (1988b)], assume that the anorthite content of the glasses is An_{90}, when in fact, many of the glasses have An contents of about An_{95-99}.

Figures 15 A and B show the olivine-pyroxene phase boundary plotted twice, once for an Fe/(Fe+Mg)x100 ratio of 30 (Figure 15A) and once for an Fe/(Fe+Mg)x100 ratio of 55 (Figure

15B). The figures illustrate that as a composition, becomes more magnesian, the olivine field expands and the olivine-pyroxene phase boundary moves away from olivine. This compositional transformation is well demonstrated by the synthetic Murchison 1300°C, IW-0.5 glass in Figure 15B, and the more magnesian 1300°C IW-1.5 glasses plotted in Figure 15A. The near overlapping of the 1300°C IW-0.5 and 1400° IW-0.5 glasses (Figure 15 B) on the olivine-pyroxene boundary suggests that this point is very likely the point where the synthetic Murchison bulk composition first encounters this phase boundary while crystallizing olivine.

The Effects of Temperature and Oxygen Fugacity on the Synthetic Murchison Experiments

The compositions of the silicate phases in the synthetic Murchison experiments indicate a variety of effects that occur with a decreasing temperature. First, the glass compositions become more plagioclase and pyroxene normative (or more eucritic) (Table 14), while coexisting pyroxenes become more calcic and coexisting olivines become more iron rich (Table 13A). Secondly, there is a increasing fraction of sodium retained in the melts (Table 13A). Despite sodium being a highly volatile element, the amount of sodium retained within the glasses is three to four times larger than in the experimental glasses of JUREWICZ *et al.* (1993). The sodium retention appears to be directly correlated to increases in the normative plagioclase content of the glasses (Table 14). The exception to this sodium trend is the 1180°C IW-1.5 glass, which appears to have suffered from incomplete equilibration and localized relict silica enrichment. There is also an increase in the Fe/(Fe+Mg) and Fe/Mn ratios of all silicate phases present (Table 13A).

The effects of lowering the oxygen fugacity are also indicated in the resulting phase compositions. The first is an obvious decrease in the Fe/(Fe+Mg) and Fe/Mn in the silicates (Table 13A). The decrease in the iron causes a mass balance effect increasing the relative amount of calcium and aluminum present within the glasses and pyroxenes. Higher Cr_2O_3 contents (Table 13A) result in the glasses as fugacity is lowered due to the increased stability of Cr^{2+} over Cr^{3+}. Reduction of the bulk charge occurs faster than melting at low to medium

temperatures (1180-1400°C)(based on the iron foil calibrations of the oxygen fugacity). Since reduction causes an increase in the normative silica content (and plagioclase content) of the charge (Figure 12) a corresponding increase in the viscosity of the melt will occur. This increased viscosity will slow the diffusion rate and will extend the time required to attain equilibrium in the experimental charge.

Comparison of Glasses Produced from the Synthetic Murchison Analogue with Eucrites

The synthetic Murchison glasses in general compare favorably with average eucrites (Figure 16A), but contain non-eucritic abundances of certain oxides. The TiO_2 contents are consistently higher than eucrites, while MnO is consistently lower. The latter of these trends can also be recognized in data of JUREWICZ *et al* (1993) and KUSHIRO and MYSEN (1979).

H-CM Chondritic Mixture Analogue Results

Synthetic H-CM and Natural 70% Allegan-30% Murchison Relationship

The synthetic H-CM composition was initially planned to be a simplified version of the natural 70% Allegan - 30% Murchison mixture, containing only the silicate portion of the natural 70% Allegan - 30% Murchison composition (the metallic iron and sulfide portions being intentionally left out). However, due to the problems caused by the adsorbed water as discussed earlier, the synthetic H-CM composition was modified. This modification increased the Fe/(Fe+Mg) ratio of the planned starting synthetic composition to a ratio of 30.5, which should have been 26, the same ratio as the natural 70% Allegan - 30% Murchison mixture. The difference caused by the modification, is equivalent to approximately 20% olivine being subtracted from the silicate portion of the natural composition. Therefore:

(Natural Allegan-Murchison) = (Synthetic H-CM) + (Metal) + (Sulfide) + (~20% Olivine).

Fe-Mn-Mg Systematics of the Synthetic H-CM Mixture

The synthetic H-CM mixture (Figure 13B) requires very little iron loss (at IW-0.5) from the bulk composition to produce typical eucritic Fe/Mn ratios of 30 to 40 within the glasses at temperatures of 1180-1200°C. This composition, unlike synthetic Murchison, does form eucritic Fe/(Fe+Mg) ratios (1180°C IW-0.5). The coexisting equilibrium silicates to this eucritic glass consist of Fo_{71} olivine and $En_{71}Wo_5$ pyroxene (Appendix II, Synthetic H-CM, 1180°C IW-0.5).

The 1400°C IW-0.5 glass (Figure 13B) also seems to represent the best candidate for a diogenitic precursor. This melt, if separated from the existing equilibrium solid phases and allowed to fractionate orthopyroxene and a small amount of olivine, should create a cumulate orthopyroxenite. Unfortunately, the glass plots substantially to the iron enriched side of the equilibrium glass iron loss curve and appears to indicate that the experiment was subject to some form of solid/melt fractionation.

Phase Equilibria of the Synthetic H-CM Mixture

The H-CM glasses plot at the lower end of the pyroxene-plagioclase boundary (Figure 14), which is different from the results of synthetic Murchison. The apparent shift is caused by the higher starting sodium content in the H-CM composition and the constraints of the projection scheme. Higher sodium causes an increase in silica in the resulting melts and makes them more plagioclase normative (Table 14) at low temperature (1180-1200°C). However, several eucrite data also fall in this area and overlap the 1180°C and 1200°C IW-0.5 glasses in the pseudoternary.

In Figure 15B, the effect of fractionation of quenched olivine on the H-CM glass compositions, which plot along the pyroxene-silica boundary (Fe/(Fe+Mg)=55) in the 1300°C IW-0.5 experiments, can be seen. If these experiments had quenched properly, the glasses should have plotted on the olivine-pyroxene peritectic, in essentially the same position as the synthetic Murchison 1300°C IW-0.5 glass. However, since olivine fractionation occurred, the

H-CM glass composition became so silica saturated that the composition moved directly across the pyroxene field to the pyroxene-silica boundary. This glass actually has a much larger range of compositions than shown, starting from its present position and trending directly away from the olivine. The other two experiments (Figure 15A) (1300°C IW-1.5 and 1400°C IW-0.5) however, plot on the olivine-pyroxene peritectic (Fe/(Fe+Mg)=30) and contain no fractionation effect.

The Effects of Temperature and Oxygen Fugacity on the Synthetic H-CM Mixture Experiments

One important difference between synthetic H-CM composition and synthetic Murchison is the formation of pigeonite at the conditions of 1300°C and IW-0.5 (Table 13B) in the H-CM composition instead of only olivine, reflecting the more pyroxene normative starting bulk composition of the synthetic H-CM mixture.

Comparison of Glasses Produced from the Synthetic H-CM Mixture with Eucrites

The glasses produced by experiments on the synthetic H-CM mixture provide the closest compositional match to the mean eucrites yet seen (Figure 16B). The best match to a eucrite was produced at 1180°C and IW-0.5. The major discrepancy was Na_2O, which is very overabundant by a factor of 1.5.

Compared to the synthetic Murchison results, the synthetic H-CM results are less variable, being no more than 20% off on any oxide, except Na_2O, at temperatures of 1180°C and 1200°C and at IW-0.5.

Series III Experiments: Natural Compositions

Natural Murchison Results

Fe-Mn-Mg Systematics of Natural Murchison

The effects of iron removal from natural Murchison on the Fe/Mn and Fe/(Fe+Mg) ratios of coexisting olivines and glass are seen in Figure 17A. Oxygen fugacities of IW-0.5 remove about 10-15% of the bulk iron within natural Murchison, but much lower oxygen fugacity conditions (IW-1.5) are needed to remove approximately 50% of the bulk iron from the starting composition and reduce Fe/Mn to eucritic values of ~50. Eucritic Fe/Mn ratios (30-45) can be produced in the glasses from natural Murchison staring material, but the Fe/(Fe+Mg) ratio is too low (45 instead of 65), so the iron loss curve for the natural Murchison glasses misses the eucritic compositional field and passes through more Mg-rich compositions (JUREWICZ *et al*, 1993).

Phase Equilibria of Natural Murchison

Compositions of the natural Murchison glass (1180°C IW-1.0) plot in LONGHI'S pseudoternary (Figure 14) close to the peritectic point. They are displaced to the plagioclase side of the peritectic point because of their high sodium contents (Table 13C).

The 1400°C IW-0.5 glasses fall on the olivine-pyroxene boundary (Fe/(Fe+Mg)x100=30) (Figure 15A) and appear to be consistent with the synthetic Murchison experiments seen in Figure 15B. Both sets plot at approximately the position where olivine fractionation path from the Murchison bulk composition first intersects the olivine-pyroxene peritectic line.

The Effects of Temperature and Oxygen Fugacity on the Natural Murchison Experiments

Modal analysis of the Series III experiments (Table 15) was used to determine the abundances of the phases present. With increasing temperature, there is an increase in the modal abundance of glass and Fe-metal present, that corresponds to a decrease in the

abundance of olivine (and possibly chromite). Lowering the oxygen fugacity however, causes increased pyroxene and metal abundances.

Comparison of the natural Murchison experiments to synthetic Murchison experiments shows that the natural compositions appear to retain more sodium than the synthetics (Table 13A and C). This is probably caused by the initial state of the sodium. In the natural compositions, the sodium is chemically bonded within the mineral sites of some silicates in Murchison. In order to volatilize the sodium these minerals must be broken down and the bonds broken first. However, in the synthetic compositions sodium is present as a relatively unstable oxide phase ($NaHCO_3 \cdot xH_2O$), that may decompose easily with increasing temperature. Because only weak bonds of Na to other elements need to be broken, it volatilizes immediately upon being heated.

Comparison of Natural Murchison to Literature Data

The natural Murchison 1180°C IW-1.0 experiment duplicates the conditions of JUREWICZ et al. (1993), and is almost identical to their result (Figures 18 and 19A). The cause of the difference between this natural Murchison experiment and the JUREWICZ et al. (1993) probably reflects a small difference in the oxygen fugacity calibration (~0.2-0.3 log units) between the two laboratories.

Comparison of Glasses Produced from Natural Murchison with Eucrites

The glasses from experiments on the natural Murchison composition do not match eucrites very well except for the 1180°C IW-1 run (Figure 19A). The glass from the 1180°C IW-0.5 run is depleted in silica (Table 13C) relative to the other Natural Murchison experiments, containing only ~42-44 wt% SiO_2, when the expected values are 47-49 wt%. A possible explanation for the anomalous results is that a heterogeneous sampling of the starting composition was taken, which may have been enriched in a CAI (calcium aluminum

inclusion) component. A high CAI component could account for the higher than expected abundances of TiO_2, CaO, and Al_2O_3, and the lower MgO content.

A substantial overabundance of sodium can be seen in the glasses of all three Natural Murchison experiments shown on the diagram.

Allegan-Murchison Mixture Results

Fe-Mn-Mg Systematics of the Allegan-Murchison Mixture

Three runs were carried out on the Allegan-Murchison mixture at a temperature of 1180°C, but were run at three different oxygen fugacities (IW-0.5, IW-1.0, & IW-1.5). A fourth experiment was carried out at a temperature of 1400°C and at an oxygen fugacity of IW-0.5 to investigate the possibility of producing a glass from which diogenites could subsequently be derived.

The equilibrium glass compositions in these charges are similar to those in the synthetic H-CM runs, but are more magnesian (Figure 17B and 13B), because the starting composition of the natural Allegan-Murchison mixture has a lower Fe/(Fe+Mg) ratio than that of the synthetic H-CM mixture. At 1180°C and oxygen fugacities of IW-0.5, the Allegan-Murchison glass and olivine show 37% reduction (Figure 17B). As a result, glass Fe/Mn ratios (55-70) substantially higher than those of eucrites are produced when eucritic Fe/(Fe+Mg) ratios are attained. At lower fugacity conditions (IW-1.5), the reverse problem occurs, with inappropriately low Fe/(Fe+Mg) ratios forming with eucritic Fe/Mn ratios.

Phase Equilibria of the Allegan-Murchison Mixture

The two Allegan-Murchison glasses (1180°C IW-0.5 & 1180°C IW-1.0) plot close to many of the synthetic H-CM glasses in the silica-olivine-plagioclase pseudoternary of Figure 14 demonstrating the relationship by fractionation (of metal, sulfide, and olivine) between the two starting compositions. Three analyses from 1180°C IW-0.5 glass seem to trend into the pyroxene field. This trend, however, appears to be an artifact of the projection caused by the

shift of the phase boundaries in the pseudoternary from the increasing Na/(Ca+Na) ratio contained within the glasses. Since the three glass analyses plotting in the pyroxene field have Na_2O contents that are 0.3 - 0.5 wt% lower than the glasses at the peritectic, a shift in the position of the peritectic point (and the phase boundaries) related to the Na/(Ca+Na) ratio is probably occurring. The composition of the 1180°C IW-1.0 glass is the best match to eucrite compositions that were made in the natural experiments. This glass plots slightly above the eucrites (probably because of the overabundance of sodium).

The 1400°C IW-0.5 glass (Figure 15) is displaced from the olivine-pyroxene peritectic line toward SiO_2. This probably indicates that quenched olivine fractionation occurred, causing the glass composition to migrate off the peritectic boundary directly away from olivine toward the silica-pyroxene cotectic line.

The Effects of Temperature and Oxygen Fugacity on the Allegan-Murchison Mixture Experiments

The compositional and modal trends for the natural Allegan-Murchison glasses are extremely similar to those in the natural Murchison experiments. The glasses from the Allegan-Murchison experiments contained the highest abundances of sodium (Table 13D) and therefore had a high albite component within the mineral normative calculations (Table 14). The Allegan-Murchison glasses tended to be more plagioclase and slightly less pyroxene normative than the natural Murchison glasses.

The modal analysis (Table 15) showed that with increasing temperature, an increase in the modal abundances of glass and Fe-metal occurs and corresponds to a decrease in the abundances of olivine (and possibly chromite). The effect of lowering the oxygen fugacity however, causes increased pyroxene and metal abundances.

Comparison of Glasses Produced by the Allegan-Murchison Mixture with Eucrites

The natural Allegan-Murchison mixture does not provide as good a match to the eucrites (Figure 19B) as the synthetic H-CM composition and has deviations from the mean eucrites. The composition however, does yield promising results for producing eucrites from chondritic sources.

Discussion

The eucrites have unique characteristics that distinguish them from other types of meteorites. Among these characteristics are the bulk composition, modal abundances of mineral phases, and the chemical composition of those phases. From these characteristics, the history of the eucrites can begin to be ascertained, from its original formation on its parent planetoid to its final arrival and deposition on Earth. Further information from the apparently related meteorites, the diogenites and howardites, can than be used to interpret a more detailed petrogenetic history of the basaltic achondrite planetoid (BAP).

Igneous rocks can be formed under a variety of circumstances. For basalts, such as the eucrites, there are essentially four dominant processes that can play a role in their formation: 1) equilibrium crystallization, 2) equilibrium melting, 3) fractional crystallization, and 4) fractional melting.

The major control of any igneous rock's formation, however, is the available source region from which the igneous composition derives. For the eucrites and diogenites, the obvious source region is material from the asteroid belt, which is where nearly all of the meteorites come from. Since the majority of meteorites are chondrites and many researchers (STOLPER, 1977; MORGAN *et al*, 1978; DREIBUS and WÄNKE, 1980; JUREWICZ *et al*, 1993) have determined BAP is likely to resemble a chondritic meteorite, chondrites of some type appear to be the preferred starting material. However, a mixture of different chondritic materials is required, if the oxygen isotopes are to be satisfied, such as a composition combining an H chondrite and a CM chondrite (DELANEY, 1993). The formation of an H-CM

planetoid appears plausible considering BUCHANAN *et al* (1993) found carbonaceous clasts in the Bholghati and EET87513 howardites, while ZOLENSKY *et al* (1992) found carbonaceous clasts in the LEW 85300 polymict eucrite, as well as in the G'Day, Kapoeta, Jodzie, Y793497 howardites and LEW 87295 polymict eucrite (ZOLENSKY *et al*, 1995). Even if these particular clasts (most of which were identified to be CM2 clasts) are not remnants of the impact that produced the planetoid but were instead deposited on BAP after its formation (which seems likely), they demonstrate that the necessary chondritic material is available to form the source region for the HED meteorites.

Equilibrium Partial Melting and Crystallization and the Basaltic Achondrite Planetoid

If we assume that equilibrium conditions existed on BAP at the time the eucrites and its associated meteorites formed, a trace of the paths of equilibrium crystallization and equilibrium melting on the olivine-plagioclase-silica pseudoternary should show what results from each process. Investigation reveals that the equilibrium melting and crystallization paths trace over one another, but in the reverse direction, and the final products formed using either melting or crystallization are identical. Therefore, equilibrium crystallization and equilibrium melting will be discussed together.

From the results of the Series II and III equilibrium partial melting experiments, a broadly eucritic melt can be produced from a chondritic source. However, the melt created will not produce appropriate Fe/Mn ratios with eucritic Fe/(Fe+Mg) ratios, and alkalis are overabundant. Ignoring the alkali problem for now (this will be discussed later in describing the formation of the basaltic achondrite planetoid), and concentrating on the synthetic H-CM and natural Allegan-Murchison experiments, since they showed more promising results than the Murchison composition, the main problem is modifying the Fe/(Fe+Mg) ratio of the bulk composition, while keeping its Fe/Mn ratio constant (or vice verse), thereby creating bulk ratios that, when partially melted (or crystallized), can produce eucritic glasses. Figure 20 demonstrates graphically what is required to achieve a satisfactory eucrite precursor

composition once a mixture like Allegan-Murchison has formed. The silicate portion of the Allegan-Murchison composition (labeled nominal H-CM in the diagram) is reduced until approximately 12 wt% FeO is converted to Fe-metal. This reduction moves the bulk composition down the iron loss path from Fe/Mn=54 to Fe/Mn=38. This composition, however, has an Fe/(Fe+Mg) of 19. Based on the natural Murchison and Allegan-Murchison experiments, this Fe/(Fe+Mg) is too low to be a eucritic precursor assuming equilibrium conditions existed, and would require an Fe/(Fe+Mg) ratio of ~30 to produce a glass with a eucritic Fe/(Fe+Mg). In order to modify the composition to a higher Fe/(Fe+Mg) ratio, approximately 20 wt% olivine must be fractionated. Extraction of the olivine moves the composition parallel to the Fe/(Fe+Mg) axis (shown by the hollow arrow) toward the synthetic H-CM bulk composition point. If olivine is the only fractionating phase, only Fe and Mg abundances are substantially modified, leaving the remaining elements essentially unaffected. When partial melting of this olivine depleted composition under reducing conditions occurs (1180°C IW-0.5), a glass with appropriate eucritic Fe/Mn and Fe/(Fe+Mg) ratios will be produced. The same calculations can be done using the bulk composition of Allegan-Murchison, instead of just the silicate portion with the same results being achieved. In this case, a much larger proportion of the original Fe budget (approximately 62 wt% FeO, assuming all Fe is FeO) must be removed by reduction. Although this modification process can be applied to any of the chondritic meteorite classes to achieve similar results [like the CM meteorites (Murchison)], it should be noted that the composition of any single chondritic type of meteorite (such as a CM) requires that larger amounts of olivine and/or Fe-metal be removed from the bulk composition before equilibrium partial melting. The composition of a single chondritic meteorite type also cannot satisfy the oxygen isotope constraints, like a mixture composition, such as natural Allegan-Murchison.

The eucrites, diogenites, and howardites all appear to be related. If the eucrites formed by equilibrium melting or crystallization processes, than the diogenites spatial and temporal relationship to the eucrites on the basaltic achondrite planetoid (BAP) would also need to be

addressed [The howardites, although important, are essentially breccias containing a combination of diogenitic and eucritic lithologies that have been altered by impact processes, and are probably not primary rock types like the eucrites or diogenites (McCARTHY *et al*, 1973; MASON *et al*, 1979). They therefore do not influence how the primary lithologies formed].

On BAP, the Fe-metal produced from the reduction of the silicate FeO to Fe-metal (and any pre-existing Fe-metal in the parent body) would most likely sink from its higher density and become a small core (~30% of total mass), while the olivine fractionation that occurred would go into the formation of an olivine rich mantle. The FeO reduction occurs because 1) the ambient oxygen fugacity in that area of the early solar system was near IW-1.0 naturally (SATO *et al*, 1973; STOLPER, 1977), 2) elemental carbon that is available within the BAP bulk composition undergoes a reaction with the silicate FeO to produce Fe-metal and CO_2, or 3) a combination of the ambient oxygen fugacity and some available carbon reacts with FeO producing Fe-metal. The exact process resulting in the FeO reduction may not be able to be determined. STOLPER (1977) found that the eucrites were saturated in five phases (pigeonite, olivine, plagioclase, spinel, and metal) at conditions very near IW-1.0. As STOLPER (1977) states:

> "if conditions of pressure and oxygen fugacity can be found at which a given rock composition has more than three phases at its liquidus, it is probable that this rock was produced by quenching of a liquid and that the generation of this liquid involved equilibria between the liquid and the liquidus phases at the conditions at which the liquidus is multiply saturated."

It is therefore very likely that the oxygen fugacity was very near IW-1.0 on the parent body (and that eucrites are very likely to result from equilibrium processes).

The above quote from STOLPER (1977) also implies that melting just above the solidus temperature for a composition like the H-CM mixture, is equivalent to the liquidus temperature of the eucrites, and therefore the eucrites likely derive from a chondritic (H-CM like) source.

The silica-olivine-plagioclase pseudoternary in Figure 21 shows the paths taken by the liquids and bulk compositions during eucrite petrogenesis. The A-M composition shows the position the composition has before both olivine fractionation and Fe reduction, while the H-CM composition shown is after fractionation and reduction. The equilibrium crystallization path begins at the bulk H-CM composition and trends directly away from olivine during olivine crystallization, until reaching the olivine-pyroxene peritectic boundary. At this point, pyroxene is produced at the expense of olivine as the bulk composition moves along the dotted path marked (a) until the peritectic point is reached and eucritic glass is left. The equilibrium melting path overplots the equilibrium crystallization path but moves in the reverse direction.

The diogenites are orthopyroxenites and appear to be mostly monomict or polymict breccias. Since brecciation usually involves some degree of surface processing or impacting on the parent body and assuming 1) the meteorite sampling seen on Earth is representative of the lithologies on BAP and 2) no large scale tectonic processes occurred on BAP, than the diogenites probably occurred as surface or near surface lithologies, like the eucrites. This would imply that if eucrites are the products of equilibrium partial melting than diogenites cannot be derived from the same magma, but rather must have formed under different petrogenetic and regional conditions, to allow alternative processes (such as fractional crystallization) to occur. It would also imply that a layered crust (TAKEDA, 1979) probably cannot exist on BAP on any planetoid-wide scale, since this would probably force the derivation of one lithology (eucrites) from the residual of another lithology (diogenites). From these implications, we can only assume that BAP contains a heterogeneous crust that varies from region to region. Then how did the diogenites form? Although it is possible to create diogenites through equilibrium partial melting, the bulk composition from which it forms must be extremely pyroxene normative, plotting on the pseudoternary either just below the olivine-pyroxene peritectic boundary in the olivine field or plotting somewhere inside the pyroxene field itself. The production of such a bulk composition from a chondritic source however becomes a problem, since the composition does not have a sufficiently large orthopyroxene

stability field (JUREWICZ *et al*, 1995) and processing involving either fractional crystallization and/or melting must also be considered to account for them.

A more reasonable possibility is that the diogenites formed by fractional crystallization of orthopyroxene from high temperature melts, like those in the 1300 - 1400°C synthetic H-CM experiments. These experimental glasses have compositions containing Fe/(Fe+Mg) ratios ~30 and Fe/Mn ratios of ~30. Fractionally crystallizing this melt would produce orthopyroxenites strikingly similar to diogenites, with the orthopyroxene being ~En75 and Fe/Mn ratios ~26.

Fractional Crystallization and BAP

MASON (1962) first suggested that the eucrites were a product of fractional crystallization from a residual liquid that had previously crystallized diogenite cumulates. This residual liquid resulted when a magnesian (olivine-rich) parent magma (that was presumably chondritic) experienced olivine fractionation at depth inside its parent body. The fractionated olivine formed the mantle, while subsequent fractionation of mafic mineral cumulates, near the surface, produced cumulate orthopyroxenites, which are represented by the diogenites. The remaining residual liquid that was left than crystallized into the eucrites.

Fractional crystallization of a bulk composition like the synthetic H-CM or natural Allegan- -Murchison would not yield a residual liquid that looked even remotely like a eucrite (Figure 21, Path b). If we assume that the diogenites formed from an olivine poor fractionally crystallized high temperature melt (like the 1300 - 1400°C synthetic H-CM glass in Figures 15 A & B), as discussed above, then the liquid remaining after orthpyroxene fractionation would be saturated with silica, pyroxene and plagioclase phases, resembling a terrestrial norite or quartz monozonite (MORSE, 1980). The reason for this silica rich melt is that during orthopyroxene fractionation the bulk composition leaves the olivine-pyroxene peritectic boundary and continues straight across the pyroxene field until intersecting the pyroxene- plagioclase boundary, between the eutectic and peritectic points. Fractionation of more

pyroxene and plagioclase phases will then persist until reaching the eutectic point, where an additional phase, a silica polymorph, will begin to crystallize to completion. The peritectic point, where eucrites would crystallize, is never reached during the entire fractional crystallization process. Even if the entire olivine-pyroxene phase boundary were a cotectic boundary [which for many reasons it is not, see DELANEY (1986a), DELANEY et al (1981), (1984), HEWINS and NEWSOM (1988), and LONGHI and PAN (1988b) for more details], at best, only a small instantaneous eucritic melt might be produced during the fractional crystallization process. However, the possibility that such a small amount of melt could account for a large proportion of the eucrites is highly unlikely. The major problem is there is no mechanism to halt the fractionating liquid at the peritectic point, and thereby inhibit it from going to completion.

One of few methods of deriving a eucritic melt, which previously crystallized the diogenites, would be to start with a composition that is substantially more Fe-rich [$Fe/(Fe+Mg) \sim 50$] than the natural or synthetic H-CM compositions, and place it initially, deep (130km+) inside the parent planetoid (BARTELS and GROVE, 1991; GROVE and BARTELS, 1992). This depth, which is equivalent to a pressure of ~500 bars to 1 kbar, effects the olivine-pyroxene peritectic boundary so that upon pyroxene fractionation, the bulk composition does not trend markedly across the pyroxene field like the synthetic H-CM would, but stays slightly above the peritectic boundary, where it would eventually intersect the pyroxene-plagioclase boundary just above the peritectic point. This magnesian composition would thereby be able to fractionate the diogenites and produce a residual liquid to crystallize some eucritic lithologies. A problem with this model however, is that the eucritic melt produced cannot be inhibited from fractionating to completion at the eutectic point. The quantity of eucritic melt produced would therefore only consist of a small fraction of the original composition.

Fractional Melting and BAP

Unlike equilibrium melting and crystallization, fractional melting does not follow the reverse path as fractional crystallization, and, in fact, results in compositions that are radically different from it. During fractional melting, melt is continuously extracted from the bulk (solid) composition as it is formed. For a composition, like the synthetic H-CM or natural Allegan-Murchison, the melt forms at the peritectic point, where the minimum melting temperature for the system, olivine-plagioclase-silica, is located and where the bulk compositions of the eucrites plots. The melt is saturated in olivine, plagioclase, and pigeonite (+spinel+metal). As this melt is extracted, the composition of the residual solids begins to move directly away from the peritectic point (Figure 21, Path d). This extraction of melt continues until plagioclase is exhausted in the residual solids. At this point, the bulk composition intersects the olivine-silica leg of the pseudoternary. A subsequent increase in the temperature, however, will not produce any additional melt, since the peritectic point of the olivine-silica binary would need to be reached in order to produce melt (There is also a corresponding absence of change in the solids). Once the olivine-silica binary peritectic is reached, melt saturated in olivine and pyroxene begins to be generated and extracted. This melt extraction causes the remaining bulk composition to move directly away from the binary peritectic point, down the olivine-silica leg of the pseudoternary, towards olivine. Melt extraction continues until pyroxene is exhausted and melting is halted for a second time (The bulk composition arrives at olivine). Increases in the temperature beyond this point, will not result in the formation of melt, until the melting temperature for the remaining olivine composition is reached. Any melt produced (and extracted) above this implausibly high temperature will only be saturated in olivine, which will eventually be exhausted and the process ended.

The production of eucrites from the H-CM composition during fractional melting is extremely easy. A substantial amount of eucritic melt is created at the beginning of fractional melting, and assuming the sampling of basaltic achondritic meteorites found on Earth is representative of the surface of BAP, the amount of melt could easily account for why the

dominant lithology seen on BAP is eucritic. The diogenites might also form by fractional melting as a residual melt that is produced after the eucritic melt is extracted. The diogenitic melt would form at the olivine-silica binary peritectic, and assuming pyroxene fractionation occurs, an orthopyroxenite would crystallize. If the diogenites did not form as a residual after the production of eucrites, than they would require, much like in equilibrium melting or crystallization, that the primary H-CM bulk composition be modified from its present position in the olivine field to a more pyroxene normative position in the pseudoternary, not producing abundant olivine normative melts upon crystallization.

A Method to Produce a Planetoid by Mixing H and CM Chondrites.

The evolution of the basaltic achondrite planetoid (BAP) has been a problem ever since the discovery of the eucrites. Most calculations of it's bulk composition (CONSOLMAGNO and DRAKE, 1977; DREIBUS *et al.* 1976, 1977; DREIBUS and WÄNKE, 1979, 1980; MORGAN *et al.*, 1977), have not dealt with the method of formation of the parent body represented by that composition. However, since the model of BOESENBERG and DELANEY (1994a & b) explicitly involves large scale mixing of two (or more) very distinctive components, the method by which they were mixed is of some importance. WETHERILL (1981) pointed out that impacts are fundamental to normal planet forming processes. Collisions were frequent in the early forming solar system. HARTMANN (1986) and HARTMANN and VAIL (1986) have argued that an extreme end member of the spectrum of impact processes involves giant impacts that can radically alter a pre-existing planetary body and completely redefine its characteristics. The BOESENBERG and DELANEY (1994a & b) view of the formation of the BAP planetoid simply applies this logic to the less extreme case of smaller asteroidal sized bodies. In the early solar system, the development of planetesimals produced H chondritic planetoids and CM chondritic planetoids that are represented by meteorites. Collision of two such objects provides a potential mechanism for mixing such apparently different precursor compositions. A result of such a "small" giant

impact would almost certainly involve the dispersal of a large proportion of the mass of the impactors after the impact. If sufficient mass were available, perhaps enough material would fall back gravitationally to form a large asteroid like Vesta, the basaltic achondrite planetoid. Total melting of the resulting planetoid could occur, because of the large energy exchange associated with impact processes, causing homogenization of the body prior to the formation of a solid crust and mantle and the onset of the magmatism that is represented by the eucrites, diogenites and howardites. A requirement of a BAP planetoid model, however, is the almost total removal of the alkali elements and other volatile elements as the basaltic achondrites have much lower alkali contents than the precursor composition. While volatilization of the alkalis is plausible, the isotopic measurements of potassium isotopes by HUMAYUN and CLAYTON (1993) appear to preclude conventional liquid-vapor volatilization mechanisms following Rayleigh fractionation laws. HASHIMOTO (1990) and DAVIS *et al.*, (1990) have shown negligible isotope fractionation during sublimation of solid forsterite samples, whereas liquid sample show marked fractionation of Mg isotopes. The isotopic indicators of volatile loss, therefore may not be independent of the mechanism by which the volatile loss occurs. Since the mixing model proposed implies that impact processes were important, it will be important to document the effect of shock modification of silicates on the mechanism of alkali volatilization and hence on volatile related isotope fractionation effects in the future. If a mechanism for alkali volatilization can be identified that avoids the constraints imposed by these potassium isotope measurements, then the "small giant impact" mechanism may be an appropriate way to construct an achondritic planetoid by mixing chondritic material from two or more sources.

Conclusions

1. Eucritic melts can be produced by equilibrium partial melting, equilibrium crystallization, or fractional melting of a chondritic composition similar to Allegan-Murchison mixture. The Fe-

Mn-Mg systematics, however, require that the bulk composition undergo a moderate amount of Fe-metal and olivine fractionation before one or more of the processes occurs.

2. The Allegan-Murchison cocktail composition of DELANEY (1993) produces a more favorable precursor composition than CM meteorites, like Murchison (or any other singular class of meteorite), even if the oxygen isotope constraint is ignored, since it requires less fractionation than any single chondritic type of meteorite (such as the CM chondrites).

3. The only compositional difference between the synthetic H-CM (or a modified form of natural Allegan-Murchison) glasses and true eucrites is the overabundance of alkalis in the glasses. The alkali content differences between the cocktail composition and natural eucrite samples requires that some unidentified mechanism (such as impact) deplete the alkali elements in the eucrites. Either the alkalis presently seen in H-chondrites were not present in the chondritic components that were mixed to form BAP or the formation of the planetoid led to the removal of the alkali elements. Further work is needed to resolve this problem.

4. Orthopyroxene fractionated from compositions similar to high temperature synthetic H-CM (1300-1400°C) partial melts can produce diogenitic lithologies, further supporting the argument that the basaltic achondrite planetoid is composed of at least two mixed chondritic classes.

References

AYLMER, D., HERZOG, G. F., KLEIN, J. and MIDDLETON, R. (1986) Beryllium-10 contents of eucrites. *Meteoritics* **21**, 329.

BARTELS, K. S. and GROVE, T. L. (1991) High-pressure experiments on magnesian eucrite compositions: Constraints on magmatic processes in the eucrite parent body. *Proc. Lunar and Planetary Science*, **21** 351-365.

BINZEL, R. P., and XU, S. (1993) Chips off of Asteroid 4 Vesta: Evidence for the parent body of basaltic achondrite meteorites. *Science* **260**, 186-191.

BOESENBERG, J. S. and DELANEY, J. S. (1994a) The composition of the Basaltic Achondrite Planetoid: A model constrained by oxygen isotopes, Fe-Mn-Mg systematics and a phase equilibrium test of that model. *Geochim. Cosmochim. Acta* (submitted).

BOESENBERG, J. S. and DELANEY, J. S. (1994b) Results of partial melting experiments on chondritic precursors of basaltic achondrites. *Meteoritics* **29**, 445-446.

BUCHANAN, P. C., ZOLENSKY, M. E., and REID, A. M. (1993) Carbonaceous chondrite clasts in the howardites Bholghati and EET87513. *Meteoritics* **28**, 659-669.

CHAPMAN, C. R. and SALISBURY, J. W. (1973) Comparisons of meteorite and asteroid spectral reflectivities. *Icarus* **19**, 507-522.51.

CHOU, I. (1987) Oxygen buffer and hydrogen sensor techniques at elevated pressures and temperatures. In G. C. Ulmer and H. L. Barnes (eds.) *Hydrothermal Experimental Techniques*, John Wiley & Sons, New York, 61-98.

CLAYTON, R. N. (1993) Oxygen isotopes in meteorites. *Ann. Rev. Earth Planet. Sci.* **21**, *115-149.*

CONSOLMAGNO, G. J. and DRAKE, M. J. (1977) Composition and evolution of the eucrite parent body: evidence from rare earth elements. *Geochim. Cosmochim. Acta* **41**, 1271-1282.

DAVIS, A. M., HASHIMOTO, A., CLAYTON, R. N., and MAYEDA, T. K. (1990) Isotope fractionation during evaporation of Mg_2SiO_4. *Nature* **347**, 655-658.

DELANEY, J. S. (1986a) Phase equilibria for basaltic achondrites. *Lunar and Planetary Science,* **XVII,**164-165.

DELANEY, J. S. (1986b) The basaltic achondrite planetoid. *Lunar and Planetary Science,* **XVII**, 166-167.

DELANEY, J. S. (1986c) A provincial model for the crust of a basaltic achondrite planetoid. *Meteoritics* **21**, 352-353.

DELANEY, J. S. (1993) Fe/Mn and oxygen isotope constraints on the compositions of the basaltic achondrite parent body. *Meteoritics* **28**, 340-341.

DELANEY, J. S. and BOESENBERG, J. S. (1993) Fe/Mn constraints on precursors of basaltic achondrites. *Lunar and Planetary Science,* **XXIV**, 391-392.

DELANEY, J. S., PRINZ, M., NEHRU, C. E., and HARLOW, G. E. (1981) A new basalt group from howardites: mineral chemistry and relationships with basaltic achondrites. *Lunar and Planetary Science* **XII**, 211-213.

DELANEY, J. S., PRINZ, M., and TAKEDA, H. (1984) The polymict eucrites. *Proc. Lunar Planet. Sci. Conf. 15th,* in *Journal of Geophysical Research,* **89**, C251-C288.

DREIBUS, G., and WÄNKE, H. (1979) On the chemical composition of the Moon and eucrite parent body and a comparison with the composition of the earth, the case of Mn, Cr and a V. *Lunar and Planetary Science* **X**, 315-317.

DREIBUS, G., and WÄNKE, H. (1980) The bulk composition of the eucrite parent asteroid and its bearing on planetary evolution. *Z. Naturforsch.* **35**a, 204-216.

DREIBUS, G., SPETTEL, B., and WÄNKE, H. (1976) Lithium as a correlated element, its condensation behavior, and its use to estimate the bulk composition of the moon and the eucrite parent body. *Proc. Lunar Sci. Conf.* **7**, 3383-3396.

DREIBUS, G., KRUSE, H., SPETTEL, B., and WÄNKE, H. (1977) The bulk composition of the moon and the eucrite parent body. *Proc. Lunar Sci. Conf.* **8**, 211-227.

FARINELLA, P., , FROESCHLÉ, C. H., and GONCZI, R. (1992) Meteorites from the asteroid 6 Hebe. *Celestial Mechanics.*, in press.

FARINELLA, P., GONCZI, R., FROESCHLÉ, C. H., and FROESCHLÉ, C. (1993) The injection of asteroid fragments into resonances, *Icarus* **101**, 174-187.

FEIERBERG, M. A. and DRAKE, M. J. (1980) The meteorite-asteroid connection: The infrared spectra of eucrites, shergottites, and Vesta. *Science* **209**, 805-807.

GLASS, B. P. (1982) *Introduction to planetary geology.* Cambridge University Press, New York, 469 pp.

GOLDSTEIN, J. I., NEWBURY, D. E., ECHLIN, P., JOY, D. C., ROMIG, A. D., JR., LYMAN, C. E., FIORI, C., and LIFSHIN, E. (1992) *Scanning electron microscopy and x-ray microanalysis*, 2nd ed. Plenum Press, New York, 820pp.

GROVE, T. L. and BARTELS, K. S. (1992) The relation between diogenite cumulates and eucrite magmas. *Proc. Lunar Planet. Sci. Conf.*, **22**, 437-445.

HARTMANN, W. K. (1986) Moon origin: The impact-trigger hypothesis. In *Origin of the Moon* (eds. W. K. HARTMANN, R. J. PHILLIPS and G. J. TAYLOR), Lunar and Planetary Institute, Houston, 579-608.

HARTMANN, W. K. and VAIL, S. M. (1986) Giant impactors: Plausible sizes and populations. In *Origin of the Moon* (eds. W. K. HARTMANN, R. J. PHILLIPS, and G. J. TAYLOR), Lunar and Planetary Institute, Houston, 551-566.

HASHIMOTO, A. (1990) Evaporation kinetics of forsterite and implications for the early solar nebula. *Nature*, **347**, 53-55.

HEINRICH, K. F. J. (1991) Strategies of electron probe data reduction. In *Electron Probe Quantitation* (eds. K. F. J. Heinrich and D. E. Newbury), Plenum Press, New York, 9-18.

HERZOG, G. F. and CRESSY, P. J. (1977) Diogenite exposure ages. *Geochim. Cosmochim. Acta* **41**, 127-134.

HERZOG, G. F., HAMPEL, W., WÄNKE, H. and HOFMEISTER, H. (1978) [26]Al production in Allende, Bereba, and Juvinas. *Meteoritics* **13**, 491.

HEWINS, R. H. and NEWSOM, H. E. (1988) Igneous activity in the early solar system. In *Meteorites and the Early Solar System* (eds. J. F. Kerridge and M. S. Matthews), University of Arizona, Tucson, 73-101.

HUEBNER, J. S. (1987) Use of gas mixtures at low pressure to specify oxygen and other fugacities of furnace atmospheres. In G. C. Ulmer and H. L. Barnes (eds.) *Hydrothermal Experimental Techniques*, John Wiley & Sons, New York, 20-60.

HUMAYUN, M. and CLAYTON, R. N. (1993) Potassium isotope cosmochemistry, volatile depletion and the origin of the earth. In *Lunar and Planetary Science*, Vol. **XXIV**, Lunar and Planetary Institute, Houston, 685-686.

JAROSEWICH, E. (1990) Chemical analyses of meteorites: a compilation of stony and iron meteorite analyses. *Meteoritics* **25**, 323-337.

JAROSEWICH, E., NELEN, J. A., and NORBERG, J. A. (1980) Reference samples for electron microprobe analysis. *Geostandards Newsletter* **4**, 43-47.

JONES, J. H. (1984) Temperature- and pressure- independent correlations of olivine/liquid partition coefficients and their application to trace element partitioning. *Contrib. Mineral. Petrol.* **88**, 126-132.

JUREWICZ, A. J. G. (1986) Appendix 2: Software used to calculate run conditions for the Deltech controlled-atmosphere furnace. In Effect of temperature, pressure, oxygen fugacity and composition on calcium partitioning, calcium-magnesium distribution and the kinetics of cation exchange between olivines and basaltic melts (Thesis for the Geology Department, Rensselaer Polytechnic Inst., Troy, NY), 206-213.

JUREWICZ, A. J. G., MITTLEFEHLDT, D. W. and JONES, J. H. (1991) Partial melting of the Allende (CV3) meteorite: implications for origins of basaltic meteorites. *Science* **252**, 695-698.

JUREWICZ, A. J. G., MITTLEFEHLDT, D. W. and JONES, J. H. (1993) Experimental partial melting of the Allende (CV) and Murchison (CM) chondrites and the origin of asteroidal basalts. *Geochim. Cosmochim. Acta* **57**, 2123-2139.

JUREWICZ, A. J. G., MITTLEFEHLDT, D. W. and JONES, J. H. (1995) Experimental partial melting of the St. Severin (LL) and Lost City (H) chondrites. *Geochim. Cosmochim. Acta* **59**, 391-408.

KINZIE, P. A. (1973) *Thermocouple Temperature Measurement*, John Wiley & Sons, New York, 1-41.

KUSHIRO, I. and MYSEN, B. O. (1979) Melting experiments on a Yamato chondrite. *Mem. Natl. Inst. Polar Res. (Japan), Spec. Issue* **15**,165-170.

LONGHI, J. and PAN, V. (1988a) Phase equilibrium constraints on the howardite - eucrite - diogenite association. *Proc. Lunar Planet Sci. Conf.* **18**, 459-470.

LONGHI, J. and PAN, V. (1988b) A reconnaissance study of phase boundaries in low-alkali basaltic liquids. *J. Petrology* **29**, 115-147.

LONGHI, J., WALKER, D., and HAYS, J. F. (1975) Fe-Mg distribution between olivine and lunar basaltic liquids. *EOS* **56**, 471.

MASON, B. (1962) *Meteorites.* Wiley, New York.

MASON, B., JAROSEWICH, E., and NELEN, J. A. (1979) The pyroxene-plagioclase achondrites. *Smithsonian Contrib. Earth Sci.*, **22**, 27-45.

McCARTHY, T. S., ERLANK, A. J., and WILLIS, J. P. (1973) On the origin of eucrites and diogenites. *Earth Planet. Sci. Lett.* **18**, 433-442.

McCORD, T. B., ADAMS, J. B., and JOHNSON, T. V. (1970) Asteroid Vesta: Spectral reflectivity and compositional implications. *Science* **168**, 1445-1447.

MORGAN, J. W., HIGUCHI, H., TAKAHASHI, H., and HERTOGEN, J. (1978) A "chondritic" eucrite parent body: inference from trace elements. *Geochim. Cosmochim. Acta* **42**, 27-38.

MORSE, S. A. (1980) *Basalts and phase diagrams.* Springer-Verlag, New York.

NAFZIGER, R. H., ULMER, G. C., and WOERMAN, E. (1971) Gaseous buffering for control of oxygen fugacity at one atmosphere. In G. C. Ulmer (ed.), *Research Techniques for High Pressure and High Temperature*, Springer-Verlag, New York, 9-41.

POWELL, R. L. (1972) Revision of the standard reference data for thermocouples. In H. H. Plumb (ed.), *Temperature: Its measurement and control in science and industry, Volume 4.* Instrument Society of America, Pittsburgh, 1579-1602.

SATO, M. (1971) Electrochemical measurements and control of oxygen fugacity and other gaseous fugacities with solid electrolyte sensors. In G. C. Ulmer (ed.), *Research Techniques for High Pressure and High Temperature*, Springer-Verlag, New York, 43-99.

SATO, M., HICKLING, N. L. and MCLANE, J. E. (1973) Oxygen fugacity values of Apollo 12, 14, and 15 lunar samples and reduced state of lunar magmas. *Proc. Fourth Lunar Sci Conf., Geochim. Cosmochim. Acta Suppl.* **4**, 1061-1079.

SCHULTZ, L. (1987) Exposure ages of basaltic achondrites and implications for the stratigraphy of their parent body. *Lunar Planet. Sci.* **XVIII**, 884-885.

STOLPER, E. (1975) Petrogenesis of eucrite, howardite, and diogenite meteorites. *Nature* **258**, 220-222.

STOLPER, E. (1977) Experimental petrology of eucritic meteorites. *Geochim. Cosmochim. Acta* **41**, 587-611.

TAKAHASHI, E. (1978) Partitioning of Ni^{2+}, Co^{2+}, Fe^{2+}, Mn^{2+}, and Mg^{2+} between olivine and silicate melts: compositional dependence of partition coefficient. *Geochim. Cosmochim. Acta* **42**, 1829-1844.

TAKAHASHI, E. (1983) Melting of a Yamato chondrite (Y-74191) up to 30 kbar. *Mem. Natl. Inst. Polar Res. (Japan), Spec. Issue* **30**, 168-180.

TAKEDA, H. (1979) A layered-crust model of a howardite parent body. *Icarus* **40**, 455-470.

TAKEI, H. (1976) Czochralski growth of Mn_2SiO_4 (Tephroite) single crystal and its properties. *J. Crystal Growth* **34**, 125-131.

TAKEI, H. (1978) Growth of fayalite (Fe_2SiO_4) single crystals by the floating-zone method. *J. Crystal Growth* **43**, 463-468.

TAKEI, H. and KOBAYASHI, T. (1974) Growth and properties of Mg_2SiO_4 single crystals. *J. Crystal Growth* **23**, 121-124.

TURRIN, R. P. (1984) Construction, maintenance and operation of an oxygen fugacity monitoring petrologic furnace. (B.A. honors thesis for Dept. of Geological Sciences, Rutgers College, Rutgers University, New Brunswick, NJ), 31 pp.

WALKER, D., and AGEE, C. B. (1988) Ureilite compaction. *Meteoritics* **23**, 81-91.

WARREN, P. H. (1985) Origin of howardites, diogenites, and eucrites: a mass balance constraint. *Geochim. Cosmochim. Acta* **49**, 577-586.

WETHERILL, G. W. (1981) The formation of the Earth from planetesimals. *Scientific American*, **244**(6), 162-174.

ZOLENSKY, M. E., HEWINS, R. H., MITTLEFEHLDT, D. W., LINDSTROM, M. M., XIAO, X., and LIPSCHUTZ, M. E. (1992) Mineralogy, petrology, and geochemistry of carbonaceous clasts in the LEW 85300 polymict eucrite. *Meteoritics* **27**, 596-604.

ZOLENSKY, M. E., WEISBERG, M. K., BUCHANAN, P. C., and MITTLEFEHLDT, D. W. (1995) Mineralogy of carbonaceous chondrite clasts in howardites and eucrites. (unpublished, in progress).

Figure Captions:

Figure 1: Oxygen isotope diagram, after CLAYTON (1992) and modified by DELANEY (1993) showing the basaltic achondrite field and several potential mixing components that may be mixed together to produce compositions on the achondrite mass fractionation line.

Figure 2: Schematic details of the Deltech VTOS/C vertical muffle tube gas mixing furnace.
- a) Alumina muffle tube
- b) Upper brass cooling head
- c) Lower brass cooling head
- d) Water outlet to upper cooling head
- e) Water inlet to upper cooling head
- f) Water outlet to lower cooling head
- g) Water inlet to lower cooling head
- h) Gas Inlet at rear of upper cooling head
- i) Gas Outlet at rear of lower cooling head
- j) Furnace thermocouple entering through the back wall of the furnace
- k) Furnace heating element
- l) Insulation
- m) Exterior metal casing surrounding furnace
- n) Hotspot location - about 3 cm high
- o) Buss bar heating element connectors
- p) Power supply connectors
- q) Removable brass cap (The sample rod and experimental charges in
    Figure 3 are inserted into the furnace through this opening.)

Figure 3: Three views detailing the experimental setup on the sample rod.
A) Generalized cross section of the sample rod showing the a) brass head, b) 40 cm long, four bore alumina tube, c) thermocouple wires, and d) support wires for the experimental charges (Figure is slightly exaggerated for clarity).

B) Close-up and detailed view of the lower section of the sample rod showing the actual setup of the experimental charges (Figure is slightly exaggerated for clarity).
- a) Four bore alumina tube
- b) Alumina rings used to aid in the support of the charges
- c) Thermocouple wires
- d) Sample rod platinum support wires
- e) Fe or Pt-Fe support wires for the experimental charges
- f) Thermocouple butt weld
- g) Experimental charges

C) A different perspective illustrating how the experimental charges were supported and positioned on the Fe or Pt-Fe support wires while in the furnace.

Figure 4: Temperature calibration setup showing the positions of the sample rod support wires, the thin Pt wires, and the Au (or Pd) wires.

Figure 5: Graph of temperature taken by sample rod thermocouple versus the furnace display readings showing that the furnace display readings, although similar to actual temperatures, linearly deviate over a broad temperature range.

Figure 6: Cross section through the lower end of oxygen fugacity sensor and thermocouple assembly. The four bore alumina rod (a) is sealed with epoxy to the inside of the yttrium-zirconia tube (b). Two of the bore holes in the alumina rod are used for the thermocouple

wires (c). A platinum wire (d), which is connected to the interior platinum foil (e) is then passed through a third bore hole. A platinum wire (f) is also attached to the exterior platinum foil (g). The fourth bore hole is used to pass oxygen into the interior of the fugacity sensor.

Figure 7: A) Schematic diagram of the original gas mixer showing that the gas flow from the high volume gas (CO) could create back pressure in the low volume gas (CO_2) line. Depending on the flow rates that were used to calibrate the oxygen fugacity initially, and those used during each experiment, the back pressure applied to the low volume gas line would result in oxygen fugacities lower than expected. The effect would be more severe on low oxygen fugacities than high ones, because the greater flowrate from the high volume gas would create a larger back pressure and reduce the fugacity further. B) Schematic diagram of the rebuilt gas mixer showing the inlets for the CO_2 and CO gases, the direction of flow, and the five pieces used in the assembly.

Figure 8: Log fO_2 vs. the A) observed and B) calculated gas mixture ratio showing the drastic differences in the observed conditions found within the furnace. In general, the observed conditions were more oxidizing than they were calculated to be by approximately ~0.5 log units.

Figure 9: Temperature vs. the A) observed and B) calculated gas mixture ratio demonstrating the drastic oxidizing conditions found in the furnace. The difference is caused by a leak, probably located near the edges of the muffle tube, where the cooling head comes in contact with the muffle tube. Air may also be able to enter along the edges of the sample rod when it is inserted into the top of the furnace.

Figure 10: Temperature vs. observed gas mixture ratio drawn from the final calibration results in Tables 8 and 9. This graph was used to determine the proper gas ratio necessary to achieve the desired oxygen fugacity conditions during the experiments.

Figure 11: Iron loss effects on the Series I experiments showing the resulting glasses and olivines plotted in an Fe/Mn vs. Fe/(Fe+Mg)x100 diagram. With increasing temperature, more platinum comes in contact with the experimental charge (the melt tends to migrate up the platinum wire) and allows greater amounts of iron to be removed. Therefore large fractionations occur at high temperature (abundant melt), such as in M17 and M19 (1580°C), and substantially less iron is removed at lower temperatures such as M4 (1180°C).

Figure 12: Silica-olivine-plagioclase pseudoternary diagram showing the effects of Fe loss on the bulk composition of synthetic Murchison. The phase boundaries seen are for an Fe/(Fe+Mg)x100=60. Pseudoternary is based on the work of LONGHI and PAN (1988b) and is projected from wollastonite.

Figure 13: Fe/Mn vs. Fe/(Fe+Mg) (molar) diagrams demonstrating the effect of iron loss on the bulk synthetic Murchison and H-CM compositions and their resulting glass compositions as a function of temperature and oxygen fugacity. The olivines in equilibrium with the glasses are also shown. The error bars shown on each experiment represent one standard deviation of compositional range. The H-CM composition is displaced toward the high Fe/(Fe+Mg) side of the Fe-loss trend. Notice in Figure A, the Fe loss curve for the glasses does not pass through the eucrite range, but it does pass through the eucrite range in Figure B for the H-CM glasses. The legend in Figure A applies to both figures.

Figure 14: Close-up view of the phase boundary intersections in the olivine-plagioclase-silica pseudoternary for an Fe/(Fe+Mg) ratio of 60. Pseudoternary is based on the work of LONGHI and PAN (1988b) and is projected from wollastonite. Eucrites (crosses) can be seen plotting on the peritectic point. Coordinates shown are for the four corners of the diagram and represent the (Olivine, Plagioclase, Silica) intersections. The intersection at the top right of

the diagram is the eutectic point. Solid line is the Orthopyroxene-Plagioclase tie line. The letters denoted within the legend are abbreviations for the natural Allegan-Murchison (AM), natural Murchison (NM), synthetic H-CM (H-CM), and the synthetic Murchison (SM) compositions. The numbers in parentheses following the compositional abbreviations are the temperature (in °C) and oxygen fugacity (relative to the IW buffer) of the experimental run.

Figure 15A and B: Two views of the olivine-pyroxene phase boundary in the olivine-plagioclase-silica pseudoternary for an Fe/(Fe+Mg) ratio of 30 (A) and 55 (B). Pseudoternary plots are based on the work of LONGHI and PAN (1988b) and is projected from wollastonite. Open symbols have an Fe/(Fe+Mg) ratio of 30 (A), while the solid symbols have an Fe/(Fe+Mg) ratio of 55 (B). Two of the experiments (solid circles and solid triangles) in Figure 15B are displaced from the olivine-pyroxene peritectic because of the fractionation of olivine during the quench. The letters denoted within the legend are abbreviations for the natural Allegan-Murchison (AM), natural Murchison (NM), synthetic H-CM (H-CM), and the synthetic Murchison (SM) compositions. The numbers in parentheses following the compositional abbreviations are the temperature (in °C) and oxygen fugacity (relative to the IW buffer) of the experimental run.

Figure 16: Normalization diagrams of the synthetic Murchison and H-CM experimental glasses to bulk average eucrites (Data taken from JAROSEWICH (1990)). The best compositional match to eucrites was produced in the H-CM 1180°C IW-0.5 experiment shown as the solid box. The open diamond (1200°C, IW-1.5) and cross (1200°C, IW-0.5) of the H-CM experiments show the drastic effects of altering the oxygen fugacity.

Figure 17: Fe/Mn vs Fe/(Fe+Mg) (molar) diagram demonstrating the effect of iron loss on the (a) bulk natural Murchison and (b) the natural Allegan (70%) - Murchison (30%) compositions and their resulting glass compositions as a function of temperature and oxygen fugacity. The olivines in equilibrium with the glasses are also shown. The error bars shown on each experiment represent one standard deviation of compositional range. Notice the Fe loss curve for the glasses does not pass through the eucrite range, but is shifted to the magnesian side of eucrites. Symbols shown in both diagrams are the same as in Figure 13 legend.

Figure 18: Normalization of literature experimental glasses to bulk average eucrites (Data taken from JAROSEWICH (1990), JUREWICZ et al.(1993), KUSHIRO and MYSEN, (1979), and STOLPER (1977)). Note the compositional variation in STOLPER'S glasses, which is dependent on what composition is being normalized to, even though he was melting eucrites.

Figure 19: Normalization diagrams of the natural Murchison and natural Allegan (70%) - Murchison (30%) experimental glasses to bulk average eucrites (Data taken from JAROSEWICH (1990)). A comparison with the work of JUREWICZ et al. (1993) in the next figure shows good agreement in terms of experimental results.

Figure 20: Fe/Mn vs Fe/(Fe+Mg)(molar) diagram showing how to modify the natural Allegan (70%) - Murchison (30%) composition into a composition similar to synthetic H-CM by using 12% reduction of FeO to Fe metal and 20% olivine fractionation.

Figure 21: Silica-olivine-plagioclase pseudoternary showing the paths taken by the liquids and the bulk composition during eucrite petrogenesis. The equilibrium crystallization path (a) and equilibrium melting path overplot each other but move in the reverse direction. The fractional crystallization path (b) follows the same trend as equilibrium crystallization initially, but moves off the peritectic boundary along the path marked as fractionation of pyroxene, then pyroxene and plagioclase, and eventually pyroxene, plagioclase, and a silica polymorph occurs. The solid evolution path taken during fractional crystallization follows the trend marked (c).

Fractional melting follows the path, marked (d), as liquid is continually removed from the bulk composition, first at the peritectic point and then at the $Oliv-SiO_2$ binary peritectic point.

Table 1. Mixtures Constrained by Oxygen Isotope Ratios to Match Basaltic Achondrite Mass Fractionation

	Murchison	Allende	LL avg.	H avg.	25 Allend-75 H	34 Allend-66 LL	30 Mur-70 H	43 Mur-57 LL
SiO_2	29.07	34.23	40.42	36.62	36.02	38.32	34.36	35.54
TiO_2	0.13	0.15	0.15	0.12	0.13	0.15	0.12	0.14
Al_2O_3	2.15	3.27	2.62	2.13	2.42	2.84	2.14	2.42
Cr_2O_3	0.48	0.52	0.49	0.51	0.51	0.50	0.50	0.49
Fe_2O_3	0.00	0.00	0.00	0.41	0.30	0.00	0.28	0.00
FeO	22.39	27.15	17.24	10.00	14.29	20.61	13.72	19.46
MnO	0.20	0.18	0.35	0.31	0.28	0.30	0.28	0.29
MgO	19.94	24.62	25.40	23.24	23.59	25.13	22.25	23.05
CaO	1.89	2.61	1.94	1.73	1.95	2.16	1.78	1.92
Na_2O	0.24	0.45	0.91	0.85	0.75	0.75	0.67	0.62
K_2O	0.04	0.03	0.11	0.09	0.08	0.08	0.08	0.08
P_2O_5	0.23	0.23	0.22	0.27	0.26	0.22	0.26	0.22
FeS	7.24	4.03	5.33	5.36	5.03	4.89	5.93	6.15
Fe-metal	0.13	0.17	2.68	15.81	11.90	1.83	11.10	1.58
Fe (total)	22.00	23.66	19.47	27.27	26.37	20.90	25.69	20.56
C	1.85	0.29	0.20	0.11	0.16	0.23	0.63	0.91
Total	85.98	97.93	98.06	97.56	97.67	98.01	94.10	92.87
Fe/Mn (t)	140.	169.	72.	114.	120.	91.	116.	93.
Fe/(Fe+Mg)	44.20	40.86	27.31	19.84	25.40	31.40	25.70	32.00

NOTE: First four columns are from JAROSEWICH (1990). Final four compositions were calculated by DELANEY (1993).
(t) Fe/Mn ratio based on total Fe.

Table 2. Chemical Compositions of Experimental Precursors.

A. Nominal Compositions of Murchison and the Allegan-Murchison Cocktail

	Natural Murchison*	70% Natural Allegan- 30% Natural Murchison*
SiO_2	33.14	35.53
TiO_2	0.15	0.11
Al_2O_3	2.45	2.10
Cr_2O_3	0.55	0.54
FeO	25.52	14.04
MnO	0.23	0.28
MgO	22.73	22.89
CaO	2.15	1.80
Na_2O	0.27	0.67
K_2O	0.05	0.08
P_2O_5	0.26	0.27
NiO	1.99	2.16
Fe-metal	0.15	12.56
FeS	8.25	6.34
C	2.11	0.67
Fe (total)	25.22	27.50
Total	100.00	100.00
Fe/Mn (t)	140	125
Fe/Mn (s)	111	106
Fe/Mn (ms)	109	54

* = Normalized anhydrous composition (based on analyses from JAROSEWICH (1990)).
(t) = Fe/Mn ratio based on total Fe
(s) = Fe/Mn ratio based on FeS free composition, but includes Fe metal.
(ms) = Fe/Mn ratio based on FeS and Fe metal free composition.

Table 2. (continued)

B. Murchison Analogue Compositions for the Series I Experiments

Fe/Mn ratio	85*	65*	45*	20*	Nominal Murchison**
SiO2	37.65	38.06	37.48	38.32	35.37
Al2O3	2.88	2.76	2.91	2.63	2.62
Cr2O3	0.52	0.51	0.48	0.49	0.58
FeO	34.51	34.08	33.84	32.86	34.63
MnO	0.40	.52	0.71	1.63	0.24
MgO	22.82	21.98	22.12	22.45	24.26
CaO	2.49	2.61	2.19	2.41	2.30
Total	100.77	100.52	99.73	100.79	100.00

* Average microprobe analyses of the four Murchison analogue compositions.
** Murchison normalized for the seven oxides contained within the compositions.
NOTE: Nominal Murchison has an Fe/Mn ratio of 142 (total Fe)[based on analyses from JAROSEWICH (1990)].

Table 2. (continued)

C. Nominal and Synthetic Compositions for the Series II Experiments

	Nominal Synthetic Murchison*	Experimental Synthetic Murchison	Nominal Synthetic H-CM**	Experimental Synthetic H-CM
SiO_2	37.18	40.19	44.64	46.04
TiO_2	0.17	0.25	0.16	0.12
Al_2O_3	2.75	3.31	2.81	3.01
Cr_2O_3	0.61	0.65	0.67	0.82
FeO	28.85(s)	27.27(s)	19.10	19.90
MnO	0.26	0.38	0.35	0.53
MgO	25.50	22.79	29.06	25.50
CaO	2.42	2.91	2.31	2.59
Na_2O	0.31	0.30	0.84	0.99
NiO	1.95	1.91	ni	ni
Total	100.00	99.96	100.00	99.50
Fe/Mn	111	71	54	37

* = Normalized anhydrous Murchison
** = Normalized silicate portion of the nominal H-CM (70% Allegan-30% Murchison) composition in Table 2A. Metal and sulfide portions were excluded from this composition.
ni = Not included in the composition
(s) = This composition excludes FeS, but includes Fe-metal as FeO. Therefore the target Fe/Mn ratio was 111, as opposed to the nominal (total Fe, including FeS) ratio of 142.
NOTE: Nominal compositions are normalized from JAROSEWICH (1990), while the experimental compositions were determined by microprobe analysis.

Table 3. Compositional Starting Materials and their Purity Levels

Starting Material	Formula	Purity
Silicon (IV) dioxide powder	SiO_2	99.999%
Titanium (IV) dioxide powder	TiO_2	99.99%
Aluminum oxide powder	Al_2O_3	99.5%
Chromium (III) oxide powder	Cr_2O_3	99.997%
Hematite powder	Fe_2O_3	97%
Manganese (II) oxide powder	MnO	99.5%
Magnesium oxide	MgO	99.5%
Calcium carbonate powder	$CaCO_3$	99.95%
Sodium hydrogen carbonate	$NaHCO_3$	~95%

Table 4. Temperature (°C) Correlation Table Between the Sample Rod Thermocouple (Tsr) and Furnace (Dfurn) Display Reading. The sample rod thermocouple shows the nominal temperature, based on the calibration to the melting points of Au and Pd.

Tsr	Dfurn	Tsr	Dfurn	Tsr	Dfurn
1050	1002	1240	1211	1430	1421
1060	1013	1250	1223	1440	1432
1070	1024	1260	1234	1450	1444
1080	1035	1270	1245	1460	1455
1090	1046	1280	1256	1470	1466
1100	1057	1290	1267	1480	1477
1110	1068	1300	1278	1490	1488
1120	1079	1310	1289	1500	1499
1130	1090	1320	1300	1510	1510
1140	1101	1330	1311	1520	1521
1150	1112	1340	1322	1530	1532
1160	1123	1350	1333	1540	1543
1170	1134	1360	1344	1550	1554
1180	1145	1370	1355	1560	1565
1190	1156	1380	1366	1570	1576
1200	1167	1390	1377	1580	1587
1210	1178	1400	1388	1590	1598
1220	1189	1410	1399	1600	1609
1230	1200	1420	1410		

Table 5. Results of the Thermocouple Calibration Experiments (Temp in °C)

Exp.	#1		#2		#3		
	Tsr	Dfurn	Tsr	Dfurn	Tsr	Dfurn	Nominal
Au	1034	1018	1061	1017	1064	1017	1064
Pd	1532	1556	1537	1555	1554	1555	1554

Tsr = sample rod thermocouple temperature
Dfurn = furnace display reading

Table 6. Initial Calibration of the Furnace Using the Oxygen Fugacity Sensor

Temp°C		Scale		ml/min		e.m.f.	IW
Tofs	Dfurn	CO	CO$_2$	CO	CO$_2$	calc	buffer
1350	1405	32	123	60.4	17.43	-780	+0.5
1350	1405	63	123	100.9	17.43	-820	IW
1350	1405	75	84	117.0	9.98	-861	-0.5
1350	1405	75	46	117.0	4.72	-901	-1.0
1350	1405	75	17	117.0	1.89	-942	-1.5
1250	1298	24	123	50.2	17.43	-816	0.5
1250	1298	51.5	123	85.1	17.43	-853	IW
1250	1298	80	100	124.0	12.80	-891	-0.5
1250	1298	80	64	124.0	6.96	-929	-1.0
1250	1298	80	26	124.0	2.70	-967	-1.5
1150	1183	17	119	41.4	16.59	-850	+0.5
1150	1183	45	119	76.5	16.59	-886	IW
1150	1183	75	107	117.0	14.13	-921	-0.5
1150	1183	75	60	117.0	6.40	-957	-1.0
1150	1183	75	20	117.0	2.10	-992	-1.5

Scale = arbitrary and unitless flowmeter reading

Tofs = Oxygen fugacity sensor themocouple temperature

Dfurn = Furnace display reading

NOTE: The e.m.f. (calculated) is measured in millivolts and the IW buffer is measured in log units relative to the buffer.

Table 7. Testing for a Leak in the Furnace

Leak Test: Part 1 (ratio of $CO:CO_2$ was 10:1)

Scale		ml/min		EMF	
CO	CO$_2$	CO	CO$_2$	(obs)	Δ log $f(O_2)$
10	32	33	3.3	-929	+0.52
40	65	70	7.0	-930	+0.51
60	82	97	9.7	-936	+0.42
80	98	124	2.4	-939	+0.38

The calculated e.m.f. value at these settings is -966 millivolts.
Operating temperature: 1150°C

Leak Test: Part 2 (ratio of $CO:CO_2$ was 20:1)

Scale		ml/min		EMF	
CO	CO$_2$	CO	CO$_2$	(obs)	Δ log $f(O_2)$
20	21.5	45	2.3	-957	+0.72
50	41	83	4.2	-965	+0.61
75	55.5	117	5.9	-969	+0.55

The calculated e.m.f. value at these settings is -1008 millivolts.
Operating temperature: 1150°C

Table 8. Calibration Using the Sample Rod Thermocouple and the Oxygen Fugacity Sensor

Temp°C		Scale		ml/min		EMF	IW
Tsr	Dfurn	CO	CO2	CO	CO2	(calc)	buffer
1350	1333	15	121	39.0	17.01	-780	+0.5
1350	1333	50	123	83.0	17.43	-821	IW
1350	1333	75	95	117.0	11.90	-861	-0.5
1350	1333	75	50	117.0	5.20	-901	-1.0
1350	1333	75	13	117.0	1.61	-942	-1.5
1250	1220	10	122	33.0	17.22	-815	+0.5
1250	1220	45	123	76.5	17.43	-854	IW
1250	1220	75	113	117.0	15.33	-891	-0.5
1250	1220	75	69	117.0	7.66	-929	-1.0
1250	1220	75	32	117.0	3.28	-967	-1.5
1150	1109	10	128	33.0	18.48	-850	+0.5
1150	1109	45	131	76.5	19.13	-886	IW
1150	1109	75	116	117.0	15.96	-921	-0.5
1150	1109	75	72	117.0	8.10	-957	-1.0
1150	1109	75	35	117.0	3.55	-992	-1.5

Table 9. Fe Foil Calibration of Iron-Wüstite Buffer

Temp°C		Scale		EMF	ml/min		EMF
Tsr	Dfurn	CO	CO2	(obs)	CO	CO2	(calc)
1350	1333	50	123	-817	83.0	17.43	-821
1250	1220	45	123	-850	76.5	17.43	-854
1150	1109	45	131	-882	76.5	19.13	-886

Table 10. Electron Microprobe Operating Conditions and Standards

El	Crystal	Bkg(1) (mm)	Bkg(2) (mm)	CF	Bsln (volts)	Win (volts)	Bias (volts)	Standard
Si	TAP	4.00	-4.00	0.179	0.5	2.0	1700	Plagioclase, Lake County
Ti	PET	1.50	-1.50	0.024	1.5	2.0	1600	Hornblende, Kakanui
Al	TAP	4.00	-5.00	0.144	0.5	2.0	1700	Anorthite, Great Sitkin Island
Cr	LIF	1.50	-1.50	0.385	0.8	2.0	1550	Chromite, Tiebaghi Mine
Fe	LIF	1.50	-1.50	0.503	0.8	2.0	1500	Fayalite (Fa 100)
Mn	LIF	4.00	-4.00	0.494	0.8	2.0	1550	Tephroite
Mg	TAP	4.00	-5.00	0.255	0.3	2.0	1700	Forsterite (Fo 100)
Ca	PET	1.50	-1.50	0.125	1.1	2.0	1600	Anorthite, Great Sitkin Island
Na	TAP	4.00	-4.00	0.014	0.4	1.5	1700	Plagioclase, Lake County
Ni	LIF	1.50	-1.50	0.003	0.5	1.0	1500	Olivine, San Carlos

El=element Bkg=Backgrounds CF=Correction factor Bsln=Baseline Win=Window

Table 11. Additonal Calibration Standards

- Anorthoclase, Kakanui
- Augite, Kakanui
- Fayalite, Rockport

- Hypersthene, Johnstown meteorite
- Olivine, Springwater meteorite
- Orthopyroxene, Tatahouine meteorite

Table 12. Experimental Parameters and Resulting Phase Assemblages

A. Series I Experiments

Synthetic Murchison Fe/Mn 85

Temp (°C)	Time (hrs)	Type	Exp #	Phases
1180	40.5	cooling	M 09	glss, oliv, pig, spin, mtl
1180	39	heating	M 13	glss, oliv, pig, spin, mtl
1253	47	heating	M 03	glss, oliv, pig, spin, mtl
1300	21	heating	M 04	glss, oliv, spin, mtl
1325	16.5	cooling	M 08	glss, oliv, mtl
1580	1	heating	M 17	glss
1580	10	heating	M 19	glss

Synthetic Murchison Fe/Mn 65

Temp (°C)	Time (hrs)	Type	Exp #	Phases
1180	40.5	cooling	M 10	glss, oliv, pig, spin, mtl
1180	39	heating	M 14	glss, oliv, pig, spin, mtl
1325	16.5	cooling	M 07	glss, oliv, mtl

Synthetic Murchison Fe/Mn 45

Temp (°C)	Time (hrs)	Type	Exp #	Phases
1180	40.5	cooling	M 11	glss, oliv, pig, spin, mtl
1325	16.5	cooling	M 06	glss, oliv, mtl

Synthetic Murchison Fe/Mn 20

Temp (°C)	Time (hrs)	Type	Exp #	Phases
1180	40.5	cooling	M 12	glss, oliv, pig, spin, mtl
1325	16.5	cooling	M 05	glss, oliv, mtl

Table 12. (continued)

B. Series II Experiments

Synthetic Murchison

Temp (°C)	Time (hrs)	Type	IW	Exp#	Phases
1180	135.5	heating	-0.5	M 29	glss, oliv, pig, spin, mtl
1180	165	cooling	-0.5	M 35	glss, oliv, pig, spin, mtl
1180	144.5	heating	-1.0	M 61	glss, oliv, pig, spin, mtl
1180	142	heating	-1.5	M 30	glss, oliv, pig, spin, mtl
1180	164	heating	-1.5	M 47	glss, oliv, pig, spin, mtl
1200	66.5	heating	-0.5	M 26	glss, oliv, pig, spin, mtl
1200	161	cooling	-0.5	M 41	glss, oliv, pig, spin, mtl
1200	69	heating	-1.5	M 27	glss, oliv, pig, spin, mtl
1200	165	cooling	-1.5	M 39	glss, oliv, pig, spin, mtl
1300	112.5	heating	-0.5	M 43	glss, oliv, mtl
1300	118	heating	-1.5	M 45	glss, oliv, pig, mtl
1400	116	heating	-0.5	M 49	glss, oliv, mtl
1400	91.5	heating	-1.5	M 51	glss, oliv, pig, mtl

Synthetic H-CM

Temp (°C)	Time (hrs)	Type	IW	Exp#	Phases
1180	144.5	heating	-0.5	H 33	glss, oliv, pig, spin, mtl
1180	165	cooling	-0.5	H 34	glss, oliv, pig, spin, mtl
1180	144.5	heating	-1.0	H 60	glss, oliv, pig, spin, mtl
1180	164	heating	-1.5	H 46	glss, oliv, pig, spin, mtl
1200	144	heating	-0.5	H 31	glss, oliv, pig, spin, mtl
1200	161	cooling	-0.5	H 40	glss, oliv, pig, spin, mtl
1200	139	heating	-1.5	H 32	glss, oliv, pig, spin, mtl
1300	112.5	heating	-0.5	H 42	glss, oliv, pig, mtl
1300	118	heating	-1.5	H 44	glss, oliv, pig, mtl
1400	116	heating	-0.5	H 48	glss, oliv, mtl
1400	91.5	heating	-1.5	H 50	glss, oliv, pig, mtl

C. Series III Experiments

Natural Murchison

Temp (°C)	Time (hrs)	Type	IW	Exp#	
1180	166	heating	-0.5	NM 55	glss, oliv, spin, mtl
1180	166.5	heating	-1.0	NM 59	glss, oliv, pig, spin, mtl
1180	169.5	heating	-1.5	NM 57	glss, oliv, pig, spin, mtl
1400	67.5	heating	-1.0	NM 63	glss, oliv, mtl

70% Allegan-30% Murchison

Temp (°C)	Time (hrs)	Type	IW	Exp#	
1180	166	heating	-0.5	AM 54	glss, oliv, pig, spin, mtl
1180	166.5	heating	-1.0	AM 58	glss, oliv, pig, spin, mtl
1180	169.5	heating	-1.5	AM 56	glss, oliv, pig, spin, mtl
1400	67.5	heating	-1.0	AM 62	glss, oliv, mtl

Table 13. Experimental Silicate Compositions

Series II Experiments

A. Synthetic Murchison

T(°C)	IW -0.5				IW -1.0	IW -1.5				Eucrite
	1180	1200	1300	1400	1180	1180	1200	1300	1400	Avg.*
Glass										
SiO2	50.18	49.58	47.92	48.53	50.53	45.20	52.43	53.52	54.89	49.15
TiO2	0.79	0.70	0.53	0.44	0.85	0.11	0.95	0.73	0.51	0.64
Al2O3	11.15	9.80	6.94	6.34	12.69	31.68	13.82	10.05	7.48	12.74
Cr2O3	0.28	0.33	0.77	0.87	0.41	0.28	0.41	0.83	0.91	0.34
FeO	19.71	21.54	24.94	25.54	16.07	1.93	11.68	12.32	6.17	17.96
MnO	0.32	0.36	0.60	0.65	0.40	0.11	0.50	0.73	0.72	0.52
MgO	6.05	7.07	11.31	12.09	6.31	2.60	8.42	12.39	20.97	6.96
CaO	10.25	9.50	6.13	6.31	10.16	16.84	10.63	9.22	7.17	10.28
Na2O	0.35	0.42	0.11	0.02	0.83	0.41	0.57	0.04	0.02	0.39
NiO	0.04	0.08	0.05	0.04	0.06	0.06	0.04	0.05	0.03	0.01
Total	99.08	99.39	99.30	100.83	98.31	99.17	99.47	99.88	98.90	98.99
Fe/Mn	60.93	59.82	41.11	38.90	40.95	16.71	22.86	16.73	8.46	34.25
Fe/(Fe+Mg)x100	64.15	62.44	54.60	53.49	58.02	29.92	42.88	35.18	13.97	59.10
Olivine										
SiO2	36.98	37.16	37.85	38.34	37.24	40.20	39.32	40.10	41.57	
TiO2	0.03	0.00	0.01	0.02	0.01	0.09	0.03	0.01	0.03	
Al2O3	0.05	0.06	0.04	0.04	0.05	0.23	0.08	0.08	0.02	
Cr2O3	0.27	0.33	0.56	0.46	0.38	0.77	0.48	0.61	0.53	
FeO	31.42	31.20	27.17	20.79	26.64	12.68	19.13	13.33	5.41	
MnO	0.40	0.43	0.52	0.43	0.45	0.52	0.63	0.60	0.47	
MgO	30.44	31.03	34.39	40.20	34.39	45.36	40.73	45.17	51.98	
CaO	0.34	0.33	0.21	0.16	0.29	0.29	0.29	0.25	0.12	
Na2O	0.01	0.00	0.00	0.01	0.02	0.01	0.00	0.00	0.02	
NiO	0.18	0.15	0.12	0.05	0.09	0.04	0.02	0.04	0.00	
Total	100.14	100.72	100.88	100.50	99.57	100.20	100.71	100.20	100.09	
Fe/Mn	77.21	72.88	51.55	48.11	59.01	24.28	29.93	21.91	11.37	
Fe/(Fe+Mg)x100	36.50	35.89	30.52	22.38	30.13	13.49	20.71	14.11	5.49	
Low Calcium Pyroxene (pigeonite)										
SiO2	54.06	53.89			53.35	56.91	55.53	57.00	56.94	
TiO2	0.08	0.07			0.09	0.07	0.15	0.07	0.03	
Al2O3	0.67	0.47			0.80	0.10	0.87	0.49	0.24	
Cr2O3	0.57	0.60			0.73	0.74	0.84	0.79	0.52	
FeO	18.90	18.94			16.51	9.37	14.48	9.32	3.86	
MnO	0.37	0.36			0.43	1.49	0.53	0.51	0.32	
MgO	22.56	23.45			24.20	27.58	26.28	31.52	36.18	
CaO	2.80	2.40			2.63	4.40	2.30	0.73	0.25	
Na2O	0.02	0.03			0.03	0.02	0.02	0.00	0.01	
NiO	0.11	0.07			0.04	0.00	0.02	0.04	0.06	
Total	100.15	100.29			98.81	100.67	101.02	100.48	98.43	
Fe/Mn	51.64	51.86			37.91	6.21	27.10	18.19	11.92	
Fe/(Fe+Mg)x100	31.78	31.00			27.48	15.61	23.41	14.11	5.62	

Table 13. Series II Experiments (continued)

B. Synthetic H-CM

T(°C)	IW -0.5				IW -1.0	IW -1.5				Eucrite
	1180	1200	1300	1400	1180	1180	1200	1300	1400	Avg.*
Glass										
SiO2	51.27	51.00	52.30	53.31	51.25	50.16	55.69	53.07	54.86	49.15
TiO2	0.54	0.58	0.42	0.19	0.60	0.69	0.57	0.47	0.34	0.64
Al2O3	12.35	12.97	8.32	4.09	13.86	17.28	14.95	9.87	8.60	12.74
Cr2O3	0.41	0.25	0.75	0.89	0.40	0.41	0.48	0.91	0.94	0.34
FeO	16.70	16.43	20.99	18.08	14.31	8.86	8.75	13.02	3.22	17.96
MnO	0.53	0.53	0.72	0.62	0.37	0.43	0.46	0.71	0.68	0.52
MgO	7.64	7.12	8.38	19.38	6.42	8.39	8.32	12.83	21.71	6.96
CaO	8.98	9.14	8.04	3.67	9.32	11.67	10.90	8.79	7.78	10.28
Na2O	0.54	0.48	0.16	0.04	0.99	0.35	0.26	0.05	0.02	0.39
Total	98.98	98.49	100.07	100.33	97.54	98.24	100.37	99.71	98.18	98.98
Fe/Mn	31.12	31.04	28.95	28.97	38.15	20.40	19.42	18.15	4.65	34.25
Fe/(Fe+Mg)x100	54.13	55.48	57.42	33.95	54.75	36.53	36.59	35.73	7.57	59.10
Olivine										
SiO2	38.13	38.04	39.19	39.71	37.42	39.28	40.01	40.06	40.16	
TiO2	0.02	0.01	0.00	0.01	0.02	0.04	0.02	0.01	0.01	
Al2O3	0.05	0.03	0.04	0.03	0.03	0.04	0.05	0.04	0.03	
Cr2O3	0.30	0.40	0.66	0.53	0.36	0.43	0.50	0.68	0.58	
FeO	26.29	24.55	21.55	15.51	24.57	14.45	13.73	14.26	3.14	
MnO	0.47	0.58	0.56	0.39	0.46	0.50	0.57	0.60	0.52	
MgO	35.25	35.83	38.88	43.97	35.82	45.36	45.46	45.05	53.39	
CaO	0.24	0.22	0.18	0.07	0.25	0.23	0.22	0.21	0.11	
Na2O	0.00	0.01	0.00	0.00	0.01	0.00	0.00	0.00	0.01	
Total	100.74	99.67	101.07	100.26	98.95	100.35	100.55	100.91	97.94	
Fe/Mn	55.54	41.97	37.79	38.93	53.87	28.25	24.09	23.48	5.96	
Fe/(Fe+Mg)x100	29.42	27.58	23.57	16.45	27.64	15.08	14.40	14.98	3.18	
Low Calcium Pyroxene (pigeonite)										
SiO2	54.89	54.81	56.27		53.05	54.56	56.59	56.74	57.15	
TiO2	0.07	0.06	0.03		0.08	0.09	0.10	0.05	0.06	
Al2O3	0.72	0.61	0.42		0.68	0.68	1.04	0.50	0.22	
Cr2O3	0.72	0.63	0.87		0.66	0.78	0.98	0.89	0.63	
FeO	17.55	15.75	13.27		15.25	10.22	9.57	10.62	5.28	
MnO	0.43	0.57	0.47		0.44	0.48	0.58	0.49	0.35	
MgO	24.33	25.49	22.89		26.02	29.00	30.31	30.70	34.68	
CaO	2.19	1.81	0.54		2.07	2.61	1.86	0.66	0.21	
Na2O	0.01	0.03	0.01		0.04	0.03	0.03	0.00	0.00	
Total	100.91	99.77	100.78		98.29	98.44	101.07	100.65	98.74	
Fe/Mn	40.12	27.96	28.05		36.32	21.17	16.31	21.68	15.19	
Fe/(Fe+Mg)x100	28.63	25.50	20.34		24.58	16.34	14.92	16.14	7.84	

Table 13. (continued)

Series III Experiments

C. Natural Murchison

T(°C)	1180	1180	1180	1400	Eucrite
IW-X	-0.5	-1.0	-1.5	-0.5	Avg.*
Glass					
SiO2	43.45	48.29	52.45	53.96	49.15
TiO2	0.82	0.62	0.59	0.35	0.64
Al2O3	14.65	13.32	14.56	7.47	12.74
Cr2O3	0.14	0.37	0.40	0.73	0.34
FeO	20.34	17.60	11.76	13.33	17.96
MnO	0.23	0.23	0.29	0.74	0.52
MgO	3.66	5.46	7.07	16.08	6.96
CaO	12.97	10.78	10.16	5.69	10.28
Na2O	0.44	0.75	0.87	0.05	0.39
NiO	0.10	0.09	0.06	0.02	0.01
Total	96.82	97.54	98.22	98.42	98.99
Fe/Mn	87.32	75.55	40.04	17.79	34.25
Fe/(Fe+Mg)x100	75.06	63.85	47.69	31.19	59.10
Olivine					
SiO2	35.22	37.51	38.54	40.11	
TiO2	0.01	0.01	0.02	0.01	
Al2O3	0.13	0.10	0.06	0.07	
Cr2O3	0.18	0.33	0.46	0.45	
FeO	33.22	28.79	19.85	11.45	
MnO	0.32	0.32	0.34	0.47	
MgO	28.86	33.12	40.33	47.12	
CaO	0.52	0.33	0.25	0.14	
Na2O	0.01	0.01	0.00	0.01	
NiO	0.17	0.15	0.06	0.05	
Total	98.64	100.67	99.93	99.88	
Fe/Mn	102.50	88.83	57.64	24.05	
Fe/(Fe+Mg)x100	39.09	32.66	21.56	11.94	
Low Calcium Pyroxene (pigeonite)					
SiO2		52.69	54.80		
TiO2		0.07	0.10		
Al2O3		0.89	0.96		
Cr2O3		0.57	0.69		
FeO		18.62	13.22		
MnO		0.32	0.36		
MgO		24.47	27.28		
CaO		1.90	2.18		
Na2O		0.03	0.04		
NiO		0.06	0.06		
Total		99.62	99.68		
Fe/Mn		57.45	37.13		
Fe/(Fe+Mg)x100		29.76	21.26		

Table 13. Series III Experiments (continued)

D. Allegan (70%) - Murchison (30%)

T(°C)	1180	1180	1180	1400	Eucrite
IW-X	-0.5	-1.0	-1.5	-0.5	Avg.*
Glass					
SiO2	52.43	51.05	52.68	53.73	49.15
TiO2	0.50	0.54	0.59	0.33	0.64
Al2O3	10.67	12.07	15.57	7.23	12.74
Cr2O3	0.29	0.31	0.35	0.76	0.34
FeO	17.78	18.21	9.77	19.76	17.96
MnO	0.26	0.31	0.30	0.63	0.52
MgO	5.68	5.11	7.76	9.66	6.96
CaO	8.31	8.98	9.79	5.68	10.28
Na2O	1.21	1.08	0.96	0.05	0.39
NiO	0.05	0.12	0.02	0.06	0.01
Total	97.17	97.78	97.79	97.89	98.99
Fe/Mn	67.52	58.00	32.16	30.97	34.25
Fe/(Fe+Mg)x100	63.12	65.90	40.87	52.53	59.10
Olivine					
SiO2	37.24	36.99	39.64	38.82	
TiO2	0.02	0.02	0.01	0.01	
Al2O3	0.05	0.07	0.07	0.04	
Cr2O3	0.31	0.48	0.39	0.47	
FeO	29.20	29.10	16.37	17.28	
MnO	0.33	0.38	0.40	0.39	
MgO	32.37	32.64	43.35	42.43	
CaO	0.27	0.30	0.23	0.12	
Na2O	0.01	0.02	0.00	0.00	
NiO	0.21	0.04	0.07	0.15	
Total	100.01	100.03	100.55	99.73	
Fe/Mn	87.37	75.61	40.41	43.75	
Fe/(Fe+Mg)x100	33.47	33.19	17.41	18.52	
Low Calcium Pyroxene (pigeonite)					
SiO2	53.59	53.41	55.65		
TiO2	0.07	0.06	0.10		
Al2O3	0.73	0.80	0.83		
Cr2O3	0.65	0.78	0.79		
FeO	17.85	17.88	12.80		
MnO	0.32	0.31	0.37		
MgO	24.20	24.48	28.29		
CaO	1.75	1.76	1.64		
Na2O	0.03	0.03	0.04		
NiO	0.13	0.05	0.03		
Total	99.32	99.58	100.55		
Fe/Mn	54.80	58.79	34.64		
Fe/(Fe+Mg)x100	29.11	28.91	20.14		

* Eucrite Avg. based on analyses from JAROSEWICH (1990)

Table 14. Mineral Normative Calculations of the Experimental Glass Compositions

Synthetic Murchison

Temp°C	IW-0.5				IW-1.0	IW-1.5				Eucrite
	1180	1200	1300	1400	1180	1180	1200	1300	1400	Avg.*
Albite	3.34	4.00	1.04	0.19	7.88	3.71	5.26	0.37	0.18	
Anorthite	30.67	26.37	19.50	17.91	32.67	84.10	36.15	27.77	20.03	
Plagioclase	34.01	30.37	20.55	18.10	40.55	87.81	41.41	28.14	20.20	43.3±2.2
Clinopyrox.	18.71	18.91	10.12	11.73	16.50	0.00	14.47	15.09	12.02	
Orthopyrox.	39.79	45.71	65.93	65.39	35.27	9.84	34.11	45.68	59.57	
Pyroxene	58.50	64.62	76.05	77.12	51.76	9.84	48.58	60.77	71.60	51.3±2.5
Ilmenite	1.17	1.03	0.78	0.64	1.25	0.15	1.36	1.04	0.70	0.8±0.4
Chromite	0.44	0.51	1.19	1.33	0.63	0.41	0.62	1.24	1.31	0.2±0.2
Quartz	5.88	3.46	0.00	0.00	5.80	1.78	8.03	8.82	6.19	4.1±1.5
Olivine	0.00	0.00	1.43	2.82	0.00	0.00	0.00	0.00	0.00	

Synthetic H-CM

Temp°C	IW-0.5				IW-1.0	IW-1.5				Eucrite
	1180	1200	1300	1400	1180	1180	1200	1300	1400	Avg.*
Albite	5.08	4.54	1.51	0.36	9.40	3.24	2.37	0.46	0.18	
Anorthite	32.78	35.03	23.14	11.03	35.29	46.95	40.21	27.23	22.95	
Plagioclase	37.86	39.57	24.65	11.39	44.69	50.18	42.58	27.69	23.12	43.3±2.2
Clinopyrox.	11.13	10.21	15.07	5.81	10.88	10.15	11.73	13.78	11.95	
Orthopyrox.	43.11	42.08	50.45	78.36	35.86	32.01	30.41	48.90	56.99	
Pyroxene	54.24	52.29	65.52	84.17	46.74	42.16	42.14	62.68	68.94	51.2±2.5
Ilmenite	0.79	0.85	0.62	0.27	0.88	0.99	0.81	0.67	0.46	0.8±0.4
Chromite	0.63	0.39	1.16	1.31	0.62	0.62	0.71	1.36	1.35	0.2±0.2
Quartz	6.49	6.90	8.05	2.87	7.07	6.05	13.76	7.60	6.12	4.1±1.5
Olivine	0.00	0.00	0.00	0.00	0.00	0.00	0.00	0.00	0.00	

Table 14. (continued)

Natural Murchison

Temp°C	1180	1180	1180	1400	Eucrite
IW-x	-0.5	-1.0	-1.5	-0.5	Avg.*
Albite	4.31	7.21	8.14	0.46	
Anorthite	41.51	35.33	37.35	20.62	
Plagioclase	45.82	42.54	45.54	21.08	43.3±2.2
Clinopyrox.	23.02	17.57	12.16	6.60	
Orthopyrox.	20.15	35.45	32.27	62.84	
Pyroxene	43.17	53.02	44.43	69.44	51.2±2.5
Ilmenite	1.25	0.92	0.86	0.50	0.8±0.4
Chromite	0.22	0.58	0.61	1.09	0.2±0.2
Quartz	0.00	2.94	8.60	7.88	4.1±1.5
Olivine	9.54	0.00	0.00	0.00	

Allegan (70%) - Murchison (30%)

Temp°C	1180	1180	1180	1400	Eucrite
IW-x	-0.5	-1.0	-1.5	-0.5	Avg.*
Albite	11.68	10.39	8.94	0.48	
Anorthite	25.47	30.10	39.60	20.90	
Plagioclase	37.15	40.49	48.54	21.39	43.3±2.2
Clinopyrox.	15.09	14.12	8.62	7.44	
Orthopyrox.	38.17	37.52	32.72	57.05	
Pyroxene	53.26	51.64	41.34	64.49	51.2±2.5
Ilmenite	0.75	0.81	0.85	0.49	0.8±0.4
Chromite	0.46	0.49	0.53	1.49	0.2±0.2
Quartz	8.39	6.58	8.74	12.44	4.1±1.5
Olivine	0.00	0.00	0.00	0.00	

* from DELANEY *et al* (1984)

Table 15. Modal Analysis of the Series III Experiments

Natural Murchison

Temp°C	1180	1180	1180	1400
IW-x	-0.5	-1.0	-1.5	-0.5
Glass	19	19	19	38
Olivine	76	72	57	42
Pyroxene	0	1	9	0
Fe-metal	5	8	16	20
Chromite	<1	<1	<1	0

Allegan (70%) - Murchison (30%)

Temp°C	1180	1180	1180	1400
IW-x	-0.5	-1.0	-1.5	-0.5
Glass	19	18	17	35
Olivine	64	57	46	48
Pyroxene	6	12	16	0
Fe-metal	10	12	20	17
Chromite	<1	<1	<1	0

Note: Fe-metal includes all FeS.

Figure 1.

Figure 2.

Upper Cooling Head

Lower Cooling Head

Figure 3.

Figure 4.

sample rod
support wires

thin Pt wires

Au (or Pd) wire
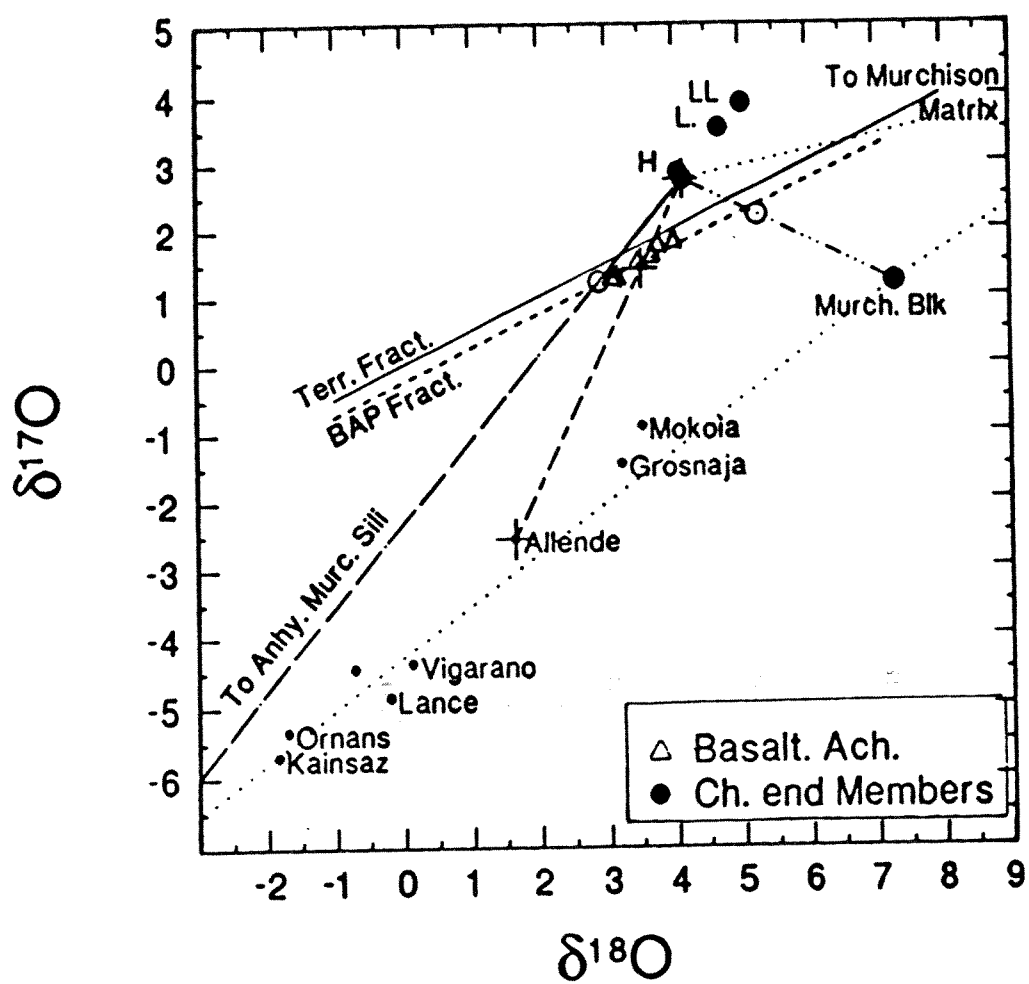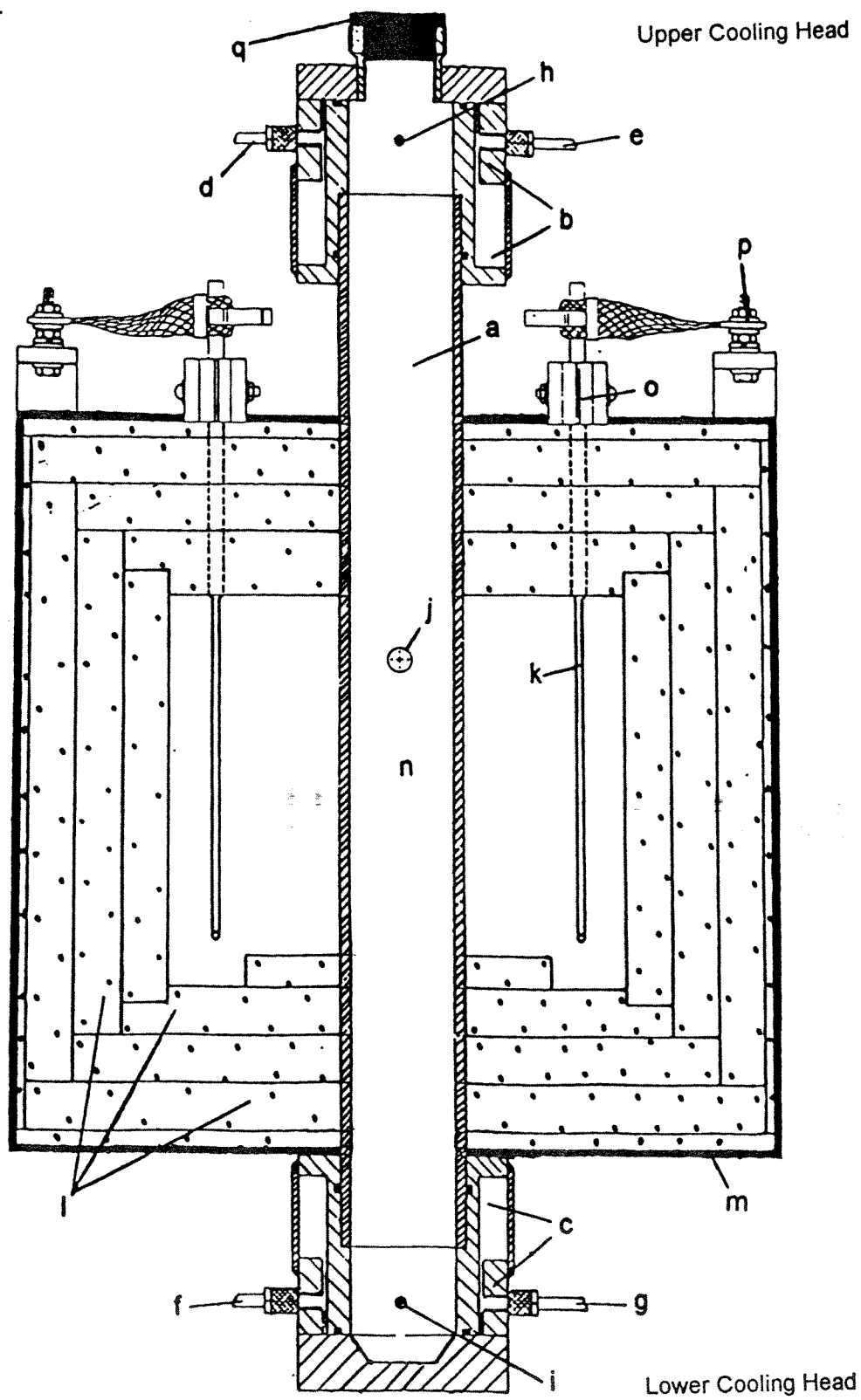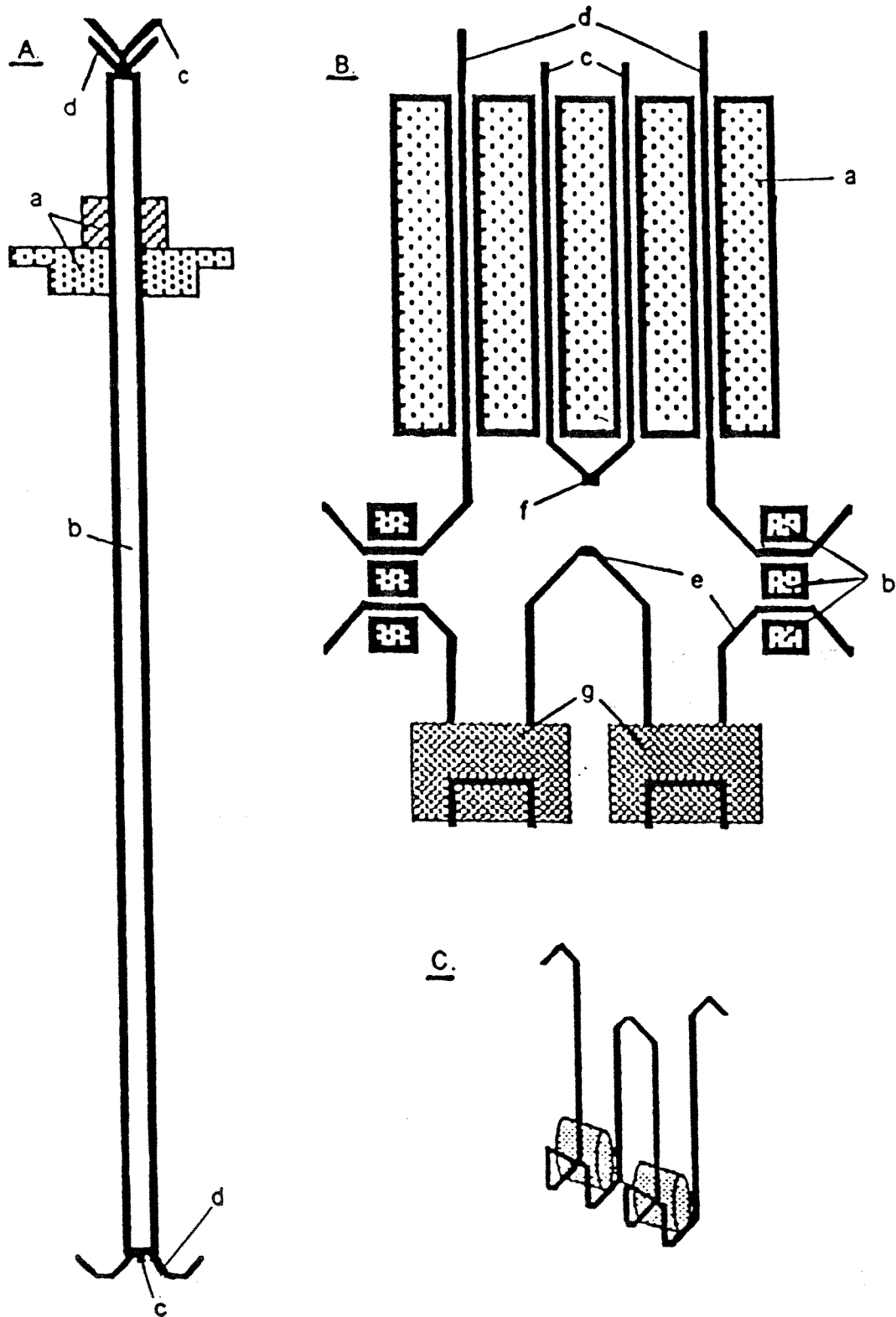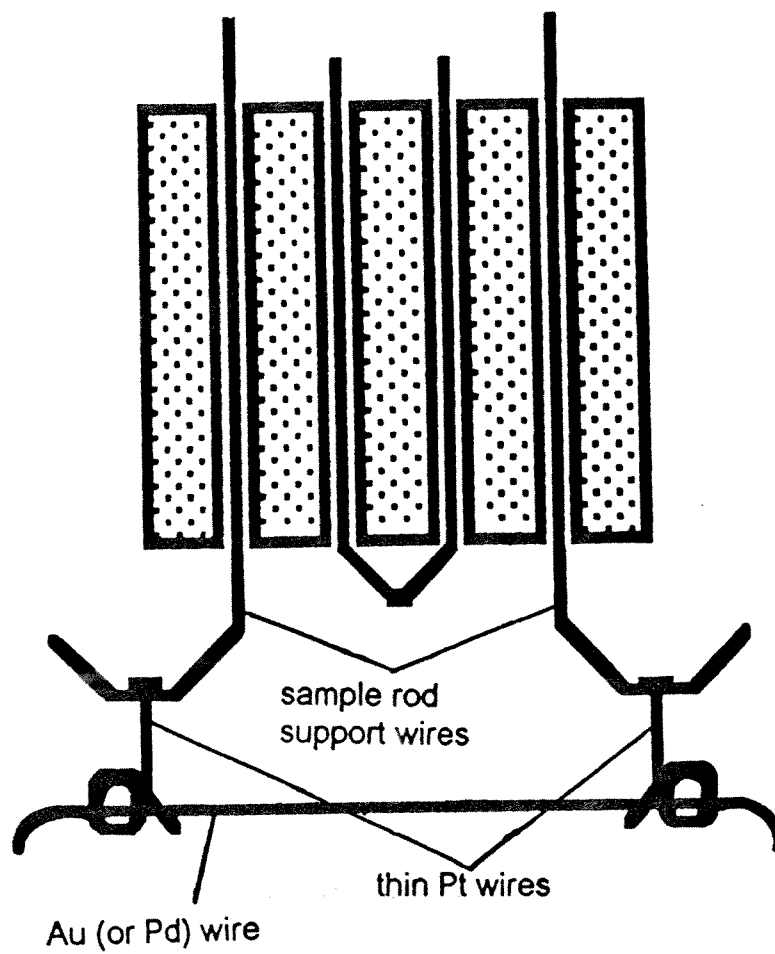
Figure 5.

Figure 6.

Figure 7A.

CO₂ inlet

CO inlet

Coiled Gas Line
To Furnace Inlet

Figure 7B.

To Furnace Inlet

In line Union connector 1/4 inch

3/16 inch outer diameter inner tube

Thin wall (0.014 inch) 1/4 inch brass tube

Union T-connector 1/4 inch tubing

CO₂ Inlet

CO Inlet

1/4 inch outer diameter outer tube with 0.028 inch wall
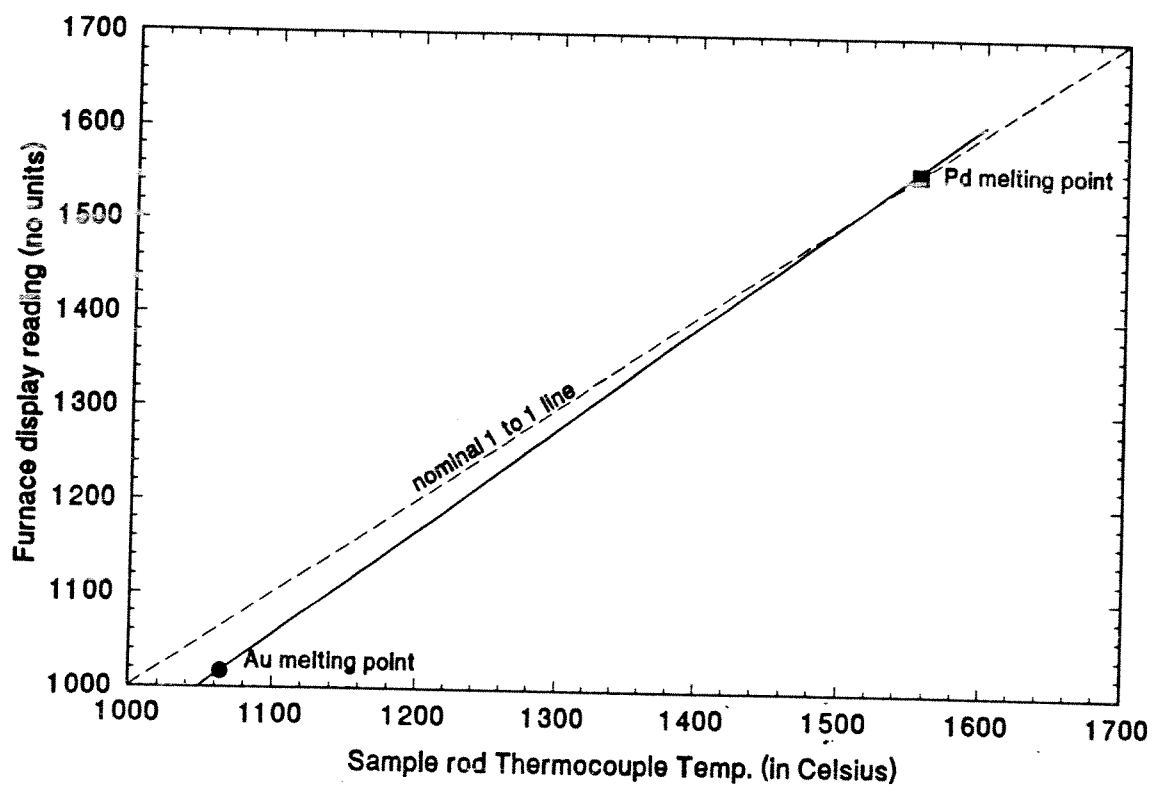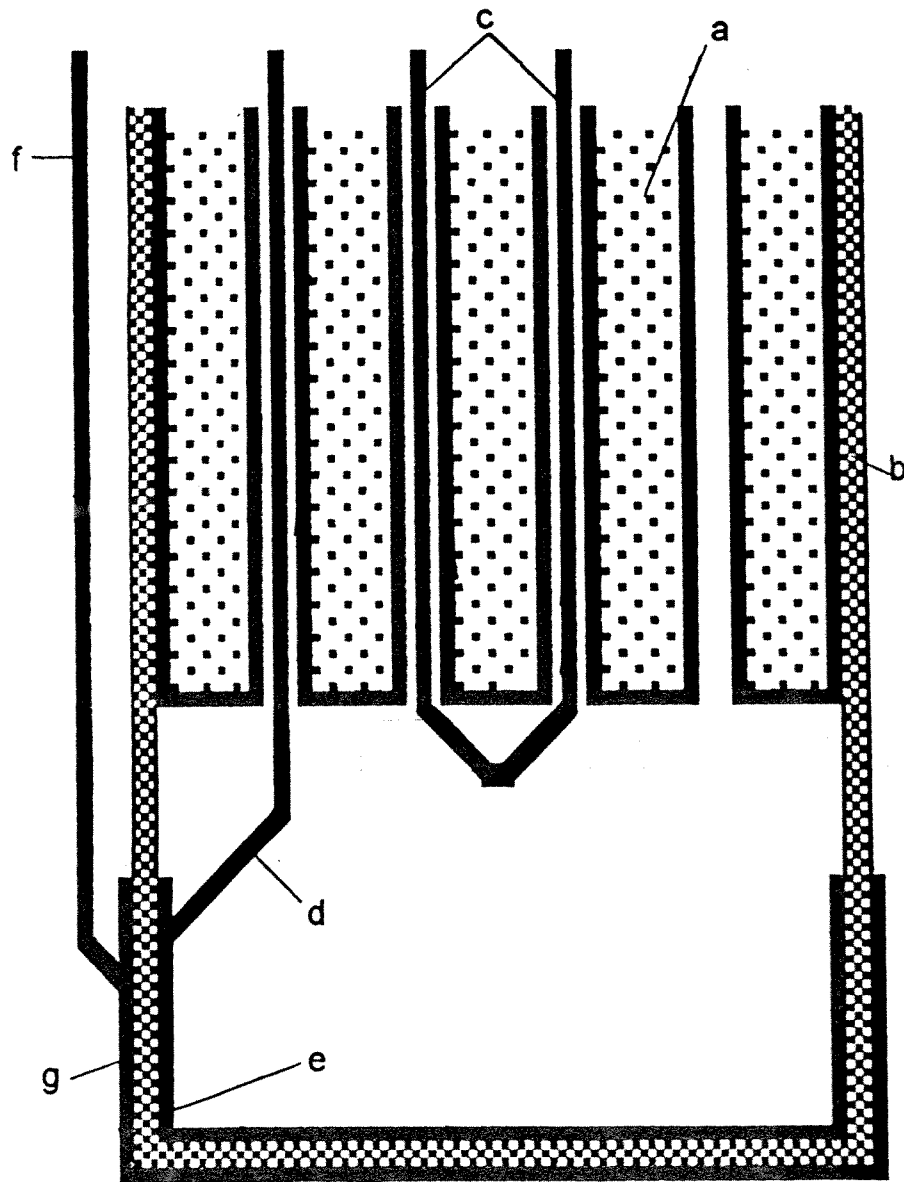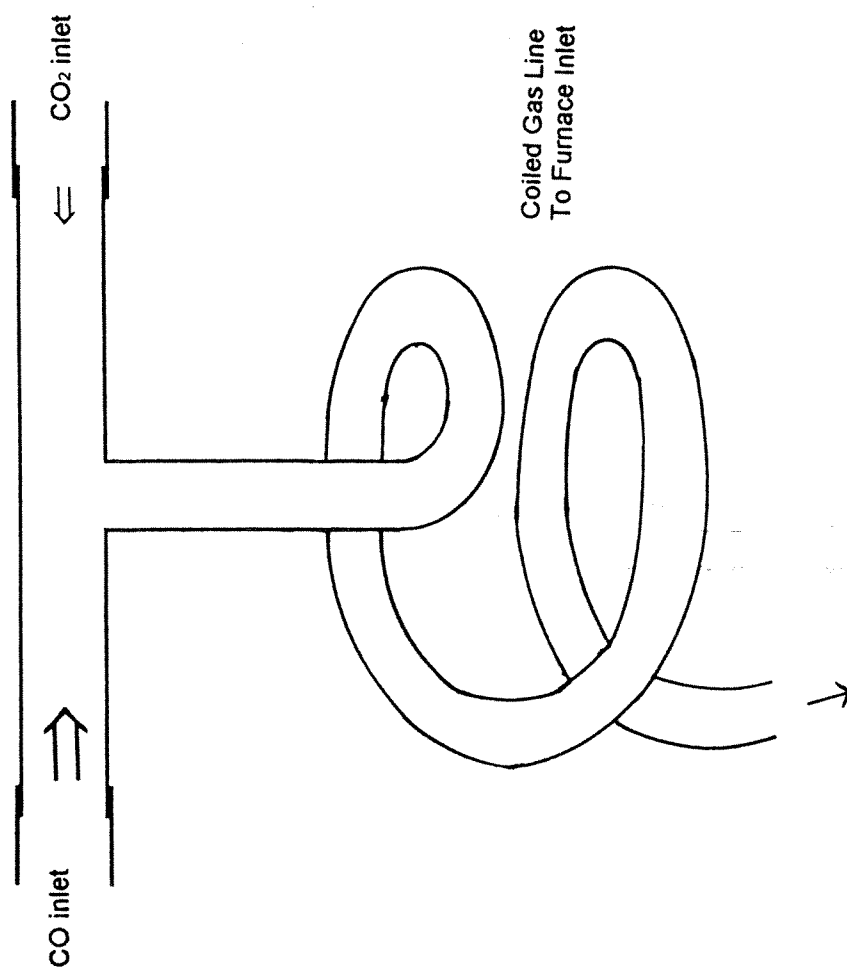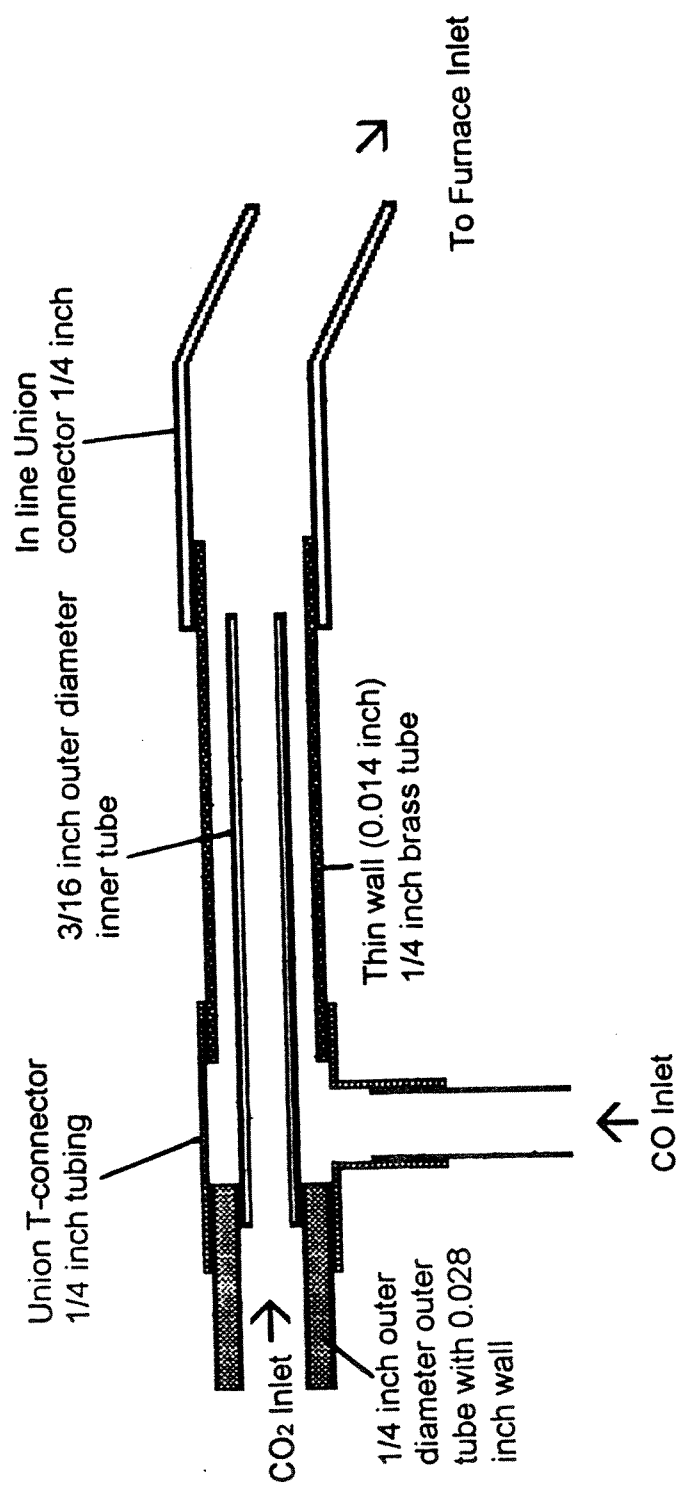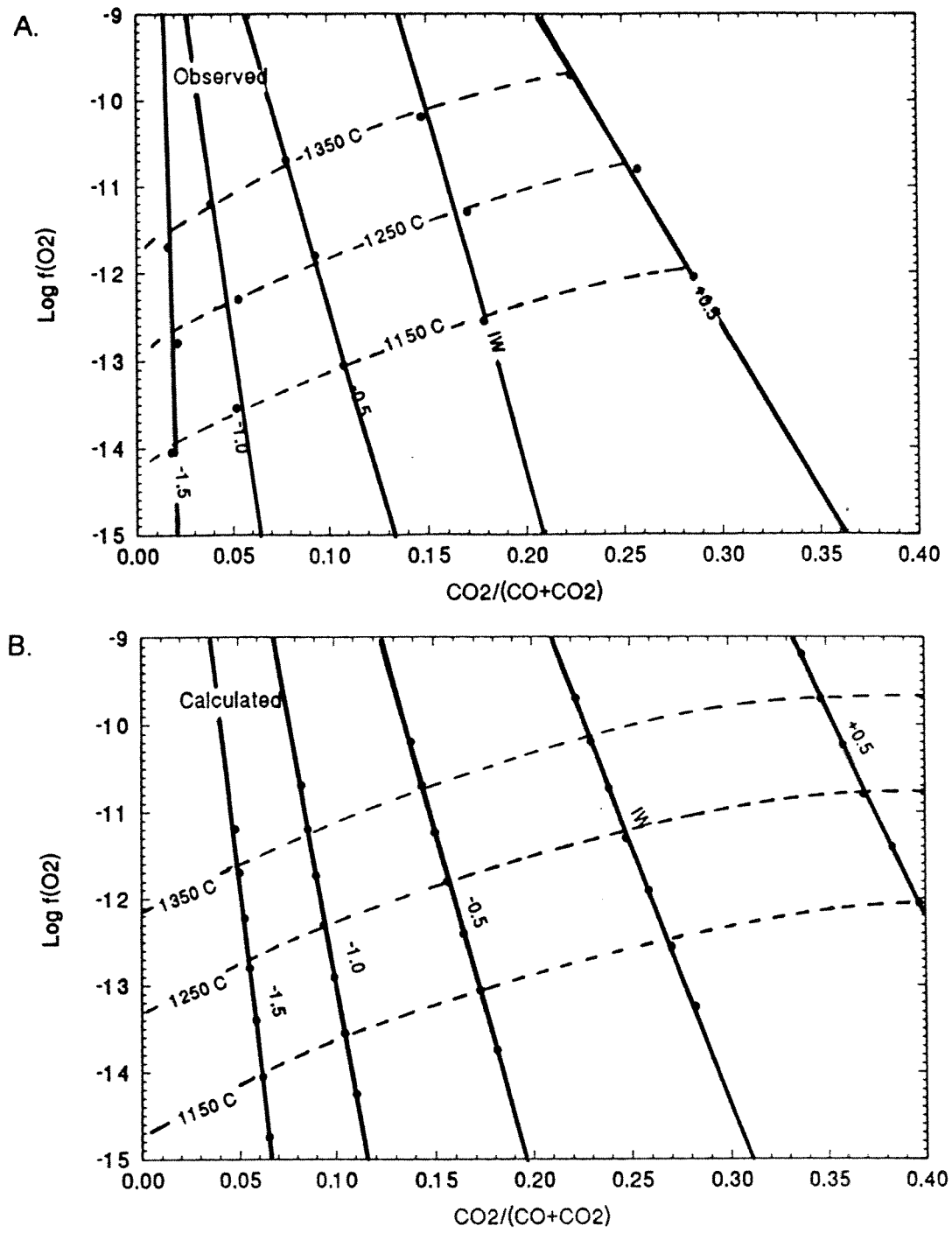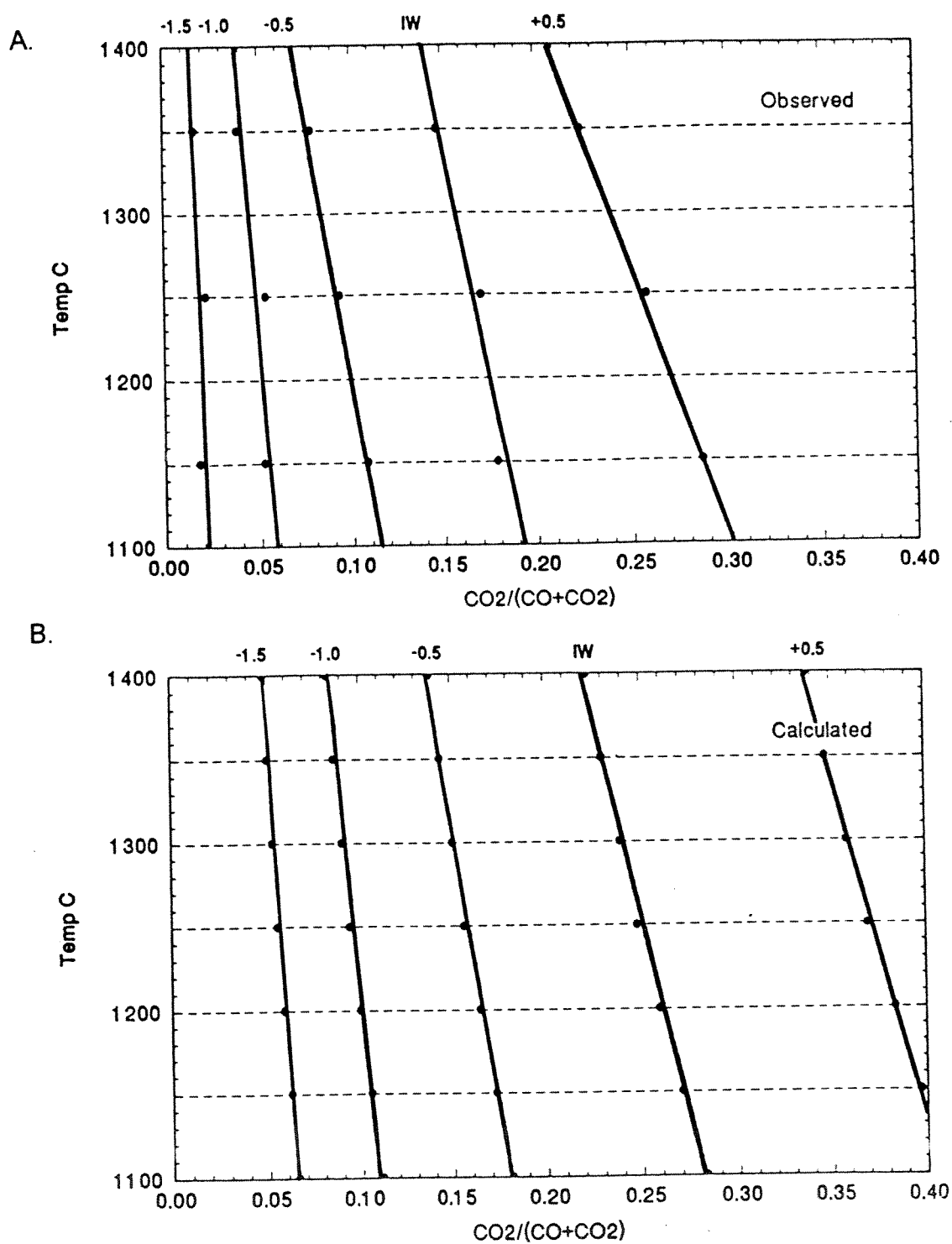
Figure 8.

Figure 9.

Figure 10.
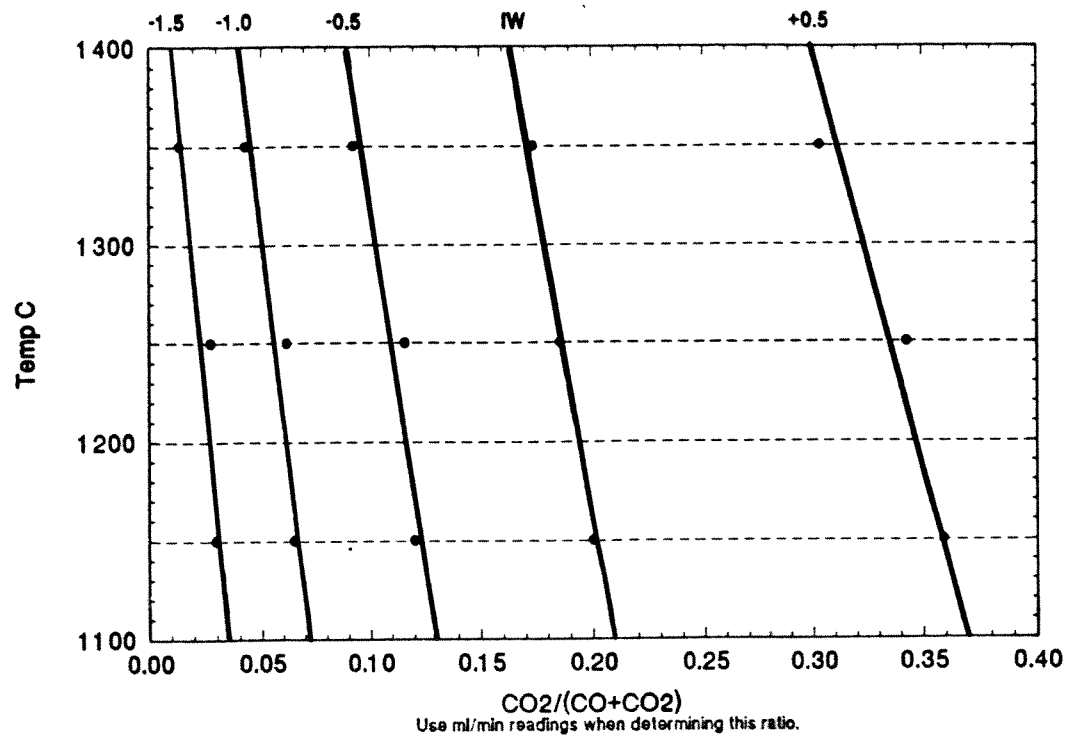
Figure 11.
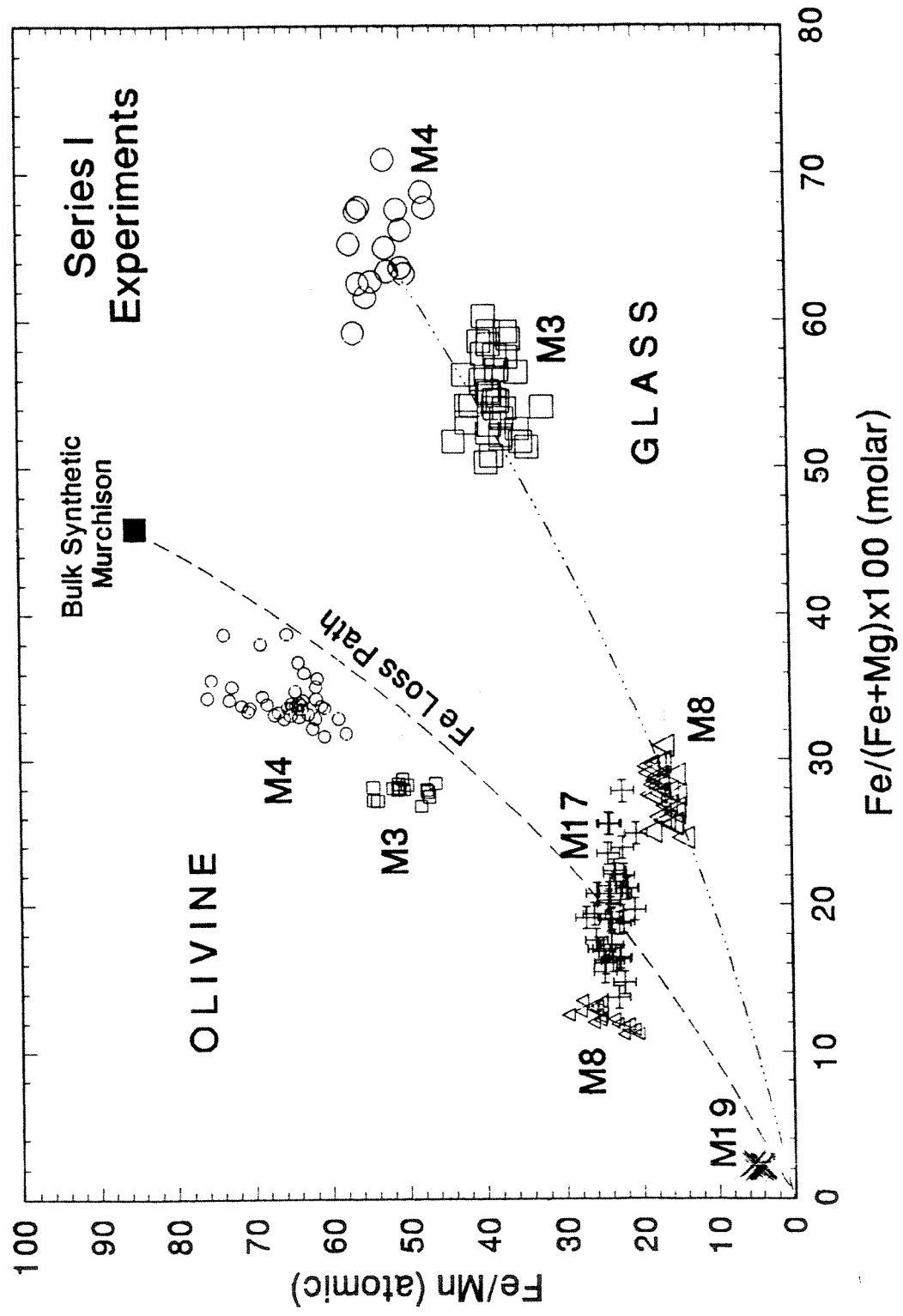
Figure 12.
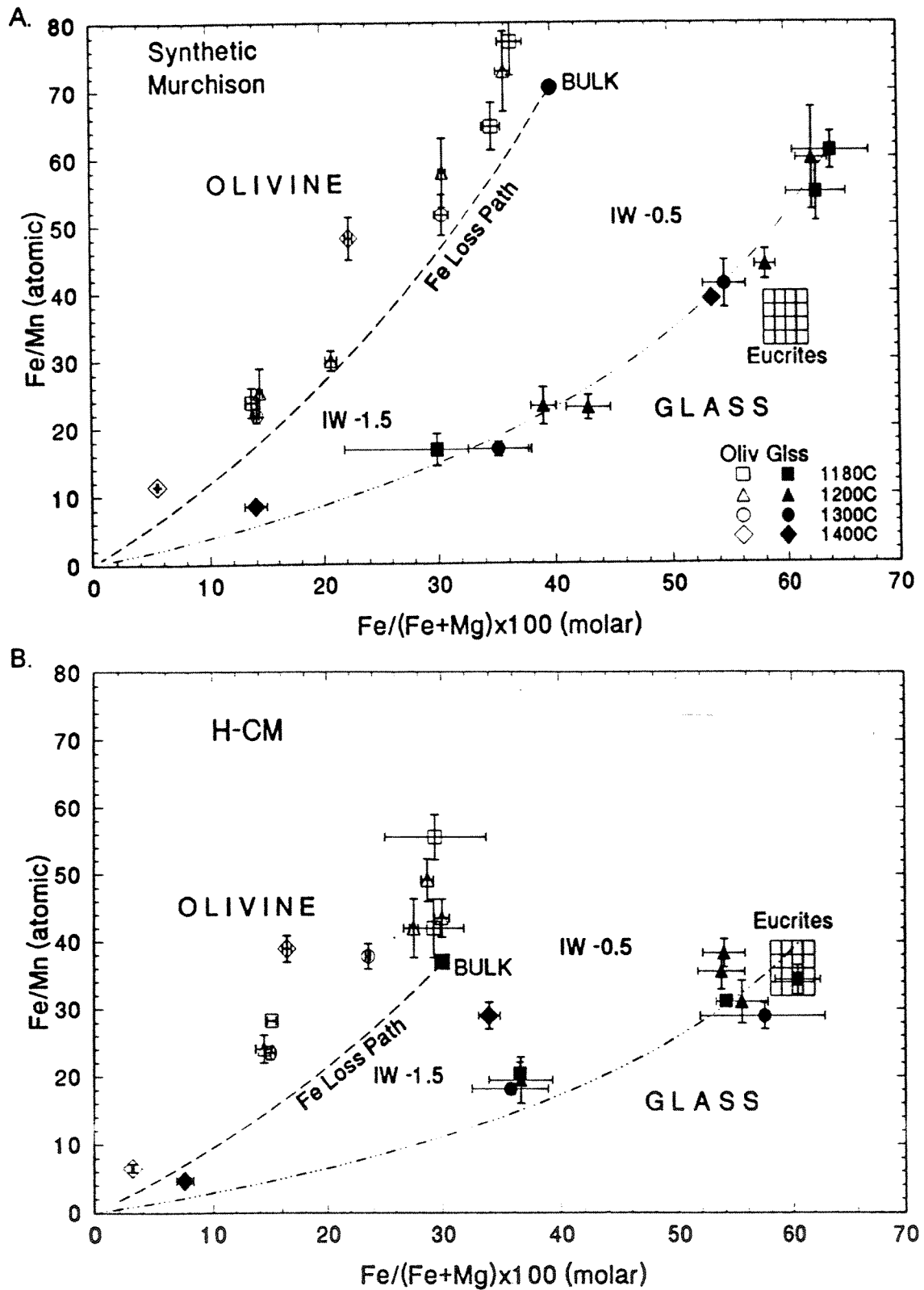
Figure 13.

Figure 14.
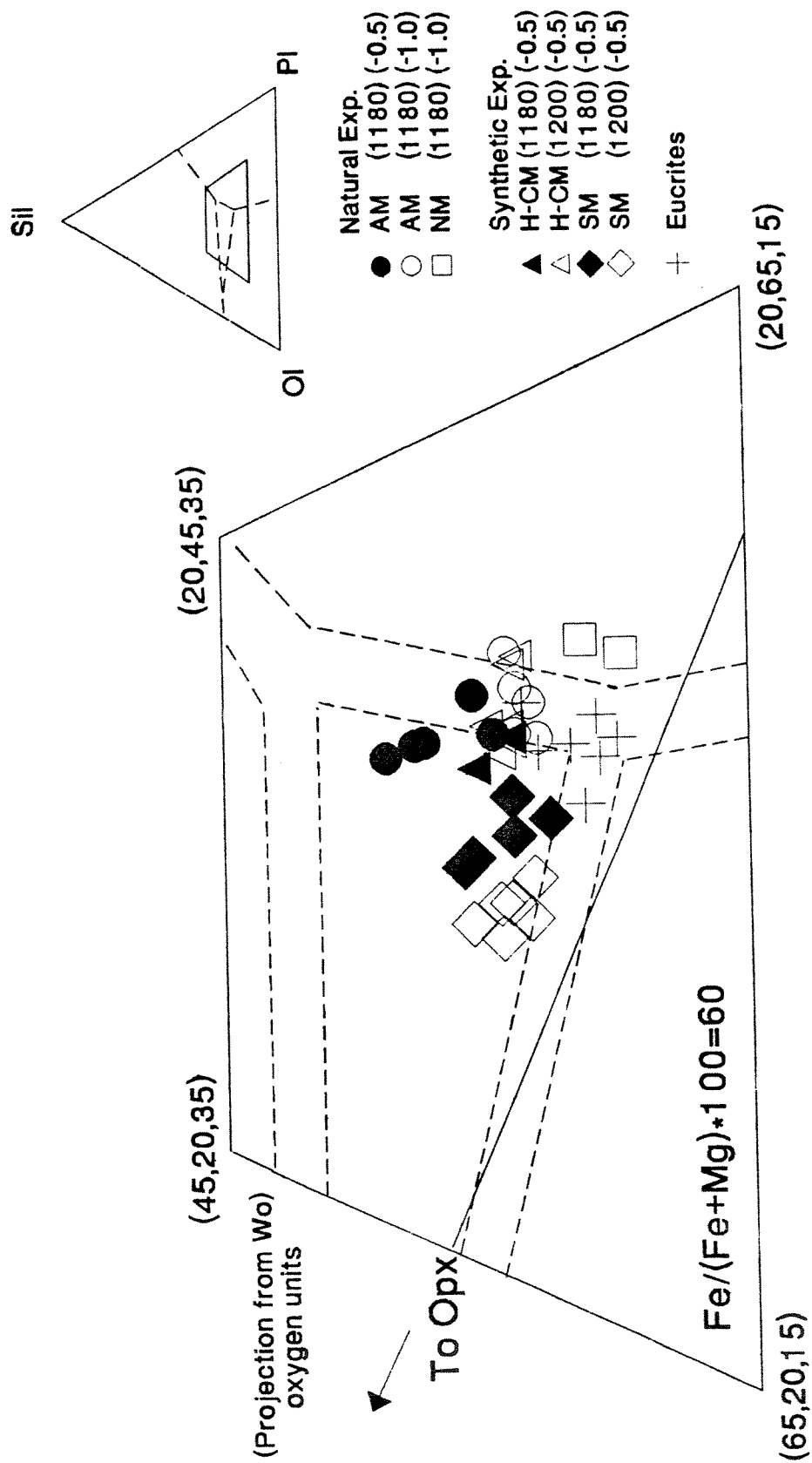
Phase boundaries represented as bands.

Figure 15.

A.

Figure 15.

Figure 16.

A. Synthetic Murchison Glasses

(Temp C)	(IW -X)
(1180)	(-0.5)
(1180)	(-0.5)
(1200)	(-0.5)
(1200)	(-0.5)
(1200)	(-1.5)

B. H-CM Glasses

(Temp C)	(IW -X)
(1180)	(-0.5)
(1180)	(-0.5)
(1200)	(-0.5)
(1200)	(-0.5)
(1200)	(-1.5)
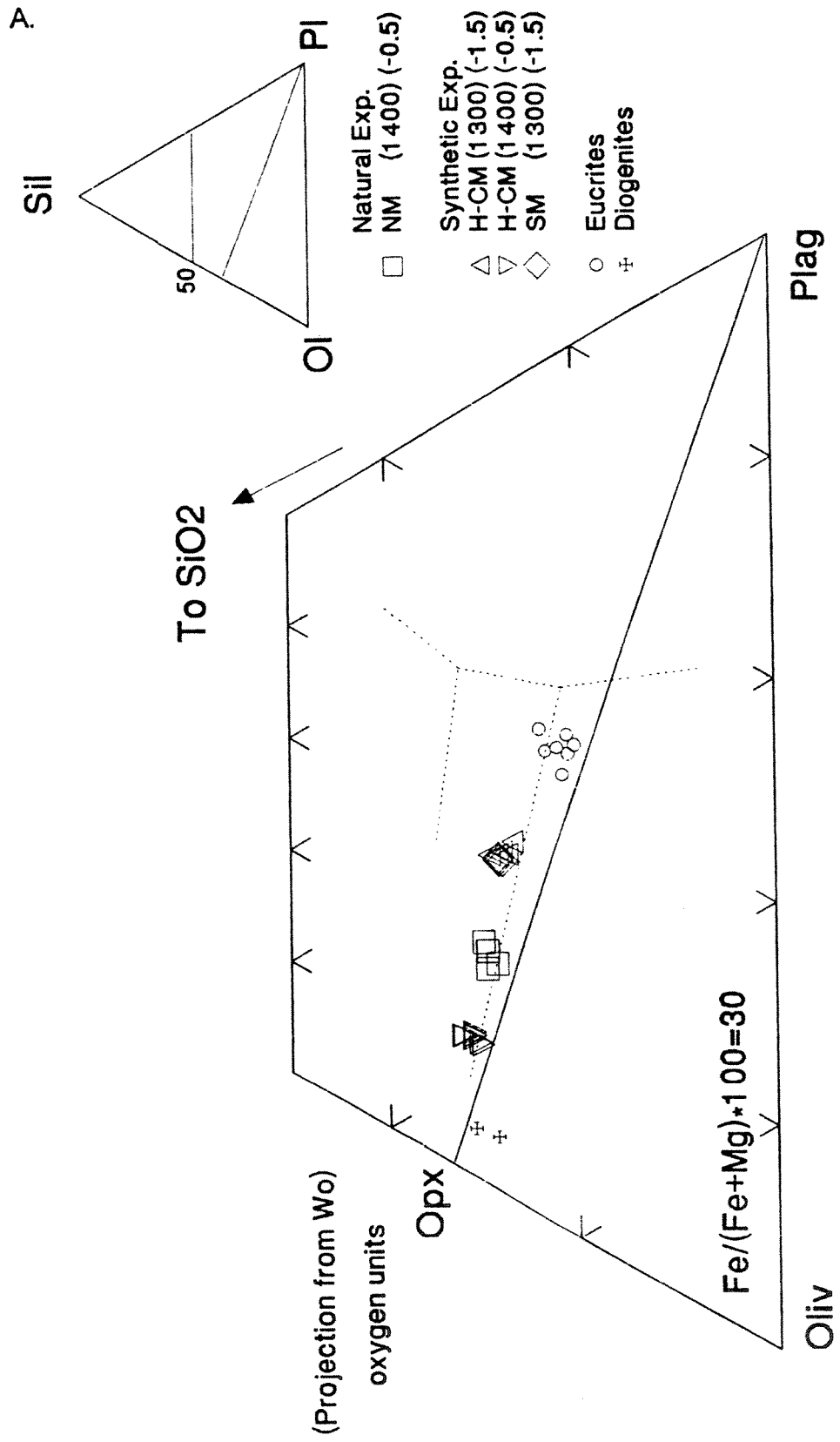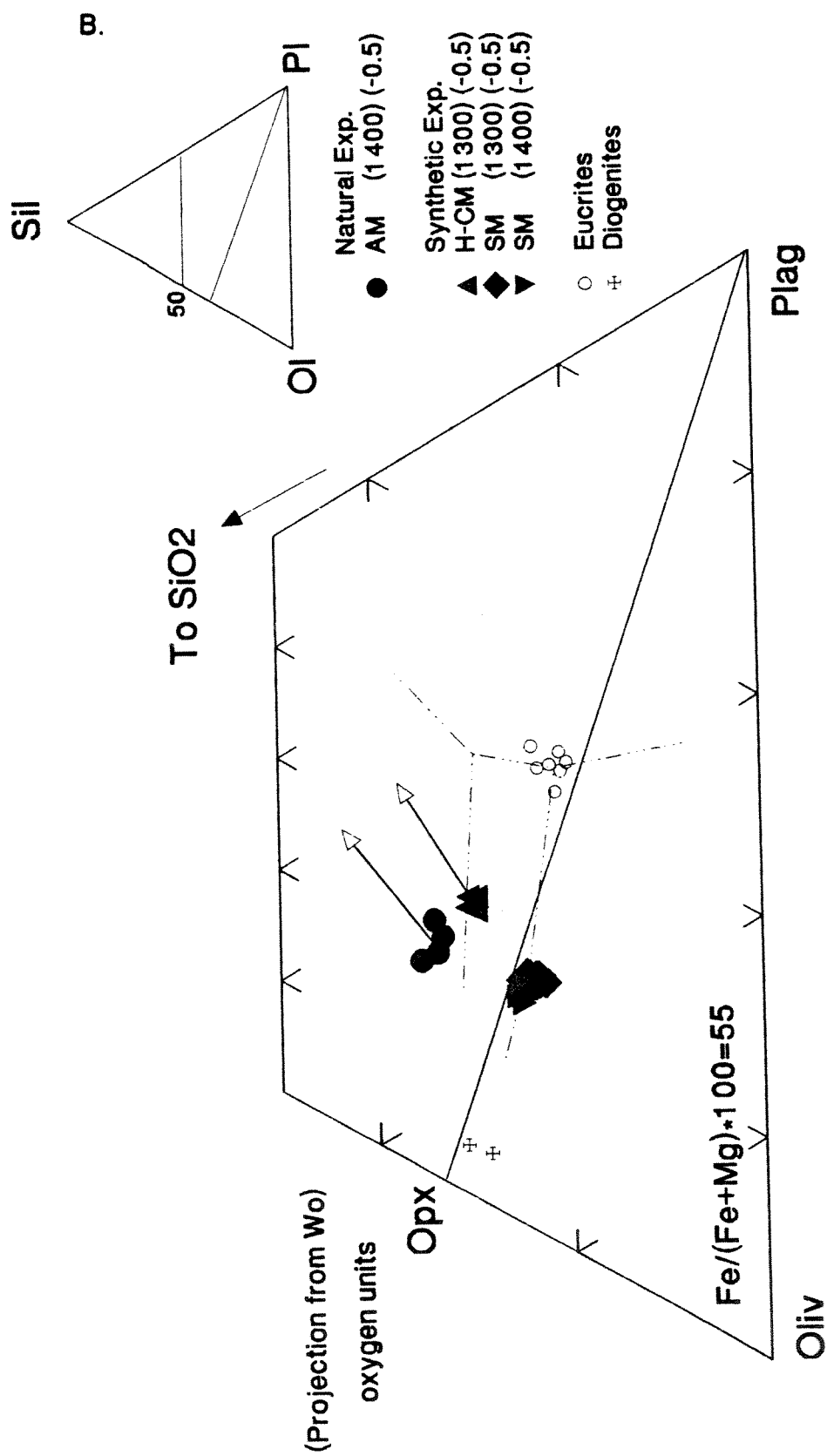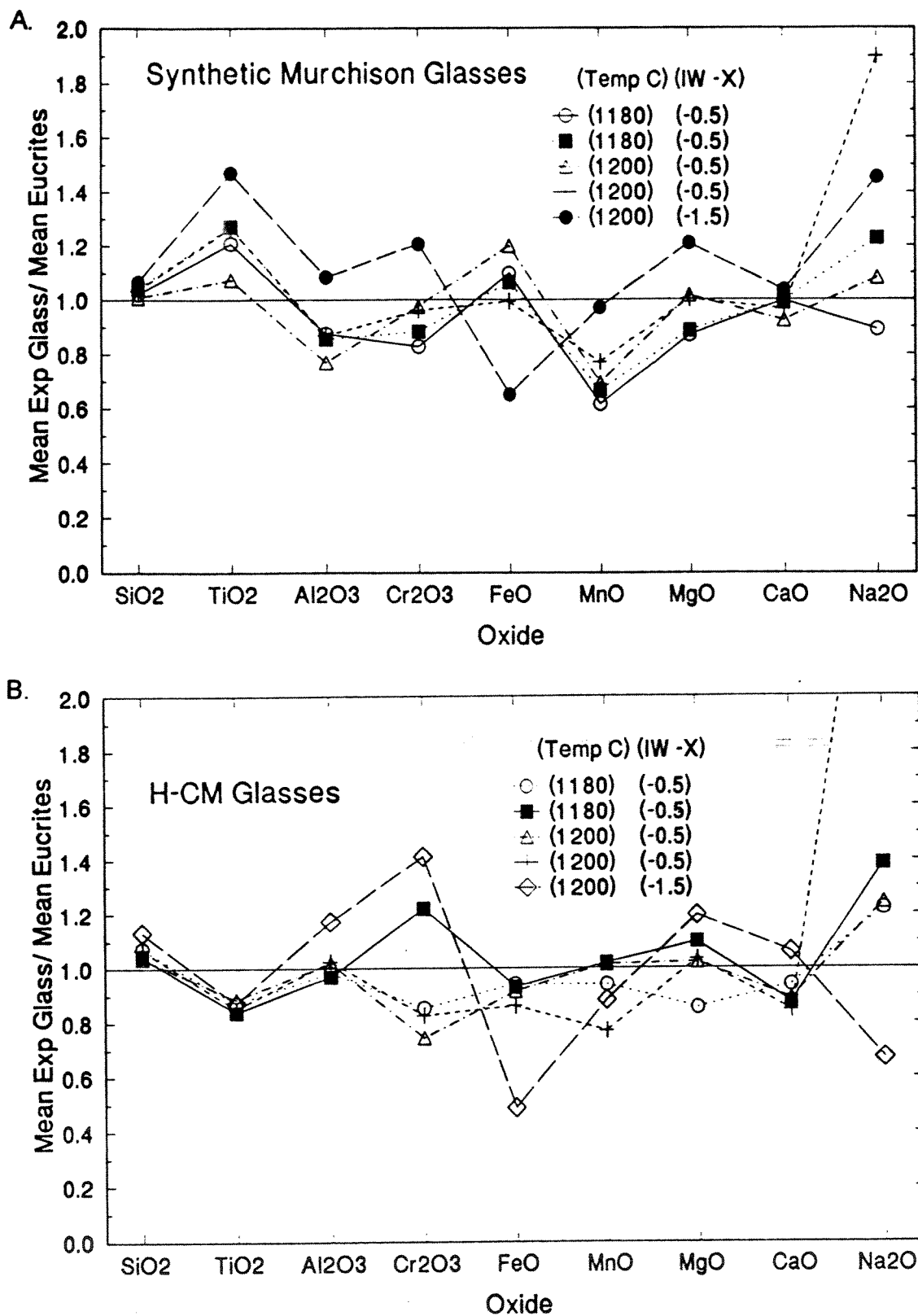
Figure 17.

A.

B.

Figure 18.

Figure 19.

A. Natural Murchison Glasses

(Temp C) (IW-X)
- ● (1180) (-0.5)
- □ (1180) (-1.0)
- △ (1180) (-1.5)

B. Allegan-Murchison Glasses

(Temp C) (IW-X)
- ● (1180) (-0.5)
- □ (1180) (-1.0)
- △ (1180) (-1.5)

Figure 20.

Figure 20.

Figure 21.

(Projection from Wo)
oxygen units
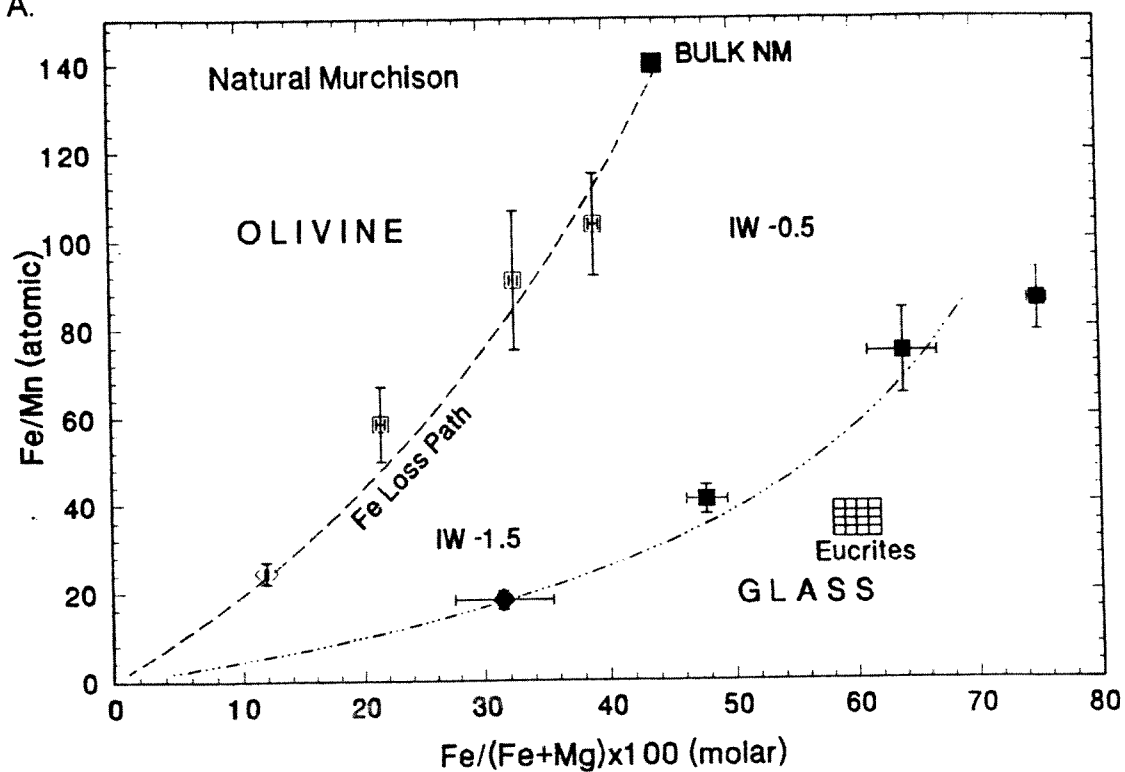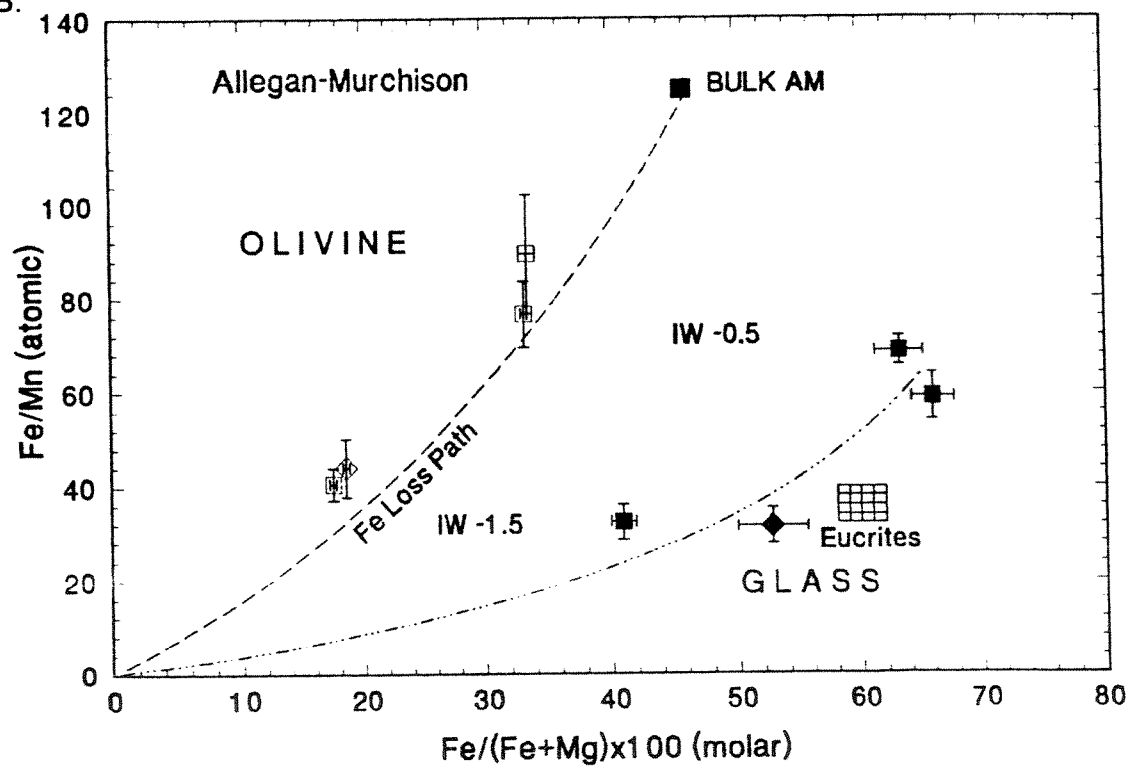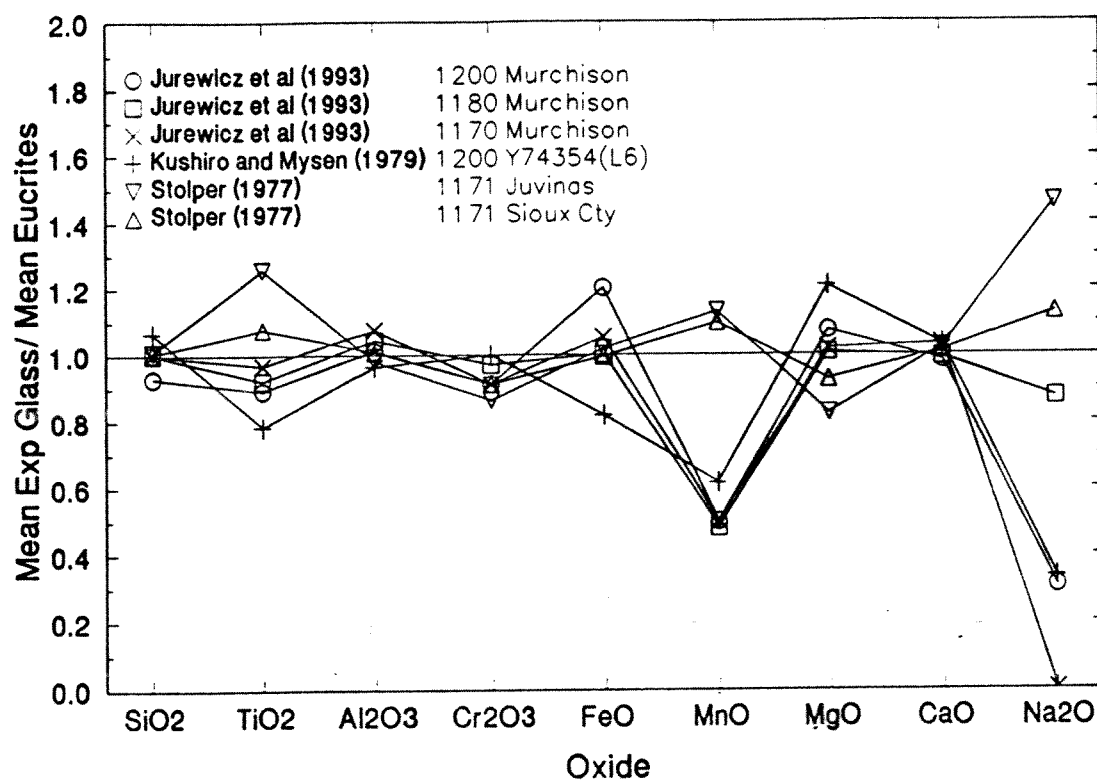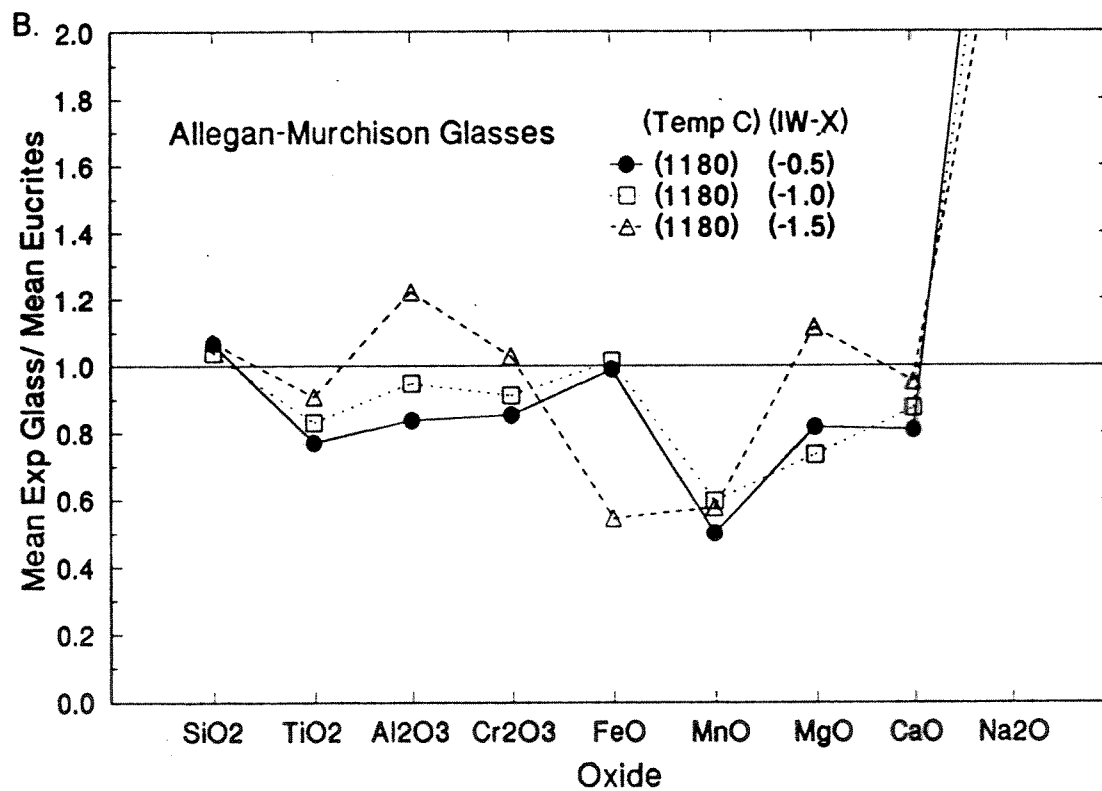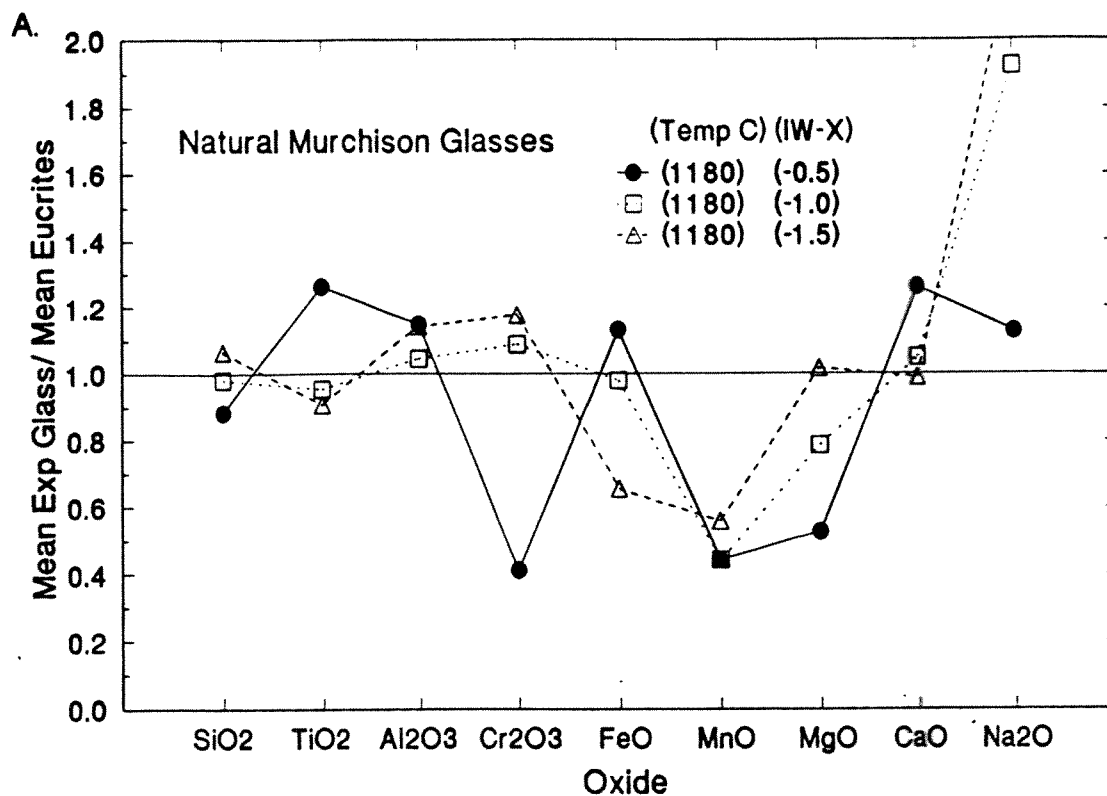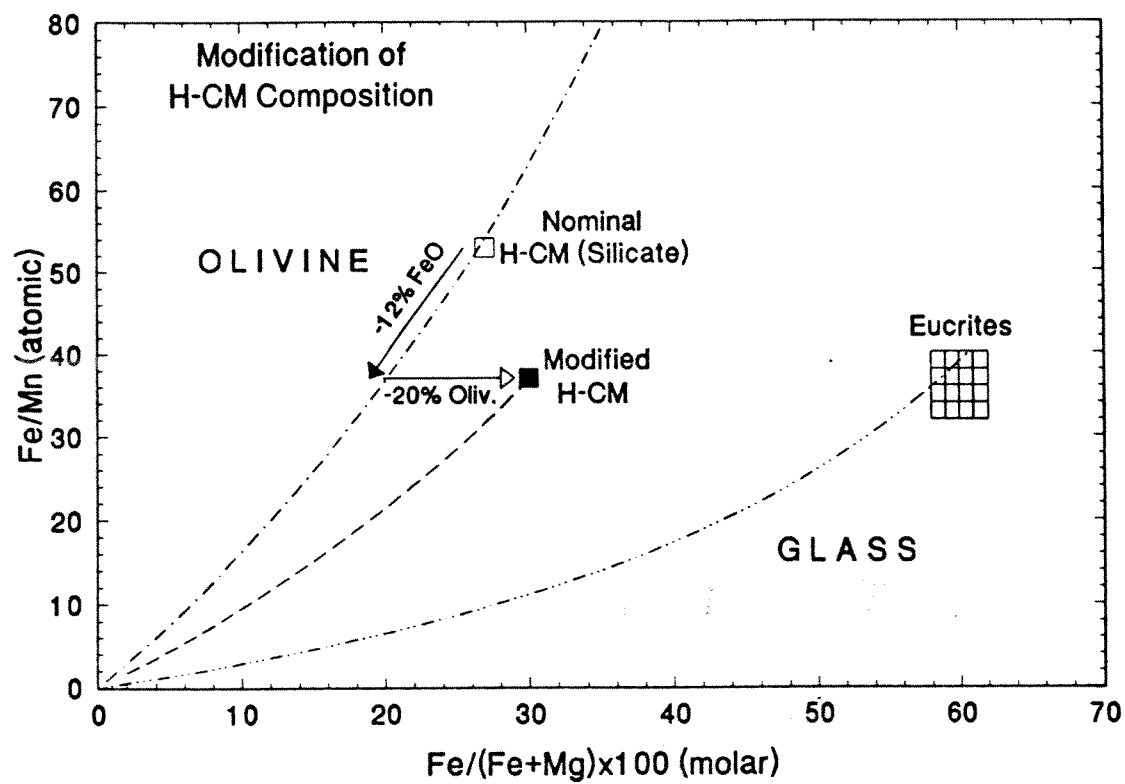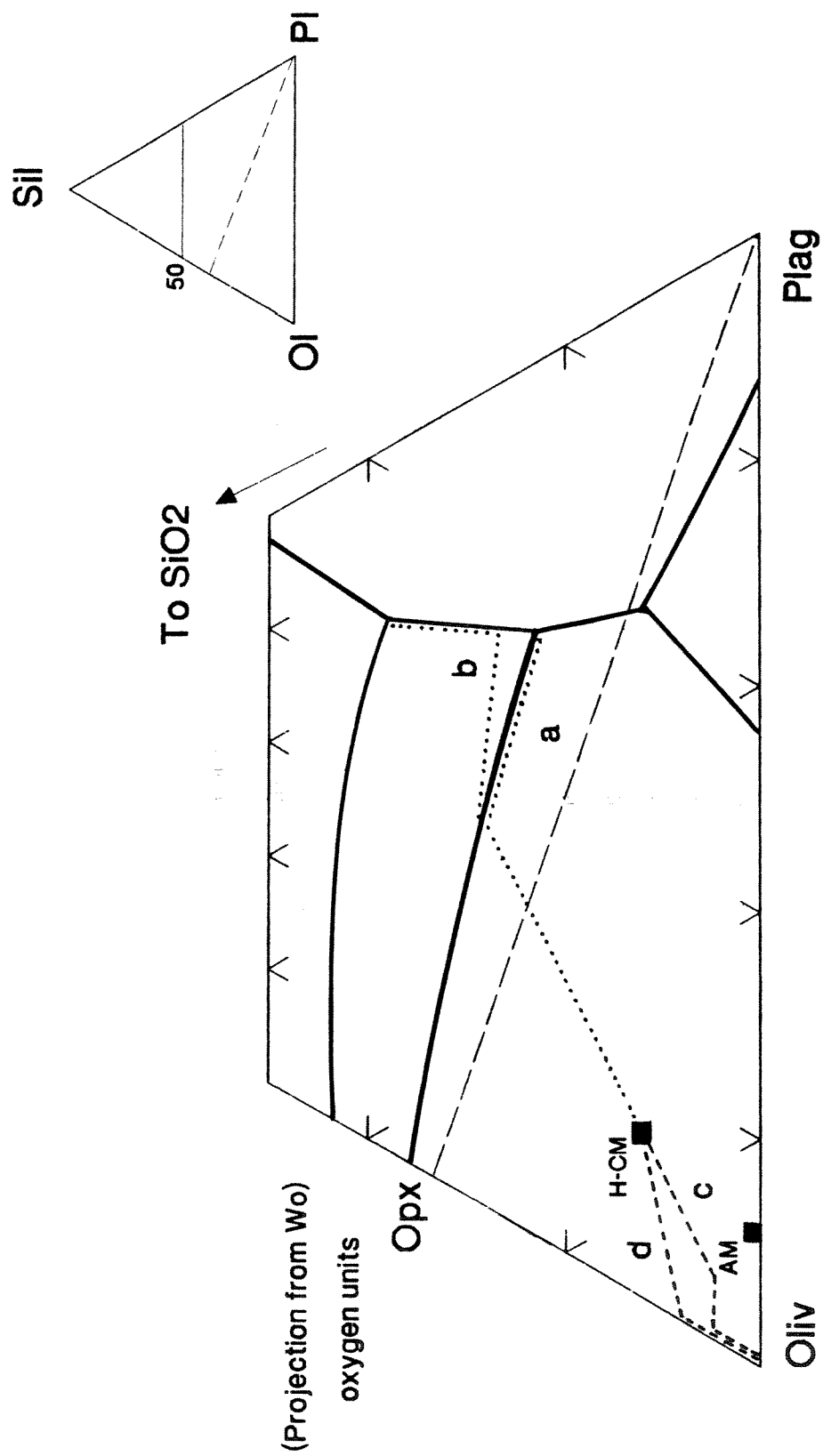
Appendix I. Chemical Analyses of Electron Microprobe Mineral Standards

Mineral	SiO$_2$	TiO$_2$	Al$_2$O$_3$	Cr$_2$O$_3$	FeO	MnO	MgO	CaO	Na$_2$O	K$_2$O	N$_i$O	Total	Ref.
Forsterite, synthetic Fo 100*	42.7	-	-	-	-	-	57.3	-	-	-	-	100.00	1
Olivine (Fo 90), San Carlos, Gils Co., AZ* USNM 111312/444	40.81	-	-	-	9.55	0.14	49.42	0.05	-	-	0.37	100.34	2
Olivine (Fo 83), Springwater meteorite** USNM 2566	38.95	-	-	0.02	16.62	0.30	43.58	-	-	-	-	99.47	2
Fayalite, synthetic Fa 100*	29.5	-	-	-	70.5	-	-	-	-	-	-	100.00	3
Fayalite, Rockport, MA** USNM 85276	29.22	0.04	-	-	67.6	2.14	-	-	-	-	-	99.70	2
Tephroite, synthetic*	29.8	-	-	-	-	70.3	-	-	-	-	-	100.10	4
Orthopyroxene, Tatahouine meteorite**	54.7	0.07	0.53	0.64	15.2	0.54	27.6	0.71	0.01	-	-	100.00	5
Hypersthene, Johnstown meteorite** USNM 746	54.09	0.16	1.23	0.75	15.22	0.49	26.79	1.52	0.05	0.05	-	100.35	2
Augite, Kakanui, New Zealand** USNM 122142	50.73	0.74	8.73	-	6.4	0.13	16.65	15.82	1.27	-	-	100.47	2
Hornblende, Kakanui, New Zealand* USNM 143965	40.37	4.72	14.90	-	11.0	0.09	12.80	10.30	2.60	2.05	-	98.83	2
Anorthite, Great Sitkin Island, AL* USNM 137041	44.00	0.03	36.03	-	0.62	-	0.02	19.09	0.53	0.03	-	100.35	2
Plagioclase (Labradorite), Lake County, OR* USNM 115900	51.25	0.05	30.91	-	0.15	0.01	0.14	13.64	3.45	0.18	-	99.78	2
Anorthoclase, Kakanui, New Zealand** USNM 133868	66.44	-	20.12	-	0.20	-	-	0.87	9.31	2.35	-	99.29	2
Chromite, Tiebaghi Mine, New Caledonia* USNM 117075	-	-	9.92	60.5	13.04	0.11	15.20	0.12	-	-	-	98.89	2

* Calibration standard
** Additional standard used to test microprobe calibration

References:
1 Takei and Kobayashi (1974)
2 Jarosewich et al (1980)
3 Takei (1978)
4 Takei (1976)
5 Rutgers University Microanalysis Laboratory standard. Analyzed by J.S. Delaney

Appendix II. Chemical Analyses of Series I, II, and III Experimental Charges

A. Series I Experiments

(Temp)　(Exp type)　(Exp #)

Synthetic Murchison Fe/Mn 85

1180°C　cooling　M09

SIO2	AL2O3	CR2O3	FEO	MNO	MGO	CAO	TOTAL	Si	Al	Cr	Fe	Mn	Mg	Ca	FEMN	FFM	WO	FS
glass																		
56.44	11.36	0.42	11.32	0.54	10.55	9.67	100.30	7992	1896	47	1341	65	2227	1467	20.70	36.90		
55.28	14.76	0.25	11.36	0.50	4.53	11.21	97.89	8010	2521	29	1377	61	979	1740	22.43	56.97		
57.66	15.59	0.25	10.77	0.44	3.80	12.31	100.82	8073	2573	28	1261	52	793	1847	24.17	59.87		
57.55	15.93	0.15	9.70	0.40	3.25	12.30	99.28	8129	2652	17	1146	48	684	1862	23.94	61.01		
58.68	16.91	0.15	8.36	0.36	3.96	12.98	101.40	8069	2741	16	961	42	812	1912	22.93	52.97		
olivine																		
40.86	0.00	0.48	12.50	0.34	46.54	0.21	100.93	1005	0	9	257	7	1706	6	36.30	13.05		
40.93	0.02	0.51	13.47	0.43	45.86	0.11	101.33	1007	1	10	277	9	1682	3	30.93	14.08		
40.41	0.02	0.32	15.05	0.41	44.34	0.15	100.70	1007	1	6	314	9	1648	4	36.24	15.92		
40.80	0.02	0.32	11.28	0.34	48.67	0.11	101.54	993	1	6	230	7	1765	3	32.76	11.47		
40.99	0.02	0.37	13.34	0.37	46.24	0.15	101.48	1006	1	7	274	8	1692	4	35.60	13.88		
40.26	0.04	0.34	14.76	0.36	44.89	0.14	100.79	1002	1	7	307	8	1666	4	40.48	15.51		
39.88	0.04	0.47	17.74	0.46	42.05	0.20	100.84	1006	1	9	374	10	1582	5	38.08	19.04		
40.11	0.04	0.37	15.86	0.46	43.36	0.24	100.44	1007	1	7	333	10	1623	6	34.04	16.94		
40.41	0.04	0.37	15.31	0.46	44.32	0.14	101.05	1006	1	7	319	10	1644	4	32.86	16.15		
40.75	0.04	0.51	13.30	0.41	45.88	0.10	100.99	1005	1	10	274	9	1687	3	32.03	13.93		
pigeonite																		
54.66	1.11	1.07	15.46	0.74	25.15	2.48	100.67	1973	47	31	467	23	1353	96	20.63	25.33	4.95	24.07
55.88	1.13	0.89	13.12	0.58	27.39	2.34	101.33	1977	47	25	388	17	1444	89	22.33	20.98	4.57	20.02
55.17	1.21	0.91	13.33	0.65	26.66	2.31	100.24	1976	51	26	399	20	1424	89	20.25	21.67	4.59	20.68
55.39	1.66	1.01	13.91	0.67	25.27	3.18	101.09	1976	70	28	415	20	1344	122	20.50	23.33	6.39	21.83
54.77	1.68	0.83	13.50	0.75	25.82	2.92	100.27	1967	71	24	406	23	1383	112	17.77	22.39	5.84	21.08
55.47	1.76	0.99	13.61	0.66	25.47	2.73	100.69	1980	74	28	406	20	1356	104	20.36	22.80	5.54	21.54
55.30	2.00	1.05	13.38	0.59	25.85	3.18	101.35	1963	84	29	397	18	1368	121	22.39	22.28	6.35	20.86
56.44	2.23	0.95	11.90	0.56	25.75	3.20	101.03	1990	93	26	351	17	1353	121	20.98	20.39	6.56	19.05
55.00	2.25	0.75	14.34	0.61	24.79	2.98	100.72	1970	95	21	430	19	1324	114	23.21	24.24	6.06	22.77
56.41	2.40	1.08	11.75	0.52	25.63	3.19	100.98	1988	100	30	346	16	1347	120	22.31	20.27	6.59	18.94
56.67	2.80	0.80	14.47	0.66	23.69	3.41	102.50	1990	116	22	425	20	1240	128	21.65	25.22	7.08	23.44

1180°C heating M13

	SIO2	AL2O3	CR2O3	FEO	MNO	MGO	CAO	TOTAL	Si	Al	Cr	Fe	Mn	Mg	Ca	FEMN	FFM	WO	FS
glass																			
	53.95	1.49	0.69	14.82	0.49	24.62	3.81	99.87	7850	256	79	1803	60	5341	594	29.86	25.03		
	52.63	4.76	0.82	15.45	1.06	19.27	5.96	99.95	7722	823	95	1896	132	4215	937	14.39	30.37		
	52.74	4.44	0.63	15.61	0.58	19.65	6.20	99.85	7739	768	73	1916	72	4299	975	26.57	30.47		
olivine																			
	38.70	0.08	0.58	23.81	0.87	36.71	0.39	101.14	1005	2	12	517	19	1421	11	27.02	26.42		
	38.32	0.21	0.29	24.79	0.35	35.86	0.57	100.39	1005	6	6	544	8	1403	16	69.93	27.83		
	38.02	0.30	0.25	23.41	0.30	36.79	0.62	99.69	999	9	5	515	7	1441	17	77.05	26.22		
	37.87	0.38	0.88	25.68	0.99	34.01	0.52	100.33	1003	12	18	569	22	1343	15	25.61	29.41		
pigeonite																			
	55.45	0.59	0.22	14.15	0.18	24.61	5.79	100.99	1991	25	6	425	5	1318	223	77.62	24.31	11.30	21.56
	54.81	0.60	0.22	14.13	0.39	24.31	6.13	100.59	1982	26	6	427	12	1311	238	35.77	24.42	11.95	21.50
	54.06	0.79	0.50	14.56	0.34	24.24	5.36	99.85	1972	34	14	444	11	1319	210	42.28	25.05	10.57	22.41
	55.41	0.81	0.18	12.29	0.96	25.34	4.91	99.90	1996	34	5	370	29	1361	189	12.64	21.03	9.72	18.99
	54.38	1.21	0.76	13.29	0.59	24.92	4.87	100.02	1968	52	22	402	18	1345	189	22.24	22.79	9.67	20.59
spinel																			
	1.37	65.53	0.15	15.30	0.10	16.88	0.63	99.96	35	1962	3	325	2	639	17	151.07	33.63		
	0.00	66.09	0.19	18.73	0.15	15.93	0.00	101.09	0	1990	4	400	3	607	0	123.29	39.62		
	0.06	67.06	0.00	13.47	0.57	18.70	0.07	99.93	2	1996	0	285	12	704	2	23.33	28.43		
	1.11	24.05	40.95	21.03	1.48	8.66	0.32	97.60	35	904	1033	561	40	412	11	14.03	55.39		
	0.13	1.66	65.23	22.20	1.25	5.69	0.08	96.24	5	72	1897	683	39	312	3	17.54	66.05		

1253°C   heating   M47

SIO2	AL2O3	CR2O3	FEO	MNO	MGO	CAO	TOTAL	Si	Al	Cr	Fe	Mn	Mg	Ca	FEMN	FFM	WO	FS
glass																		
49.31	10.11	0.75	20.43	0.48	8.64	8.88	98.60	7525	1818	90	2607	62	1966	1452	42.02	56.25		
49.23	10.20	0.75	20.38	0.52	9.12	8.76	98.96	7485	1828	90	2592	67	2067	1427	38.70	54.84		
49.21	10.24	0.75	20.26	0.48	9.80	8.30	99.04	7462	1830	90	2570	62	2216	1349	41.67	53.01		
49.46	10.24	0.70	20.75	0.54	8.26	9.05	99.00	7528	1837	84	2642	70	1874	1476	37.94	57.60		
49.16	10.28	0.44	20.40	0.53	9.45	8.58	98.84	7476	1843	53	2595	68	2143	1398	38.00	53.99		
49.29	10.32	0.86	19.81	0.61	9.09	8.70	98.68	7496	1850	103	2520	79	2061	1418	32.06	54.08		
48.95	10.41	0.58	20.40	0.57	8.51	9.21	98.63	7478	1875	70	2607	74	1938	1508	35.34	56.44		
49.08	10.56	0.77	20.58	0.56	7.81	9.14	98.50	7509	1904	93	2633	73	1781	1498	36.29	58.68		
49.68	10.68	0.66	19.72	0.49	8.44	8.93	98.60	7542	1911	79	2504	63	1910	1453	39.74	55.93		
50.02	10.71	0.77	20.01	0.54	8.01	9.00	99.06	7566	1909	92	2531	69	1806	1459	36.59	57.44		
olivine																		
37.20	0.00	0.58	25.33	0.46	36.05	0.25	99.87	988	0	12	562	10	1427	7	54.37	28.13		
37.63	0.00	0.60	25.34	0.49	35.70	0.27	100.03	996	0	13	561	11	1409	8	51.06	28.32		
37.20	0.02	0.60	24.88	0.52	35.96	0.25	99.43	990	1	13	554	12	1427	7	47.24	27.80		
36.54	0.02	0.61	24.98	0.49	35.82	0.22	98.68	982	1	13	562	11	1436	6	50.34	27.96		
37.52	0.04	0.67	23.89	0.50	36.33	0.25	99.19	996	1	14	530	11	1437	7	48.14	26.80		
37.89	0.04	0.57	25.61	0.50	35.47	0.22	100.30	1000	1	12	566	11	1396	6	50.57	28.66		
37.80	0.04	0.67	25.28	0.49	36.15	0.21	100.64	994	1	14	556	11	1417	6	50.94	28.02		
37.18	0.04	0.60	25.36	0.49	36.15	0.28	100.10	985	1	13	562	11	1428	8	51.10	28.08		
37.91	0.04	0.56	25.29	0.50	35.72	0.24	100.26	1000	1	12	558	11	1405	7	49.94	28.27		
36.75	0.06	0.67	25.20	0.48	36.00	0.28	99.44	981	2	14	563	11	1433	8	51.84	28.04		
36.71	0.06	0.57	24.97	0.52	35.83	0.22	98.88	984	2	12	560	12	1432	6	47.41	27.94		
37.97	0.06	0.69	24.77	0.45	36.94	0.21	101.09	991	2	14	541	10	1437	6	54.35	27.20		
37.95	0.06	0.09	24.77	0.52	36.43	0.22	100.04	1000	2	2	546	12	1431	6	47.03	27.45		
37.67	0.06	0.57	24.52	0.45	36.63	0.25	100.15	992	2	12	540	10	1438	7	53.80	27.16		
37.48	0.06	0.47	25.29	0.54	35.53	0.27	99.64	996	2	10	562	12	1408	8	46.24	28.36		
37.89	0.08	0.25	24.88	0.48	35.77	0.25	99.60	1003	2	5	551	11	1412	7	51.18	27.91		
pigeonite																		
54.45	0.36	0.70	14.16	0.41	27.18	1.93	99.19	1978	15	20	430	13	1472	75	34.10	22.47	3.80	21.76
54.83	0.45	0.75	15.14	0.49	26.86	1.51	100.03	1981	19	21	457	15	1447	58	30.51	23.84	2.98	23.31
54.36	0.45	0.85	14.86	0.40	26.71	1.30	98.93	1983	19	25	453	12	1452	51	36.68	23.63	2.60	23.17
54.13	0.60	0.85	15.64	0.62	26.31	1.34	99.49	1973	26	24	477	19	1430	52	24.91	24.76	2.67	24.34
54.62	0.60	0.82	14.78	0.44	26.86	1.13	99.25	1983	26	24	449	14	1454	44	33.17	23.42	2.26	23.05
55.60	0.62	0.75	14.23	0.43	26.93	1.29	99.85	1998	26	21	428	13	1443	50	32.67	22.71	2.59	22.27
54.36	0.66	0.96	14.77	0.56	26.99	1.26	99.56	1971	28	28	448	17	1459	49	28.04	23.28	2.50	22.90
54.21	0.81	1.02	15.27	0.43	26.76	1.18	99.68	1967	35	29	463	13	1448	46	35.06	24.08	2.34	23.68
54.15	0.83	0.82	13.55	0.41	27.46	1.76	98.98	1966	36	24	411	13	1487	68	32.63	21.54	3.48	20.93
54.62	0.85	0.92	14.87	0.45	26.33	1.29	99.33	1983	36	28	451	14	1425	50	32.63	23.88	2.60	23.43
54.47	0.87	1.05	14.97	0.53	26.88	1.44	100.21	1965	37	30	452	16	1446	56	27.89	23.60	2.85	23.13
53.91	0.93	0.96	15.36	0.50	25.77	1.23	98.66	1977	40	28	471	16	1409	48	30.33	24.85	2.51	24.43
spinel																		
0.11	13.83	53.89	22.01	0.44	7.66	0.08	98.02	4	549	1434	619	13	384	3	49.39	60.95		
0.15	13.96	52.54	21.56	0.44	8.39	0.07	97.11	5	556	1405	610	13	423	3	48.38	58.33		
1.24	17.44	46.92	22.94	0.40	8.90	0.00	97.84	41	675	1219	630	11	436	0	56.63	58.51		

1300°C heating   M04

SIO2	AL2O3	CR2O3	FEO	MNO	MGO	CAO	TOTAL	Si	Al	Cr	Fe	Mn	Mg	Ca	FEMN	FFM	WO	FS
glass
44.91	8.09	0.56	26.28	0.46	9.92	7.25	97.47	7199	1529	71	3523	62	2371	1245	56.41	59.15		
44.93	8.43	0.35	28.80	0.52	9.78	6.02	98.83	7154	1582	44	3835	70	2322	1027	54.68	61.59		
43.88	7.54	0.39	29.34	0.52	9.58	5.68	96.93	7169	1452	50	4009	72	2333	994	55.71	62.50		
47.19	9.28	0.64	25.87	0.45	7.49	7.51	98.43	7413	1718	79	3399	60	1754	1264	56.76	65.20		
47.32	8.36	0.64	26.79	0.51	8.41	7.61	99.64	7388	1539	79	3498	67	1958	1273	51.87	63.34		
46.89	8.35	0.61	25.88	0.49	7.56	7.51	97.29	7470	1568	77	3448	68	1796	1282	52.15	64.94		
46.99	8.91	0.58	25.71	0.47	8.34	7.88	98.88	7361	1645	72	3369	62	1948	1323	54.01	62.63		
46.75	9.50	0.66	25.65	0.51	8.11	6.99	98.17	7355	1762	82	3375	68	1902	1178	49.66	63.14		
47.03	9.04	0.72	25.39	0.50	7.88	8.07	98.63	7380	1672	89	3332	66	1843	1357	50.14	63.57		
46.67	8.79	0.67	26.88	0.53	7.41	7.94	98.89	7361	1634	84	3546	71	1743	1342	50.08	66.16		
47.42	8.51	0.66	27.17	0.48	7.09	7.82	99.15	7451	1576	82	3570	64	1661	1317	55.89	67.43		
46.04	8.84	0.66	27.16	0.53	7.03	8.02	98.28	7331	1659	83	3617	71	1669	1368	50.60	67.51		
47.54	9.15	0.64	25.67	0.54	6.58	8.30	98.42	7474	1696	80	3376	72	1542	1398	46.94	67.65		
45.70	8.35	0.70	28.10	0.50	7.25	8.10	98.70	7292	1570	88	3750	68	1725	1385	55.49	67.66		
46.34	8.98	0.79	27.31	0.57	6.65	8.19	98.83	7341	1677	99	3618	76	1571	1390	47.31	68.72		
45.29	9.24	0.77	28.55	0.54	6.25	8.17	98.81	7235	1740	97	3814	73	1489	1398	52.20	70.95		
olivine
37.14	0.04	0.47	29.69	0.48	32.48	0.27	100.57	998	1	10	667	11	1301	8	61.07	33.71		
37.22	0.06	0.26	29.24	0.46	32.85	0.25	100.34	1000	2	6	657	10	1315	7	62.76	33.13		
37.01	0.06	0.48	28.79	0.46	32.78	0.25	99.83	998	2	10	649	11	1318	7	61.80	32.83		
37.22	0.06	0.19	28.33	0.45	33.28	0.28	99.81	1001	2	4	637	10	1334	8	62.16	32.15		
36.90	0.06	0.19	29.99	0.46	32.07	0.27	99.96	999	2	4	679	11	1295	8	61.69	34.22		
36.67	0.06	0.48	29.65	0.46	32.27	0.27	99.86	994	2	10	672	11	1304	8	63.64	33.83		
37.14	0.06	0.23	29.55	0.45	32.43	0.28	100.14	1001	3	5	666	10	1303	8	64.84	33.65		
37.29	0.08	0.39	29.13	0.45	32.98	0.28	100.60	998	3	8	652	10	1316	8	63.92	32.96		
36.84	0.08	0.57	29.59	0.45	32.10	0.25	99.88	997	3	12	670	10	1296	7	64.92	33.91		
36.71	0.08	0.00	29.78	0.46	32.20	0.25	99.48	998	3	0	677	11	1305	7	63.92	33.98		
37.27	0.08	0.47	27.66	0.45	33.33	0.27	99.53	998	3	10	622	10	1336	8	60.69	31.60		
36.58	0.08	0.23	28.96	0.44	32.65	0.18	99.12	995	3	5	659	10	1324	5	64.99	33.06		
36.84	0.08	0.47	29.31	0.45	32.02	0.31	99.48	1000	3	10	665	10	1296	9	64.31	33.75		
36.50	0.09	0.61	29.47	0.48	32.43	0.25	99.83	989	3	13	668	11	1311	7	60.62	33.58		
36.60	0.13	0.45	29.53	0.46	31.74	0.31	99.22	998	4	10	673	11	1290	9	63.38	34.11		
spinel
3.59	22.98	33.18	27.26	0.30	11.24	0.11	98.66	113	852	826	718	8	527	4	89.72	57.27		
7.72	23.56	29.90	25.33	0.31	14.69	0.07	101.58	227	817	695	623	8	644	2	80.68	48.87		

1325°C   cooling   M08

M08 SIO2	AL2O3	CR2O3	FEO	MNO	MGO	CAO	TOTAL	Si	Al	Cr	Fe	Mn	Mg	Ca	FEMN	FFM	WO	FS
glass																		
57.85	7.03	0.99	10.83	0.61	14.87	6.44	98.62	8267	1184	112	1294	74	3168	986	17.53	28.53		
59.47	7.09	0.77	9.98	0.57	15.64	6.28	99.80	8334	1171	85	1170	68	3268	943	17.29	25.96		
59.58	7.09	0.63	9.66	0.62	14.89	6.45	98.92	8403	1179	70	1140	74	3131	975	15.38	26.23		
58.25	7.12	0.83	10.82	0.59	15.12	6.44	99.17	8269	1191	93	1285	71	3200	980	18.11	28.20		
59.15	7.20	0.80	9.85	0.58	15.65	6.59	99.82	8297	1190	89	1156	69	3273	990	16.77	25.69		
59.90	7.22	0.94	9.97	0.65	14.36	6.66	99.70	8401	1194	104	1170	77	3003	1001	15.14	27.52		
58.51	7.22	0.89	10.72	0.65	15.29	6.35	99.63	8262	1202	99	1266	78	3219	961	16.28	27.75		
58.83	7.29	0.86	10.10	0.65	15.27	6.42	99.42	8295	1212	96	1191	78	3210	970	15.34	26.59		
57.81	7.31	0.89	11.03	0.58	14.82	6.51	98.95	8240	1228	100	1315	70	3149	994	18.78	29.00		
57.89	7.35	0.95	11.00	0.62	14.91	6.72	99.44	8218	1230	107	1306	75	3156	1022	17.52	28.79		
58.85	7.35	0.91	10.18	0.61	15.30	6.59	99.79	8275	1218	101	1197	73	3208	993	16.48	26.74		
59.58	7.37	0.98	9.57	0.53	13.17	7.44	98.64	8440	1231	110	1134	64	2782	1129	17.83	28.50		
58.68	7.52	1.01	10.18	0.58	14.64	6.66	99.27	8293	1253	113	1203	69	3085	1009	17.33	27.61		
58.58	7.61	0.96	10.51	0.58	13.70	6.90	98.84	8326	1275	108	1249	70	2903	1051	17.89	29.59		
59.30	7.77	0.89	10.41	0.67	13.96	6.94	99.94	8327	1286	99	1223	80	2923	1044	15.34	28.94		
olivine																		
40.33	0.04	0.53	11.42	0.50	48.40	0.11	101.33	986	1	10	234	10	1764	3	22.55	11.63		
40.78	0.02	0.69	11.13	0.52	47.79	0.14	101.07	997	1	13	228	11	1742	4	21.13	11.49		
40.69	0.06	0.73	11.49	0.52	47.55	0.14	101.18	996	2	14	235	11	1735	4	21.82	11.87		
39.94	0.02	0.63	11.80	0.49	47.31	0.13	100.32	988	1	12	244	10	1746	3	23.78	12.21		
40.46	0.02	0.47	12.30	0.48	47.16	0.14	101.03	995	1	9	253	10	1729	4	25.30	12.70		
40.75	0.04	0.60	11.35	0.48	46.97	0.17	100.34	1004	1	12	234	10	1725	4	23.35	11.88		
40.84	0.02	0.76	11.50	0.43	46.97	0.10	100.69	1003	1	15	236	9	1720	4	26.41	12.02		
40.54	0.04	0.66	11.82	0.46	46.89	0.15	100.51	1000	1	13	244	10	1724	3	25.37	12.33		
40.50	0.04	0.64	11.63	0.45	46.89	0.10	100.30	1000	1	12	240	9	1726	4	25.52	12.16		
40.09	0.02	0.44	12.23	0.43	46.73	0.15	100.05	995	1	9	254	9	1730	3	28.08	12.74		
40.18	0.00	0.58	12.59	0.48	46.56	0.11	100.48	995	0	11	261	10	1719	3	25.90	13.10		
40.03	0.06	0.67	12.36	0.46	46.41	0.13	100.12	994	2	13	257	10	1719	3	28.53	12.93		
39.66	0.02	0.67	12.41	0.46	45.98	0.15	99.35	994	1	13	260	10	1718	4	26.64	13.09		
39.94	0.00	0.51	12.71	0.45	45.58	0.13	99.32	1001	0	10	266	10	1703	3	27.89	13.46		
40.75	0.02	0.66	12.59	0.49	45.40	0.11	100.02	1012	1	13	262	10	1681	3	25.37	13.39		

1580°C heating M17

SIO2	AL2O3	CR2O3	FEO	MNO	MGO	CAO	TOTAL	Si	Al	Cr	Fe	Mn	Mg	Ca	FEMN	FFM	WO	FS
glass																		
49.08	3.95	0.80	13.28	0.54	29.30	3.50	100.45	7135	677	92	1615	67	6351	545	24.28	20.10		
48.93	3.84	0.48	12.67	0.52	30.16	3.30	99.90	7128	659	55	1544	64	6550	515	24.06	18.92		
48.65	3.82	0.77	15.43	0.68	27.23	4.31	100.89	7134	660	89	1892	84	5953	677	22.40	23.86		
49.57	3.80	0.80	13.88	0.57	28.52	3.43	100.57	7206	651	92	1688	70	6181	534	24.04	21.26		
49.14	3.78	0.76	12.53	0.54	30.21	3.30	100.26	7131	647	87	1521	66	6536	513	22.91	18.72		
48.20	3.74	0.76	13.57	0.52	28.83	3.43	99.05	7125	652	89	1678	65	6354	543	25.77	20.72		
48.80	3.72	0.79	12.97	0.49	30.04	3.22	100.03	7115	639	91	1582	61	6530	503	26.13	19.35		
49.33	3.70	0.75	11.63	0.46	31.67	2.98	100.52	7106	628	85	1401	56	6801	460	24.96	16.97		
49.76	3.68	0.73	12.71	0.56	30.44	3.11	100.99	7163	624	83	1530	68	6533	480	22.41	18.82		
49.16	3.67	0.76	14.00	0.63	29.08	3.54	100.84	7146	629	87	1702	78	6302	551	21.94	21.06		
48.76	3.63	0.66	12.08	0.46	31.52	3.08	100.19	7071	620	76	1465	57	6814	479	25.93	17.58		
48.84	3.59	0.76	13.10	0.62	29.71	3.62	100.24	7122	617	88	1598	77	6459	566	20.86	19.64		
48.29	3.57	0.00	13.50	0.49	31.77	3.05	100.67	7014	611	0	1640	60	6880	475	27.20	19.11		
48.73	3.57	0.67	11.62	0.50	33.26	2.46	100.81	7006	605	76	1397	61	7129	379	22.95	16.27		
48.78	3.48	0.76	11.68	0.45	31.79	2.91	99.85	7083	596	87	1419	55	6882	453	25.63	16.98		

1580°C   heating   M19

SIO2	AL2O3	CR2O3	FEO	MNO	MGO	CAO	TOTAL	Si	Al	Cr	Fe	Mn	Mg	Ca	FEMN	FFM	WO	FS
glass																		
56.86	4.35	0.28	1.33	0.28	33.63	3.85	100.58	7694	694	30	151	32	6785	558	4.69	2.16		
56.56	4.36	0.39	1.39	0.26	33.25	3.68	99.89	7704	700	42	158	30	6753	537	5.28	2.28		
56.76	4.38	0.23	1.47	0.28	34.06	3.79	100.97	7660	697	25	166	32	6853	548	5.18	2.35		
56.65	4.38	0.00	1.31	0.30	34.12	3.82	100.58	7666	699	0	148	34	6884	554	4.31	2.10		
56.74	4.38	0.47	1.38	0.32	33.79	3.76	100.84	7667	698	50	156	37	6807	544	4.26	2.23		
56.54	4.38	0.28	1.31	0.30	33.56	3.79	100.13	7685	702	30	149	35	6801	548	4.41	2.13		
56.95	4.40	0.41	1.34	0.30	33.61	3.79	100.80	7691	700	44	151	34	6767	550	5.88	2.18		
56.80	4.42	0.38	1.31	0.22	33.49	3.78	100.41	7696	706	41	148	25	6765	550	4.24	2.14		
56.39	4.46	0.35	1.33	0.31	33.74	3.82	100.36	7654	714	38	151	36	6828	552	5.49	2.15		
56.93	4.46	0.34	1.39	0.25	33.71	3.82	100.90	7681	709	36	157	29	6781	552	4.94	2.25		
56.89	4.46	0.23	1.25	0.25	33.91	3.79	100.81	7677	709	25	141	29	6823	547	3.80	2.02		
56.97	4.50	0.00	1.31	0.34	34.07	3.82	100.98	7675	715	0	148	39	6844	547	4.25	2.10		
56.69	4.50	0.38	1.29	0.30	33.99	3.69	100.84	7654	716	41	146	34	6842	534		2.07		

Synthetic Murchison Fe/Mn 65

1180°C   cooling   M10

SIO2	AL2O3	CR2O3	FEO	MNO	MGO	CAO	TOTAL	Si	Al	Cr	Fe	Mn	Mg	Ca	FEMN	FFM	WO	FS
glass																		
56.52	9.94	0.83	9.57	0.61	12.80	8.06	98.33	8082	1675	94	1145	74	2729	1235	15.49	29.00		
53.68	10.15	0.70	11.09	0.77	14.28	8.38	99.05	7745	1726	80	1338	94	3072	1296	14.22	29.71		
55.43	11.56	0.45	10.06	0.67	11.42	9.28	98.87	7929	1949	51	1204	81	2435	1422	14.83	32.35		
57.72	15.80	0.18	8.54	0.45	2.49	12.77	97.95	8221	2652	20	1017	54	529	1949	18.74	63.57		
57.27	16.19	0.10	8.77	0.41	2.49	12.30	97.53	8188	2728	11	1049	50	531	1884	21.12	64.37		
59.20	16.65	0.25	6.54	0.40	4.16	12.49	99.69	8188	2714	27	757	47	858	1851	16.14	45.54		
olivine																		
40.56	0.00	0.32	11.01	0.43	47.62	0.10	100.04	1000	0	6	227	9	1751	3	25.28	11.43		
39.86	0.02	0.37	14.61	0.71	43.97	0.22	99.76	1004	1	7	308	15	1651	6	20.32	15.59		
38.68	0.02	0.31	16.61	0.68	43.11	0.15	99.56	988	1	6	355	15	1641	4	24.12	17.64		
39.34	0.02	0.34	13.19	0.50	45.76	0.17	99.32	990	1	7	278	11	1717	5	26.05	13.85		
39.47	0.02	0.42	11.95	0.50	46.73	0.13	99.22	989	1	8	250	11	1745	3	23.60	12.48		
39.83	0.02	0.47	11.63	0.53	46.24	0.10	98.82	999	1	9	244	11	1729	3	21.67	12.29		
39.36	0.02	0.28	11.60	0.41	47.47	0.14	99.28	984	1	6	242	9	1769	4	27.94	12.00		
38.87	0.04	0.56	14.85	0.61	43.79	0.13	98.85	991	1	11	317	13	1665	4	24.04	15.88		
40.43	0.04	0.41	11.36	0.58	47.41	0.17	100.40	997	1	8	234	12	1742	4	19.34	11.78		
39.41	0.04	0.32	12.53	0.52	45.68	0.11	98.61	995	1	6	265	11	1720	3	23.79	13.26		
38.02	0.04	0.50	16.12	0.71	42.43	0.25	98.07	986	1	10	349	16	1640	7	22.42	17.43		
39.49	0.04	0.39	15.34	0.59	43.48	0.15	99.48	1001	1	8	325	13	1643	4	25.67	16.42		
39.32	0.08	0.31	10.69	0.48	47.17	0.11	98.16	990	2	6	225	10	1770	3	21.99	11.22		
38.81	0.30	0.98	14.78	0.65	42.81	0.28	98.61	993	9	20	316	14	1633	8	22.45	16.11		
pigeonite																		
54.75	0.91	1.17	13.98	0.90	25.90	2.39	100.00	1977	39	33	422	28	1395	92	15.34	22.90	5.03	22.84
54.77	0.98	1.11	13.65	0.83	26.60	2.20	100.14	1971	42	32	411	25	1427	85	16.24	22.05	4.37	20.78
54.19	1.00	1.01	13.57	0.85	26.10	2.24	98.96	1974	43	29	413	26	1417	87	15.76	22.26	4.62	21.06
54.51	1.02	0.86	13.19	0.94	26.33	2.43	98.26	1976	44	25	400	29	1423	94	13.85	21.60	5.17	21.45
54.43	1.21	1.08	12.23	0.85	27.01	2.45	99.26	1966	52	31	369	26	1454	95	14.21	19.97	5.44	19.56
54.72	1.23	0.99	12.85	0.90	26.38	2.60	99.67	1973	52	28	387	27	1418	100	14.10	21.14	5.72	20.31
54.32	1.83	0.94	12.50	0.81	25.19	2.74	98.33	1980	79	27	381	25	1369	107	15.24	21.47	6.23	20.34

1180°C   heating   M14

	SIO2	AL2O3	CR2O3	FEO	MNO	MGO	CAO	TOTAL	Si	Al	Cr	Fe	Mn	Mg	Ca	FEMN	FFM	WO	FS
glass	55.79	11.20	0.22	13.39	0.56	6.47	10.87	98.50	8134	1925	25	1633	69	1406	1698	23.61	52.53		
	55.89	11.18	0.23	13.38	0.55	6.58	10.66	98.47	8144	1920	26	1631	68	1429	1664	24.02	52.13		
	55.64	11.24	0.26	13.33	0.55	6.32	10.92	98.26	8133	1936	30	1630	68	1377	1710	23.93	53.00		
	55.48	11.26	0.22	13.28	0.56	6.38	10.74	97.92	8132	1945	25	1628	70	1394	1687	23.41	52.66		
olivine	37.97	0.04	0.25	25.52	0.81	35.28	0.42	100.29	1003	1	5	564	18	1390	12	31.11	28.60		
	37.97	0.06	0.34	25.15	0.85	35.68	0.38	100.43	1000	2	7	554	19	1402	11	29.21	28.06		
	38.23	0.09	0.64	25.64	0.76	35.17	0.52	101.05	1003	3	13	563	17	1376	15	33.31	28.78		
	38.68	0.13	0.77	24.61	0.76	35.28	0.45	100.68	1012	4	16	539	17	1377	13	31.97	27.88		
	38.49	0.15	0.35	22.85	1.07	37.24	0.39	100.54	1002	5	7	498	24	1446	11	21.09	25.30		
	38.32	0.17	0.09	25.40	0.72	36.21	0.45	101.36	999	5	2	554	16	1408	13	34.83	28.01		
	37.31	0.26	0.20	24.71	1.10	34.44	0.55	98.57	1003	8	4	555	25	1380	16	22.18	28.33		
	37.72	0.36	0.38	23.44	0.89	35.70	0.60	99.09	1001	11	8	520	20	1412	17	26.00	26.64		
	38.19	0.51	0.39	24.15	1.03	34.21	0.83	99.31	1014	16	8	536	23	1354	24	23.15	28.02		
	38.40	0.51	0.58	25.55	0.66	35.15	0.70	101.55	1001	16	12	557	15	1366	20	38.22	28.75		
	37.63	0.51	0.20	25.82	1.07	34.74	0.62	100.59	994	16	4	571	24	1369	18	23.83	29.07		
pigeonite	56.78	0.59	0.22	13.46	0.67	23.36	4.86	99.94	2043	25	6	405	20	1253	187	19.84	24.13	10.04	21.71
	55.22	0.70	0.22	13.56	0.98	23.38	5.46	99.52	2010	30	6	413	30	1269	213	13.66	24.12	11.06	21.45
	54.51	0.85	0.76	14.73	0.72	24.49	4.86	100.92	1969	36	22	445	22	1319	188	20.20	24.92	9.53	22.54
	55.00	0.87	0.31	14.63	1.07	24.06	4.53	100.47	1991	37	9	443	33	1298	176	13.50	24.96	9.01	22.72
	55.56	1.04	0.72	14.24	1.70	23.63	4.41	101.13	1998	37	20	428	52	1267	170	8.27	24.52	8.86	22.34
	54.62	1.08	0.44	13.51	0.62	24.79	4.90	99.92	1979	44	13	409	19	1339	190	21.51	23.16	9.72	20.91
	54.53	1.15	0.80	14.61	1.32	24.34	3.55	100.23	1979	46	23	443	41	1317	138	10.93	24.62	7.12	22.87
	54.06	1.17	0.82	14.67	1.08	22.57	5.30	99.65	1982	50	24	450	34	1234	208	13.41	26.20	10.81	23.36
	54.49	1.23	0.66	12.98	0.49	23.83	6.45	100.07	1975	50	19	393	15	1288	250	26.16	23.20	12.87	20.21
	54.83	1.25	0.76	13.20	0.54	24.62	5.08	100.26	1977	52	22	398	16	1324	196	24.14	22.90	10.15	20.58
	54.79		0.89	14.01	1.82	24.31	3.89	100.96	1974	53	25	422	56	1306	150	7.60	23.67	7.77	21.83
spinel	0.81	64.41	1.75	16.43	0.53	17.13	0.29	101.35	21	1927	35	349	11	648	8	30.61	34.59		
	0.15	65.81	0.13	16.44	0.23	17.48	0.00	100.24	4	1979	3	351	5	665	0	70.57	34.37		
	8.75	12.34	42.71	23.16	1.12	10.79	0.80	99.67	275	457	1062	609	30	506	27	20.42	53.21		

1325°C   cooling   M07

SiO2	AL2O3	CR2O3	FEO	MNO	MGO	CAO	TOTAL	Si	Al	Cr	Fe	Mn	Mg	Ca	FEMN	FFM	WO	FS
glass																		
48.91	8.88	0.69	12.88	0.67	16.48	8.65	97.16	7359	1575	82	1621	85	3697	1394	18.98	30.00		
57.61	9.30	0.67	13.11	0.68	7.41	10.69	99.47	8304	1580	76	1581	83	1592	1651	19.04	48.54		
52.37	9.66	0.75	13.12	0.77	10.93	9.42	97.02	7820	1700	89	1639	97	2433	1507	16.82	39.30		
52.76	11.02	0.79	12.67	0.72	8.87	10.33	97.16	7843	1931	93	1575	91	1966	1645	17.37	43.37		
olivine																		
39.60	0.04	0.54	13.43	0.62	45.27	0.18	99.68	994	1	11	282	13	1694	5	21.39	14.17		
39.00	0.04	0.64	13.59	0.56	44.82	0.21	98.86	989	1	13	288	12	1695	6	23.96	14.45		
39.15	0.04	0.70	13.16	0.57	43.87	0.20	97.69	1002	1	14	282	12	1674	5	22.80	14.31		
39.32	0.02	0.60	13.14	0.58	43.41	0.20	97.27	1009	1	12	282	13	1662	6	22.37	14.42		
39.32	0.21	0.56	13.32	0.58	43.34	0.31	97.64	1007	6	11	285	13	1654	9	22.68	14.61		
pigeonite																		
56.61	0.45	0.70	8.85	0.53	30.79	0.71	98.64	2006	19	20	262	16	1626	27	16.49	13.77	1.40	13.58
55.97	0.53	0.75	8.56	0.52	31.02	0.74	98.09	1994	22	21	255	16	1648	28	16.25	13.30	1.45	13.10
55.47	0.76	0.94	9.03	0.56	30.19	0.81	97.76	1989	32	27	271	17	1614	31	15.92	14.24	1.61	14.01
56.86	0.89	1.08	9.03	0.53	29.73	1.15	99.27	2005	37	30	266	16	1563	43	16.82	14.43	2.30	14.10
55.92	1.25	0.91	9.01	0.57	29.32	1.48	98.46	1992	52	26	268	17	1557	56	15.61	14.57	2.97	14.13
56.27	1.76	0.94	8.61	0.53	29.13	1.67	98.91	1990	73	26	255	16	1536	63	16.04	14.10	3.38	13.62
55.86	2.34	0.76	9.40	0.61	28.10	2.43	99.50	1976	98	21	278	18	1482	92	15.22	15.64	4.92	14.87

Synthetic Murchison Fe/Mn 45
1180°C   cooling   M11

SIO2	AL2O3	CR2O3	FEO	MNO	MGO	CAO	TOTAL	Si	Al	Cr	Fe	Mn	Mg	Ca	FEMN	FFM	WO	FS
glass																		
58.10	14.15	0.23	9.70	0.68	4.08	11.73	98.67	8259	2371	26	1153	82	865	1787	14.08	54.92		
56.63	15.06	0.23	11.01	0.67	3.33	12.08	99.01	8098	2538	26	1317	81	710	1851	16.23	62.47		
56.35	15.63	0.13	11.42	0.79	2.93	12.23	99.48	8041	2629	15	1363	96	623	1870	14.27	65.47		
57.81	15.66	0.10	11.40	0.67	2.74	12.61	100.99	8108	2589	11	1337	80	573	1895	16.80	67.21		
55.43	16.16	0.16	11.72	0.75	2.55	12.49	99.26	7954	2733	18	1407	91	546	1921	15.43	68.84		
58.49	16.16	0.29	8.59	0.61	3.95	12.22	100.31	8134	2649	32	999	72	819	1821	13.90	52.86		
56.97	16.65	0.19	10.72	0.74	2.59	12.20	100.06	8037	2769	21	1265	88	545	1844	14.30	66.64		
58.43	17.01	0.10	9.07	0.68	2.32	12.45	100.06	8152	2797	11	1058	80	483	1861	13.17	65.28		
54.47	18.10	0.13	11.71	0.75	2.17	13.28	100.61	7736	3030	15	1391	90	459	2021	15.42	71.67		
52.52	18.97	0.26	9.48	0.62	4.81	13.12	99.78	7477	3183	29	1129	75	1021	2001	15.10	50.74		
olivine																		
40.80	0.02	0.31	12.56	0.68	46.43	0.13	100.93	1005	1	6	259	14	1705	3	18.24	13.08		
40.07	0.02	0.35	15.22	0.83	45.03	0.14	101.66	994	1	7	316	17	1665	4	18.11	15.80		
39.81	0.02	0.28	18.86	0.99	41.07	0.25	101.28	1007	1	6	399	21	1549	7	18.81	20.26		
40.43	0.02	0.45	14.14	0.76	45.13	0.11	101.04	1003	1	9	293	16	1669	3	18.37	14.83		
39.94	0.04	0.50	19.79	1.10	39.61	0.25	101.23	1015	1	10	421	24	1501	7	17.76	21.63		
40.56	0.06	0.39	14.14	0.76	44.87	0.14	100.92	1006	2	8	293	16	1660	4	18.37	14.90		
40.67	0.13	0.35	15.58	0.75	43.53	0.28	101.29	1011	4	7	324	16	1614	7	20.51	16.59		
pigeonite																		
55.41	0.79	0.91	14.87	1.19	26.50	2.04	101.71	1974	33	26	443	36	1407	78	12.34	23.49	3.96	22.56
55.35	1.10	0.94	15.86	1.28	24.95	2.36	101.84	1979	46	27	474	39	1330	90	12.23	25.73	4.68	24.53
55.26	1.11	1.24	16.00	1.42	24.49	2.42	101.94	1978	47	35	479	43	1307	93	11.13	26.19	4.83	24.92
55.02	1.72	1.05	14.29	1.16	24.57	2.24	100.05	1985	73	30	431	35	1322	87	12.16	24.11	4.62	23.00
55.20	1.81	1.01	14.97	1.15	25.75	2.34	102.23	1958	76	28	444	35	1361	89	12.85	24.13	4.61	23.02
54.38	1.95	1.13	14.23	1.29	24.95	2.63	100.56	1959	83	32	429	39	1340	102	10.89	23.71	5.32	22.45

1325°C cooling   M06

SIO2	AL2O3	CR2O3	FEO	MNO	MGO	CAO	TOTAL	Si	Al	Cr	Fe	Mn	Mg	Ca	FEMN	FFM	WO	FS
glass																		
53.44	8.52	0.89	13.59	1.14	14.92	7.61	100.11	7739	1454	102	1646	140	3221	1181	11.77	32.87		
53.44	8.54	0.85	14.23	1.06	14.86	7.68	100.66	7718	1454	97	1719	130	3200	1189	13.25	34.05		
53.51	8.60	0.80	14.07	0.98	14.23	8.09	100.28	7752	1469	92	1705	120	3074	1256	14.18	34.80		
53.44	8.60	0.76	13.73	1.06	15.12	7.72	100.43	7718	1464	87	1658	130	3256	1195	12.79	32.88		
53.31	8.60	0.80	14.29	1.12	14.91	7.82	100.85	7694	1463	91	1725	137	3208	1209	12.60	34.02		
53.59	8.75	0.75	13.23	1.10	14.53	8.06	100.01	7756	1493	86	1601	135	3135	1250	11.88	32.87		
53.53	8.88	0.98	12.45	0.93	15.09	7.98	99.84	7731	1512	112	1504	114	3249	1235	13.22	30.90		
53.70	9.03	0.73	12.72	1.05	15.04	7.89	100.16	7734	1533	83	1532	128	3230	1218	11.96	31.33		
53.59	9.03	0.83	12.80	1.03	15.04	7.85	100.17	7723	1534	95	1543	126	3231	1212	12.27	31.49		
53.66	9.07	0.89	12.71	1.01	15.39	7.93	100.66	7696	1533	101	1525	123	3291	1219	12.43	30.87		
53.87	9.13	0.98	12.84	1.06	15.09	7.89	100.86	7713	1541	111	1537	129	3221	1210	11.96	31.46		
olivine																		
40.58	0.02	0.50	12.92	0.66	45.95	0.14	100.77	1003	1	10	267	14	1694	4	19.33	13.53		
40.61	0.02	0.42	13.88	0.81	45.66	0.11	101.51	1001	1	8	286	17	1678	3	16.92	14.44		
40.84	0.04	0.69	13.53	0.80	45.43	0.21	101.54	1005	1	13	279	17	1667	6	16.70	14.19		
40.71	0.04	0.53	14.01	0.74	45.08	0.17	101.28	1006	1	10	290	15	1661	5	18.69	14.73		
40.58	0.02	0.47	14.32	0.85	45.02	0.18	101.33	1004	1	9	296	16	1661	5	19.11	15.02		
40.82	0.02	0.51	14.91	0.90	44.85	0.13	102.09	1005	1	10	307	18	1646	3	17.32	15.58		
40.05	0.02	0.57	14.74	0.76	44.74	0.20	101.22	996	1	10	307	19	1659	5	16.17	15.45		
40.11	0.04	0.56	14.32	0.87	44.69	0.15	100.63	1000	1	11	299	16	1662	4	18.60	15.11		
40.50	0.00	0.63	14.74	0.87	44.45	0.20	101.39	1004	0	11	306	18	1643	5	16.73	15.54		
40.20	0.04	0.54	14.54	0.84	43.94	0.14	100.24	1007	1	12	305	18	1641	4	17.09	15.51		
pigeonite																		
58.19	0.40	0.72	8.38	0.71	32.45	0.73	101.58	1998	16	20	241	21	1661	27	11.65	12.52	1.38	12.35
57.66	0.49	0.85	9.56	0.76	31.92	0.69	101.93	1986	20	23	275	22	1639	25	12.42	14.22	1.30	14.04
57.76	0.53	0.88	9.92	0.77	31.35	0.64	101.85	1993	22	24	286	23	1613	24	12.72	14.90	1.22	14.72
57.59	0.72	1.08	9.55	0.66	31.34	0.62	101.56	1990	29	30	276	19	1614	23	14.29	14.45	1.19	14.28

Synthetic Murchison Fe/Mn 20

1180°C   cooling   M12

SIO2	AL2O3	CR2O3	FEO	MNO	MGO	CAO	TOTAL	Si	Al	Cr	Fe	Mn	Mg	Ca	FEMN	FFM	WO	FS
glass
59.24	14.13	0.31	8.79	2.12	4.59	10.84	100.02	8293	2332	34	1029	251	958	1626	4.09	45.97		
58.25	15.34	0.26	9.07	1.76	3.37	11.67	99.72	8198	2545	29	1068	210	707	1760	5.09	53.80		
58.36	15.63	0.31	9.02	1.89	2.77	11.52	99.50	8223	2596	35	1063	226	582	1739	4.71	56.83		
58.53	15.82	0.18	8.67	1.68	2.17	12.41	99.46	8241	2626	20	1021	200	456	1872	5.10	60.89		
58.06	16.34	0.07	8.59	1.77	2.87	11.84	99.54	8161	2707	8	1010	211	601	1783	4.79	55.42		
olivine
40.31	0.00	0.47	15.05	2.40	42.25	0.15	100.63	1014	0	9	317	51	1585	4	6.19	16.22		
39.94	0.02	0.44	14.59	2.14	43.03	0.13	100.29	1006	1	9	307	46	1617	4	6.73	15.61		
39.96	0.02	0.41	13.60	2.07	43.76	0.13	99.95	1006	1	8	286	44	1642	4	6.49	14.51		
41.14	0.02	0.39	10.91	1.69	46.15	0.13	100.43	1014	1	8	225	35	1696	3	6.37	11.50		
40.43	0.02	0.32	13.78	1.96	43.48	0.17	100.16	1014	1	6	289	42	1626	5	6.94	14.77		
41.31	0.02	0.42	11.33	1.69	46.34	0.18	101.29	1012	1	8	232	35	1692	5	6.62	11.85		
41.29	0.02	0.56	12.90	1.96	45.05	0.13	101.91	1013	1	11	265	41	1648	3	6.50	13.55		
40.54	0.04	0.41	14.61	2.17	42.90	0.13	100.80	1015	1	8	306	46	1601	3	6.65	15.66		
40.24	0.04	0.44	14.76	2.35	42.96	0.21	101.00	1008	1	9	309	50	1604	6	6.20	15.75		
40.26	0.04	0.37	13.03	2.05	44.16	0.13	100.04	1009	1	7	273	44	1650	3	6.28	13.89		
pigeonite
55.60	1.10	1.27	11.93	2.85	25.44	2.69	100.88	1987	46	36	357	86	1356	103	4.13	19.83	5.42	18.75
55.20	1.19	1.07	13.15	3.20	24.59	2.57	100.97	1984	50	30	395	97	1318	99	4.06	21.83	5.18	20.70
55.45	1.55	1.07	12.45	2.93	25.88	2.24	101.57	1971	65	30	370	88	1372	85	4.20	20.23	4.45	19.33
55.52	1.83	1.14	12.99	3.25	24.29	2.88	101.90	1976	77	32	387	98	1289	110	3.95	21.80	5.83	20.53

1325°C cooling M05

SIO2	AL2O3	CR2O3	FEO	MNO	MGO	CAO	TOTAL	Si	Al	Cr	Fe	Mn	Mg	Ca	FEMN	FFM	WO	FS
glass
54.66	7.22	0.99	5.93	2.54	22.78	6.02	100.14	7681	1196	110	697	302	4773	906	2.31	12.07		
51.32	7.37	0.50	6.70	2.40	25.53	6.45	100.27	7293	1235	56	796	289	5409	982	2.76	12.26		
57.74	7.60	0.82	6.33	2.51	18.60	7.02	100.62	8030	1246	90	736	296	3857	1046	2.49	15.06		
56.16	7.63	0.83	5.36	2.38	21.79	5.72	99.87	7840	1256	92	626	281	4535	856	2.22	11.50		
52.82	8.24	0.80	6.41	2.57	21.49	5.72	98.05	7597	1397	91	771	313	4608	882	2.46	13.55		
49.91	9.77	0.80	6.28	2.60	23.43	6.56	99.35	7153	1650	91	753	316	5006	1007	2.38	12.39		
50.34	10.22	0.56	6.88	2.61	19.15	8.20	97.96	7335	1755	65	838	322	4160	1280	2.60	15.76		
52.82	12.49	0.79	6.99	2.75	10.38	11.29	97.51	7711	2149	91	853	340	2259	1766	2.51	24.72		
53.91	13.26	0.60	7.05	2.81	8.90	12.35	98.88	7759	2249	68	849	343	1910	1905	2.48	27.37		
54.10	14.11	0.47	7.24	2.83	8.59	12.90	100.24	7693	2365	53	861	341	1821	1965	2.53	28.48		
olivine
41.74	0.13	0.57	6.88	2.14	48.91	0.46	100.83	1010	4	11	139	44	1764	12	3.17	7.15		
41.38	0.04	0.64	7.15	2.22	48.83	0.24	100.50	1006	1	12	145	46	1770	6	3.18	7.41		
40.63	0.02	0.48	7.32	2.21	48.81	0.22	99.69	998	1	9	150	46	1787	6	3.27	7.58		
pigeonite
58.83	0.59	0.83	4.17	2.04	34.09	0.88	101.43	1998	24	22	118	59	1726	32	2.02	6.22	1.65	6.12
58.83	0.91	0.76	4.52	2.08	33.71	1.13	101.94	1992	36	20	128	60	1702	41	2.15	6.77	2.12	6.63
58.02	1.11	0.92	4.39	1.92	34.31	0.80	101.47	1973	45	25	125	55	1740	29	2.26	6.50	1.50	6.41
57.87	2.04	0.83	4.64	1.99	32.37	2.03	101.77	1969	82	22	132	57	1642	74	2.30	7.21	3.88	6.93
57.46	2.95	0.79	5.00	2.20	29.56	2.41	100.37	1984	120	22	144	64	1522	89	2.24	8.34	4.90	7.94

B. Series II Experiments

(Temp) f(O₂) (Exp type) (Exp #)

Synthetic Murchison

1180°C   IW-0.5   heating   M29

	SIO2	TIO2	AL2O3	CR2O3	FEO	MNO	MGO	CAO	NA2O	NIO	TOTAL	Si	Ti	Al	Cr	Fe	Mn	Mg	Ca	Na	Ni	FEMN	FFM	WO	FS
glass																									
	50.57	0.75	10.52	0.32	20.33	0.36	6.80	9.99	0.27	0.00	99.91	7602	85	1864	38	2556	46	1524	1609	79	0	55.76	61.95		
	50.17	0.72	10.66	0.29	19.21	0.30	7.44	9.51	0.31	0.17	98.78	7589	82	1901	35	2430	38	1678	1541	91	21	63.22	58.61		
	48.84	0.80	11.32	0.28	21.01	0.32	5.99	10.37	0.34	0.00	99.27	7445	92	2034	34	2679	41	1361	1694	100	0	64.83	65.63		
	49.70	0.82	11.40	0.24	19.61	0.32	6.16	10.21	0.39	0.08	98.93	7534	93	2037	29	2486	41	1392	1659	115	10	60.51	63.43		
	49.75	0.76	10.75	0.27	20.35	0.33	6.39	10.11	0.44	0.06	98.90	7552	87	1923	32	2584	42	1446	1644	130	7	60.89	63.44		
olivine																									
	37.18	0.05	0.04	0.07	30.72	0.39	30.72	0.32	0.03	0.22	99.74	1012	1	1	2	699	9	1247	9	2	5	77.76	35.77		
	36.78	0.09	0.04	0.28	32.84	0.41	29.45	0.35	0.00	0.18	100.42	1005	2	1	6	751	9	1200	10	0	4	79.08	38.30		
	37.14	0.05	0.04	0.20	31.18	0.39	31.06	0.31	0.01	0.06	100.43	1005	1	1	4	706	9	1254	9	0	1	78.93	35.86		
	36.65	0.00	0.04	0.26	31.27	0.39	30.51	0.35	0.01	0.00	99.47	1004	0	1	6	716	9	1246	10	0	0	79.16	36.34		
	37.67	0.00	0.04	0.38	30.80	0.44	31.17	0.39	0.04	0.23	101.13	1011	1	1	8	691	10	1247	11	1	5	69.11	35.48		
	36.52	0.07	0.08	0.35	31.06	0.37	30.54	0.35	0.04	0.28	99.66	999	1	3	8	711	9	1246	10	2	6	82.88	36.17		
	37.59	0.05	0.08	0.37	30.75	0.41	30.79	0.34	0.04	0.25	100.67	1013	1	3	8	693	9	1237	10	2	5	74.04	35.73		
	36.58	0.01	0.05	0.26	30.72	0.44	30.55	0.32	0.00	0.21	99.14	1004	0	2	6	705	10	1250	9	0	5	68.93	35.88		
	36.88	0.01	0.03	0.23	31.68	0.39	29.93	0.32	0.00	0.18	99.65	1010	0	1	5	726	9	1222	9	0	4	80.20	37.08		
	36.82	0.02	0.05	0.34	33.21	0.40	29.68	0.33	0.00	0.19	101.04	1002	0	2	7	756	9	1204	10	0	4	81.97	38.38		
pigeonite																									
	54.77	0.02	0.59	0.48	19.30	0.37	23.15	2.29	0.01	0.10	101.08	1995	1	25	14	588	11	1257	89	1	3	51.50	31.67	4.59	30.21
	53.98	0.07	0.87	0.73	18.51	0.41	22.85	2.27	0.00	0.33	100.02	1986	2	38	21	570	13	1254	89	0	10	44.58	31.03	4.65	29.58
	52.80	0.12	0.98	0.61	19.36	0.43	21.74	2.50	0.00	0.06	98.60	1981	3	43	18	607	14	1216	100	0	2	44.45	33.07	5.19	31.35
	54.71	0.07	0.43	0.53	18.58	0.31	22.46	3.73	0.03	0.09	100.95	1998	2	19	15	567	10	1223	146	2	3	59.18	31.53	7.50	29.16
	53.96	0.10	0.66	0.62	19.02	0.37	22.45	3.13	0.04	0.04	100.40	1985	3	29	18	585	12	1231	123	3	1	50.76	32.01	6.32	29.99
	54.13	0.10	0.51	0.47	18.64	0.31	22.72	2.91	0.04	0.04	99.87	1995	3	22	14	575	10	1249	115	3	1	59.37	31.35	5.90	29.50
spinel																									
	0.21	0.93	11.19	52.66	26.69	0.36	5.84	0.14	0.01	0.00	98.03	7	24	457	1441	773	11	301	5	1	0	73.19	71.24		
	0.13	1.05	11.34	51.24	26.96	0.35	5.84	0.10	0.01	0.17	97.19	5	28	467	1416	788	10	304	4	1	5	76.05	71.46		
	0.11	1.07	12.91	49.20	26.95	0.39	6.25	0.08	0.00	0.06	97.05	4	28	528	1349	782	11	323	3	2	2	68.22	70.02		
	0.39	1.25	16.50	44.40	27.09	0.35	6.63	0.21	0.03	0.05	96.87	13	32	662	1194	771	11	336	8	0	1	76.41	69.00		
	0.40	1.12	16.25	46.12	26.62	0.34	6.56	0.17	0.02	0.26	97.86	13	28	646	1229	751	10	330	6	1	7	77.30	68.86		
	0.09	1.20	21.21	41.30	28.27	0.31	6.16	0.10	0.00	0.11	98.75	3	30	821	1073	777	9	302	4	0	1	90.03	71.45		
metal																									
	0.06	0.10	0.08	0.15	61.91	0.00	0.00	0.06	0.00	72.48	134.84	13	16	20	26	11221	0	0	14	0	12637				
	0.00	0.00	0.00	0.15	60.56	0.00	0.01	0.00	0.00	74.74	135.46	0	0	0	26	10954	0	3	0	0	13004				
	0.00	0.01	0.00	0.27	72.34	0.02	0.00	0.00	0.00	61.35	133.99	0	2	0	46	13175	4	0	0	0	10748				

1180°C   IW-0.5   cooling   M35

	SIO2	TIO2	AL2O3	CR2O3	FEO	MNO	MGO	CAO	NA2O	NIO	TOTAL	Si	Ti	Al	Cr	Fe	Mn	Mg	Ca	Na	Ni	FEMN	FFM	WO	FS
glass																									
	50.36	0.83	10.07	0.34	19.34	0.31	6.93	9.79	0.46	0.00	98.43	7655	95	1804	41	2459	40	1571	1595	136	0	61.60	60.42		
	50.75	0.77	10.13	0.28	19.50	0.34	6.33	10.02	0.42	0.03	98.57	7704	88	1813	34	2476	44	1433	1630	124	4	56.63	62.64		
	51.05	0.84	10.28	0.33	19.26	0.36	6.09	10.51	0.48	0.12	99.31	7694	95	1826	39	2428	46	1368	1697	140	15	52.82	63.19		
	51.09	0.80	10.30	0.31	19.85	0.32	6.95	9.86	0.49	0.01	99.98	7652	90	1818	37	2486	41	1552	1582	142	1	61.25	60.96		
	51.52	0.78	10.30	0.29	19.39	0.35	6.77	10.05	0.44	0.00	99.89	7701	88	1815	34	2424	44	1509	1610	128	0	54.70	60.95		
	51.92	0.85	10.37	0.25	19.22	0.34	7.03	9.95	0.53	0.03	100.49	7702	95	1813	29	2385	43	1555	1581	152	4	55.81	59.88		
	49.40	0.82	10.54	0.31	19.94	0.31	6.43	10.28	0.40	0.03	98.46	7552	94	1899	37	2550	40	1466	1684	119	4	63.51	62.87		
	51.94	0.77	10.54	0.25	19.39	0.34	6.86	9.88	0.57	0.00	100.54	7702	86	1842	29	2405	43	1517	1570	164	0	56.31	60.66		
	50.10	0.82	10.62	0.31	20.01	0.37	6.23	10.23	0.49	0.06	99.24	7591	93	1897	37	2536	47	1407	1661	144	7	53.40	63.54		
	50.53	0.82	10.66	0.28	19.48	0.35	6.42	10.33	0.43	0.38	99.68	7607	93	1892	33	2453	45	1441	1666	126	46	54.95	62.28		
	48.86	0.82	10.68	0.34	19.54	0.32	6.77	9.89	0.50	0.00	97.72	7516	95	1936	41	2514	42	1553	1630	149	0	60.29	61.19		
olivine																									
	37.33	0.03	0.04	0.34	30.73	0.45	31.32	0.34	0.00	0.17	100.75	1006	1	1	7	692	10	1258	10	0	4	67.42	35.31		
	36.97	0.03	0.04	0.28	30.26	0.45	32.02	0.34	0.00	0.18	100.57	997	1	1	6	683	10	1287	10	0	4	66.39	34.47		
	36.90	0.02	0.04	0.29	30.07	0.44	31.11	0.34	0.00	0.24	99.45	1006	0	1	6	686	10	1265	10	0	5	67.47	34.98		
	37.59	0.03	0.06	0.34	29.99	0.46	31.70	0.36	0.01	0.29	100.82	1009	1	2	7	673	12	1268	10	0	6	64.36	34.49		
	36.30	0.05	0.06	0.35	31.40	0.52	31.29	0.38	0.00	0.14	100.50	987	1	2	8	714	12	1269	11	1	3	59.61	35.80		
	36.50	0.05	0.06	0.38	31.42	0.52	31.89	0.35	0.00	0.24	101.41	983	1	2	8	708	12	1281	10	0	5	59.65	35.39		
	37.03	0.05	0.06	0.34	29.58	0.52	32.28	0.35	0.00	0.17	100.38	998	1	2	7	667	10	1297	10	0	4	56.16	33.75		
	36.71	0.03	0.06	0.29	30.37	0.44	32.07	0.31	0.00	0.19	100.47	992	0	2	6	687	10	1292	9	0	4	68.14	34.52		
	37.87	0.02	0.06	0.26	29.71	0.45	32.78	0.34	0.00	0.15	101.64	1005	0	2	5	659	10	1297	9	0	3	65.18	33.53		
	37.44	0.02	0.06	0.31	30.90	0.45	32.27	0.34	0.01	0.25	102.04	996	1	2	7	688	10	1281	10	0	5	67.79	34.77		
	37.25	0.03	0.08	0.29	30.44	0.43	32.55	0.34	0.00	0.19	101.61	994	1	3	6	679	10	1295	10	1	4	69.89	34.24		
	37.44	0.03	0.08	0.31	30.93	0.48	30.43	0.41	0.00	0.17	100.28	1014	1	3	7	701	11	1229	12	0	4	63.62	36.11		
	38.06	0.02	0.08	0.29	30.35	0.46	31.87	0.34	0.00	0.13	101.60	1012	0	3	6	675	10	1264	10	0	3	65.14	34.64		
	38.21	0.02	0.21	0.31	29.82	0.46	31.59	0.38	0.00	0.18	101.18	1018	0	7	7	664	10	1255	11	0	4	64.00	34.43		
spinel																									
	0.34	0.57	13.45	69.72	30.08	0.36	5.31	0.06	0.00	0.10	119.99	10	12	448	1558	711	9	224	2	0	2	82.49	75.37		
	0.24	0.55	8.39	49.80	30.94	0.41	5.22	0.13	0.00	0.08	95.76	9	15	362	1440	946	13	285	5	0	2	74.50	76.09		

1180°C IW-1.0 heating M61

	SIO2	TIO2	AL2O3	CR2O3	FEO	MNO	MGO	CAO	NA2O	NIO	TOTAL	Si	Ti	Al	Cr	Fe	Mn	Mg	Ca	Na	Ni	FEMN	FFM	WO	FS
glass																									
	50.51	0.88	12.15	0.38	16.25	0.31	7.25	9.96	0.77	0.00	98.46	7560	99	2143	45	2034	39	1618	1597	223	0	51.76	55.11		
	50.04	0.82	12.19	0.37	15.88	0.35	6.73	10.12	0.78	0.05	97.33	7574	93	2175	44	2010	45	1519	1641	229	6	44.80	56.25		
	49.59	0.85	12.19	0.22	15.88	0.22	7.11	10.05	0.80	0.15	97.06	7532	97	2182	26	2017	28	1610	1636	236	18	71.27	55.18		
	49.44	0.87	12.43	0.37	15.89	0.34	7.23	9.71	0.82	0.11	97.21	7498	99	2222	44	2016	44	1635	1578	241	13	46.14	54.56		
	50.70	0.80	12.53	0.28	16.67	0.43	6.17	10.12	0.89	0.03	98.62	7590	90	2211	33	2087	55	1377	1623	258	4	38.28	59.32		
	51.19	0.93	12.68	0.32	15.93	0.36	6.09	10.40	0.74	0.00	98.64	7624	104	2226	38	1984	45	1352	1660	214	0	43.69	58.67		
	50.77	0.87	12.75	0.54	16.66	0.46	5.80	10.26	0.77	0.15	99.03	7575	98	2242	64	2079	58	1290	1640	223	18	35.76	60.66		
	50.10	0.78	12.75	0.70	16.38	0.37	6.07	10.17	0.82	0.00	98.14	7538	88	2261	83	2061	47	1362	1640	239	0	43.71	59.40		
	50.42	0.83	12.85	0.28	16.83	0.46	5.97	10.70	0.81	0.00	99.15	7527	93	2261	33	2101	58	1329	1712	234	0	36.12	60.24		
	50.10	0.93	12.96	0.41	15.98	0.49	5.65	10.37	0.90	0.11	97.90	7549	105	2302	49	2014	63	1269	1674	263	13	32.20	60.19		
	51.69	0.92	13.09	0.35	16.78	0.48	5.74	10.79	1.04	0.22	101.10	7561	101	2257	40	2053	59	1252	1691	295	26	34.52	61.02		
	51.39	0.80	13.11	0.50	15.12	0.44	6.30	10.00	0.92	0.13	98.71	7619	89	2291	59	1875	55	1393	1589	264	16	33.93	56.43		
	51.17	0.88	13.19	0.39	15.17	0.34	6.12	9.93	0.94	0.08	98.21	7620	99	2315	46	1889	43	1359	1584	271	10	44.05	57.41		
olivine																									
	37.01	0.00	0.02	0.38	26.82	0.46	34.24	0.31	0.03	0.13	99.40	995	0	1	8	603	10	1372	9	2	3	57.57	30.37		
	37.31	0.00	0.02	0.37	26.28	0.44	34.41	0.32	0.01	0.09	99.25	1000	0	1	8	589	10	1376	9	1	2	58.97	29.84		
	37.78	0.02	0.02	0.23	25.78	0.45	34.94	0.31	0.00	0.08	99.61	1005	0	1	5	574	10	1386	9	0	2	56.56	29.12		
	37.35	0.00	0.04	0.44	26.12	0.44	35.20	0.25	0.03	0.27	100.14	993	0	1	9	581	10	1395	7	2	6	58.61	29.25		
	36.69	0.00	0.06	0.41	26.71	0.44	34.17	0.32	0.00	0.17	98.97	991	0	2	9	603	10	1376	9	0	4	59.94	30.33		
	37.27	0.03	0.06	0.37	27.11	0.44	34.14	0.25	0.01	0.05	99.73	998	1	2	8	607	10	1363	7	1	1	60.83	30.66		
	37.33	0.03	0.06	0.37	27.07	0.40	34.01	0.29	0.03	0.04	99.63	1000	1	2	8	607	9	1358	8	2	1	66.82	30.73		
	37.44	0.00	0.06	0.39	26.17	0.46	34.36	0.31	0.01	0.06	99.26	1003	0	2	8	586	10	1372	9	1	1	56.17	29.78		
	36.97	0.07	0.08	0.47	26.98	0.50	34.54	0.25	0.03	0.00	99.89	989	1	3	10	604	11	1378	7	2	0	53.28	30.30		
	37.29	0.00	0.09	0.38	27.33	0.44	33.92	0.32	0.03	0.03	99.83	998	0	3	8	612	10	1354	9	2	1	61.33	30.97		
pigeonite																									
	53.48	0.05	0.72	0.67	16.66	0.39	24.18	2.53	0.01	0.06	98.75	1978	1	31	20	515	12	1334	100	1	2	42.18	27.69	5.11	26.28
	53.63	0.10	0.81	0.80	16.44	0.48	24.11	2.83	0.04	0.04	99.28	1974	3	35	23	506	15	1323	112	3	1	33.82	27.44	5.71	25.88
	52.93	0.12	0.87	0.73	16.44	0.43	24.31	2.53	0.03	0.01	98.40	1966	3	38	21	511	14	1346	101	2	0	37.75	27.30	5.11	25.91
spinel																									
	0.68	1.12	15.06	46.42	24.26	0.39	7.73	0.15	0.01	0.10	95.92	23	29	606	1254	693	11	394	5	1	3	61.42	63.12		
	0.39	1.08	15.44	46.70	23.88	0.39	7.49	0.60	0.07	0.09	96.13	13	28	620	1259	681	11	381	22	5	2	60.46	63.47		
metal																									
	0.15	0.07	0.06	0.20	106.52	0.00	0.08	0.00	0.07	29.34	136.49	32	11	15	33	18817	0	25	0	29	4986				
	0.00	0.00	0.00	0.13	106.88	0.00	0.02	0.00	0.03	30.32	137.18	0	0	0	22	18812	0	6	0	12	5143				

1180°C   IW-1.5   heating   M30

SIO2	TIO2	AL2O3	CR2O3	FEO	MNO	MGO	CAO	NA2O	NIO	TOTAL	Si	Ti	Al	Cr	Fe	Mn	Mg	Ca	Na	Ni	FEMN	FFM	WO	FS
glass																								
44.62	0.05	31.84	0.05	1.59	0.11	3.30	16.89	0.29	0.07	98.81	6283	5	5284	6	187	13	693	2548	79	8	14.27	20.97		
44.82	0.22	31.95	0.75	2.50	0.13	2.89	16.96	0.32	0.00	100.42	6242	23	5244	83	291	15	600	2531	86	0	18.99	32.12		
46.16	0.07	31.26	0.04	1.71	0.10	1.60	16.68	0.63	0.12	98.27	6508	7	5195	4	202	12	336	2520	172	14	16.88	36.67		
olivine																								
39.47	0.13	0.28	0.86	12.77	0.46	45.08	0.28	0.03	0.10	99.46	991	2	8	17	268	10	1687	8	1	2	27.41	13.64		
39.47	0.18	0.81	2.25	13.06	0.54	44.09	0.34	0.00	0.05	100.79	982	3	24	44	272	11	1635	9	0	1	23.88	14.16		
39.79	0.12	0.42	1.13	12.86	0.54	44.19	0.32	0.00	0.00	99.37	999	2	12	22	270	11	1655	9	0	0	23.51	13.95		
39.83	0.17	0.68	0.86	12.45	0.56	43.43	0.56	0.01	0.19	98.74	1005	3	20	17	263	12	1634	15	0	4	21.95	13.77		
40.46	0.02	0.15	0.57	12.49	0.58	47.26	0.27	0.00	0.04	101.84	989	0	4	11	255	12	1723	7	0	1	21.26	12.83		
41.08	0.08	0.06	0.53	12.62	0.50	44.90	0.28	0.03	0.04	100.12	1019	1	2	10	262	11	1660	7	1	1	24.92	13.55		
pigeonite																								
56.91	0.07	0.10	0.74	9.37	1.49	27.58	4.40	0.02	0.00	100.68	2009	2	4	21	277	45	1452	166	1	0	6.21	15.61	8.78	14.60
56.88	0.05	0.08	0.75	9.26	1.51	27.34	4.51	0.01	0.00	100.39	2014	1	3	21	274	45	1443	171	1	0	6.05	15.56	9.06	14.52
56.99	0.08	0.02	0.74	9.44	1.48	27.45	4.32	0.02	0.00	100.54	2015	2	1	21	279	44	1447	164	1	0	6.30	15.77	8.66	14.77
spinel																								
0.08	2.65	6.14	60.79	15.96	0.96	10.44	0.12	0.01	0.00	97.15	3	68	248	1644	457	28	532	4	1	0	16.41	44.90		
0.21	3.11	21.63	43.60	15.09	0.80	13.78	0.20	0.00	0.00	98.42	6	73	790	1068	391	21	637	7	0	0	18.62	37.24		
0.47	3.49	19.63	45.10	15.70	0.51	13.28	0.11	0.00	0.16	98.46	15	82	723	1115	410	14	619	4	0	4	30.39	39.36		
2.09	3.47	20.91	40.71	16.28	0.51	12.96	0.84	0.02	0.00	97.80	65	81	765	999	422	13	599	28	1	0	31.52	40.80		
metal																								
0.11	0.00	0.02	0.15	121.39	0.18	0.03	0.04	0.05	7.33	129.30	24	0	5	26	22531	34	10	10	22	1309				
0.13	0.07	0.06	0.04	120.52	0.00	0.00	0.10	0.01	6.96	127.89	29	12	16	7	22602	0	0	24	4	1256				

1180°C   IW-1.5   heating   M47

SIO2	TIO2	AL2O3	CR2O3	FEO	MNO	MGO	CAO	NA2O	NIO	TOTAL	Si	Ti	Al	Cr	Fe	Mn	Mg	Ca	Na	Ni	FEMN	FFM	WO	FS
glass																								
44.59	0.25	30.22	0.05	1.77	0.15	5.03	16.84	0.49	0.00	99.18	6278	26	5015	6	208	18	1056	2510	134	0	11.65	16.26		
42.50	0.19	33.70	0.13	2.14	0.08	4.75	16.74	0.37	0.00	100.59	5921	20	5534	14	249	9	987	2499	100	0	26.41	20.02		
43.60	0.16	33.77	0.18	2.23	0.12	2.69	17.07	0.48	0.14	100.45	6076	17	5547	20	260	14	559	2549	130	16	18.35	31.20		
42.84	0.17	35.28	0.05	1.73	0.11	2.21	17.99	0.46	0.07	100.92	5944	18	5769	5	201	13	457	2674	124	8	15.53	29.93		
olivine																								
38.76	0.07	0.32	0.60	12.74	0.57	44.86	0.33	0.00	0.12	98.37	985	1	10	12	271	12	1700	9	0	2	22.07	13.66		
39.35	0.25	0.52	0.49	12.26	0.80	44.68	0.77	0.01	0.14	99.27	990	5	15	10	258	17	1675	21	0	3	15.13	13.22		
39.99	0.17	1.18	0.44	12.22	0.67	43.85	0.85	0.03	0.16	98.56	999	3	35	9	255	14	1634	23	1	3	18.01	13.42		
40.02	0.12	0.34	0.54	12.66	0.73	44.12	0.36	0.00	0.11	99.00	1007	2	10	11	267	16	1656	10	0	2	17.12	13.75		
spinel																								
0.33	3.53	20.07	43.40	16.07	0.71	13.01	0.09	0.02	0.08	97.31	10	84	748	1085	425	19	613	3	1	2	22.35	40.19		
metal																								
0.00	0.53	0.01	0.25	119.12	0.00	0.00	0.08	0.04	13.12	133.13	0	88	3	43	21464	0	0	14	17	2274				

1200°C   IW-0.5   heating   M26

	SIO2	TIO2	AL2O3	CR2O3	FEO	MNO	MGO	CAO	NA2O	NIO	TOTAL	Si	Ti	Al	Cr	Fe	Mn	Mg	Ca	Na	Ni	FEMN	FFM	WO	FS
glass																									
	49.50	0.67	9.56	0.41	21.66	0.35	7.46	9.47	0.34	0.17	99.59	7541	77	1717	49	2760	45	1694	1546	100	21	61.10	61.34		
	49.31	0.68	9.69	0.06	21.16	0.41	6.77	9.68	0.42	0.11	98.29	7593	79	1759	7	2725	53	1554	1597	125	14	50.96	62.89		
	50.30	0.68	9.56	0.37	21.03	0.32	7.44	9.40	0.39	0.00	99.49	7623	78	1708	44	2666	41	1681	1526	115	0	64.89	60.75		
	49.76	0.70	9.89	0.35	21.34	0.36	7.22	9.21	0.49	0.07	99.39	7568	80	1773	42	2715	46	1637	1501	145	9	58.53	61.72		
	49.30	0.74	10.19	0.35	21.73	0.41	6.45	9.75	0.49	0.16	99.58	7520	85	1832	42	2772	53	1467	1594	145	20	52.33	64.59		
	49.31	0.72	9.91	0.45	22.33	0.31	7.08	9.47	0.40	0.00	99.98	7500	82	1777	54	2841	40	1606	1543	118	0	71.12	63.32		
olivine																									
	36.80	0.00	0.00	0.34	31.71	0.44	31.02	0.32	0.00	0.15	100.78	997	0	0	7	719	10	1253	9	0	3	71.15	36.26		
	37.03	0.00	0.02	0.32	30.76	0.37	30.64	0.31	0.00	0.10	99.55	1010	0	1	7	702	9	1246	9	0	2	82.08	35.87		
	36.45	0.00	0.02	0.34	30.94	0.41	31.52	0.35	0.00	0.00	100.03	992	0	1	7	704	9	1279	10	0	0	74.50	35.34		
	36.93	0.00	0.04	0.39	31.04	0.44	30.54	0.31	0.00	0.01	99.84	1007	0	2	8	708	10	1241	9	0	3	69.65	36.12		
	37.10	0.00	0.06	0.34	31.17	0.37	31.22	0.32	0.00	0.00	100.59	1003	0	2	7	705	8	1258	9	0	0	83.17	35.75		
	37.35	0.00	0.06	0.35	31.17	0.37	30.99	0.32	0.00	0.00	100.61	1008	0	3	7	704	8	1247	9	0	0	83.17	35.92		
	36.84	0.00	0.08	0.34	30.99	0.45	31.27	0.38	0.00	0.22	100.57	997	0	3	7	702	10	1262	11	0	5	67.99	35.54		
	37.08	0.00	0.08	0.04	31.39	0.45	31.27	0.34	0.00	0.18	100.83	1001	0	3	13	709	9	1259	10	0	4	68.87	35.84		
	36.65	0.00	0.13	0.63	31.07	0.40	31.26	0.29	0.00	0.15	100.58	993	0	4	10	704	9	1263	8	0	3	76.68	35.63		
	37.16	0.00	0.25	0.45	32.51	0.44	30.00	0.39	0.00	0.15	101.35	1003	0	8	8	734	10	1208	11	0	3	72.94	37.61		
	37.80	0.05	0.02	0.39	30.79	0.39	30.77	0.28	0.01	0.15	100.65	1018	1	1	5	693	10	1235	8	1	3	77.94	35.79		
	37.55	0.02	0.04	0.22	30.58	0.45	30.99	0.34	0.01	0.13	100.32	1014	0	1	9	691	10	1248	10	1	3	67.09	35.44		
	37.24	0.00	0.04	0.40	30.87	0.45	31.17	0.31	0.01	0.22	100.71	1005	0	1	9	697	10	1254	9	1	5	67.73	35.53		
	36.89	0.01	0.03	0.33	30.76	0.40	30.67	0.33	0.02	0.09	99.53	1007	0	1	7	703	9	1249	10	1	2	75.92	35.84		
	37.08	0.01	0.01	0.34	30.86	0.41	31.05	0.31	0.00	0.28	100.35	1005	0	0	7	699	9	1255	9	0	6	74.31	35.62		
pigeonite																									
	53.10	0.00	0.21	0.44	19.01	0.36	23.64	2.77	0.03	0.08	99.64	1971	0	9	13	590	11	1309	110	2	2	52.14	30.90	5.45	29.22
	53.95	0.12	0.68	0.73	18.69	0.40	24.08	2.10	0.03	0.04	100.82	1970	3	29	21	571	12	1311	82	2	1	46.13	30.14	4.16	28.88
	53.99	0.09	0.52	0.69	18.92	0.31	23.52	2.63	0.03	0.14	100.84	1976	2	22	20	579	10	1283	103	2	4	60.26	30.93	5.22	29.32
	53.47	0.06	0.70	0.65	18.98	0.40	23.16	2.07	0.03	0.00	99.51	1960	2	31	19	588	13	1279	82	2	0	46.85	31.28	4.19	29.97
	54.95	0.07	0.26	0.50	19.11	0.35	22.84	2.43	0.05	0.08	100.63	2009	2	11	14	584	11	1245	95	4	2	53.91	31.76	4.92	30.19
spinel																									
	0.17	1.05	13.38	51.29	26.63	0.36	6.20	0.13	0.00	0.22	99.43	6	27	532	1368	752	10	312	5	0	6	73.03	69.99		
	0.06	1.03	8.01	56.61	27.25	0.31	5.21	0.11	0.00	0.09	98.68	2	27	331	1571	800	9	273	4	0	3	86.78	73.95		
	0.09	0.95	8.81	55.48	26.71	0.36	5.55	0.10	0.01	0.03	98.09	3	25	364	1539	784	11	290	4	1	1	73.25	72.25		
	0.11	1.08	11.45	52.65	26.95	0.34	6.06	0.11	0.01	0.04	98.80	4	28	463	1429	774	10	310	4	1	1	78.25	70.74		
	0.21	1.06	18.08	44.12	27.02	0.31	6.86	0.14	0.00	0.07	97.87	7	27	713	1167	756	9	342	5	0	2	86.05	68.30		
metal																									
	0.00	0.02	0.00	0.09	65.81	0.05	0.00	0.00	0.00	70.54	136.51	0	3	0	15	11798	9	0	0	0	12164				
	0.04	0.02	0.00	0.09	66.73	0.03	0.00	0.00	0.00	68.50	135.41	9	3	0	15	12050	5	0	0	0	11898				
	0.22	0.03	0.02	0.05	71.27	0.01	0.00	0.00	0.03	64.98	136.61	47	5	5	8	12716	2	0	0	12	11152				

1200°C   IW-0.5   cooling   M41

	SIO2	TIO2	AL2O3	CR2O3	FEO	MNO	MGO	CAO	NA2O	NIO	TOTAL	Si	Ti	Al	Cr	Fe	Mn	Mg	Ca	Na	Ni	FEMN	FFM	WO	FS
glass	49.46	0.83	11.03	0.35	17.25	0.40	7.00	9.98	0.78	0.05	97.13	7571	96	1990	42	2209	52	1598	1637	232	6	42.58	57.25		
	51.58	0.82	11.05	0.31	18.44	0.39	6.95	9.84	0.71	0.04	100.13	7657	92	1933	36	2289	49	1538	1565	204	5	46.68	59.06		
	51.49	0.82	11.11	0.32	17.83	0.41	6.99	9.95	0.73	0.03	99.68	7661	92	1948	38	2219	52	1551	1586	211	4	42.94	58.07		
	50.78	0.81	11.14	0.34	17.74	0.40	6.89	9.91	0.74	0.02	98.77	7632	92	1974	40	2230	51	1544	1596	216	2	43.79	58.30		
olivine	37.99	0.02	0.04	0.38	27.43	0.43	34.44	0.28	0.00	0.06	101.07	1003	0	1	8	606	10	1355	8	0	1	62.98	30.73		
	38.49	0.02	0.06	0.31	27.25	0.48	34.70	0.32	0.00	0.15	101.78	1007	0	2	6	598	11	1354	9	0	3	56.05	30.42		
	37.22	0.02	0.06	0.32	27.24	0.53	33.79	0.29	0.00	0.11	99.58	999	0	2	7	612	12	1353	8	0	2	50.75	30.95		
	37.89	0.02	0.06	0.34	27.13	0.49	34.42	0.31	0.00	0.11	100.77	1003	0	2	7	600	11	1358	9	0	2	54.67	30.49		
	36.21	0.03	0.06	0.31	27.30	0.45	34.85	0.32	0.00	0.15	101.68	1002	1	2	6	599	10	1362	9	0	3	59.90	30.37		
	37.74	0.03	0.08	0.37	27.42	0.44	33.64	0.34	0.01	0.13	100.20	1006	1	3	8	611	10	1337	10	1	3	61.53	31.22		
	38.36	0.02	0.08	0.29	26.93	0.44	34.72	0.35	0.00	0.10	101.29	1007	0	2	6	591	10	1359	10	0	2	60.43	30.17		
	37.99	0.02	0.08	0.31	27.44	0.48	34.79	0.32	0.01	0.09	101.53	999	0	2	6	603	11	1363	9	1	2	56.44	30.51		
	37.63	0.02	0.09	0.29	26.86	0.53	34.17	0.35	0.00	0.11	100.05	1003	0	3	6	599	12	1357	10	0	2	50.04	30.42		
	38.10	0.00	0.17	0.38	27.26	0.41	34.17	0.29	0.01	0.17	100.96	1006	0	5	8	602	9	1345	8	1	4	65.65	30.77		
pigeonite	55.45	0.07	0.43	0.54	16.39	0.44	25.73	2.06	0.03	0.05	101.19	1991	2	18	15	492	13	1377	79	2	1	36.78	26.14	4.04	25.08
	55.67	0.07	0.51	0.56	16.11	0.44	25.92	2.06	0.03	0.05	101.42	1991	2	21	16	482	13	1382	79	2	1	36.15	25.67	4.04	24.63
	55.17	0.10	0.72	0.63	16.47	0.45	25.60	1.99	0.03	0.04	101.20	1982	3	30	18	495	14	1371	77	2	1	36.14	26.33	3.92	25.30
	55.32	0.08	0.83	0.56	16.71	0.49	24.87	1.99	0.01	0.05	100.91	1993	2	35	16	503	15	1336	77	1	1	33.67	27.15	3.98	26.07
	54.47	0.10	0.89	0.70	15.76	0.43	24.95	2.27	0.03	0.00	99.60	1984	3	38	20	480	13	1355	89	2	0	36.19	25.98	4.57	24.79
spinel	0.28	0.63	9.90	52.37	30.93	0.36	5.32	0.11	0.00	0.09	99.99	10	16	404	1435	897	11	275	4	0	3	84.82	75.85		
	0.28	0.70	10.88	50.98	28.70	0.41	6.48	0.11	0.01	0.14	98.69	10	18	444	1395	831	12	334	4	1	4	69.11	70.57		
metal	0.06	0.00	0.02	0.06	58.54	0.01	0.02	0.00	0.00	82.37	141.08	12	0	5	10	10174	2	6	0	0	13771				
	0.19	0.02	0.04	0.10	57.87	0.04	0.05	0.00	0.00	82.61	140.92	39	3	10	16	10051	7	15	0	0	13802				

1200°C IW-1.5 heating M27

	SiO2	TiO2	AL2O3	CR2O3	FEO	MNO	MGO	CAO	NA2O	NiO	TOTAL	Si	Ti	Al	Cr	Fe	Mn	Mg	Ca	Na	Ni	FEMN	FFM	WO	FS
glass																									
	58.21	0.72	12.24	0.50	8.14	0.36	7.19	10.86	0.37	0.03	98.62	8238	77	2042	56	963	43	1517	1647	102	3	22.33	38.18		
	58.70	0.79	12.13	0.43	8.55	0.36	6.85	11.31	0.48	0.04	99.63	8247	83	2009	48	1005	43	1435	1703	131	5	23.45	40.47		
	58.56	0.72	12.13	0.48	8.04	0.47	7.03	10.67	0.43	0.06	98.60	8281	77	2022	54	951	56	1482	1617	118	7	16.89	38.20		
	58.71	0.68	12.12	0.43	8.42	0.34	7.42	10.75	0.41	0.06	99.34	8253	72	2008	48	990	40	1555	1619	112	7	24.45	38.29		
olivine																									
	40.69	0.00	0.04	0.63	13.89	0.57	45.25	0.25	0.00	0.00	101.32	1005	0	1	12	287	12	1665	7	0	0	24.06	14.60		
	40.43	0.00	0.06	0.60	13.69	0.63	45.66	0.27	0.00	0.00	101.34	998	0	2	12	283	13	1681	7	0	0	21.45	14.30		
	38.49	0.00	0.08	0.61	13.73	0.59	44.24	0.25	0.00	0.00	97.99	987	0	2	12	294	13	1691	7	0	0	22.97	14.73		
	40.71	0.00	0.08	0.64	13.71	0.58	45.37	0.27	0.00	0.09	101.36	1004	0	2	12	283	12	1668	7	0	0	23.34	14.41		
	40.01	0.00	0.11	0.69	13.46	0.58	45.32	0.24	0.00	0.09	100.50	996	0	3	14	280	12	1682	6	0	2	22.91	14.19		
	40.33	0.03	0.06	0.56	13.46	0.62	45.75	0.25	0.00	0.23	101.29	996	1	2	11	278	13	1685	7	0	5	21.43	14.07		
	40.66	0.04	0.04	0.50	13.31	0.51	44.72	0.29	0.01	0.04	100.12	1012	1	1	10	277	11	1660	8	0	1	25.77	14.23		
	40.28	0.01	0.03	0.55	13.61	0.44	46.09	0.28	0.01	0.10	101.40	994	0	1	11	281	9	1695	7	0	2	30.54	14.15		
pigeonite																									
	56.63	0.00	0.55	0.83	10.05	0.49	29.13	3.01	0.00	0.00	100.69	1991	0	23	23	295	15	1527	113	0	0	20.25	16.09	5.81	15.15
	56.52	0.00	0.91	0.92	9.48	0.44	29.75	2.80	0.00	0.00	100.82	1979	0	38	25	278	13	1553	105	0	0	21.27	15.06	5.39	14.25
	55.30	0.00	1.19	1.07	9.60	0.59	29.90	2.62	0.00	0.14	100.27	1952	0	50	30	283	18	1573	99	0	4	16.07	15.12	5.02	14.36
	55.75	0.27	1.21	1.05	9.88	0.44	30.24	2.45	0.00	0.08	101.29	1948	7	50	30	289	13	1575	92	0	2	22.17	15.38	4.66	14.67
	56.27	0.18	1.27	0.94	9.21	0.57	29.48	2.28	0.00	0.04	100.20	1977	5	53	26	271	17	1544	86	0	1	15.95	14.77	4.48	14.11
	56.84	0.19	1.30	1.17	9.13	0.72	30.46	2.06	0.00	0.08	101.87	1965	5	53	32	264	21	1570	76	0	2	12.52	14.23	3.95	13.67
	56.29	0.21	1.53	0.99	9.47	0.43	28.97	2.28	0.00	0.00	100.17	1979	6	63	28	278	13	1518	86	0	0	21.74	15.39	4.53	14.69
	55.62	0.30	1.61	1.13	9.51	0.57	29.86	2.66	0.00	0.11	101.26	1943	8	66	31	278	17	1555	100	0	3	16.47	15.02	5.11	14.25
	57.06	0.22	1.68	1.20	9.20	0.58	29.46	2.24	0.00	0.06	101.64	1974	6	69	33	266	17	1520	83	0	2	15.66	14.77	4.40	14.12
	55.92	0.18	1.81	1.24	9.04	0.43	29.38	2.56	0.00	0.00	100.56	1959	5	75	34	265	13	1535	96	0	0	20.76	14.62	5.04	13.88
spinel																									
	0.11	0.65	34.35	33.92	13.53	0.46	14.03	0.01	0.00	0.04	97.10	3	15	1201	796	336	12	621	0	0	1	29.04	34.69		
	2.61	0.65	28.97	34.80	14.38	0.43	16.17	0.31	0.03	0.04	98.39	77	14	1007	812	355	11	711	10	2	1	33.02	32.95		
	0.47	0.75	24.43	42.56	15.26	0.44	14.61	0.18	0.00	0.05	98.75	14	17	880	1028	390	11	666	6	0	1	34.24	36.55		
	0.60	0.68	31.08	39.18	14.59	0.37	13.53	0.17	0.00	0.06	100.26	18	15	1073	907	357	9	591	5	0	1	38.93	37.33		
	0.26	0.68	29.65	35.78	14.13	0.39	14.82	0.18	0.01	0.05	95.95	8	16	1068	865	361	10	675	6	1	1	35.77	34.51		
metal																									
	0.17	0.00	0.00	0.18	118.32	0.01	0.07	0.03	0.00	11.44	130.22	37	0	0	31	21817	2	23	7	0	2029				
	1.20	0.00	0.02	0.00	117.26	0.08	2.22	0.10	0.00	12.61	133.47	252	0	0	0	20628	14	696	23	0	2134				
	0.02	0.00	0.02	0.09	121.24	0.00	0.03	0.00	0.00	11.47	132.87	4	0	5	15	21953	0	10	0	0	1998				
	0.04	0.00	0.04	0.18	124.37	0.00	0.02	0.03	0.00	12.05	136.73	8	0	10	30	21872	0	6	0	0	2038				
	0.62	0.00	0.04	0.18	119.44	0.01	1.58	0.00	0.00	12.04	133.91	131	0	10	30	21129	2	498	7	0	2049				
	0.96	0.00	0.13	0.01	117.93	0.13	0.40	0.06	0.00	13.21	132.83	205	0	33	2	21099	24	128	14	4	2273				
	0.11	0.07	0.08	0.12	120.39	0.00	0.02	0.00	0.01	11.17	131.97	24	11	21	21	21904	0	6	0	0	1955				
	0.02	0.05	0.00	0.10	117.83	0.00	0.05	0.03	0.05	12.51	130.64	4	8	0	17	21698	0	16	7	21	2216				

1200°C IW-1.5 cooling M39

	SiO2	TiO2	AL2O3	CR2O3	FEO	MNO	MGO	CAO	NA2O	NIO	TOTAL	Si	Ti	Al	Cr	Fe	Mn	Mg	Ca	Na	Ni	FEMN	FFM	WO	FS
glass																									
	51.64	0.93	13.34	0.45	12.94	0.52	8.52	10.63	0.58	0.04	99.59	7523	102	2291	52	1577	64	1850	1659	164	5	24.57	45.16		
	52.22	0.92	13.36	0.39	12.68	0.49	8.29	10.48	0.54	0.00	99.37	7594	101	2290	45	1542	60	1797	1633	152	0	25.55	45.36		
	53.80	1.00	13.94	0.42	10.39	0.46	8.01	10.44	0.67	0.05	99.18	7725	108	2359	48	1248	56	1715	1606	187	6	22.30	41.34		
	52.76	0.92	13.98	0.37	11.67	0.53	8.62	10.52	0.57	0.03	99.97	7584	99	2369	42	1403	65	1847	1620	159	3	21.74	42.32		
	51.79	0.98	14.11	0.42	11.35	0.54	8.52	11.03	0.50	0.10	99.34	7509	107	2411	48	1376	66	1842	1714	141	12	20.75	41.91		
	52.39	0.98	14.19	0.41	11.04	0.49	8.56	10.70	0.54	0.05	99.35	7562	106	2414	47	1333	60	1842	1655	151	6	22.25	41.20		
olivine																									
	38.59	0.02	0.08	0.47	19.75	0.61	40.81	0.29	0.01	0.00	100.63	989	0	2	10	423	13	1559	8	0	0	31.97	21.21		
	39.62	0.03	0.08	0.44	19.63	0.63	40.39	0.29	0.00	0.01	101.12	1007	1	2	9	417	14	1530	8	0	0	30.76	21.28		
	39.36	0.03	0.08	0.48	19.07	0.67	40.77	0.27	0.00	0.05	100.78	1002	1	2	10	406	14	1548	7	0	1	28.10	20.63		
	39.77	0.03	0.09	0.48	18.72	0.63	40.72	0.28	0.00	0.03	100.75	1010	1	3	10	398	14	1541	8	0	1	29.34	20.36		
	39.24	0.05	0.09	0.51	18.50	0.62	40.94	0.31	0.00	0.01	100.27	1002	1	3	10	395	13	1558	8	0	0	29.46	20.09		
pigeonite																									
	55.49	0.13	0.72	0.82	15.62	0.52	25.75	2.17	0.03	0.01	101.26	1986	3	30	23	467	16	1374	83	2	0	29.66	25.17	4.29	24.09
	56.89	0.17	0.85	0.77	13.05	0.53	26.83	2.28	0.01	0.00	101.38	2005	5	35	21	385	16	1410	86	1	0	24.31	21.25	4.54	20.28
	54.43	0.15	0.91	0.85	14.25	0.48	26.56	2.25	0.01	0.04	99.93	1966	4	39	24	431	15	1431	87	1	1	29.31	22.95	4.44	21.94
	55.30	0.15	1.02	0.91	15.01	0.59	25.97	2.50	0.03	0.04	101.52	1972	4	43	26	448	18	1381	96	2	1	25.12	24.25	4.92	23.06

1300°C IW-0.5 heating M43

	SIO2	TIO2	AL2O3	CR2O3	FEO	MNO	MGO	CAO	NA2O	NIO	TOTAL	Si	Ti	Al	Cr	Fe	Mn	Mg	Ca	Na	Ni	FEMN	FFM	WO	FS
glass																									
	48.44	0.50	6.69	0.76	25.65	0.62	11.29	6.34	0.09	0.10	100.48	7446	58	1212	92	3298	81	2587	1044	27	12	40.85	55.28		
	48.63	0.50	6.69	0.75	23.93	0.57	12.32	5.83	0.11	0.01	99.34	7484	58	1213	91	3080	74	2827	961	33	1	41.45	51.50		
	48.05	0.57	6.71	0.83	25.72	0.67	11.52	6.30	0.11	0.01	100.49	7396	66	1217	101	3311	87	2644	1039	33	1	37.90	54.80		
	47.02	0.55	6.73	0.77	24.29	0.59	11.57	6.13	0.09	0.05	97.79	7403	65	1249	96	3198	79	2716	1034	27	6	40.65	53.37		
	47.37	0.55	6.76	0.80	23.68	0.62	11.57	6.16	0.11	0.03	97.65	7441	65	1252	99	3111	83	2710	1037	34	4	37.71	52.70		
	47.64	0.52	6.76	0.83	25.94	0.61	11.29	6.37	0.11	0.05	100.12	7376	61	1234	102	3359	80	2606	1057	33	6	41.99	55.57		
	46.68	0.52	6.76	0.72	24.10	0.62	11.52	6.09	0.11	0.05	97.17	7396	62	1262	90	3194	83	2721	1034	34	6	38.38	53.24		
	46.68	0.52	6.82	0.73	23.97	0.59	11.67	6.23	0.11	0.04	97.36	7379	62	1271	91	3169	79	2750	1055	34	5	40.11	52.83		
	48.37	0.53	6.84	0.76	25.96	0.57	11.54	6.25	0.13	0.06	101.01	7403	61	1234	92	3323	74	2633	1025	39	7	44.97	55.11		
	48.46	0.55	6.92	0.85	25.95	0.62	11.29	6.20	0.11	0.08	101.03	7414	63	1248	103	3321	80	2575	1016	33	10	41.33	55.56		
	48.09	0.47	7.14	0.72	26.19	0.57	12.44	5.41	0.12	0.04	101.19	7340	54	1285	87	3343	74	2831	885	36	5	45.37	53.51		
olivine																									
	37.74	0.03	0.04	0.64	26.89	0.54	34.69	0.24	0.00	0.06	100.87	998	1	1	13	594	12	1367	7	0	1	49.17	30.12		
	37.99	0.00	0.04	0.56	27.25	0.54	33.84	0.21	0.00	0.05	100.48	1008	0	1	12	605	12	1339	6	0	1	49.83	30.92		
	37.99	0.02	0.04	0.54	27.81	0.52	34.27	0.20	0.00	0.06	101.45	1001	0	1	11	613	12	1347	6	0	1	52.80	31.10		
	37.82	0.00	0.04	0.53	26.26	0.50	34.31	0.20	0.00	0.24	99.90	1007	0	1	11	585	11	1361	6	0	5	51.86	29.87		
	38.57	0.00	0.04	0.51	27.69	0.49	34.70	0.21	0.01	0.05	102.27	1006	0	1	11	604	11	1349	6	1	1	55.80	30.75		
	37.20	0.00	0.04	0.53	27.71	0.53	34.16	0.22	0.00	0.08	100.47	992	0	1	11	618	12	1359	6	0	2	51.62	31.09		
	37.48	0.00	0.04	0.56	27.80	0.49	33.79	0.21	0.00	0.00	100.37	1000	0	1	12	620	11	1344	6	0	0	56.02	31.40		
	37.76	0.02	0.04	0.54	27.65	0.52	33.91	0.21	0.00	0.01	100.66	1003	0	1	11	614	12	1343	6	0	0	52.50	31.20		
	38.38	0.02	0.04	0.53	28.05	0.53	34.85	0.22	0.01	0.22	100.85	1009	0	1	11	573	12	1366	6	1	5	48.53	29.37		
	37.42	0.02	0.04	0.58	27.00	0.53	34.67	0.22	0.01	0.24	100.73	993	0	1	12	599	12	1371	6	1	5	50.30	30.22		
	37.95	0.02	0.06	0.61	27.06	0.49	34.62	0.21	0.00	0.24	101.26	1000	0	2	13	596	11	1360	6	0	5	54.53	30.31		
	37.93	0.02	0.06	0.56	26.84	0.58	34.89	0.20	0.00	0.22	101.30	998	0	2	12	591	13	1369	6	0	5	45.69	29.95		

1300°C IW-1.5 heating M45

	SiO2	TiO2	Al2O3	Cr2O3	FeO	MnO	MgO	CaO	Na2O	NiO	TOTAL	Si	Ti	Al	Cr	Fe	Mn	Mg	Ca	Na	Ni	FEMN	FFM	WO	FS
glass	52.61	0.68	9.45	0.76	12.07	0.74	13.96	9.02	0.05	0.05	99.39	7646	74	1619	87	1467	91	3025	1405	14	6	16.10	32.01		
	52.24	0.72	9.58	0.86	11.50	0.74	14.41	8.47	0.04	0.00	98.56	7628	79	1649	99	1404	92	3137	1325	11	0	15.34	30.31		
	53.01	0.68	9.73	0.85	13.21	0.74	14.14	8.52	0.05	0.13	101.06	7605	73	1645	96	1585	90	3024	1310	14	15	17.63	33.73		
	52.80	0.69	9.55	0.78	12.23	0.73	14.20	8.88	0.03	0.02	99.91	7633	75	1627	89	1479	89	3060	1375	8	2	16.54	31.95		
olivine	40.20	0.00	0.04	0.57	13.28	0.63	45.10	0.21	0.00	0.04	100.07	1003	0	1	11	277	13	1678	6	0	1	20.81	14.08		
	40.09	0.02	0.06	0.64	13.28	0.59	45.58	0.20	0.00	0.04	100.50	997	0	2	13	276	12	1690	5	0	1	22.22	13.96		
	39.75	0.00	0.06	0.61	13.57	0.56	45.15	0.20	0.00	0.03	99.93	996	0	2	12	284	12	1686	5	0	1	23.93	14.34		
	40.84	0.02	0.11	0.60	12.99	0.59	45.17	0.49	0.00	0.05	100.86	1009	0	3	12	268	12	1664	13	0	1	21.74	13.80		
	40.73	0.03	0.15	0.69	13.43	0.62	45.68	0.22	0.01	0.03	101.59	1001	1	4	13	276	13	1674	6	0	1	21.39	14.06		
pigeonite	56.89	0.05	0.36	0.72	9.80	0.52	32.00	0.69	0.00	0.05	101.08	1979	1	15	20	285	15	1660	26	0	1	18.61	14.55	1.30	14.36
	56.31	0.05	0.43	0.76	9.69	0.49	30.29	0.73	0.00	0.10	98.85	2000	1	18	21	288	15	1604	28	0	3	19.53	15.10	1.44	14.88
	57.76	0.07	0.49	0.75	8.76	0.53	32.25	0.76	0.00	0.04	101.41	1991	2	20	20	253	15	1657	28	0	1	16.32	13.12	1.44	12.93
	56.91	0.08	0.51	0.82	9.85	0.46	31.37	0.71	0.01	0.00	100.72	1985	2	21	23	287	14	1632	27	1	0	21.14	14.87	1.35	14.67
	57.19	0.08	0.51	0.77	10.34	0.45	31.34	0.67	0.00	0.05	100.40	1985	2	21	21	300	13	1622	25	0	1	22.69	15.51	1.27	15.31
	56.74	0.08	0.53	0.79	8.38	0.58	31.45	0.81	0.00	0.05	99.41	1994	2	22	22	246	17	1647	30	0	1	14.27	12.89	1.57	12.88
	57.23	0.08	0.57	0.89	8.40	0.56	31.97	0.76	0.00	0.00	100.46	1989	2	23	24	244	16	1657	28	0	0	14.81	12.74	1.45	12.55

1400°C IW-0.5 heating M49

SIO2	TIO2	AL2O3	CR2O3	FEO	MNO	MGO	CAO	NA2O	NIO	TOTAL	Si	Ti	Al	Cr	Fe	Mn	Mg	Ca	Na	Ni	FEMN	FFM	WO	FS
glass
48.52	0.46	6.26	0.89	25.44	0.65	12.11	6.18	0.03	0.05	100.59	7444	53	1132	108	3264	84	2770	1016	9	6	38.64	53.35		
48.58	0.47	6.16	0.88	25.39	0.63	12.23	6.35	0.02	0.06	100.77	7442	54	1112	107	3253	82	2793	1042	6	7	39.79	53.08		
48.44	0.45	6.41	0.86	25.45	0.65	12.01	5.91	0.01	0.03	100.22	7451	52	1162	105	3274	85	2754	974	3	4	38.66	53.56		
48.86	0.46	6.38	0.87	25.71	0.66	11.94	6.66	0.02	0.04	101.60	7432	53	1144	105	3271	85	2708	1086	6	5	38.46	53.94		
48.71	0.42	6.33	0.87	25.41	0.65	12.01	5.98	0.01	0.03	100.42	7473	48	1145	106	3261	84	2747	983	3	4	38.60	53.52		
olivine
37.93	0.00	0.04	0.47	20.55	0.40	40.31	0.18	0.00	0.00	99.88	983	0	1	10	446	9	1558	5	0	0	50.73	22.14		
39.39	0.08	0.04	0.45	20.91	0.48	40.23	0.14	0.00	0.00	101.72	1000	2	1	9	444	10	1523	4	0	0	43.01	22.46		
37.87	0.03	0.04	0.45	20.74	0.45	40.62	0.18	0.00	0.11	100.49	978	1	1	9	448	10	1563	5	0	2	45.51	22.16		
38.34	0.00	0.04	0.47	20.21	0.40	39.88	0.15	0.00	0.05	99.54	994	0	1	10	438	9	1542	4	0	1	49.89	22.04		
36.02	0.00	0.04	0.50	21.11	0.41	40.18	0.18	0.03	0.10	100.57	982	0	1	10	456	9	1547	5	2	2	50.84	22.66		
38.51	0.02	0.06	0.44	21.21	0.43	39.96	0.15	0.01	0.04	100.83	990	0	2	9	456	9	1532	4	0	1	48.70	22.84		

1400°C IW-1.5 heating M51

	SIO2	TIO2	AL2O3	CR2O3	FEO	MNO	MGO	CAO	NA2O	NIO	TOTAL	Si	Ti	Al	Cr	Fe	Mn	Mg	Ca	Na	Ni	FEMN	FFM	WO	FS
glass																									
	55.17	0.51	7.11	0.84	6.03	0.74	22.10	6.97	0.03	0.06	99.55	7750	54	1177	93	709	88	4629	1049	8	7	8.05	13.06		
	55.23	0.48	7.30	0.87	6.17	0.71	21.92	6.80	0.01	0.00	99.48	7758	51	1209	97	725	84	4591	1023	3	0	8.58	13.42		
	54.14	0.49	7.34	0.93	5.79	0.73	21.84	6.94	0.01	0.07	98.27	7706	52	1231	105	689	88	4634	1058	3	8	7.83	12.74		
	54.44	0.51	7.43	0.92	6.27	0.67	21.58	7.00	0.03	0.00	98.85	7713	54	1241	103	743	80	4559	1063	8	0	9.24	13.81		
	54.20	0.54	7.50	0.96	6.60	0.79	19.79	7.50	0.02	0.09	98.00	7769	58	1267	109	791	96	4229	1152	6	10	8.25	15.46		
	55.55	0.49	7.64	1.03	6.32	0.78	20.24	7.67	0.02	0.02	99.75	7799	52	1264	114	742	93	4237	1154	5	2	8.00	14.63		
	55.53	0.57	8.06	0.85	6.03	0.64	19.34	7.32	0.02	0.00	98.37	7865	61	1346	95	714	77	4084	1111	5	0	9.30	14.65		
olivine																									
	40.24	0.10	0.01	0.54	5.34	0.46	52.16	0.13	0.01	0.00	98.99	981	2	0	10	109	10	1896	3	0	0	11.46	5.41		
	41.57	0.03	0.02	0.53	5.41	0.47	51.98	0.12	0.02	0.00	100.15	999	1	1	10	109	10	1863	3	1	0	11.36	5.49		
	40.87	0.04	0.04	0.54	5.33	0.46	51.88	0.14	0.00	0.00	99.30	992	1	1	10	108	9	1877	4	0	0	11.44	5.42		
	40.76	0.07	0.02	0.54	5.46	0.46	52.21	0.12	0.00	0.00	99.64	987	1	1	10	111	9	1884	3	0	0	11.72	5.52		
pigeonite																									
	57.04	0.06	0.27	0.56	3.65	0.30	36.43	0.24	0.01	0.00	98.57	1976	2	11	15	106	9	1882	9	1	0	12.01	5.30	0.44	5.27
	55.67	0.06	0.32	0.55	3.79	0.37	35.60	0.29	0.00	0.02	98.68	1970	2	13	15	112	11	1878	11	0	1	10.11	5.60	0.55	5.57
	56.85	0.01	0.21	0.48	4.07	0.34	35.93	0.27	0.02	0.12	98.29	1979	0	9	13	119	10	1865	10	1	3	11.82	5.94	0.50	5.91
metal																									
	0.00	0.00	0.02	0.09	98.36	0.00	0.08	0.00	0.05	42.11	140.71	0	0	5	15	16954	0	25	0	20	6982				

Synthetic H-CM

1180°C IW-0.5 heating H33

SIO2	TIO2	AL2O3	CR2O3	FEO	MNO	MGO	CAO	NA2O	TOTAL	Si	Ti	Al	Cr	Fe	Mn	Mg	Ca	Na	FEMN	FFM	WO	FS
glass																						
51.96	0.58	12.34	0.28	17.19	0.52	6.80	9.21	0.54	99.42	7684	65	2151	33	2126	65	1499	1459	155	32.64	57.61		
52.01	0.50	12.41	0.28	17.07	0.46	6.72	9.29	0.53	99.27	7696	56	2164	33	2112	58	1482	1473	152	36.64	57.84		
53.51	0.58	12.49	0.32	16.13	0.45	5.89	9.82	0.48	99.67	7831	64	2154	37	1974	56	1285	1540	136	35.39	59.55		
53.31	0.57	12.49	0.29	17.19	0.52	5.54	9.78	0.43	100.12	7807	63	2156	34	2106	65	1210	1535	122	32.64	62.30		
52.46	0.58	12.60	0.35	16.85	0.53	5.52	9.91	0.51	99.31	7754	64	2195	41	2083	66	1216	1570	146	31.39	61.89		
53.38	0.58	12.64	0.26	17.21	0.46	5.52	9.74	0.41	100.20	7805	64	2178	30	2105	57	1203	1526	116	36.94	62.55		
52.65	0.58	12.70	0.25	16.75	0.48	5.65	9.78	0.43	99.27	7768	64	2209	29	2067	60	1243	1546	123	34.45	61.34		
olivine																						
38.12	0.02	0.02	0.31	24.17	0.50	36.06	0.27	0.01	99.48	1006	0	1	6	534	11	1419	8	1	47.73	27.17		
38.57	0.00	0.02	0.28	28.12	0.68	32.73	0.28	0.00	100.68	1024	0	1	6	624	15	1295	8	0	40.83	32.26		
38.08	0.00	0.02	0.26	24.46	0.56	35.38	0.25	0.00	99.01	1012	0	1	5	544	13	1402	7	0	43.13	27.77		
37.25	0.05	0.04	0.28	28.14	0.88	33.36	0.31	0.00	100.31	998	1	1	6	630	20	1332	9	0	31.57	31.80		
37.48	0.02	0.04	0.23	27.17	0.58	32.25	0.28	0.00	98.05	1020	0	1	5	619	13	1309	8	0	46.25	31.87		
39.13	0.02	0.04	0.28	24.28	0.56	37.41	0.28	0.01	102.00	1006	0	1	6	522	13	1434	8	1	42.81	26.53		
37.57	0.00	0.04	0.23	25.11	0.56	36.08	0.28	0.00	99.88	994	0	1	5	556	13	1423	8	0	44.27	27.90		
38.68	0.00	0.04	0.37	23.94	0.59	37.36	0.27	0.00	101.25	1002	0	1	8	519	13	1443	7	0	40.06	26.27		
37.99	0.00	0.04	0.26	27.83	0.70	33.20	0.31	0.00	100.33	1013	0	1	5	620	16	1319	9	0	39.25	31.73		
38.23	0.02	0.06	0.37	23.49	0.52	35.77	0.25	0.00	98.71	1015	0	2	8	521	12	1415	7	0	44.60	26.76		
38.25	0.02	0.08	0.50	28.15	0.68	32.98	0.32	0.00	100.98	1014	0	2	10	624	15	1303	9	0	40.87	32.12		
pigeonite																						
55.49	0.05	0.28	0.57	16.17	0.36	23.20	3.68	0.07	99.87	2022	1	12	16	493	11	1260	144	5	44.35	27.93	8.09	26.34
54.62	0.03	0.40	0.50	16.30	0.40	24.13	2.45	0.04	98.87	2008	1	17	15	501	12	1323	97	3	40.23	27.29	5.23	26.26
55.86	0.10	0.64	0.67	14.65	0.94	26.65	2.48	0.00	101.99	1980	3	27	19	434	28	1409	94	0	15.39	23.21	5.56	22.32
56.05	0.07	0.64	0.63	14.56	0.65	26.51	2.25	0.00	101.36	1993	2	27	18	433	20	1405	86	0	22.12	23.31	4.14	22.54
55.09	0.07	0.77	0.58	15.06	0.63	27.31	1.79	0.00	101.30	1966	2	32	16	450	19	1453	68	0	23.60	23.39	3.23	23.21

1180°C   IW-0.5   cooling   H34

	SIO2	TIO2	AL2O3	CR2O3	FEO	MNO	MGO	CAO	NA2O	TOTAL	Si	Ti	Al	Cr	Fe	Mn	Mg	Ca	Na	FEMN	FFM	WO	FS
glass	51.28	0.54	12.07	0.42	16.79	0.53	7.66	8.92	0.49	98.70	7637	60	2119	49	2091	67	1701	1423	141	31.28	54.19		
	51.26	0.55	12.64	0.41	16.62	0.53	7.62	9.04	0.59	99.26	7587	61	2205	48	2057	66	1682	1434	169	30.96	54.07		
	51.21	0.55	12.31	0.41	16.71	0.53	7.71	8.99	0.44	98.86	7611	61	2157	48	2077	67	1708	1432	127	31.13	53.92		
	51.36	0.55	12.27	0.42	16.75	0.51	7.59	8.87	0.48	98.80	7634	61	2150	49	2082	64	1682	1413	138	32.43	54.39		
olivine	39.11	0.02	0.04	0.26	22.87	0.43	37.72	0.25	0.01	100.71	1012	0	1	5	495	9	1455	7	1	52.51	25.26		
	38.68	0.02	0.04	0.29	24.13	0.41	37.95	0.20	0.01	101.73	997	0	1	6	520	9	1459	6	0	58.11	26.17		
	37.55	0.02	0.04	0.34	28.71	0.48	32.76	0.15	0.00	100.05	1008	0	1	7	645	11	1311	4	0	59.06	32.78		
	37.16	0.03	0.04	0.31	30.27	0.50	31.70	0.35	0.00	100.36	1003	1	1	7	683	11	1276	10	0	59.77	34.68		
	37.25	0.00	0.04	0.32	30.26	0.56	31.82	0.27	0.00	100.52	1004	0	1	7	682	13	1278	8	0	53.35	34.56		
	38.17	0.02	0.06	0.26	24.17	0.44	37.39	0.21	0.01	100.73	996	0	2	5	527	10	1454	6	1	54.24	26.48		
	39.00	0.00	0.06	0.35	23.59	0.45	37.39	0.22	0.00	101.06	1009	0	2	7	510	10	1442	6	0	51.76	26.01		
pigeonite	54.66	0.07	0.53	0.76	17.91	0.45	23.40	2.62	0.00	100.40	1996	2	23	22	547	14	1274	103	0	39.30	29.81	5.29	28.23
	54.23	0.05	0.59	0.72	20.11	0.46	22.29	2.24	0.00	100.69	1993	1	26	21	618	14	1221	88	0	43.16	33.34	4.54	31.83
	53.66	0.05	0.60	0.60	19.41	0.45	23.56	2.01	0.00	100.34	1974	1	26	17	597	14	1292	79	0	42.59	31.38	4.00	30.12
	55.97	0.08	0.74	0.58	16.76	0.36	25.10	1.69	0.00	101.28	2004	2	31	16	502	11	1340	65	0	45.97	27.09	3.38	26.17
	54.64	0.07	0.91	0.89	16.69	0.45	25.07	1.58	0.00	100.30	1981	2	39	26	506	14	1355	61	0	36.62	26.99	3.17	26.14
	56.16	0.10	0.96	0.77	14.40	0.43	26.56	2.98	0.07	102.43	1978	3	40	21	424	13	1395	112	5	33.07	23.16	5.78	21.82
spinel	0.28	0.93	8.60	54.25	25.33	0.44	6.48	0.08	0.00	96.39	10	25	359	1521	751	13	343	3	0	56.84	67.86		

1180°C   IW-1.0   heating   H60

	SIO2	TIO2	AL2O3	CR2O3	FEO	MNO	MGO	CAO	NA2O	TOTAL	Si	Ti	Al	Cr	Fe	Mn	Mg	Ca	Na	FEMN	FFM	WO	FS
glass																							
	50.85	0.62	13.60	0.31	14.85	0.36	6.80	9.35	0.96	97.70	7587	70	2392	37	1853	46	1513	1495	278	40.73	54.32		
	50.92	0.53	13.64	0.44	14.43	0.35	6.42	9.47	0.82	97.02	7631	60	2409	52	1809	44	1434	1521	238	40.71	55.02		
	51.15	0.57	13.64	0.38	14.65	0.36	6.72	9.30	0.89	97.67	7619	64	2395	45	1825	45	1492	1484	257	40.18	54.27		
	51.28	0.63	13.81	0.38	15.04	0.41	6.60	9.16	1.13	98.44	7595	70	2411	44	1863	51	1457	1454	325	36.22	55.25		
	51.62	0.63	13.81	0.48	14.09	0.36	6.43	9.42	1.04	97.88	7650	70	2412	56	1746	45	1421	1496	299	38.64	54.37		
	51.54	0.68	13.91	0.38	14.97	0.32	6.70	9.39	0.97	98.86	7592	75	2415	44	1844	40	1471	1482	277	46.19	54.96		
olivine																							
	37.46	0.02	0.02	0.37	24.37	0.41	36.35	0.24	0.00	99.24	995	0	1	8	541	9	1439	7	0	58.69	27.20		
	37.63	0.02	0.02	0.39	24.84	0.45	35.78	0.28	0.01	99.46	999	0	1	8	552	10	1417	8	1	54.50	27.89		
	37.55	0.00	0.02	0.35	24.49	0.46	35.96	0.25	0.00	99.13	999	0	1	7	545	10	1427	7	0	52.57	27.50		
	37.40	0.05	0.02	0.29	24.61	0.63	36.78	0.29	0.01	100.13	987	1	1	6	543	14	1448	8	1	38.57	27.10		
	37.33	0.03	0.02	0.23	25.23	0.49	36.06	0.22	0.00	99.61	992	1	1	5	561	11	1429	6	0	50.84	28.03		
	37.59	0.02	0.02	0.35	24.83	0.44	35.42	0.22	0.01	98.90	1003	0	1	7	554	10	1410	6	1	55.72	28.08		
	37.63	0.00	0.04	0.35	24.79	0.40	36.28	0.21	0.01	99.71	996	0	1	7	549	9	1432	6	1	61.19	27.58		
	37.42	0.00	0.04	0.39	24.19	0.39	35.65	0.25	0.01	98.34	1002	0	1	8	542	9	1423	7	1	61.24	27.45		
	37.76	0.02	0.04	0.54	24.51	0.46	36.30	0.22	0.01	99.86	997	0	1	11	541	10	1429	6	1	52.61	27.33		
	37.82	0.02	0.04	0.38	24.66	0.49	34.90	0.28	0.01	98.60	1011	0	1	8	552	11	1391	8	1	49.69	28.23		
	36.99	0.00	0.06	0.28	24.64	0.37	35.85	0.28	0.00	98.47	992	0	2	6	553	8	1434	8	0	65.75	27.71		
pigeonite																							
	52.11	0.13	0.57	0.80	14.23	0.63	27.52	2.24	0.13	98.36	1926	4	25	23	440	20	1516	89	9	22.30	22.26	4.30	21.30
	52.01	0.07	0.64	0.69	15.67	0.30	26.21	2.14	0.01	97.74	1940	2	28	20	489	9	1458	86	1	51.57	24.99	4.19	23.95
	53.51	0.10	0.64	0.61	15.43	0.44	25.62	1.99	0.04	98.38	1974	3	28	18	476	14	1409	79	3	34.62	25.07	3.98	24.07
	53.98	0.05	0.64	0.53	15.53	0.35	26.03	2.31	0.03	99.45	1970	1	28	15	474	11	1416	90	2	43.81	24.93	4.54	23.80
	53.16	0.10	0.77	0.70	14.90	0.50	25.37	1.96	0.04	97.50	1975	3	34	21	463	16	1405	78	3	29.42	24.57	3.98	23.60
	53.55	0.03	0.81	0.61	15.76	0.43	25.37	1.78	0.00	98.34	1976	1	35	18	486	13	1396	70	0	36.19	25.66	3.58	24.74

1180°C IW-1.5 heating H46

	SiO2	TIO2	AL2O3	CR2O3	FEO	MNO	MGO	CAO	NA2O	TOTAL	Si	Ti	Al	Cr	Fe	Mn	Mg	Ca	Na	FEMN	FFM	WO	FS
glass																							
	49.50	0.68	17.18	0.44	8.75	0.45	8.29	11.67	0.31	97.26	7253	75	2967	51	1072	56	1811	1832	88	19.20	36.48		
	50.83	0.70	17.38	0.39	8.97	0.41	8.49	11.67	0.39	99.23	7292	76	2939	44	1076	50	1816	1794	108	21.60	36.58		
	51.54	0.78	16.72	0.41	8.90	0.52	8.64	11.59	0.31	99.41	7372	84	2819	46	1065	63	1843	1776	86	16.90	35.85		
	51.32	0.70	16.70	0.39	8.68	0.75	8.31	11.21	0.30	98.36	7408	76	2841	45	1048	92	1788	1734	84	11.43	35.79		
	52.11	0.72	17.06	0.29	8.75	0.53	8.04	12.02	0.39	99.91	7408	77	2859	33	1040	64	1704	1831	108	16.30	37.05		
olivine																							
	38.89	0.08	0.04	0.40	14.29	0.50	45.84	0.23	0.00	100.27	976	2	1	8	300	11	1715	6	0	28.22	14.81		
	39.67	0.02	0.05	0.47	14.61	0.51	44.88	0.23	0.01	100.45	993	0	1	9	306	11	1675	6	0	28.29	15.36		
	39.03	0.02	0.04	0.42	14.33	0.51	45.43	0.22	0.00	100.00	982	0	1	8	301	11	1703	6	0	27.74	14.95		
pigeonite																							
	53.47	0.14	0.53	0.82	10.53	0.41	29.29	2.61	0.03	97.83	1948	4	23	24	321	13	1591	102	2	25.36	16.67	5.03	15.83
	53.98	0.09	0.62	0.72	10.44	0.52	28.85	2.10	0.02	97.33	1968	2	27	21	318	16	1568	82	1	19.82	16.73	4.13	16.04
	55.34	0.07	0.75	0.77	10.05	0.54	28.98	3.07	0.04	99.61	1971	2	31	22	299	16	1539	117	3	18.38	16.14	5.94	15.18
	55.47	0.08	0.82	0.82	9.85	0.46	28.87	2.68	0.02	99.00	1981	2	35	23	294	14	1537	103	1	21.14	15.94	5.27	15.10

1200°C   IW-0.5   heating   H31

	SIO2	TIO2	AL2O3	CR2O3	FEO	MNO	MGO	CAO	NA2O	TOTAL	Si	Ti	Al	Cr	Fe	Mn	Mg	Ca	Na	FEMN	FFM	WO	FS
glass																							
	50.64	0.58	12.64	0.37	16.63	0.58	7.81	8.79	0.42	98.46	7558	65	2224	44	2076	73	1738	1406	122	28.31	53.40		
	50.77	0.58	12.85	0.38	16.71	0.52	7.69	9.09	0.43	99.02	7539	65	2249	45	2075	65	1703	1446	124	31.73	54.00		
	51.15	0.58	12.85	0.06	16.47	0.57	7.26	8.84	0.50	98.28	7625	65	2258	7	2053	72	1614	1412	145	28.53	54.92		
	50.66	0.58	12.87	0.34	16.40	0.49	7.38	9.23	0.47	98.42	7560	65	2264	40	2047	62	1642	1476	136	33.05	54.57		
	50.49	0.60	13.77	0.15	16.36	0.53	6.14	9.57	0.44	98.05	7556	68	2429	18	2048	67	1370	1535	128	30.48	58.76		
	50.92	0.68	13.89	0.16	16.33	0.57	6.15	9.57	0.53	98.80	7558	76	2430	19	2027	72	1361	1522	153	28.29	58.59		
olivine																							
	37.50	0.00	0.00	0.42	24.29	0.54	36.21	0.22	0.00	99.18	997	0	0	9	540	12	1435	6	0	44.41	27.17		
	38.42	0.00	0.00	0.47	24.71	0.63	35.96	0.22	0.00	100.41	1008	0	0	10	542	14	1407	6	0	38.73	27.62		
	37.82	0.00	0.02	0.38	25.24	0.66	35.75	0.27	0.00	100.14	999	0	1	8	558	15	1408	8	0	37.76	28.16		
	38.19	0.02	0.02	0.50	24.92	0.61	35.57	0.22	0.00	100.05	1007	0	1	10	550	14	1399	6	0	40.34	28.02		
	38.04	0.02	0.04	0.38	24.49	0.66	35.57	0.10	0.00	99.30	1009	0	1	8	543	15	1407	3	0	36.64	27.65		
	38.32	0.05	0.06	0.32	24.74	0.50	36.01	0.24	0.03	100.27	1006	1	2	7	543	11	1410	7	2	48.85	27.66		
	38.06	0.02	0.06	0.41	24.02	0.54	35.88	0.27	0.03	99.29	1008	0	2	9	532	12	1416	8	2	43.92	27.13		
	37.85	0.00	0.04	0.41	24.47	0.61	35.50	0.25	0.00	99.13	1006	0	1	9	544	14	1407	7	0	39.61	27.69		
	38.17	0.01	0.05	0.30	24.04	0.50	35.99	0.22	0.01	99.29	1010	0	2	6	532	11	1419	6	1	47.47	27.10		
pigeonite																							
	55.11	0.05	0.51	0.60	15.39	0.63	25.24	2.24	0.05	99.82	1999	1	22	17	467	19	1365	87	4	24.12	25.22	4.49	24.09
	53.89	0.07	0.91	0.79	15.46	0.75	25.97	1.57	0.01	99.42	1967	2	39	23	472	23	1413	61	1	20.35	24.73	3.12	23.96
	55.22	0.05	0.66	0.60	15.95	0.49	25.12	2.01	0.03	100.13	1999	1	28	17	483	15	1355	78	2	32.14	26.05	4.04	25.00
	55.28	0.07	0.47	0.64	16.21	0.52	25.90	1.67	0.04	100.80	1990	2	20	18	488	16	1390	64	3	30.78	25.77	3.29	24.92
	54.53	0.05	0.51	0.54	15.75	0.48	25.22	1.58	0.01	98.67	2000	1	22	16	483	15	1379	62	1	32.40	25.74	3.20	24.91
spinel																							
	0.77	0.57	12.55	53.57	23.43	0.46	7.28	0.20	0.00	98.83	26	14	496	1422	658	13	364	7	0	50.29	63.54		
	0.98	0.57	14.17	51.08	22.90	0.44	7.63	0.21	0.00	97.98	33	14	559	1351	641	12	381	8	0	51.39	61.98		
	0.24	0.50	12.13	54.02	23.54	0.50	7.31	0.11	0.00	98.35	8	13	485	1449	668	14	370	4	0	46.48	63.49		
	0.28	0.60	15.57	50.06	22.91	0.45	7.48	0.13	0.00	97.48	9	15	616	1328	643	13	374	5	0	50.27	62.43		

1200°C   IW-0.5   cooling   H40

	SiO2	TiO2	AL2O3	CR2O3	FEO	MNO	MGO	CAO	NA2O	TOTAL	Si	Ti	Al	Cr	Fe	Mn	Mg	Ca	Na	FEMN	FFM	WO	FS
glass	53.21	0.53	12.74	0.25	15.68	0.40	7.33	8.55	1.20	99.90	7752	58	2188	29	1910	49	1592	1335	339	38.70	53.79		
	52.69	0.55	12.81	0.29	16.16	0.41	7.06	8.72	1.21	99.90	7706	60	2208	34	1977	51	1539	1366	343	38.92	55.42		
	52.95	0.55	12.94	0.26	15.86	0.40	7.35	8.56	1.20	100.08	7711	60	2221	30	1932	49	1596	1336	339	39.15	54.01		
	52.31	0.58	13.19	0.25	14.68	0.40	7.56	8.51	1.11	98.59	7693	64	2286	29	1806	50	1658	1341	317	36.24	51.40		
	51.94	0.53	13.19	0.29	15.18	0.39	7.38	8.66	1.25	98.81	7654	59	2291	34	1871	49	1621	1367	357	38.43	52.84		
	51.73	0.52	13.19	0.28	15.50	0.36	7.58	8.62	1.17	98.99	7624	58	2291	33	1911	45	1666	1361	334	42.51	52.76		
	52.39	0.55	13.21	0.29	15.30	0.37	7.48	8.33	1.21	99.14	7682	61	2283	34	1876	46	1635	1309	344	40.83	52.74		
	52.97	0.58	13.28	0.26	15.77	0.43	6.86	8.83	1.19	100.17	7705	63	2277	30	1919	53	1488	1376	336	36.21	55.46		
	52.46	0.57	13.40	0.29	15.27	0.41	7.10	8.93	1.04	99.47	7673	63	2310	34	1868	51	1548	1399	295	36.77	53.88		
	52.56	0.55	13.42	0.26	14.97	0.40	7.21	8.73	1.02	99.12	7695	61	2316	30	1833	50	1574	1369	290	36.95	53.03		
olivine	37.93	0.00	0.02	0.25	25.86	0.49	35.30	0.24	0.00	100.09	1004	0	1	5	572	11	1393	7	0.00	52.11	28.96		
	38.44	0.00	0.02	0.26	26.37	0.54	35.42	0.25	0.00	101.36	1006	0	1	5	577	12	1382	7	0.00	48.22	29.28		
	38.38	0.00	0.02	0.31	25.92	0.53	35.20	0.28	0.01	100.65	1009	0	1	6	570	12	1380	8	0.51	48.29	29.06		
	38.70	0.02	0.04	0.32	25.86	0.54	35.53	0.24	0.00	101.29	1010	0	1	7	565	12	1383	7	0.00	47.28	28.82		
	38.25	0.00	0.04	0.32	26.37	0.49	35.25	0.22	0.01	100.98	1005	0	1	7	580	11	1381	6	0.51	53.14	29.40		
	38.64	0.02	0.04	0.26	25.94	0.53	36.41	0.25	0.01	102.11	1001	0	1	5	562	12	1406	7	0.50	48.32	28.39		
	38.55	0.02	0.04	0.29	26.22	0.48	36.25	0.25	0.01	102.11	1000	0	1	6	569	11	1402	7	0.50	53.93	28.71		
	38.34	0.02	0.04	0.37	24.86	0.54	36.16	0.22	0.00	100.55	1005	0	1	8	545	12	1413	6	0.00	45.46	27.66		
	38.70	0.02	0.04	0.29	25.78	0.56	35.75	0.27	0.00	101.41	1009	0	1	6	562	12	1389	8	0.00	45.45	28.62		
pigeonite	55.67	0.07	0.43	0.58	16.13	0.50	26.18	2.39	0.05	102.00	1983	2	18	16	481	15	1390	91	3	31.85	25.48	4.61	24.30
	54.83	0.12	0.79	0.75	16.24	0.52	24.84	2.73	0.05	100.87	1980	3	34	21	490	16	1337	106	4	30.84	26.60	5.42	25.16
spinel	0.30	0.58	6.99	58.96	23.65	0.43	7.43	0.11	0.00	98.45	10	15	286	1620	687	13	385	4	0	54.30	63.35		

1200°C   IW-1.5   heating   H32

	SIO2	TIO2	AL2O3	CR2O3	FEO	MNO	MGO	CAO	NA2O	TOTAL	Si	Ti	Al	Cr	Fe	Mn	Mg	Ca	Na	FEMN	FFM	WO	FS
glass																							
	51.69	0.72	16.65	0.58	8.98	0.54	9.29	11.19	0.22	99.86	7358	77	2793	65	1069	65	1971	1707	61	16.42	34.42		
	52.33	0.67	16.46	0.53	8.98	0.40	9.53	11.38	0.16	100.44	7396	71	2742	59	1062	48	2008	1723	44	22.17	34.05		
	53.72	0.62	16.51	0.51	8.59	0.44	9.29	11.26	0.18	101.12	7504	65	2718	56	1004	52	1935	1685	49	19.28	33.56		
	56.39	0.48	13.96	0.42	8.61	0.35	7.61	11.12	0.24	99.18	7976	51	2327	47	1019	42	1605	1685	66	24.29	38.22		
	59.86	0.47	13.23	0.35	8.00	0.34	7.18	10.35	0.27	100.05	8291	49	2160	38	927	40	1483	1536	73	23.23	37.84		
	59.36	0.46	13.27	0.46	8.83	0.52	7.07	10.54	0.38	100.88	8214	48	2164	50	1022	61	1459	1563	102	16.77	40.21		
	59.03	0.44	13.20	0.45	8.70	0.48	7.13	10.55	0.38	100.36	8209	46	2164	49	1012	57	1478	1572	102	17.90	39.73		
	53.15	0.67	16.32	0.54	9.29	0.60	9.46	10.79	0.26	101.07	7460	71	2700	60	1091	71	1980	1623	71	15.29	34.71		
olivine																							
	39.28	0.02	0.04	0.44	15.57	0.61	44.14	0.21	0.00	100.31	990	0	1	9	328	13	1658	6	0	25.20	16.41		
	39.34	0.02	0.06	0.53	13.62	0.52	45.63	0.20	0.00	99.92	986	0	2	11	286	11	1706	5	0	25.86	14.26		
	39.47	0.03	0.04	0.57	13.50	0.63	45.98	0.20	0.00	100.42	985	1	1	11	282	13	1710	5	0	21.16	14.05		
	39.88	0.00	0.06	0.47	13.48	0.56	45.53	0.22	0.00	100.20	995	0	2	9	281	12	1694	6	0	23.77	14.16		
	39.90	0.00	0.02	0.48	13.51	0.57	46.18	0.24	0.00	100.87	990	0	1	9	280	12	1708	6	0	23.35	13.99		
	39.90	0.02	0.06	0.51	13.51	0.56	46.08	0.22	0.03	100.86	996	0	2	10	280	12	1704	6	0	23.82	14.04		
	40.18	0.02	0.04	0.45	13.64	0.52	45.78	0.22	0.00	100.88	996	0	1	9	283	11	1692	6	1	25.90	14.24		
	40.69	0.02	0.06	0.54	13.48	0.52	44.67	0.25	0.00	100.23	1013	0	2	11	281	11	1657	7	0	25.60	14.40		
	40.78	0.02	0.06	0.48	13.28	0.65	45.81	0.22	0.00	101.30	1004	0	2	9	273	14	1682	6	0	20.17	13.89		
	40.64	0.02	0.04	0.55	13.71	0.52	44.76	0.23	0.01	100.48	1010	0	1	11	285	11	1659	6	0	26.03	14.58		
pigeonite																							
	56.74	0.12	0.94	1.01	9.13	0.54	30.96	1.89	0.04	101.37	1970	3	38	28	265	16	1602	70	3	16.69	14.08	3.60	13.57
	56.99	0.06	0.64	0.94	10.63	0.64	29.12	2.22	0.02	101.27	1993	2	26	26	311	19	1518	83	1	16.40	16.82	4.31	16.10
	56.11	0.17	1.85	1.16	8.86	0.65	30.47	1.99	0.02	101.28	1950	4	76	32	258	19	1579	74	1	13.46	13.88	3.84	13.35
	56.54	0.07	0.72	0.82	9.66	0.51	30.68	1.33	0.03	100.37	1982	2	30	23	283	15	1604	50	2	18.70	14.89	2.56	14.51
spinel																							
	0.47	0.48	26.57	37.99	14.37	0.50	14.79	0.17	0.00	95.34	15	11	976	936	374	13	687	6	0	28.38	34.84		
	0.83	0.43	25.49	40.68	15.48	0.43	14.33	0.22	0.01	97.90	25	10	921	986	397	11	655	7	1	35.55	37.34		
	2.85	0.42	24.68	40.06	14.05	0.49	13.45	0.48	0.04	96.52	88	10	893	973	361	13	616	16	2	28.31	36.47		

1300°C   IW-0.5   heating   H42

	SIO2	TIO2	AL2O3	CR2O3	FEO	MNO	MGO	CAO	NA2O	TOTAL	Si	Ti	Al	Cr	Fe	Mn	Mg	Ca	Na	FEMN	FFM	WO	FS
glass	51.64	0.38	7.94	0.83	19.62	0.63	10.21	7.08	0.12	98.45	7807	43	1415	99	2481	81	2301	1147	35	30.75	51.02		
	52.11	0.38	7.99	0.79	20.60	0.71	10.25	7.30	0.16	100.29	7771	43	1404	93	2569	90	2279	1166	46	28.65	52.03		
	51.77	0.42	8.29	0.66	20.94	0.74	9.09	7.84	0.15	99.90	7773	47	1467	78	2630	94	2035	1261	44	27.94	55.26		
	52.21	0.44	8.14	0.81	20.32	0.73	9.12	8.04	0.15	99.96	7812	50	1436	96	2543	93	2034	1289	44	27.48	54.45		
olivine	39.21	0.00	0.02	0.66	21.16	0.57	38.97	0.21	0.00	100.80	1007	0	1	13	455	12	1492	6	0	36.65	23.20		
	39.43	0.00	0.02	0.70	21.64	0.59	39.00	0.17	0.00	101.55	1007	0	1	14	462	13	1485	5	0	36.21	23.58		
	38.83	0.00	0.04	0.67	21.43	0.54	38.48	0.20	0.00	100.19	1005	0	1	14	464	12	1485	6	0	39.18	23.66		
	39.19	0.00	0.04	0.61	21.81	0.59	38.95	0.17	0.01	101.37	1004	0	1	12	467	13	1487	5	0	36.50	23.75		
	39.30	0.02	0.06	0.67	21.69	0.53	39.00	0.15	0.00	101.42	1005	0	2	14	464	11	1487	4	0	40.41	23.64		
pigeonite	56.35	0.03	0.32	0.76	13.10	0.44	28.93	0.50	0.01	100.44	1998	1	13	21	388	13	1529	19	1	29.40	20.12	0.97	19.92
	56.18	0.02	0.34	0.86	12.85	0.44	29.03	0.49	0.01	100.22	1995	1	14	24	382	13	1537	19	1	28.84	19.76	0.96	19.57
	56.86	0.03	0.34	0.76	13.23	0.46	28.78	0.52	0.03	101.01	2004	1	14	21	390	14	1512	20	2	28.40	20.35	1.01	20.15
	55.75	0.03	0.40	0.86	13.34	0.48	28.75	0.49	0.01	100.08	1989	1	17	24	398	14	1529	19	1	29.27	20.51	0.96	20.31
	56.31	0.05	0.40	0.86	13.33	0.45	28.87	0.52	0.03	100.85	1992	1	17	24	394	14	1523	20	2	27.42	20.42	1.01	20.21
	56.33	0.02	0.43	0.89	13.24	0.45	28.45	0.55	0.00	100.36	2000	0	18	25	393	14	1506	21	0	29.05	20.56	1.08	20.33
	56.16	0.00	0.45	0.91	13.47	0.48	28.97	0.52	0.01	100.97	1986	1	19	25	398	14	1528	20	1	27.71	20.53	1.01	20.33
	56.52	0.02	0.45	0.86	13.32	0.45	28.44	0.53	0.01	100.60	2002	1	19	24	395	14	1502	21	1	29.23	20.66	1.04	20.44
	55.94	0.03	0.47	0.88	13.29	0.49	29.10	0.55	0.01	100.76	1982	1	20	25	394	15	1537	21	1	26.78	20.24	1.06	20.03
	56.12	0.05	0.51	0.96	13.42	0.49	28.74	0.59	0.00	100.88	1987	1	21	27	397	15	1517	22	0	27.04	20.60	1.15	20.36
	56.12	0.03	0.51	0.95	12.92	0.48	28.95	0.56	0.00	100.52	1989	1	21	27	383	14	1530	21	0	26.58	19.87	1.09	19.66

1300°C IW-1.5 heating H44

SiO2	TIO2	AL2O3	CR2O3	FEO	MNO	MGO	CAO	NA2O	TOTAL	Si	Ti	Al	Cr	Fe	Mn	Mg	Ca	Na	FEMN	FFM	WO	FS
glass																						
53.48	0.45	9.75	0.98	12.65	0.71	13.93	8.21	0.04	100.20	7694	49	1653	111	1522	87	2988	1266	11	17.59	33.11		
53.03	0.45	9.88	0.95	13.15	0.72	13.85	8.20	0.05	100.28	7647	49	1679	108	1586	88	2978	1267	14	18.03	34.10		
52.44	0.45	9.96	0.95	12.67	0.70	14.14	8.65	0.04	100.00	7588	49	1699	109	1533	86	3050	1341	11	17.87	32.84		
52.67	0.42	9.98	0.92	12.70	0.74	13.94	8.42	0.04	99.83	7624	46	1703	105	1538	91	3008	1306	11	16.95	33.16		
51.26	0.47	10.35	0.98	12.21	0.71	13.85	8.17	0.05	98.05	7550	52	1797	114	1504	89	3041	1289	14	16.98	32.46		
olivine																						
40.39	0.00	0.02	0.64	14.37	0.58	45.47	0.17	0.00	101.64	997	0	1	12	297	12	1673	4	0	24.46	14.97		
39.69	0.00	0.04	0.69	14.54	0.61	44.49	0.21	0.00	100.27	995	0	1	14	305	13	1663	6	0	23.53	15.39		
40.11	0.02	0.06	0.72	13.86	0.61	45.20	0.24	0.00	100.82	997	0	2	14	288	13	1675	6	0	22.43	14.58		
pigeonite																						
54.92	0.02	0.36	0.86	11.63	0.46	29.63	0.57	0.00	98.45	1980	1	15	25	351	14	1593	22	0	24.96	17.92	1.11	17.72
56.50	0.03	0.36	0.82	11.73	0.46	29.91	0.60	0.00	100.41	1993	1	15	23	346	14	1573	23	0	25.18	17.90	1.16	17.70
57.38	0.07	0.42	0.85	12.09	0.45	29.96	0.62	0.01	101.85	1996	2	17	23	352	13	1554	23	1	26.53	18.33	1.19	18.11
57.06	0.03	0.53	0.89	9.13	0.56	31.50	0.71	0.01	100.42	1990	1	22	25	266	17	1638	27	1	16.10	13.87	1.36	13.68
56.37	0.05	0.55	0.98	10.85	0.45	30.13	0.71	0.01	100.10	1988	1	23	27	320	13	1585	27	1	23.81	16.69	1.38	16.46
57.31	0.05	0.62	0.94	9.80	0.52	31.40	0.70	0.00	101.34	1986	1	25	26	284	15	1623	26	0	18.61	14.78	1.33	14.58
55.60	0.07	0.68	0.88	8.56	0.53	31.84	0.76	0.01	98.93	1969	2	28	25	253	16	1681	29	1	15.95	13.00	1.46	12.81

1400°C   IW-0.5   heating   H48

	TIO2	AL2O3	CR2O3	FEO	MNO	MGO	CAO	NA2O	TOTAL	Si	Ti	Al	Cr	Fe	Mn	Mg	Ca	Na	FEMN	FFM	WO	FS
SIO2																						
glass																						
53.59	0.18	3.97	0.91	18.06	0.59	19.00	3.62	0.04	100.01	7871	20	687	106	2219	73	4161	570	11	30.22	34.38		
54.28	0.18	3.99	0.86	17.57	0.53	19.60	3.62	0.05	100.73	7886	20	683	99	2135	65	4245	564	14	32.73	33.12		
53.10	0.18	4.04	0.89	18.35	0.63	19.91	3.69	0.05	100.89	7760	20	696	103	2243	78	4338	578	14	28.76	33.68		
52.99	0.20	4.06	0.86	18.35	0.63	19.63	3.69	0.04	100.50	7773	22	702	100	2251	78	4293	580	11	28.76	33.99		
53.25	0.20	4.08	0.95	18.00	0.61	19.52	3.60	0.04	100.30	7806	22	705	110	2207	76	4266	565	11	29.14	33.70		
52.76	0.23	4.12	0.85	17.43	0.67	19.42	3.60	0.05	99.18	7808	26	719	99	2158	84	4285	571	14	25.69	33.06		
53.14	0.18	4.21	0.82	18.01	0.62	19.42	3.51	0.04	100.00	7810	20	729	95	2214	77	4255	553	11	28.68	33.82		
53.38	0.18	4.23	0.96	18.87	0.67	18.55	4.06	0.05	101.00	7809	20	729	111	2309	83	4046	636	14	27.81	35.86		
olivine																						
39.73	0.00	0.02	0.50	15.62	0.40	43.86	0.08	0.00	100.26	1000	0	1	10	329	9	1645	2	0	38.56	16.58		
40.48	0.05	0.02	0.57	15.57	0.39	44.55	0.01	0.00	101.64	1002	1	1	11	322	8	1645	0	0	39.42	16.32		
39.94	0.02	0.02	0.56	14.91	0.37	44.19	0.10	0.00	100.16	1002	0	1	11	313	8	1653	3	0	39.79	15.85		
38.96	0.02	0.02	0.53	15.50	0.40	44.16	0.08	0.03	99.70	987	0	1	11	328	9	1668	2	1	38.26	16.38		
40.26	0.00	0.02	0.50	15.75	0.41	43.84	0.08	0.00	100.91	1006	0	1	10	329	9	1633	2	0	37.93	16.70		
40.11	0.00	0.02	0.54	15.50	0.36	44.49	0.08	0.00	101.15	999	0	1	11	323	8	1652	2	0	42.51	16.29		

1400°C IW-1.5 heating H50

	SiO2	TiO2	AL2O3	CR2O3	FEO	MNO	MGO	CAO	NA2O	TOTAL	Si	Ti	Al	Cr	Fe	Mn	Mg	Ca	Na	FEMN	FFM	WO	FS
glass	54.48	0.37	8.39	0.95	3.24	0.71	21.91	7.78	0.04	97.87	7699	39	1398	106	383	85	4616	1178	11	4.51	7.53		
	55.17	0.37	8.49	0.93	3.09	0.66	22.17	7.59	0.02	98.49	7727	39	1402	103	362	78	4629	1139	5	4.62	7.14		
	54.74	0.37	8.50	0.96	3.46	0.74	21.12	7.92	0.01	97.83	7741	39	1417	107	409	89	4453	1200	3	4.62	8.27		
	54.95	0.35	8.67	0.99	3.19	0.69	21.82	7.64	0.01	98.32	7716	37	1435	110	375	82	4568	1150	3	4.56	7.46		
	55.32	0.23	8.72	0.93	2.79	0.59	22.16	7.74	0.03	98.53	7733	24	1437	103	326	70	4618	1159	8	4.67	6.51		
	54.52	0.38	8.83	0.88	3.58	0.72	21.11	8.00	0.02	98.03	7700	40	1470	98	423	86	4445	1211	5	4.91	8.54		
olivine	40.16	0.01	0.03	0.58	3.14	0.52	53.39	0.07	0.01	97.90	981	0	1	11	64	11	1944	2	0	5.96	3.18		
	39.39	0.08	0.04	0.55	3.11	0.43	53.16	0.15	0.03	96.93	972	1	1	11	64	9	1957	4	1	7.14	3.16		
	38.73	0.04	0.05	0.64	3.00	0.45	53.87	0.16	0.00	96.93	958	1	1	13	62	9	1986	4	0	6.58	3.02		
pigeonite	57.18	0.08	0.16	0.59	6.70	0.33	33.77	0.17	0.00	98.98	1331	1	4	11	130	7	1172	4	0	20.05	9.97	0.32	9.98
	56.56	0.03	0.26	0.61	2.47	0.40	36.96	0.25	0.01	97.55	1314	1	7	11	48	8	1280	6	0	6.10	3.59	0.47	3.60
	57.13	0.05	0.29	0.67	3.87	0.37	35.59	0.26	0.01	98.24	1324	1	8	12	75	7	1230	6	0	10.33	5.72	0.49	5.72
	57.16	0.03	0.29	0.65	2.25	0.40	36.93	0.26	0.00	97.97	1320	1	8	12	43	8	1272	6	0	5.55	3.29	0.49	3.29

C. Series III Experiments

| (Temp) | (fO₂) | (Exp type) | (Exp #) |

Natural Murchison

| 1180°C | IW-0.5 | | heating | | NM55 |

	SIO2	TIO2	AL2O3	CR2O3	FEO	MNO	MGO	CAO	NA2O	NIO	TOTAL	Si	Ti	Al	Cr	Fe	Mn	Mg	Ca	Na	Ni	FEMN	FFM	WO	FS
glass																									
	43.54	0.75	14.13	0.18	20.97	0.25	4.01	12.94	0.43	0.10	97.30	6898	89	2638	23	2778	34	947	2197	132	13	82.82	73.91		
	42.30	0.85	14.55	0.16	21.91	0.22	3.88	12.93	0.40	0.09	97.29	6750	102	2737	20	2924	30	923	2211	124	12	98.33	75.42		
	43.64	0.83	14.78	0.12	21.15	0.25	3.70	12.83	0.47	0.17	97.94	6865	98	2741	15	2783	33	868	2163	143	22	83.53	75.54		
	43.09	0.78	15.25	0.18	21.57	0.23	3.33	13.70	0.43	0.08	98.64	6764	92	2822	22	2832	31	779	2304	131	10	92.60	77.76		
	43.73	0.95	15.49	0.12	20.16	0.21	3.18	14.31	0.44	0.13	98.71	6812	111	2844	15	2627	28	739	2389	133	16	94.79	77.42		
olivine																									
	34.76	0.02	0.04	0.13	33.35	0.32	28.92	0.46	0.01	0.13	98.14	981	0	1	3	788	8	1217	14	1	3	102.90	39.13		
	35.77	0.03	0.04	0.19	32.56	0.31	28.83	0.46	0.01	0.22	98.42	1000	1	1	4	762	7	1202	14	1	5	103.70	38.64		
	35.83	0.00	0.06	0.06	33.38	0.30	29.35	0.53	0.00	0.11	99.62	992	0	2	1	773	7	1212	16	0	2	109.86	38.81		
	35.04	0.02	0.06	0.16	33.36	0.35	28.74	0.53	0.03	0.23	98.52	985	0	2	4	785	8	1205	16	2	5	94.11	39.27		
	35.00	0.02	0.09	0.20	33.40	0.31	28.74	0.53	0.01	0.15	98.45	988	0	3	4	786	7	1206	16	1	3	106.38	39.32		
	35.19	0.00	0.09	0.15	33.23	0.37	28.74	0.52	0.00	0.27	98.56	983	0	3	3	780	9	1203	16	0	6	88.68	39.17		
	34.85	0.02	0.09	0.16	33.35	0.31	28.80	0.53	0.00	0.17	98.28	981	0	3	4	786	7	1211	16	0	4	106.22	39.23		
	35.09	0.03	0.09	0.26	33.82	0.27	29.05	0.48	0.00	0.13	99.22	981	1	3	6	790	6	1210	14	0	3	123.68	39.38		
	35.09	0.00	0.11	0.06	32.54	0.36	29.20	0.52	0.01	0.11	98.00	987	0	4	1	766	9	1225	16	1	2	89.25	38.30		
	35.75	0.02	0.26	0.19	33.15	0.30	28.70	0.66	0.01	0.15	99.19	994	0	9	4	771	7	1190	20	1	3	109.10	39.18		
	35.66	0.00	0.32	0.22	32.91	0.37	28.88	0.52	0.03	0.22	99.13	992	0	10	5	766	9	1198	15	2	5	87.82	38.82		
	34.57	0.00	0.36	0.35	33.60	0.28	28.40	0.49	0.01	0.11	98.17	977	0	12	8	794	7	1197	15	1	3	118.48	39.76		
spinel																									
	0.26	0.78	25.98	34.00	26.78	0.23	7.31	0.10	0.00	0.18	95.62	9	19	1007	884	736	6	358	4	0	5	114.95	66.88		
	2.65	0.52	35.81	21.95	26.18	0.17	9.43	0.46	0.07	0.14	97.38	80	12	1277	525	663	4	425	15	4	3	152.04	60.66		
metal																									
	0.13	0.05	0.00	0.09	75.89	0.03	0.00	0.00	0.00	64.28	140.47	27	8	0	15	13171	5	0	0	0	10732				

1180°C   IW-1.0   heating   NM59

SIO2	TIO2	AL2O3	CR2O3	FEO	MNO	MGO	CAO	NA2O	NIO	TOTAL	Si	Ti	Al	Cr	Fe	Mn	Mg	Ca	Na	Ni	FEMN	FFM	WO	FS
glass																								
48.56	0.63	13.16	0.34	18.09	0.22	5.12	11.06	0.70	0.09	97.97	7409	72	2367	41	2309	28	1165	1808	207	11	81.19	65.93		
48.61	0.63	13.49	0.35	17.28	0.26	4.92	11.47	0.46	0.00	97.47	7422	72	2428	42	2207	34	1120	1877	136	0	65.62	65.67		
48.62	0.62	13.44	0.36	17.98	0.24	5.11	11.25	0.56	0.02	98.20	7393	71	2409	43	2287	31	1158	1833	165	2	73.97	65.78		
48.48	0.62	13.23	0.38	18.21	0.24	5.02	11.32	0.59	0.04	98.13	7393	71	2378	46	2322	31	1141	1850	174	5	74.92	66.46		
48.51	0.63	13.48	0.33	17.59	0.23	4.99	11.11	0.68	0.04	97.59	7409	72	2427	40	2247	30	1136	1818	201	5	75.51	65.84		
olivine																								
36.88	0.03	0.06	0.29	28.61	0.28	33.21	0.32	0.03	0.19	99.90	994	1	2	6	645	6	1334	9	2	4	100.89	32.48		
37.40	0.00	0.06	0.25	28.08	0.35	32.57	0.32	0.03	0.17	99.23	1010	0	2	5	635	8	1312	9	2	4	79.21	32.46		
37.40	0.00	0.06	0.35	28.61	0.28	33.36	0.32	0.01	0.25	100.64	999	0	2	7	639	6	1328	9	1	5	100.89	32.38		
37.91	0.02	0.06	0.32	28.56	0.35	32.96	0.32	0.01	0.15	100.66	1010	0	2	7	636	8	1309	9	1	3	80.57	32.58		
37.46	0.00	0.06	0.23	28.50	0.31	32.91	0.32	0.03	0.09	99.91	1006	0	2	5	640	7	1318	9	2	2	90.77	32.58		
38.10	0.03	0.06	0.28	28.68	0.40	33.28	0.24	0.00	0.20	101.27	1009	1	2	6	635	9	1314	7	0	4	70.79	32.44		
37.76	0.00	0.06	0.44	28.64	0.25	32.83	0.31	0.01	0.18	100.48	1009	0	2	9	640	6	1307	9	1	4	113.11	32.76		
37.50	0.00	0.06	0.22	29.40	0.26	33.11	0.32	0.01	0.04	100.92	1000	0	2	5	656	6	1317	9	1	1	111.65	33.15		
37.29	0.00	0.08	0.34	28.87	0.31	33.08	0.32	0.01	0.09	100.39	999	0	2	7	647	7	1322	9	1	2	91.95	32.75		
37.78	0.00	0.08	0.37	28.42	0.36	33.08	0.31	0.01	0.08	100.49	1008	0	2	8	634	8	1316	9	1	2	77.95	32.39		
37.87	0.02	0.11	0.34	29.20	0.23	33.29	0.36	0.00	0.14	101.56	1002	0	3	8	646	5	1314	10	0	3	125.35	32.89		
36.97	0.00	0.11	0.23	29.36	0.36	33.53	0.32	0.03	0.14	101.05	988	0	3	7	656	8	1335	9	2	3	80.52	32.81		
37.50	0.02	0.13	0.22	28.96	0.32	33.16	0.43	0.01	0.13	100.88	1000	0	4	5	646	7	1318	12	1	3	89.36	32.76		
37.48	0.00	0.19	0.39	28.55	0.39	33.23	0.31	0.00	0.20	100.74	999	0	6	8	637	9	1321	9	0	4	72.28	32.38		
37.55	0.03	0.21	0.48	28.48	0.34	33.43	0.35	0.01	0.06	100.94	998	1	7	10	633	8	1325	10	1	1	82.71	32.21		
37.31	0.03	0.23	0.47	29.80	0.35	32.96	0.35	0.00	0.24	101.74	991	1	7	10	662	8	1306	10	0	5	84.07	33.52		
pigeonite																								
52.69	0.07	0.89	0.57	18.62	0.32	24.47	1.90	0.03	0.06	99.62	1949	2	39	17	576	10	1350	75	2	2	57.45	29.76	3.75	28.65

1180°C IW-1.5 heating NM57

	SIO2	TIO2	AL2O3	CR2O3	FEO	MNO	MGO	CAO	NA2O	NIO	TOTAL	Si	Ti	Al	Cr	Fe	Mn	Mg	Ca	Na	Ni	FEMN	FFM	WO	FS
glass																									
	52.35	0.55	14.08	0.35	11.89	0.28	7.10	10.28	1.01	0.11	98.00	7676	61	2433	41	1458	35	1552	1615	287	13	41.93	47.89		
	51.86	0.65	14.76	0.38	11.41	0.30	7.13	10.38	0.90	0.04	97.81	7603	72	2551	44	1399	37	1559	1631	256	5	37.55	46.72		
	52.84	0.58	14.38	0.42	11.30	0.28	7.06	10.13	0.86	0.06	97.91	7713	64	2474	48	1379	35	1536	1584	243	7	39.85	46.75		
	53.08	0.58	14.44	0.44	12.05	0.25	6.85	10.00	0.77	0.09	98.55	7715	63	2474	51	1465	31	1484	1557	217	11	47.59	49.16		
	52.41	0.60	14.45	0.45	11.94	0.30	7.43	9.81	0.73	0.08	98.20	7651	66	2486	52	1458	37	1617	1534	207	9	39.30	46.84		
	52.52	0.57	14.61	0.41	11.91	0.31	6.60	10.65	0.93	0.06	98.57	7656	62	2510	47	1458	38	1434	1663	263	7	37.93	49.65		
	51.88	0.58	14.87	0.35	11.78	0.27	7.83	9.58	0.80	0.01	97.95	7586	64	2563	40	1452	33	1707	1501	227	7	43.08	45.29		
	52.69	0.63	14.93	0.38	11.84	0.30	6.53	10.45	0.93	0.06	98.74	7654	69	2556	44	1439	37	1414	1627	262	7	38.97	49.78		
olivine																									
	38.51	0.02	0.04	0.41	19.99	0.40	40.41	0.22	0.00	0.04	100.04	993	0	1	8	431	9	1553	6	0	1	49.34	21.63		
	38.08	0.03	0.04	0.51	20.01	0.28	40.66	0.27	0.00	0.03	99.91	984	1	1	10	432	6	1567	7	0	1	70.56	21.57		
	38.38	0.02	0.06	0.51	20.33	0.28	40.96	0.24	0.01	0.04	100.83	983	1	2	10	436	6	1565	7	0	1	71.69	21.71		
	38.04	0.05	0.08	0.50	19.99	0.35	40.24	0.29	0.01	0.05	99.60	986	1	2	10	434	8	1556	8	1	1	56.39	21.71		
	38.89	0.00	0.04	0.41	20.13	0.43	39.08	0.28	0.01	0.08	99.35	1009	0	1	8	437	9	1512	7	1	2	46.22	22.31		
	38.89	0.02	0.04	0.45	19.70	0.35	40.44	0.25	0.01	0.09	100.18	999	0	1	8	423	8	1548	7	0	2	55.57	21.38		
	38.29	0.02	0.04	0.45	19.45	0.32	40.26	0.24	0.00	0.08	99.15	994	0	1	9	422	7	1558	7	0	2	60.01	21.25		
	38.98	0.02	0.06	0.44	19.54	0.32	40.92	0.25	0.00	0.03	100.56	996	0	2	9	418	7	1559	7	0	1	60.29	21.05		
	38.83	0.03	0.13	0.53	19.52	0.35	40.03	0.24	0.00	0.11	99.77	1001	1	4	11	421	8	1538	7	0	2	55.07	21.40		
pigeonite																									
	56.09	0.13	0.79	0.60	13.64	0.28	26.99	2.28	0.07	0.11	100.98	1992	3	33	17	405	8	1429	87	5	3	48.10	21.99	4.50	21.00
	54.06	0.05	0.93	0.56	13.26	0.46	27.49	2.11	0.04	0.08	99.04	1962	1	40	16	402	14	1487	82	3	2	28.46	21.14	4.13	20.27
	55.00	0.08	1.13	0.61	13.20	0.37	27.23	2.20	0.03	0.19	100.04	1972	2	48	17	396	11	1456	85	2	5	35.22	21.25	4.34	20.33
	54.47	0.07	0.83	0.79	12.80	0.36	27.99	1.99	0.01	0.00	99.31	1965	3	35	23	386	11	1505	77	1	0	35.11	20.30	3.89	19.51
	54.43	0.12	0.89	0.72	13.75	0.35	26.50	2.21	0.04	0.03	99.04	1977	3	38	21	418	11	1435	86	3	0	38.79	22.41	4.41	21.43
	54.87	0.12	1.06	0.75	12.90	0.35	27.47	2.18	0.03	0.04	99.77	1970	3	45	21	387	11	1470	84	2	1	36.39	22.73	4.30	21.84
	54.70	0.10	1.10	0.79	13.02	0.34	27.26	2.27	0.03	0.00	99.61	1969	3	47	22	392	10	1463	88	2	0	37.81	21.01	4.48	20.07
metal																									
	0.06	0.00	0.00	0.15	114.73	0.04	0.00	0.00	0.00	17.56	132.54	13	0	0	26	20857	7	0	0	0	3071				
	0.06	0.02	0.00	0.13	119.26	0.01	0.22	0.00	0.00	13.31	133.01	13	3	0	22	21548	2	71	0	0	2313				
	0.02	0.00	0.00	0.01	121.43	0.03	0.00	0.00	0.00	11.90	133.39	4	0	0	2	21917	5	0	0	0	2066				

148

1400°C   IW-0.5   heating   NM63

	SIO2	TIO2	AL2O3	CR2O3	FEO	MNO	MGO	CAO	NA2O	NIO	TOTAL	Si	Ti	Al	Cr	Fe	Mn	Mg	Ca	Na	Ni	FEMN	FFM	WO	FS
glass																									
	52.20	0.33	6.35	0.73	13.79	0.85	18.64	4.72	0.05	0.00	97.66	7727	37	1108	85	1707	107	4114	749	14	0	16.02	28.80		
	52.37	0.35	6.65	0.69	14.27	0.74	18.34	5.71	0.05	0.00	99.17	7668	39	1148	80	1748	92	4004	896	14	0	19.04	29.91		
	52.48	0.38	6.80	0.80	14.37	0.79	17.21	5.85	0.05	0.00	98.73	7719	42	1179	93	1768	98	3774	922	14	0	17.96	31.34		
	52.10	0.37	6.84	0.83	15.49	0.96	15.31	6.56	0.04	0.00	98.50	7743	41	1198	98	1925	121	3392	1045	12	0	15.93	35.40		
olivine																									
	40.07	0.00	0.01	0.44	11.52	0.53	46.90	0.14	0.01	0.16	99.78	996	0	0	9	239	11	1738	4	0	3	21.46	12.04		
	40.09	0.00	0.02	0.48	11.46	0.54	47.47	0.14	0.00	0.03	100.23	991	0	1	9	237	11	1750	4	0	1	20.95	11.86		
	39.88	0.01	0.02	0.41	11.60	0.41	47.45	0.11	0.00	0.00	99.88	990	0	1	8	241	9	1755	3	0	0	27.94	12.01		
	39.95	0.01	0.03	0.38	11.48	0.41	46.82	0.12	0.00	0.00	99.20	997	0	1	7	240	9	1742	3	0	0	27.65	12.04		
	40.11	0.00	0.04	0.35	11.54	0.56	47.39	0.14	0.03	0.10	100.26	992	0	1	7	239	12	1747	4	1	2	20.35	11.95		
	40.46	0.00	0.04	0.37	11.46	0.40	47.14	0.14	0.03	0.00	100.04	1000	0	1	7	237	8	1737	4	1	0	28.29	11.95		
	40.46	0.00	0.04	0.51	11.64	0.45	46.88	0.13	0.01	0.11	100.23	1000	0	1	10	241	9	1727	3	0	2	25.54	12.17		
	40.07	0.03	0.04	0.44	11.31	0.45	47.34	0.14	0.01	0.00	99.83	993	1	1	9	234	9	1750	4	0	0	24.82	11.76		
	40.13	0.00	0.05	0.47	11.46	0.49	47.52	0.13	0.01	0.05	100.30	991	0	1	9	237	10	1750	3	0	1	23.09	11.86		
	40.22	0.00	0.06	0.47	11.41	0.50	47.17	0.10	0.00	0.09	100.02	996	0	1	9	236	10	1741	3	0	2	22.53	11.89		
	39.81	0.00	0.06	0.56	11.48	0.44	47.37	0.15	0.03	0.06	99.96	988	0	2	11	238	9	1752	4	1	1	25.76	11.91		
	40.19	0.03	0.06	0.54	11.39	0.48	46.76	0.12	0.03	0.04	99.62	999	1	2	11	237	10	1732	3	0	1	23.43	11.96		
	40.24	0.05	0.08	0.50	11.26	0.43	46.91	0.14	0.03	0.00	99.64	999	1	2	10	234	9	1736	4	1	0	25.86	11.81		
	39.86	0.00	0.08	0.41	11.28	0.45	47.44	0.15	0.00	0.09	99.76	990	0	2	8	234	9	1756	4	0	2	24.75	11.71		
	40.11	0.02	0.36	0.42	11.50	0.48	46.21	0.29	0.00	0.00	99.39	999	0	11	8	240	10	1716	8	0	0	23.66	12.19		

70% Allegan-30% Murchison

	1180°C	IW-0.5		heating		AM54																			
	SiO2	TIO2	AL2O3	CR2O3	FEO	MNO	MGO	CAO	NA2O	NIO	TOTAL	Si	Ti	Al	Cr	Fe	Mn	Mg	Ca	Na	Ni	FEMN	FFM	WO	FS
glass																									
	52.35	0.47	10.37	0.31	17.32	0.25	5.80	8.24	1.17	0.06	96.34	7979	54	1863	37	2208	32	1318	1346	346	7	68.40	62.05		
	52.50	0.52	10.51	0.32	17.97	0.25	5.55	8.26	0.96	0.09	96.93	7969	59	1880	38	2281	32	1256	1343	283	11	70.97	63.91		
	52.39	0.50	10.64	0.26	18.68	0.26	5.60	8.65	1.39	0.03	98.40	7884	57	1887	31	2351	33	1256	1395	406	4	70.94	64.58		
	52.33	0.52	10.77	0.32	17.56	0.25	5.14	8.54	1.47	0.00	96.90	7949	59	1928	38	2231	32	1164	1390	433	0	69.35	65.10		
	52.56	0.47	11.05	0.25	17.37	0.27	6.30	7.86	1.05	0.08	97.26	7918	53	1962	30	2189	34	1415	1269	307	10	63.52	60.16		
olivine																									
	37.25	0.03	0.00	0.26	28.66	0.37	33.03	0.25	0.01	0.20	100.06	1001	1	0	6	644	8	1324	7	1	4	76.48	32.60		
	37.25	0.03	0.02	0.29	28.84	0.28	33.20	0.27	0.01	0.05	100.24	999	1	1	6	647	6	1328	8	1	1	101.70	32.66		
	37.05	0.03	0.02	0.42	29.20	0.35	32.28	0.27	0.00	0.09	99.71	1002	1	1	9	661	8	1302	8	0	2	82.37	33.53		
	37.74	0.00	0.02	0.28	28.77	0.34	32.70	0.28	0.01	0.22	100.36	1010	0	1	6	644	8	1305	6	1	5	83.55	32.92		
	37.33	0.05	0.02	0.37	29.02	0.36	32.50	0.20	0.01	0.18	100.04	1005	1	1	8	653	8	1304	6	1	4	79.59	33.23		
	36.97	0.02	0.02	0.34	28.96	0.37	32.66	0.24	0.01	0.22	99.81	999	0	1	7	654	8	1315	7	1	5	77.28	33.08		
	37.87	0.00	0.02	0.34	29.54	0.32	31.65	0.27	0.00	0.24	100.25	1018	0	1	7	664	7	1268	8	0	5	91.15	34.24		
	37.10	0.02	0.02	0.32	29.28	0.39	32.22	0.24	0.00	0.18	99.77	1003	0	1	7	662	9	1299	7	0	4	74.13	33.61		
	37.35	0.00	0.04	0.28	29.00	0.40	32.73	0.28	0.01	0.18	100.27	1003	0	1	6	651	9	1310	8	1	4	71.58	33.05		
	37.31	0.03	0.04	0.22	30.05	0.28	31.84	0.27	0.00	0.22	100.26	1006	1	1	5	678	6	1280	8	0	5	105.97	34.50		
	37.35	0.03	0.08	0.32	29.32	0.27	32.45	0.35	0.05	0.11	100.33	1003	1	3	7	659	6	1300	10	3	2	107.22	33.53		
	37.42	0.02	0.08	0.28	28.47	0.28	32.71	0.28	0.00	0.15	99.69	1007	0	3	6	641	6	1313	8	0	3	100.39	33.70		
	36.88	0.03	0.09	0.31	29.23	0.41	32.60	0.28	0.00	0.38	100.21	994	1	3	7	659	9	1311	8	0	8	70.39	33.31		
	37.59	0.02	0.11	0.37	28.82	0.28	32.47	0.24	0.00	0.29	100.19	1009	0	3	8	647	6	1299	7	0	6	101.63	33.13		
	37.25	0.05	0.19	0.25	28.47	0.27	32.83	0.31	0.01	0.23	99.86	1002	1	6	5	640	6	1316	9	1	5	104.11	32.62		
pigeonite																									
	53.95	0.08	0.49	0.57	17.72	0.31	24.19	1.60	0.03	0.15	99.09	1991	2	21	17	547	10	1331	63	2	4	56.44	28.98	3.24	28.04
	53.03	0.05	0.76	0.64	17.84	0.31	24.04	1.90	0.03	0.04	98.64	1972	1	33	19	555	10	1333	76	2	1	56.82	29.24	3.84	28.12
	53.83	0.07	0.81	0.66	18.29	0.32	23.86	1.75	0.03	0.22	98.84	1979	2	35	19	562	10	1308	69	2	7	56.43	29.91	3.54	28.85
	53.55	0.08	0.87	0.72	17.55	0.35	24.71	1.74	0.03	0.13	99.73	1966	2	38	21	539	11	1353	68	2	4	49.51	28.33	3.47	27.34
spinel																									
	0.13	1.32	6.80	52.92	25.79	0.27	5.34	0.03	0.00	0.15	92.75	5	37	300	1565	807	9	298	1	0	5	94.31	72.48		
	0.09	1.20	7.33	54.60	26.18	0.30	5.46	0.04	0.00	0.11	95.31	3	33	314	1568	795	9	296	2	0	3	86.16	72.29		
metal																									
	0.09	0.02	0.00	0.03	56.94	0.03	0.00	0.00	0.00	85.08	142.19	19	3	0	5	9824	5	0	0	0	14120				
	0.04	0.03	0.00	0.00	60.57	0.01	0.05	0.00	0.01	92.33	153.04	8	4	0	0	9714	2	14	0	4	14244				

1180°C IW-1.0 heating AM58

	SIO2	TIO2	AL2O3	CR2O3	FEO	MNO	MGO	CAO	NA2O	NIO	TOTAL	Si	Ti	Al	Cr	Fe	Mn	Mg	Ca	Na	Ni	FEMN	FFM	WO	FS
glass																									
	50.45	0.50	11.92	0.41	18.76	0.31	5.26	8.98	1.00	0.14	97.73	7677	57	2138	49	2388	40	1193	1464	295	17	59.75	65.94		
	51.26	0.57	11.96	0.22	17.97	0.28	5.47	8.76	1.13	0.15	97.77	7747	65	2130	26	2271	36	1232	1419	331	18	63.37	64.17		
	51.45	0.55	12.32	0.29	17.91	0.33	4.61	9.21	1.12	0.06	97.85	7767	62	2192	35	2281	42	1038	1490	328	7	53.59	67.68		
	50.06	0.52	11.34	0.42	17.75	0.26	6.42	8.88	1.01	0.03	96.69	7672	60	2048	51	2275	34	1467	1458	300	4	67.41	60.26		
	50.68	0.48	11.39	0.38	17.75	0.28	6.27	8.87	1.00	0.00	97.10	7719	55	2045	46	2261	36	1424	1448	295	0	62.59	60.77		
olivine																									
	36.73	0.02	0.04	0.38	29.16	0.44	32.85	0.31	0.00	0.03	99.96	992	0	1	8	659	10	1323	9	0	1	65.44	33.07		
	37.01	0.00	0.04	0.48	29.07	0.34	32.45	0.31	0.03	0.00	99.73	1000	0	1	10	657	8	1308	9	2	0	84.42	33.31		
	36.95	0.03	0.04	0.44	29.14	0.37	32.62	0.27	0.03	0.00	99.89	997	1	1	9	658	8	1313	8	2	0	77.76	33.24		
	37.33	0.05	0.06	0.51	29.82	0.36	32.68	0.25	0.00	0.06	101.12	997	1	2	11	666	8	1302	7	0	1	81.79	33.72		
	37.31	0.00	0.06	0.34	29.14	0.34	33.16	0.31	0.00	0.00	100.66	998	0	2	7	652	8	1322	9	0	0	84.62	32.89		
	36.54	0.05	0.06	0.48	28.93	0.37	32.63	0.28	0.03	0.00	99.37	992	1	2	10	657	8	1321	8	2	0	77.20	33.07		
	36.73	0.00	0.09	0.37	29.01	0.36	32.40	0.35	0.04	0.08	99.43	997	0	3	8	658	8	1311	10	2	2	79.56	33.29		
	36.69	0.00	0.13	0.94	28.33	0.41	32.02	0.34	0.01	0.01	98.88	999	0	4	20	645	9	1300	10	1	0	68.22	33.01		
	37.59	0.03	0.15	0.34	29.33	0.41	32.91	0.32	0.01	0.14	101.23	1000	1	5	7	653	9	1306	9	1	3	70.63	33.17		
pigeonite																									
	52.91	0.07	0.76	0.83	17.73	0.36	24.34	1.79	0.05	0.00	98.84	1964	2	33	24	550	11	1347	71	4	0	48.63	28.84	3.60	27.80
	53.91	0.05	0.77	0.77	17.88	0.35	24.90	1.71	0.04	0.01	100.39	1967	1	33	22	546	11	1355	67	3	0	50.44	28.55	3.38	27.59
	53.46	0.03	0.79	0.73	17.75	0.22	24.23	1.79	0.03	0.09	99.12	1975	1	34	21	548	7	1335	71	2	3	79.66	29.02	3.61	27.97
	52.97	0.08	0.83	0.83	17.91	0.27	24.51	1.82	0.01	0.11	99.34	1958	2	36	24	554	8	1351	72	1	3	65.50	28.95	3.63	27.89
	53.80	0.07	0.87	0.75	18.13	0.36	24.44	1.67	0.04	0.06	100.19	1969	2	38	22	555	11	1334	65	3	2	49.72	29.21	3.33	28.24
	51.86	0.12	1.00	0.80	19.16	0.37	24.06	1.67	0.03	0.04	99.11	1937	3	44	24	598	12	1340	67	2	1	51.13	30.69	3.31	29.68

1180°C IW-1.5 heating AM56

	SIO2	TIO2	AL2O3	CR2O3	FEO	MNO	MGO	CAO	NA2O	NIO	TOTAL	Si	Ti	Al	Cr	Fe	Mn	Mg	Ca	Na	Ni	FEMN	FFM	WO	FS
glass																									
	52.88	0.62	14.74	0.37	9.98	0.26	8.41	9.58	1.08	0.06	97.98	7661	68	2517	42	1209	32	1817	1487	303	7	37.90	39.55		
	52.76	0.52	15.17	0.34	9.67	0.28	7.26	10.12	1.06	0.00	97.18	7695	57	2608	39	1180	35	1579	1582	300	0	34.10	42.24		
	52.76	0.58	15.70	0.37	9.91	0.28	7.66	9.84	0.96	0.03	98.09	7626	63	2675	42	1198	34	1651	1524	269	3	34.95	41.55		
	52.18	0.62	15.70	0.38	9.58	0.32	7.79	9.65	0.80	0.00	97.02	7612	68	2700	44	1169	40	1694	1508	226	0	29.56	40.27		
	52.46	0.60	16.00	0.37	9.69	0.34	7.78	9.84	0.88	0.01	97.97	7587	65	2728	42	1172	42	1678	1525	247	1	28.14	40.54		
	53.06	0.58	16.12	0.29	9.79	0.32	7.66	9.70	1.00	0.00	98.52	7622	63	2729	33	1176	39	1640	1493	279	0	30.21	41.19		
olivine																									
	39.69	0.00	0.04	0.39	16.16	0.43	43.38	0.25	0.00	0.03	100.37	1000	0	1	8	341	9	1630	7	0	1	37.11	17.21		
	39.90	0.02	0.06	0.28	16.08	0.43	43.82	0.22	0.00	0.20	101.01	999	0	2	6	337	9	1635	6	0	4	36.92	16.99		
	39.66	0.00	0.06	0.28	16.56	0.40	43.26	0.24	0.00	0.17	100.63	999	0	2	6	349	9	1624	6	0	3	40.88	17.60		
	39.19	0.03	0.06	0.44	16.39	0.39	43.09	0.25	0.01	0.04	99.88	994	1	2	9	348	8	1630	7	0	1	41.49	17.51		
	39.64	0.05	0.08	0.41	16.48	0.37	43.18	0.22	0.00	0.01	100.42	999	0	2	8	347	8	1623	6	0	0	43.98	17.56		
	39.94	0.05	0.08	0.41	16.35	0.41	43.14	0.22	0.01	0.04	100.64	1004	1	2	8	344	9	1616	6	0	1	39.37	17.46		
	40.03	0.00	0.08	0.38	16.08	0.34	43.59	0.21	0.00	0.11	100.83	1003	0	2	8	337	7	1628	6	0	2	46.70	17.08		
	39.06	0.00	0.13	0.57	16.89	0.44	43.36	0.21	0.00	0.00	100.66	986	0	4	11	357	9	1633	6	0	0	37.90	17.85		
pigeonite																									
	55.90	0.07	0.55	0.82	12.84	0.34	28.39	1.58	0.04	0.00	100.53	1985	2	23	23	381	10	1503	60	3	0	37.29	20.13	3.08	19.51
	54.47	0.07	0.62	0.56	13.71	0.34	28.06	1.57	0.11	0.08	99.59	1966	2	26	16	414	10	1510	61	8	2	39.81	21.40	3.04	20.75
	55.75	0.10	0.66	0.79	13.33	0.36	27.36	1.68	0.01	0.00	100.04	1993	3	28	22	399	11	1458	64	1	0	36.56	21.34	3.33	20.63
	55.60	0.12	0.83	0.88	12.56	0.35	28.45	1.57	0.04	0.05	100.45	1975	3	35	25	373	11	1507	60	3	1	35.43	19.74	3.06	19.13
	55.71	0.12	1.08	0.89	12.71	0.43	28.09	2.03	0.03	0.00	101.09	1970	3	45	25	376	13	1481	77	2	0	29.18	20.10	3.95	19.31
	56.50	0.12	1.23	0.83	11.68	0.39	29.41	1.39	0.01	0.04	101.60	1973	3	51	23	341	12	1531	52	1	1	29.57	18.11	2.69	17.62
spinel																									
	0.73	0.62	21.75	45.51	17.16	0.43	11.21	0.08	0.01	0.08	97.58	23	15	811	1139	454	12	529	3	1	2	39.40	45.66		
	0.09	1.62	7.60	55.41	20.16	0.45	9.22	0.04	0.01	0.05	94.65	3	43	318	1553	598	14	487	2	1	1	44.23	54.41		
metal																									
	0.00	0.02	0.00	0.03	101.07	0.01	0.07	0.00	0.01	35.62	136.83	0	3	0	5	17894	2	22	0	4	6066				
	0.06	0.00	0.02	0.25	96.68	0.10	0.00	0.00	0.00	18.34	115.45	15	0	6	49	20183	21	0	0	0	3683				

1400°C   IW-0.5   heating   AM62

SIO2	TIO2	AL2O3	CR2O3	FEO	MNO	MGO	CAO	NA2O	NIO	TOTAL	Si	Ti	Al	Cr	Fe	Mn	Mg	Ca	Na	Ni	FEMN	FFM	WO	FS
glass																								
53.48	0.32	5.91	0.86	21.65	0.67	10.55	5.58	0.05	0.10	99.17	8051	36	1049	102	2726	85	2368	900	15	12	31.91	52.63		
52.44	0.25	6.48	0.82	19.79	0.70	11.86	5.09	0.04	0.00	97.47	7965	29	1160	98	2514	90	2686	828	12	0	27.91	47.53		
51.58	0.33	6.90	0.80	21.28	0.63	10.08	5.55	0.04	0.03	97.22	7927	38	1250	97	2735	82	2309	914	12	4	33.35	53.35		
52.88	0.40	7.37	0.67	19.08	0.58	10.86	5.53	0.07	0.00	97.44	7991	45	1313	80	2411	74	2447	895	21	0	32.48	48.89		
olivine																								
38.17	0.00	0.02	0.58	17.44	0.37	41.93	0.10	0.00	0.19	98.80	987	0	1	12	377	8	1616	3	0	4	46.54	18.84		
38.34	0.03	0.02	0.47	17.32	0.40	42.18	0.10	0.00	0.14	99.03	988	1	1	10	373	9	1620	4	0	3	42.75	18.64		
39.21	0.00	0.02	0.35	16.93	0.32	41.97	0.10	0.00	0.20	99.10	1004	0	1	7	363	7	1603	4	0	4	52.24	18.39		
38.77	0.02	0.02	0.51	17.43	0.40	42.23	0.13	0.00	0.19	99.70	992	0	1	10	373	9	1610	4	0	4	43.02	18.72		
39.94	0.00	0.04	0.44	16.80	0.40	43.16	0.13	0.01	0.19	101.11	1002	0	1	9	352	8	1614	3	0	4	41.47	17.85		
38.25	0.02	0.04	0.44	17.06	0.35	42.80	0.11	0.01	0.05	99.13	983	0	1	9	367	8	1640	3	0	1	48.13	18.21		
39.00	0.02	0.04	0.44	17.17	0.44	42.28	0.10	0.00	0.09	99.58	996	0	1	9	367	10	1610	3	0	2	38.53	18.47		
38.53	0.00	0.04	0.50	17.61	0.46	42.56	0.10	0.01	0.25	100.06	984	0	1	10	376	10	1621	3	0	5	37.80	18.75		
39.15	0.00	0.04	0.50	17.61	0.30	42.85	0.13	0.00	0.00	100.58	991	0	1	10	373	6	1618	4	0	0	57.96	18.67		
39.26	0.02	0.06	0.44	17.20	0.40	42.43	0.08	0.00	0.18	100.07	998	0	2	9	366	9	1608	2	0	4	42.46	18.45		
39.04	0.02	0.06	0.42	17.19	0.41	42.60	0.13	0.00	0.32	100.19	992	0	2	8	365	9	1615	4	0	7	41.40	18.38		
38.23	0.03	0.06	0.56	17.61	0.48	42.23	0.17	0.00	0.06	99.43	983	1	2	11	379	10	1619	5	0	1	36.22	18.86		

Cation mineral formulas based on:

24000 oxygens for glass
4000 oxygens for olivine (ideal olivine = 3000 cations per 4000 oxygens)
6000 oxygens for pigeonite (ideal pyroxene= 4000 cations per 6000 oxygens)
4000 oxygens for spinel (ideal spinel = 3000 cations per 4000 oxygens)
24000 oxygens for metal

$FEMN = (FeO/71.846) / (MnO/70.938)$

$FFM = (FeO/71.846) / [(FeO/71.846)+(MnO/70.938)+(MgO/40.304)]$

$WO = (CaO/56.08) / [(CaO/56.08)+(FeO/71.846)+(MgO/40.304)]$

$FS = (FeO/71.846) / [(CaO/56.08)+(FeO/71.846)+(MgO/40.304)]$